THE ANELASTIC STRUCTURE AND DEEP GEOLOGY OF THE DERBYSHIRE DOME FROM HIGH FREQUENCY RAYLEIGH WAVES

by

Andrew James William McDonald

(BSc, The University of Leeds)

Submitted in accordance with the requirements

for the degree of

Doctor of Philosophy

The University of Leeds

Department of Earth Sciences

July 1984

ABSTRACT

This work is an investigation of the anelastic structure of the Derbyshire Dome and adjacent areas from the analysis of high frequency, 0.6 - 4.2 Hz, fundamental mode Rayleigh waves observed from quarry blasts within the study area.

Seismic field experiments, designed and implemented to record Rayleigh waves accurately, are discussed together with the data preparation sequence. The effects of possible errors on timing and amplitude measurements are investigated and reduced.

Time domain measurements indicate the Carboniferous Limestone district of the Derbyshire Dome consists of smaller provinces the boundaries of which are marked by sudden changes in group velocity and co-incide with geological surface features. Similar provinces are not found in the adjacent Millstone Grit district. Approximate estimates of group velocity are higher over the limestone than over the Millstone Grit district.

Transformation into the frequency domain facilitates the determination of group arrival times and amplitude spectrum of each Rayleigh wave recorded. Least squares interstation analyses provide estimates of group slowness dispersion for the districts and component provinces and the Rayleigh wave specific attenuation factor, $Q_\gamma^{-1}(\nu)$, as a function of frequency for certain districts and provinces.

Group slowness which ranges from 0.33 - 1.1 s km^{-1}, increasing generally with frequency, is higher in the Millstone Grit district. $Q_\gamma^{-1}(\nu)$ ranges between 0.01 and 0.08 showing no marked correlation with surface lithology.

Models of shear wave velocity, $\beta(z)$, and intrinsic specific

attenuation factor for shear waves, $Q_\beta^{-1}(z)$, with depth, z, are obtained for the upper 1.5 km of the crust in each district and province from the inversion of the observed dispersion and $Q_\gamma^{-1}(\nu)$ data using linearised and Hedgehog techniques for $\beta(z)$ and similar methods for $Q_\beta^{-1}(z)$.

The deep geology of the area is inferred from the $\beta(z)$ models. The limestone district is divided by a major basement fault, to which surface features may be related. The Carboniferous Limestone of different provinces is underlain directly by Ordovician mudstones or Devonian sandstones. A sedimentary basin, of 1.5 km thickness, displaying rhythmic sedimentation is postulated within the Millstone Grit district.

Fluid saturation conditions are inferred from the $Q_\beta^{-1}(z)$ models. On comparison with previous laboratory work values of Q_β^{-1} which exhibit a possible frequency dependence imply partial saturation of the upper layers of the limestone district whilst field estimates of Q_β^{-1} not exhibiting any frequency dependence imply the Millstone Grit district to be fully saturated at all levels. Two mechanisms of dissipation based on the petrographic character of the rock and fluid flow are believed to operate jointly.

List of Contents.

List of Figures.

Chapter Two.

Chapter Five.

Plate 1 The Source - a quarry blast in Ballidon Quarry.

Total charge size 1252 kg

Number of holes 10

Delay interval 25 ms

Height of face 15 m

Top: Quarry face prior to blast.

Bottom: During blast - firing sequence from right to left. 59

List of Tables.

Key to Symbols and Abbreviations.

Symbols:

All symbols used in this thesis are defined in the text but those which refer to particular quantities are given below for reference. Where a given symbol is used for more than one quantity the particular usage will be apparent from the context.

α compressional wave velocity (km s^{-1}),
roll off of Gaussian filter used in the multiple filter technique.

β shear wave velocity (km s^{-1}),
seismometer damping co-efficient.

γ attenuation co-efficient for Rayleigh waves (km^{-1}).

η exponent of frequency for frequency dependent intrinsic shear wave specific attenuation factor.

θ azimuth ($^{\circ}$),
the Levenberg-Marquardt smoothing parameter - the degree of damping in matrix inversions.

λ wavelength (m or km).

ν frequency (Hz).

ρ density (km m^{-3})

σ Poisson's ratio,
standard deviation of an observed quantity.

τ period (s).

ω angular frequency (rad s^{-1}).

$\Delta\nu$ fundamental harmonic frequency (Hz).

δt sampling interval (s)

c	phase velocity (km s^{-1}).
h	thickness (m or km).
k	wavenumber (m^{-1} or km^{-1}).
K	seismometer coupling factor (V m^{-1} s).
p	slowness (s km^{-1}).
Q^{-1}	general specific attenuation factor.
Q_α^{-1}	intrinsic compressional wave specific attenuation factor.
Q_β^{-1}	intrinsic shear wave specific attenuation factor.
Q_γ^{-1}	observed Rayleigh wave specific attenuation factor.
r	distance from source (km).
t	time (s).
U	group velocity (km s^{-1}).
x	any general distance or displacement (m or km).
z	depth (m or km).

Abbreviations:

BGS	British Geological Survey (formerly the Institute of Geogical Sciences.)
c.l.	confidence level
dc	signal, or level, with a frequency of 0 Hz (strictly direct current).
d.u.	digitiser units.
emf	electro-motive force.
ep	extended period (for seismometers with natural period of 1.5 s).
FFT	Fast Fourier Transform.
FORTRAN	FORmula TRANslation - a high level computer language.
FTAN	Frequency - Time ANalysis.

ACKNOWLEDGEMENTS

I have conducted this research with the Global Seismology Research Group (GSRG) of the British Geological Survey (BGS) in Edinburgh as a research student of the Department of Earth Sciences, the University of Leeds. I would like to thank the heads of both departments for the use of their facilities and for accepting me as a student.

It is with pleasure that I acknowledge the guidance and help given to me by my supervisors Dr Paul Burton (BGS) and Dr Graham Stuart (Leeds). Their interest and encouragement at all stages of this project from the deployment of the equipment, sometimes in very poor weather conditions, to discussions on the results has sustained my often failing enthusiasm.

I would also like to thank Robert McGonigle (BGS) for his help both in the field and, more importantly, in the large computing component of this project; answering patiently my many questions.

Thanks are due to Robert Jones, manager of the Natural Environment Research Council's Seismological Equipment Pool, for his assisstance with the equipment. I would like to acknowledge the late John Parker, also of the Seismological Equipment Pool, whose quiet and efficient manner contributed significantly to the smooth running of the field experiments.

The many hours of field work and fruitful discussions shared with David Rogers whilst working on the various aspects of the seismological investigation of the Derbyshire Dome are happily acknowledged.

Many other people have had some association with this project and I hope I will be forgiven for not thanking them explicitly for

their aid. My fellow students both in the BGS and at Leeds are thanked for their stimulating discussions and friendship. The staff of the GSRG gave of their time and expertise freely, for which I am most grateful.

I am also grateful to the Natural Environment Research Council who supported the project through the award of a research studentship grant.

Last, but not least, I am indebted to the quarry managers, shot firing teams, land owners and farmers of the field work area. Without their friendly co-operation, which was a pleasant aspect of the study, a succesful conclusion of this project would have been difficult to achieve.

CHAPTER ONE

INTRODUCTION

1.1 THE PROJECT.

When subjected to small strains, for example during the passage of a seismic wave in the far field, earth materials behave in an anelastic manner resulting in the dissipation of energy from the seismic wave. This behaviour can be observed as a decay in amplitude of the seismic wave with distance in excess of that due to the geometrical spreading of the wave front. Attenuation, often poorly determined, is, therefore, an important parameter required together with the seismic wave velocities to provide a complete description of seismic wave propagation. Anderson & Archambeau (1964) were fully aware of the significance of attenuation when they stated: "The attenuation of seismic energy in the earth, being a direct measure of anelasticity, is potentially an important source of information regarding the composition, state and temperature of the deep interior."

The research reported in this thesis is an investigation of the anelastic properties of the shallow upper crust of the Derbyshire Dome and adjacent areas of central England (Fig 1.1). The principal aim of this project was to obtain reliable estimates of the specific attenuation factor for Rayleigh waves, $Q_\gamma^{-1}(\nu)$, as a function of frequency, ν, and thence the distribution with depth, z, of the intrinsic specific attenuation factor for shear waves, $Q_\beta^{-1}(z)$ from mathematical inversion techniques. To achieve this required the

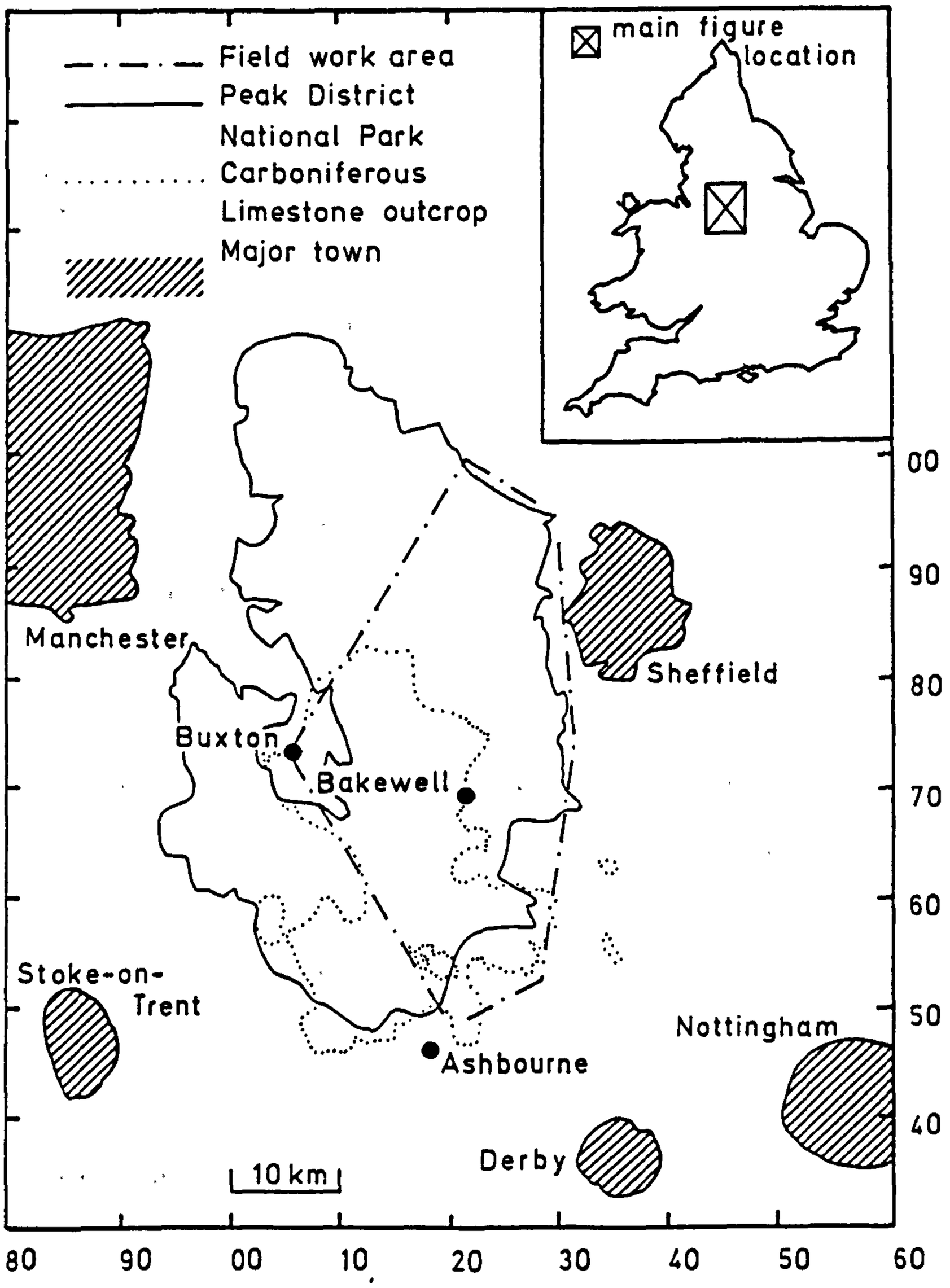

Figure 1.1 Map showing location of the field work area. All maps may be located by the 10 km grid references given which lie in parts of the National Grid squares SD, SE, SJ, SK respectively for this figure and SE and SK for all other maps.)

prior knowledge of the shear wave velocity structure, $\beta(z)$, which itself was obtained from the inversion of the observed Rayleigh wave group velocity dispersion. A more complete description of the anelastic structure and further insight into the deep geology of the study area would result from the shear wave velocity and attenuation models thus obtained.

A primary objective of this project was the acquisition of good quality data appropriate to the aims of the study. High frequency, 0.5-5 Hz, Rayleigh waves were recorded from quarry blasts located conveniently in the study area. The field experiments were designed specifically to record Rayleigh waves to their best advantage and employed methods of data acquisition and preparation adapted especially to the purpose. These data would then be processed in the frequency domain using techniques developed by Evans (1981) from the low frequency teleseismic methods of, for example, Burton (1973).

The Derbyshire Dome and adjacent areas were chosen as the study area for a number of reasons. A seismic refraction study of the Derbyshire Dome (Rogers 1980) had indicated a high amplitude phase in the signals from quarry blasts which was assumed to be of surface wave type and in particular Rayleigh waves. Further, the area provided the opportunity to study the anelastic properties of different lithologies namely the Carboniferous Limestone of the Derbyshire Dome and the terrigenous sediments of the Millstone Grit in the surrounding areas. Estimates of intrinsic attenuation* could then be compared with previous laboratory measurements.

A low velocity layer below the high velocity limestone had been

* Throughout this thesis, unless stated otherwise, the term 'intrinsic attenuation' is used to refer to the intrinsic specific attenuation factor for body waves to a medium and in particular to Q_β^{-1}, the specific attenuation factor for shear waves.

assumed to exist (Burton pers. com.) being inferred from the later refraction study of Rogers (1983). Such a layer is 'hidden' to normal refraction methods but surface wave analysis techniques should be able to resolve this particular problem and provide estimates of shear wave velocity and thickness of the low velocity layer. In this way the present work would also be a complement to the earlier body wave refraction study.

To summarise, the aims of this project were four fold:

1) to obtain models of $\beta(z)$ and $Q_\beta^{-1}(z)$ from reliable estimates of Rayleigh wave group velocity dispersion and attenuation as functions of frequency and to use these to provide a greater insight to the deep geology of the area,
2) to compare the field estimates of attenuation for different lithologies with the results of laboratory measurements of intrinsic attenuation,
3) to attempt to demonstrate the applicability of surface waves in determining structure when refraction experiments are not ideal, that is when there may be a velocity inversion with depth,
4) to design field experiments which would provide the best appropriate data to achieve the aims above.

The nature of this project has dictated the form of this thesis. The various anelastic parameters used are defined in the following section. Preliminary discussions on high frequency surface waves and their uses are followed by background information on the geology and previous geophysical work in the region. The experimental design, data acquisition and preparation are described together with preliminary time domain observations on the seismograms in chapter 2. Frequency domain processing techniques are discussed in chapter 3 and the estimates of Rayleigh wave group

velocity dispersion and attenuation presented. Subsequent chapters introduce the inversion techniques which were used to provide the models of the anelastic structure of the area. The whole is concluded by an attempt to present the results of this thesis in the context of previous work.

1.2 DEFINITION of ANELASTIC PARAMETERS.

Any dispersed wave train, for example the fundamental mode Rayleigh wave, may be formed by the superposition of a number of travelling waves of different amplitude, frequency and initial phase. Following Dziewonski & Hales (1972), the recorded seismogram may be represented by

$$f(r,t) = \int_0^\infty A(r,\theta,\omega)\exp[i(\omega t-\phi(r,\theta,\omega))]d\omega, \qquad (1.1)$$

where r is the distance from source

θ is the azimuth to the source

ω is the angular frequency

t is time.

$A(r,\theta,\omega)$ and $\phi(r,\theta,\omega)$ are the real amplitude and phase delay functions respectively which constitute the recorded, complex Fourier spectrum of the signal, $F_r(\omega)$, where

$$F_r(\omega) = A(r,\theta,\omega)\exp(-i\phi(r,\dot{\theta},\omega)). \qquad (1.2)$$

The amplitude function depends, in general, on a number of terms such that

$$A(r,\theta,\omega) = S(\theta,\omega)I(\omega)D(r,\omega)G(r). \tag{1.3}$$

The phase delay function may be represented by

$$\phi(r,\theta,\omega) = \phi_s(\theta,\omega) + \phi_i(\omega) + \phi_d(r,\omega) \tag{1.4}$$

where S, ϕ_s are the amplitude and phase terms due to the source,

I, ϕ_i are the corresponding terms representing the recording system response,

D, ϕ_d represent the effects of the propagation path

and G is the geometrical spreading which affects amplitude only.

The group velocity, $U(\omega)$, may be defined to be the velocity with which the maximum energy propagates. The phase velocity, $c(\omega)$, is the velocity at which the individual plane waves travel. Both velocities are related to $\phi(r,\theta,\omega)$.

Consider, therefore, a monochromatic wave of frequency ω_o. Its velocity may be found from the condition

$$\omega_o t - \phi(r,\theta,\omega) = \text{const.} \tag{1.5}$$

If we assume that ϕ_s, ϕ_i are known and have been corrected for and that

$$\phi = \phi_d = k(\omega_o)r, \tag{1.6}$$

where k is the wavenumber then

$$\omega_o t - k(\omega_o) r = \text{const}, \tag{1.7}$$

differentiating with respect to r yields

$$\omega_o \frac{dt}{dr} - k(\omega_o) = 0, \tag{1.8}$$

that is

$$\frac{dt}{dr} = \frac{k(\omega_o)}{\omega_o} . \tag{1.9}$$

Clearly, this is an inverse velocity, a slowness, and gives an expression for the phase velocity

$$c(\omega) = \frac{\omega}{k} . \tag{1.10}$$

We now use the method of stationary phase (Båth 1968, pp43-48) as applied to the time domain representation of the signal equation (1.1) and consider

$$\Phi(\omega) = \omega t - \phi(r,\theta,\omega). \tag{1.11}$$

As above removing ϕ_s, ϕ_i and substituting for ϕ_d we obtain

$$\Phi(\omega) = \omega t - k(\omega) r, \tag{1.12}$$

differentiating with respect to ω

$$\frac{d\Phi}{d\omega} = t - \frac{rdk}{d\omega}, \tag{1.13}$$

which has a stationary value at

$$t = \frac{rdk}{d\omega}. \tag{1.14}$$

Again we have a velocity such that

$$U(\omega) = \frac{r}{t} = \frac{d\omega}{dk}. \tag{1.15}$$

Applying this result to (1.1) yields

$$f(r,t) = \frac{U(\omega_u)\, A(\omega_u)}{\left[2\pi\, r\, U'(\omega_u)\right]^{\frac{1}{2}}} \exp\left[i(\omega_u t - k_u r \pm \frac{\pi}{4}\right], \tag{1.16}$$

for frequency ω_u at which the stationary phase method holds.

[Note: Båth (1968) and Brune et al. (1960) using the stationary phase method consider the problem from the spatial aspect with $\omega=\omega(k)$. We, however, consider the problem with $k=k(\omega)$ as throughout this thesis we are concerned with the frequency dependence of the anelastic parameters.]

From (1.16) for a given r and t the surface wave has the form of a monochromatic wave of frequency ω_u. This enables group velocity to be measured directly from the seismogram (Grant & West

1965, p97). Phase velocity, however, can be determined from the record only if peaks may be correlated between the seismograms unambiguously.

Group velocity obviously is a derivative property of phase velocity. For a given group velocity dispersion curve the phase velocity can only be determined to within the accuracy of an arbitrary constant of integration. Any attempt to invert group velocity data to obtain a velocity-depth model will, therefore, include a further degree of non-uniqueness compared to the inversion of phase velocity data (Sato 1958, Pilant & Knopoff 1970, Knopoff 1972). The measurement of phase velocity requires either the knowledge of the initial phase of the source or the use of interstation techniques (Bloch & Hales 1968). Group velocity, then, can be obtained more readily from seismograms and consequently determinations and inversions of group velocity data are more common than phase velocity.

The above derivations are strictly only applicable when

$$\frac{tU''(\omega)}{[tU'(\omega)]^{3/2}} < \varepsilon, \qquad (1.17)$$

where ε is small. This condition must be fulfilled to make equation (1.16) a valid approximation to the integral (1.1) which was solved using a Taylor expansion to second order only (Båth 1968).

Expression (1.17) cannot be satisfied when $U'(\omega) \to 0$, that is when a turning point in the group velocity dispersion curve exists thus producing an Airy phase in the seismogram which appears as a relatively high amplitude phase. A turning point may occur in the group velocity dispersion curve of high frequency Rayleigh waves if

either a low velocity layer of sufficient thickness exists at depth or if there is a large contrast in shear wave velocity as may be found, for example, between an unconsolidated surficial layer and the underlying bedrock. A separate treatment for the Airy phase has been given by Pekeris (1948).

The problems associated with the stationary phase method are removed if the analysis is conducted in the frequency domain. In this case, amplitude measurements are not limited to the apparent periods seen on individual seismograms and which may not be comparable directly between different seismograms and stations but are determined at each harmonic frequency. Also, the variation in Rayleigh wave amplitude with distance as a function of frequency corresponding to (1.16) does not require the group velocity derivative which may contain large errors (Burton 1974).

The dissipation of energy from a travelling wave, observed as a decay in amplitude with distance, provides a physically realisable measure of attenuation. For a harmonic signal this decay, except at the source, is exponential (Knopoff 1964a)

$$A_r = A_o \exp(-\gamma r), \tag{1.18}$$

where A_r is the amplitude at distance r

and A_o is the amplitude at zero distance

The contribution to the amplitude function, equation (1.3), by the propagation path, therefore, is

$$D(r,\omega) = \exp(-\gamma(\omega) r), \tag{1.19}$$

where $\gamma(\omega)$ is the spatial attenuation co-efficient.

An alternative measure of attenuation is given by Q^{-1}, the specific attenuation factor, defined by Knopoff (1964a)

$$Q^{-1} = \frac{\Delta E}{2\pi E}, \qquad (1.20)$$

where ΔE is the energy dissipated per cycle of a harmonic wave in a given volume

and E is the peak elastic energy of the system in the same volume.

Being dimensionless Q^{-1} provides a useful means of comparing the intrinsic anelasticity of different materials.

The specific attenuation factor for Rayleigh waves, Q_γ^{-1}, may be related to γ by

$$Q_\gamma^{-1}(\omega) = \frac{2U(\omega)}{\omega}\ \gamma(\omega). \qquad (1.21)$$

In this case the group velocity, $U(\omega)$, is used being the velocity of energy transport rather than the phase velocity (Brune 1962).

It has been shown that an attenuative medium must produce an intrinsic dispersion (Futterman 1962). This causal relation between intrinsic attenuation and dispersion, further highlighted by Burton (1977) for surface waves, implies that the observed dispersion $U(\omega)$ contains a component due to the layered velocity structure and a second, the causal dispersion, caused by the attenuation. The magnitude of the former is much larger, usually, than the causal dispersion (Carpenter & Davies 1966).

Equation (1.16) shows the amplitude of the monochromatic wave

of frequency ω_u to have an inverse square root dependence on distance. This provides the final contribution to the amplitude function, that of geometrical spreading of the wavefront with

$$G = r^{-1/2}. \tag{1.22}$$

The amplitude function is now (Burton 1974),

$$A(r,\phi,\omega) = r^{-1/2} \exp\left[\frac{-\omega r}{2U(\omega)} Q_\gamma^{-1}(\omega)\right] S(\theta,\omega)I(\omega). \tag{1.23}$$

The effect of the recording system can be removed by dividing the Fourier spectrum $F_r(r,\theta,\omega)$ of equation (1.2) by the instrument transfer function to obtain the true spectrum of the signal, $F(r,\theta,\omega)$, such that

$$F(r,\theta,\omega) = \frac{F_r(r,\theta,\omega)}{In(\omega)} \tag{1.24}$$

$$= \frac{A(r,\theta,\omega)}{I(\omega)} \exp[-i(\phi(r,\theta,\omega) - \phi_i(\omega)],$$

where $In(\omega)$ is the instrument transfer function, $I(\omega)\exp[-i\phi_i(\omega)]$. In the time domain this process of instrument correction involves the deconvolution of the relevant time functions.

Single station estimates of $Q_\gamma^{-1}(\omega)$ are only possible if the source function can be estimated (MacBeth & Burton 1983). Using two or more stations distributed along the same azimuth the source term reduces to a constant for each frequency. Alternatively, using two or more events at approximately the same epicentre and recorded at

the same site then the path term reduces to a constant at each frequency which permits the comparison of the sources or the determination of the source function (Marshall & Burton 1971). In certain circumstances the source may be considered to be circular, for example some nuclear explosions (Burton 1973), and in this case the azimuthal restriction may be lifted. The geometry of a quarry blast, however, is unlikely to produce a circular radiation pattern. This necessitates either a knowledge of the source function or the use of recording stations having a limited variation in azimuth to the source.

Finally, the vertical component of displacement, u_z, of the fundamental mode Rayleigh wave propagating over a half space is given by (Bullen 1979, p90)

$$u_z = a\{-0.85\exp(-0.85kz) + 1.47\exp(-0.39kz)\}\cos\{k(x-ct)\}, \qquad (1.25)$$

At depth of one wavelength, $z = \lambda$ and

$$u_z(\lambda) \approx 0.2u_z(0), \qquad (1.26)$$

which implies that to a first approximation a fundamental mode Rayleigh wave will sample the crust to a depth of one wavelength; the energy being reduced to about 95% of that at the surface.

1.3 ATTENUATION.

1.3.1 Mechanisms of Dissipation.

A great number of mechanisms have been invoked to account for the

dissipation of seismic energy by earth materials. Jackson & Anderson (1970), Johnston et al. (1979) and Mavko et al. (1979) provide good reviews of this topic. Throughout this section 'attenuation' refers to the general quantity Q^{-1}, the specific attenuation factor.

Any proposed mechanism of dissipation must satisfy observations made on earth materials. Laboratory experiments, especially on dry rocks, have shown that Q^{-1} may be independent of frequency over a broad frequency range, 10^{-2}-10^{7} Hz, (Birch & Bancroft 1938, Born 1941: and others).

The presence of pore fluids may, however, affect the attenuation in a number of ways. Firstly, Q^{-1} acquires a frequency dependence related to the degree of saturation which increases with increasing pore fluid content (Born 1941, Wyllie et al. 1962). Attenuation in liquids has been shown to be proportional to frequency (Pinkerton 1947) and may explain the frequency dependent component in saturated rocks. This effect may be important in porous rocks although Hamilton (1972) suggests it is negligible even in unconsolidated, marine sediments. Secondly, the attenuation for water saturated rocks is higher by up to a factor of three than for the same rocks having been dried; this increase depending on the degree of saturation in a complex way (Clark et al. 1980).

The type of pore fluid also effects the attenuation and has been shown to be higher in water saturated rocks than for those saturated with organic fluids such as benzene (Tittmann et al. 1980). Laboratory observations of this kind have important implications for energy exploration in the field (Kjartansson 1979).

Attenuation has been shown to decrease with increasing

confining pressure as a result of cracks in the sample closing (Birch & Bancroft 1938). The effect of cracks is further demonstrated by attenuation being an order of magnitude higher in limestone than for single crystal calcite (Peselnick & Zietz 1959).

At the low strains associated with seismic waves attenuation is independent of strain amplitude (Mavko 1979). For larger strains above 10^{-6}, however, attenuation increases rapidly with increasing strain (Winkler & Nur 1978).

Generally, Q^{-1} is independent of temperature for low temperatures relative to the melting point but at higher temperatures attenuation increases possibly due to partial melting, thermal cracking or phase changes in the pore fluid (Gordon & Davies 1968).

Mechanisms for dissipation on atomic dimensions have been summarised by Jackson & Anderson (1970). Crystal imperfections migrating in response to the applied stress, diffusion and solid-solid phase change are amongst the mechanisms reviewed. Such microscopic effects, however, may be of little significance to field measurements of attenuation within the upper crust.

Frictional sliding between grain boundaries has been proposed as a primary mechanism of dissipation (Born 1941). Such a mechanism would be expected to be independent of frequency and would explain the observed dependence of attenuation on pressure and the degree of saturation. As a mechanism of dissipation, however, frictional sliding has been criticised by Winkler (1979). He concludes on experimental and theoreticical grounds that at normal pressures such energy losses could only occur at strains greater than 10^{-6}.

An important group of mechanisms especially in crustal rocks depend upon fluid interactions. At high frequencies inertial flow

and viscous shear relaxation are significant (Biot 1956, Walsh 1969). At lower seismic frequencies, however, the viscous dissipation of energy due to the flow of fluids between cracks or into partially filled pores becomes dominant (Mavko & Nur 1975, O'Connell & Budiansky 1977).

Further fluid mechanisms include thermal relaxation in fully saturated conditions (Kjartansson & Denlinger 1977), the wetting effect of water on grain boundaries at low saturation and the chemical weakening of the rock matrix (Johnston et al. 1979).

We would expect, therefore, that different mechanisms will pertain to different physical conditions. For fully saturated rocks the loss of energy may be due to fluid flow between cracks or thermal relaxation whilst for partially saturated rocks fluid droplets will move within pores in response to compression. The effect of such mechanisms will depend upon the saturate and its physical properties. At higher frequencies inertial fluid flow will contribute significantly to the total attenuation.

For the low pressures and temperatures which pertain in the shallow upper crust and for observations at geophysical frequencies fluid flow mechanisms must be the primary cause of anelasticity. Any measurements of Q^{-1} within the upper crust could, then, provide information on the saturation conditions existing in a study area.

1.3.2 Laboratory and In Situ Determinations of Q^{-1}.

Two main techniques are used in the laboratory to determine Q^{-1}. A further method has also been used during in situ investigations of attenuation. We are concerned here with laboratory and in situ determinations rather than the field

observations which are discussed in the following section.

The resonance technique requires the specimen, usually in the form of a bar, to be excited into its normal modes of mechanical vibration. Measurements on the width of resonance curves or the time decay of the vibrations can yield estimates of Q^{-1} (Birch & Bancroft 1938, Born 1941, Wyllie *et al.* 1962, Winkler 1979, Clark *et al.* 1980: and others).

The second technique measures the variation in amplitude of ultrasonic pulses between two transducers coupled to the specimen. Such experiments are conducted, normally, above 50 kHz with compressional and shear pulses being generated by the appropriate transducers. Alternatively, controlled pulse amplitudes may be compared between the sample and a reference material of low Q^{-1} (Krishnamurthi & Balakrishna 1957, Peselnick & Zietz 1959, Toksöz *et al.* 1979, Frisillo & Stewart 1980: and others).

The only determination of Rayleigh wave attenuation in the laboratory was reported by Knopoff & Porter (1963). Their experimental arrangement and analysis technique were similar, in miniature, to the field experiments described in this thesis. A series of transducers were placed on the polished surface of a granite bar and the decay in amplitude with distance of the vertical motion measured. Estimates of γ were made by plotting the ratio of the power spectrum of a signal to that of a reference frequency against distance; the slope giving γ.

A theory of wavelet propagation has been employed to obtain *in situ* estimates of attenuation in a shale sequence (Ricker 1953). Later work on the same sequence, using spectral ratio techniques, did not, however, support the earlier findings (McDonal *et al.* 1958). The original theory has been criticised by Collins & Lee

(1956) and Savage (1969) with an alternative relation between travel time and pulse width being proposed by Gladwin & Stacey (1974).

A number of measures of Q^{-1} for different rock types using the above methods are provided in Table 1.1. Reported values of Q are converted to Q^{-1} as are values of γ where possible. The estimates presented are for 'normal' conditions of pressure, saturation et cetera and details of the variation of Q^{-1} with different physical conditions may be found in the references cited.

1.4 SURFACE WAVES and the STUDY of ANELASTICITY.

1.4.1 Previous Studies of Surface Waves.

It has been shown that fundamental mode Rayleigh waves penetrate to a depth of approximately one wavelength. This implies that with normal dispersion the lower frequency phases will penetrate deeper structures than the later arriving high frequency phases. The structure sampled by different frequencies will, therefore, be an average of the physical properties to a depth of one wavelength and consequently each frequency will be affected by a slightly different average.

The structure of the lower crust and upper mantle may be delineated from measurements on the passage of travelling surface waves within the 0.005-0.01 Hz frequency band. Knopoff (1972) has produced a suite of phase velocity dispersion curves each characteristic of a particular tectonic environment. Attenuation at these frequencies has been reviewed by Jackson & Anderson (1970). Patton (1980) reviews the existing data and regionalises both phase velocity and attenuation for the Eurasian Continent. Jacob (1969a),

TABLE 1.1 Attenuation Co-efficients of Earth Materials

Material	Attenuation $Q^{-1} \times 10^{-3}$	Frequency	Excitation method	
Amherst sandstone	19.2	0.93 - 12.8 kHz	Lr	(c)
Sandstone	41.6	50 - 120 Hz	F	(e)
Berea sandstone	28.6 - 10	400 kHz	C	(1)
	17.5	5 - 20 kHz	C	(k)
	16.9		S	
Tennessee sandstone	8.7		C	
	8.3		S	
Coconino sandstone	13.0		C	
	11.9		S	
Boise sandstone	6.0		C	
	6.3		S	
Wingate sandstone	21.1	5 - 20 kHz	C	
	21.7		S	
Hunton limestone	15.4	2.8 - 10.6 kHz	Lr	(c)
Oolitic limestone	22.2	50 - 120 Hz	F	(e)
Shelly limestone	15.9		F	
Solenhofen limestone	9.1	3 - 15 MHz	Cp	(h)
	5.3		Sp	
	1.1 - 5.4	4 Hz - 10 MHz	S	(i)
I-1 limestone	6.1	5 - 10 MHz	Cp	(h)
	~2.5		Sp	
H-1 limestone	5.3		Cp	
Indiana limestone	2.4	5 - 20 kHz	C	(k)
	2.6		S	
Leuders limestone	3.2		C	
	2.0		S	
Austin chalk	1.5	5 - 20 kHz	C	(k)
	1.3		S	
Sylvan shale	13.7	3.4 - 128 kHz	Lr	(c)
Orchard cap rock	22.2	1.1 - 6.6 kHz	Lr	(c)
(gypsum & anhydrite)	19.2	0.1 - 2 kHz	Tr	
Cockfield Yequa form.	14.9	3.6 - 10.9 kHz	Lr	(c)
Quincy granite	10.0	0.14 1.6 kHz	Lr	(b)
	5 - 6.7		Tor	
Granite	17.5	50 - 120 kHz	F	(e)
Westerly granite	12.7	0.05 - 4 kHz	Rwp	(j)

TABLE 1.1 cont.

Material	Attenuation $Q^{-1} \times 10^{-3}$	Frequency	Excitation method	
Diorite	8.0	50 -120 kHz	F	(e)
Diabase glass	0.3	50 - 90 kHz		(d)
Dolerite	11.1	50 - 120 Hz	F	(e)
Kanan Road basalt	0.7 - 1.3		S	(n)
Sioux quartzite	5.9	5 - 20 kHz	C	(k)
	6.5		S	
Orthoquartzite	~2.5		S	(n)
Silica	0.8	1 - 10 Hz		(a)
Calcite	0.5	3 - 10 MHz	Cp	(h)
In situ measurements				
Beaufort Sea sediments	23.3*	125 Hz	C	(m)
	14.9**		C	
Pierre shale	~43+	50 - 450 Hz	C	(g)
	~69++		C	
	~100	20 - 125 Hz	Sh	

Laboratory measurements of attenuation co-efficient γ dB cm^{-1}

Limestone	11.1	2.1 MHz	Up	(f)
Shale	13.3		Up	
Dolerite	14.6		Up	
Deccantrap	10.7		Up	
Marble	14.6		Up	

Notes: 1) Where possible reported Q and γ values have been converted into Q^{-1} values.
2) References, given as lower case letters in parentheses, are tabulated in Table 1.1a
3) Abbreviations: C- compressional resonance, Cp- compressional pulses, F- flexural, Lr- longitudinal resonance, Rwp- Rayleigh wave pulses, Sh- horizontally travelling shear wave, Sp- shear pulses, Tor- torsional resonance, Tr- transverse resonance, Up- ultrasonic pulses.
4) * for section between 549 - 1193 m
** for section between 945 - 1311 m
+ for total section length
++ for section between 250' - 750'

Table 1.1a References for Table 1.1.

a) Gemant, A., & Jackson, W., 1937. Measurements of internal friction in some dielectric materials. Phil. Mag. 23, 960-983

b) Birch, F., & Bancroft, D., 1938. Elasticity and internal friction in a long column of granite. Bull. seism. Soc. Am. 28, 243-254

c) Born, W.T., 1941. The attenuation constant of earth materials. Geophysics 6, 132-148

d) Birch, F., 1942. Handbook of physical constants. Geol. Soc. Am. Spec. Paper 36.

e) Bruckshaw, J., & Mahanta, P., 1954. The variation of elastic constants of rocks with frequency. Petroleum 17, 14-18

f) Krishnamurthi, M., & Balakrishna, S., 1957. Attenuation of sound in rocks. Geophysics 22, 268-274

g) McDonal, F.J., Angona, F.A., Mills, R.L., Sengbush, R.L., Van Nostrand, R.G., & White, J.E., 1958. Attenuation of shear and compressional waves in Pierre Shale. Geophysics 23, 421-439

h) Peselnick, L., & Zietz, I., 1959. Internal friction of fine grained limestones at ultrasonic frequencies. Geophysics 24, 285-296

i) Peselnick, L., & Outerbridge, W.F., 1961. Internal friction in shear and shear modulus of Solenhofen limestone over a frequency range of 10^7 cycles per second. J. geophys. Res. 66, 581-588

j) Knopoff, L., & Porter, L.D., 1963. Attenuation of surface waves in a granular material. J. geophys. Res. 68, 2191-2197

k) Clark, V.A., Tittmann, B.R., & Spencer, T.W., 1980. Effect of volatiles on attenuation (Q^{-1}) and velocity in sedimentary rocks. J. geophys. Res. 85, 5190-5198

l) Frisillo, A., & Stewart, T.J., 1980. Effect of partial gas/brine saturation on ultrasonic absorption in sandstone. J. geophys. Res. 85, 5209-5211

m) Ganley, D.C., & Kanasewich, E.R., 1980. Measurement of absorption and dispersion from check shot surveys. J. geophys. Res. 85, 5219-5226

n) Tittmann, B.R., Clark, V.A., Richardson, J.M., & Spencer, T.W., 1980. Possible mechanism for seismic attenuation in rocks containing small amounts of volatiles. J. geophys. Res. 85, 5199-5208

Stuart (1978) and Clark & Stuart (1981) have presented models of shear wave velocity in the region of the British Isles.

A number of studies in the frequency band 0.01-0.1 Hz have been conducted using surface waves mainly from nuclear explosions. Keller et al. (1976) and Bache et al. (1978) have obtained crustal structures from the observed dispersion whilst Burton (1974) provides estimates of attenuation at the lower frequencies in this band.

Souriau et al. (1980) have utilised earthquake data to provide estimates of attenuation within this frequency band over the Massif Central, France. Their data require the intrinsic shear wave attenuation to be frequency dependent complementing work by Mitchell (1980) in eastern North America. Earthquake data are also used by Correig et al. (1982) to regionalise attenuation co-efficients and dispersion velocities in Europe. No studies of surface waves at these frequencies have been made for Britain.

Within this study we are concerned with waves in the frequency band between 0.5 Hz and 5 Hz. At these frequencies the first few kilometres of the crust are sampled. McEvilly & Stauder (1965) indicated the sensitivity of surface waves to the sedimentary thickness by fitting curves of theoretical dispersion from models to the observed data. The acceptable models were dependent on the thickness and velocity of the upper layer overlying the half-space. They suggested, therefore, that such studies would provide an inexpensive method of delineating sedimentary basins; useful to the oil industry. (A similar conclusion had been reached earlier by Oliver & Ewing (1958) using data from a local earthquake in the eastern USA with frequencies in the lower band of 0.08-0.5 Hz). A low velocity layer at depth was required by Herrmann (1969) to model

the observed dispersion across the Cincinnati Arch (USA) demonstrating that such 'hidden' layer problems are tractable to surface wave analysis.

Velocity structures derived from large scale refraction surveys may contain little information about the near surface due to the distribution of sources and stations. Berry & Fuchs (1973) and Clee et al. (1974) used observed Rayleigh waves to infer a low velocity surface layer of 1-2 km thickness. Inclusion of this layer in their interpretations of the crust of Canada improved the accuracy of their models and synthetic seismograms.

Within the British Isles high frequency surface waves have been reported by Collette et al. (1967) and Hall (1978) during refraction experiments. The low velocities (0.74-1.03 km s^{-1}) measured by Collette et al. (1967) for waves of frequency around 3 Hz were taken to be due to the character of the sediments in the North Sea and the noticeable difference north and south of Flamborough Head to the change in thickness.

An extensive study of surface waves in this frequency band has been conducted previously by Evans (1981). Using data from the Scottish part of the LISPB experiment (Bamford et al. 1976) initial observations were used to delineate seven major provinces which could be correlated with the surface geology. Phase slowness varied from 0.33-0.61 s km^{-1} overall and showed generally an increase with increasing geologic age of the province. Inversions to obtain shear velocity models showed β to increase with depth within the metamorphics north of the Highland Boundary Fault. Lower velocities are given within the Old Red Sandstone basin. The velocities from these inversions tend to be slightly lower than previously determined shear wave velocities (Assumpção & Bamford 1978).

MacBeth (1983) has also analysed high frequency surface waves from natural and artificial seismic sources in Scotland. In the Midland Valley of Scotland the shear wave velocity was shown to increase from 1.5 km s^{-1} at the surface to 3.5 km s^{-1} at approximately 2 km. Analysis of higher mode Rayleigh waves permitted the resolution of the shear wave velocity at greater depths returning a value of 3.8 km s^{-1} at 17 km. These values compare favourably with those given by Evans (1981).

Few determinations of attenuation have been attempted within this frequency band. Båth (1975) in an investigation of the R_g phase recorded across Sweden from a number of shallow events provides an estimate of Q_γ^{-1} ranging between 0.003 and 0.006. No correction was made, however, for possible Airy phase propagation which has an amplitude dependence on distance in the time domain different to that of the remainder of the fundamental mode Rayleigh wave (Pekeris 1948). Measurements on the L_g phase, a complex mixture of Love and Rayleigh mode propagation (Panza & Calcagnile 1975), have yielded values of $Q_\gamma^{-1} \sim 10^{-3}$. Chow et al. (1980) used L_g to determine Q_γ^{-1} in southern Africa, obtaining a value of 0.002 before and after applying a correction for Airy phase propagation. This value is higher than that of Nuttli (1973) who obtained Q_γ^{-1} of 0.001 for cratonic regions in North America and is thought to be due to the anomalous conditions of the East African Rift System. Such investigations on L_g, whilst being in the frequency band of interest, are conducted over a greater distance than the studies of the fundamental mode Rayleigh wave which are considered within this thesis.

Evans (1981) in his study of the anelastic properties of surface waves in Scotland measured Q_γ^{-1} with an overall range of

0.015-0.05 for five of his geologic provinces. These values of Q_γ^{-1} are noticably higher than those reported above. Inverting the observed data he obtained Q_β^{-1} in the range 0.015-0.04 showing a general increase with depth. Shear wave attenuation was shown to fit the data better if a frequency dependence was included. Not all of the observations, however, were explained by this dependence. He interprets his observations of Q_β^{-1} in terms of rock type, structure and the saturation conditions within each province.

Single station estimates of $Q_\beta^{-1}(z)$ have also been given for the Midland Valley of Scotland by MacBeth (1983). The intrinsic shear wave attenuation was shown to be well resolved in the top 400 m returning a value of 0.02 but showed little correlation with the surface geology. Similar analysis techniques were applied to the LISPB data and provide a range of Q_β^{-1} from 0.02 to 0.09 again in the first few hundred metres. Again these results are compatible with those of Evans (1981).

Surface waves of frequency greater than 5 Hz are of interest to seismic reflection prospectors. Such waves may be of large amplitude compared to the body wave reflections (Waters 1981) and measures are taken to suppress the surface waves by suitable spatial or frequency filtering. To achieve this noise tests are made to determine the dispersive characteristics of the prospect area (Al-Husseini *et al.* 1981). Whilst the data from these tests are used to design reflection profile source-receiver arrays to minimise ground roll they could also provide approximate velocity models for preliminary processing.

1.4.2 The Advantages of Using Surface Waves.

An interesting difference between the laboratory and field determinations of attenuation is that the former have concentrated on body wave type excitations whilst the latter have utilised chiefly surface wave observations. Measurements of body wave attenuation have been made in the field (McDonal *et al.* 1958, Newman & Worthington 1980) but such determinations are subject to large errors which may be reduced by using the appropriate surface wave mode.

For our purposes the appropriate surface wave is the vertical component of the fundamental Rayleigh mode. The main advantages are that the Rayleigh wave may be sampled at various points along its ray (the Earth's surface) and that the geometric spreading correction may be calculated accurately (Anderson *et al.* 1965). This allows amplitudes to be compared directly at different stations. For body waves, however, each arrival at individual stations will be that of a different ray. These rays will have been affected by their individual paths and to correct for this requires a knowledge of reflection and transmission co-efficients, the degree of mode conversion and the velocity structure. Further, the losses due to wavefront expansion will be complicated and varying between the rays. The angle of incidence to the surface will also affect the recorded amplitude (O'Brien 1967).

The recording and identification of crustal shear waves even with three component instrumentation has posed many problems (Assumpcao & Bamford 1978, Hales *et al.* 1980). The specific attenuation factor for shear waves may be greater than that for compressional waves by a factor of at least two (Anderson *et al.* 1965) resulting in much smaller recorded amplitudes. Further, the

interaction with the free surface produces reflections, mode conversions and amplitude variations due to the angle of incidence (Evans 1983). The determination of shear wave velocity and attenuation from body wave observations can be subject to large errors. More reliable estimates of these shear wave parameters can be obtained, therefore, from the inversion of surface wave data.

1.5 GEOLOGICAL and GEOPHYSICAL SETTING of the REGION.

1.5.1 Introduction.

The field work area, encompassing parts of north Derbyshire and South Yorkshire, may be divided into two districts of distinct geologic and physiographic character. The Derbyshire Dome, a broad plateau of Lower Carboniferous Limestone, in the southern part of the area forms the White Peak of the Peak District National Park. Comprising the northern district, and on the flanks of the Dome, are series of Upper Carboniferous clastic sediments which have been shaped into the more rugged topography of the Dark Peak. The field work area is enclosed within a broader region of similar geologic character and development which also includes younger, Permo-Triassic sediments. The various lithologies observed at outcrop in the region range from Lower Carboniferous (Viséan) to Permo-Triassic (Ladinian) age.

Contemporaneous with the limestones of the southern district is a suite of extrusive and instrusive, basic igneous rocks. Significant lead-zinc mineralisation is also found within the limestones forming the South Pennine Orefield (Dunham 1952, Ineson & Ford 1982).

The region has received much attention because of the economic mineral resources of the southern district. Details of mining for lead are given in the Domesday Book of 1086 whilst archeological finds indicate that the Romans were well acquainted with the district's potential (Lewis 1971). Scientific research into all aspects of the regional geology flourished in the 19th century and has continued to the present day. Geophysical investigations, however, have not been conducted to the same extent and are limited to a few surveys conducted from 1970 onwards. It is from this wealth of published work that the following synthesis has been produced; the two bibliographies of Ford & Mason (1967) and Ford (1972) have been of much help. The published Geological Survey's of Sheets 86, 87, 99, 100, 111, 112, 124 also contain much information.

1.5.2 Petrology.

1.5.2i Carboniferous Limestone.

The exposed rocks of the Lower Carboniferous belong to the Viséan stage and consist of a series of limestones and limestone/shales. A standard nomenclature for these formations is given by Aitkenhead & Chisholm (1982).

The limestones were deposited in three main facies (Ford 1968a): The shelf or massif facies is the most extensive consisting of shallow water, fine grained calcarenites which are found north east of Dove Dale. To the south west the second facies exhibits basinal characteristics being comprised of more thinly bedded limestones often separated by thin mudstone or shale partings. Thach (1965) takes these features together with the absence of particular fossil algae to indicate a deep water, aphotic

environment.

The least extensive facies consists of poorly sorted, highly fossiliferous limestones deposited as reef-like structures at the margins of the shelf separating the two facies described above.

The limestones have undergone varying amounts of diagenesis. Silicification in the form of chert is restricted to upper horizons within the shelf limestones and is of post depositional origin. Dolomitsation, common in the south of the Dome (Ford 1968a), shows cross-cutting relationships with the limestone and may be due to sub-surface effects in the Permian (Kent 1957). Dolomitic bands of this type within the limestone may be of significance in seismic investigations by facilitating the propagation of high velocity direct waves (Bayerley & Brooks 1980, Rogers 1983).

Primary dolomites have been proven at depth in the Woo Dale and Ryder Point bore holes (Cope 1973, Chisholm & Butcher 1981). These deposits are distinct to the secondary dolomites above and are believed to be persistant, but diachronous, over the shelf (Aitkenhead & Chisholm 1982).

1.5.2ii Upper Carboniferous Clastic Sediments.

a) Millstone Grit: The Namurian of the region is represented by the Millstone Grit which surrounds the Dome to the west, north and east. It is of chiefly deltaic facies and occurs as a repetitious series of cyclothems.

Prior to the deltaic sedimentation deep water deposits were laid down in the basins surrounding the Viséan limestone shelf. The Edale Shales, a series of shales, mudstones and sub-ordinate limestones attain a maximum thickness of 370 m to the north of the shelf (Stevenson & Gaunt 1971). As the water began to shallow with

the approach of the shore line from the north east the Mam Tor Beds, a sequence of distal turbidites (Allen 1960), were deposited attaining a thickness of 140 m.

True rhythmic sedimentation did not start until the shore line was at its most southerly point and the basins at their shallowest. A generalised cyclothem follows the sequence; shale, mudstone and sandy shale, sandstone, seat earth (ganister) and coal (Ford 1968b). Each cyclothem may be 150 m thick with the sandstones, which are usually coarse and feldspathic, reaching a thickness of 30 m. The coals and seat earths are normally only centimetres thick.

Sedimentation within the basins appears to have been continuous whilst at the shelf margins there is considerable overlap of the younger beds onto older ones. A marked erosional contact with the Carboniferous Limestone suggests that at least 90 m of the limestone sequence is missing.

On the west and east of the Dome the Millstone Grit thins southwards from its maximum thickness of 1200 m to the north as it approaches what was St Georges Land (Anderton et al. 1979, p145). A considerable thickness of shales has been proven by borehole, however, in the basin separating the limestone shelf and St. Georges Land, the Widmerpool Gulf.

b) Coal Measures: Only small outcrops of the Westphalian aged Lower Coal Measures lie within the field work area. Rocks of this age, therefore, have not been sampled extensively.

These rocks are a continuation of the cyclical sedimentation of the Namurian upon which they are conformable. Deposited in a wide swampy, paralic environment (Francis 1979) the character of the cyclothems is changed with the coarser, clastic sediments decreasing

in importance (Edwards & Trotter 1954). The Lower Coal Measures attain a thickness of 350 m within the region (Eden et al. 1957) but thins towards the south in a similar manner to the Millstone Grit.

1.5.2iii Permo-Triassic Sediments.

Lower and Middle Triassic sandstones and mudstones are found outside the field work area in the south of the region. Fragments of Bunter Sandstone (Sherwood Sandstone Group ?) have been found, however, in Tertiary solution hollows in the Carboniferous Limestone of the field work area (Walsh et al. 1980).

A simplified regional geology map for the lithologies discussed above is given in Fig 1.2.

1.5.2iv Igneous Rocks

Extensive studies of the igneous rocks of the area have been conducted by Bemrose (1894, 1907) and more recently by Walters & Ineson (1981), Ineson & Walters (1983). Of limited outcrop, these rocks comprise a varied assemblage of basaltic lavas, tuffs and vent agglomerates contemporaneous with the Carboniferous Limestone. Doleritic intrusions, showing Namurian emplacement dates, are also found. At subcrop, however, these deposits cannot be considered to be minor in volume or areal extent. This is especially so on the eastern side of the Derbyshire Dome and may be of significance for seismic investigations in this district.

1.5.3 Sub-Carboniferous Basement.

Information concerning the nature of the sub-Carboniferous basement is limited to a few significant boreholes and small outcrops within

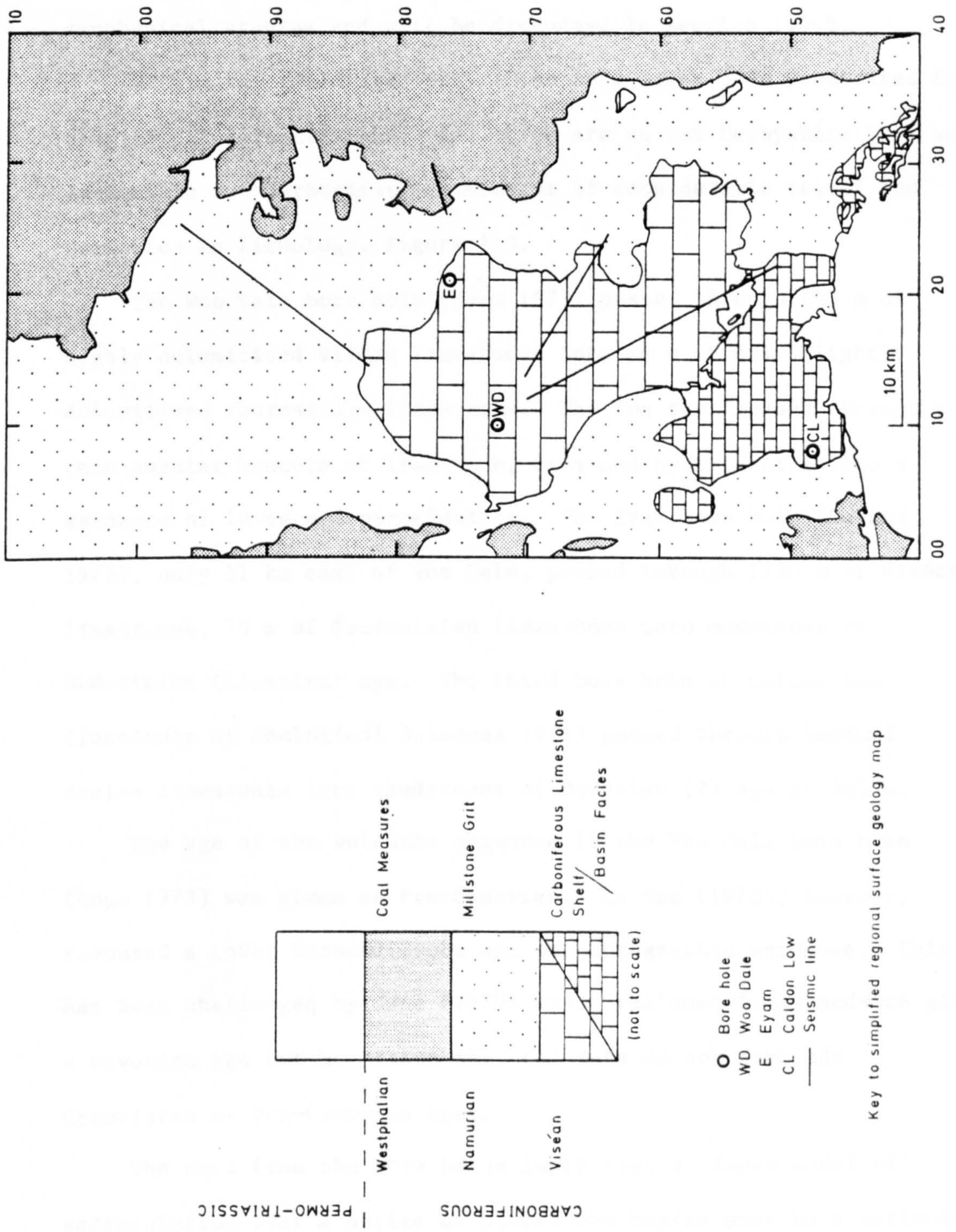

Figure 1.2 Map of the simplified surface geology of the region.

and outside the area of present study. Further data come from geophysical studies and will be discussed in section 1.5.5.

Within the field area only three bore holes have penetrated the base of the Carboniferous. All three are on the Derbyshire Dome and indicate a sub-Carboniferous basement of considerable relief and variation in lithology, Figure 1.3.

The Woo Dale bore hole (Cope 1973) passed through 243 m of highly dolomitised Viséan limestones into 28 m of only slightly dolomitised Tournaisian limestones. The log then passes through a thin angular breccia of limestone, lava and pyroclastics into a sequence of lavas and pyroclastics. The Eyam bore hole (Dunham 1973), only 11 km east of Woo Dale, passed through 1730 m of Viséan limestones, 73 m of Tournaisian limestones into mudstones of Ordovician (Llanvirn) age. The third bore hole at Caldon Low (Institute of Geological Sciences 1978) passed through basinal facies limestones into sandstones of Devonian (?) age at 365 m.

The age of the volcanic sequence in the Woo Dale bore hole (Cope 1973) was given as Pre-Cambrian. La Bas (1972), however, favoured a Lower Carboniferous age on petrographic evidence. This has been challenged by Cope (1979) using radiometric methods to give a Devonian age but he states that the data do not preclude Ordovician or Pre-Cambrian ages.

The data from the bore holes imply that a simple model of sedimentation over a series of blocks and basins must be questioned. Miller & Grayson (1982) replace the original hypothesis by tilt blocks bounded by basement fault scarps. Thick sedimentary sequences, seen for example in the Eyam bore hole, can develop in the down slope position whilst condensed sequences, as in the Woo Dale bore hole, will be found near the fault scarp. Chisholm (pers.

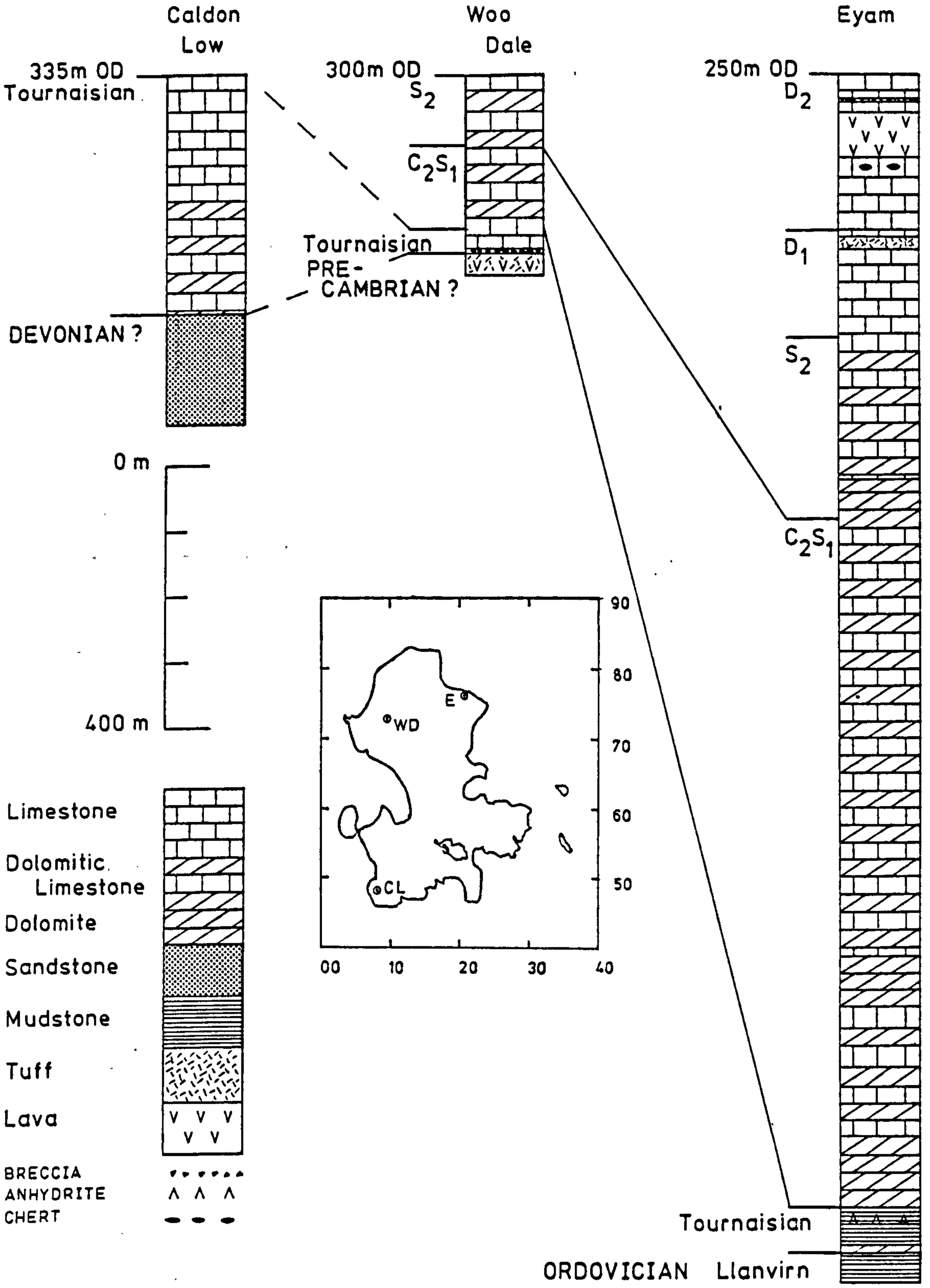

Figure 1.3 The logs and locations of the deep bore holes of the region. (Carboniferous Limestone outcrop indicated on inset map.)

com.) supports this theory and, further, suggests the presence of Devonian sediments below the Carboniferous on the downthrow side of the fault scarp to the west of Buxton.

Further data regarding the depth to the sub-Carboniferous basement is limited. Chisholm & Butcher (1981) conclude that the base of the Carboniferous Limestone cannot be far below 28 m OD from the increase in detrital quartz in dolomite chippings from a bore hole near Matlock. Cores from other bore holes, mainly in the basinal regions surrounding the Derbyshire Dome, have either not penetrated the Carboniferous sediments or, in Lincolnshire and Nottinghamshire, have proven Cambrian quartzites to lie below Lower Carboniferous or Devonian sediments (Kent 1967). Wills (1978) has postulated that Cambrian quartzites lie below the mudstones of the Eyam bore hole.

Kent (1967) has further suggested that the Derbyshire block is linked structurally to the Pre-Cambrian of the Charnwood Forest, having a similar trend. This view is supported by Wills (1978) from the aero-magnetic map of the region. This would then make the Derbyshire block the north western limit of St. Georges Land to which Charnwood and the proven shallow basement of Norfolk belonged in Carboniferous times.

1.5.4 Structural Geology of the Region.

The major structure of the region is referred to, commonly, as the Derbyshire Dome. The structure contours of Shirley & Horsfield (1945) and Shirley (1959) indicate that this is a misnomer with the structure being far from simple. Ford & Ineson (1971) describe it as a complex of fairly gentle folds with a general E-W trend rising

to N-S line culmination. For convenience and to remain consistent with the literature, however, the term 'Dome' will be retained when referring to the limestone outcrop of the southern district of the field work area.

The E-W trend seen over the shelf swings round to N-S or NNW-SSE in the basinal facies of Dove Dale with the limestones indicating intense folding and crumpling (Prentice 1951). Fold trends may be deflected occasionally by reef limestone masses and some of the steep dips shown may be depositional. The eastward plunging fold axes may be traced into the Millstone Grit and Coal Measures to the east where they assume a N-S trend.

Faults on the western margin of the Dome are generally normal with similar trends to the folding. Over the shelf, however, E-W, NW-SE, ENE-WSW and ESE-WNW trends are shown. The major Bonsall and Gulf Faults, having NW-SE trends, produce a graben-like feature by down throwing in opposite directions. Chisholm (pers. com.) suggests that these faults are related to a basement feature which may be the Derby Fault of Wills (1978).

Strong N-S folding and faulting exists in the Upper Carboniferous rocks in the west of the northern district (Stevenson & Gaunt 1971). The central and eastern parts, however, are characterised by a series of gentle, E-W trending folds. The asymmetric Edale Anticline shows an increased dip to the south due possibly to the proximity of the shelf block (Stevenson & Gaunt 1971). Faulting is rare within these parts but increases to the north east and east of the region within the upper Namurian and Westphalian sediments. The youngest rocks in the east and south of the region exhibit only a gentle, regional dip to the east.

The variation in trend of the different structures has made it

difficult to determine the causative stress regime. In an attempt to resolve this problem Weaver (1974) conducted a systematic analysis of the joints in the southern part of the Derbyshire Dome. A dominant conjugate joint set of NW-SE, NE-SW trends has been observed within all lithologies except for the western, marginal limestones and would suggest a compressive stress orientated in an E-W direction. To accommodate all the structures, however, this stress field must have been modified by local, basement influences and also be variable in time. This joint pattern has also been observed in the northern district by Moseley & Ahmed (1967). The major structures of the region are given in Figure 1.4.

1.5.5 Previous Geophysical Investigations.

In contrast to the wealth of published work on the regional geology very few geophysical surveys have been reported in the literature. Both seismic and gravimetric methods have been used on regional scales with other techniques being used over more localised areas for specific investigations such as mineral reconnaissance.

1.5.5i Seismic Surveys.

Three major surveys have been conducted within the region. The LISPB GAMMA line (Bamford et al. 1976) ended to the north of Buxton covering part of the northern district. A second line in the south (Whitcombe & Maguire 1981) extended from the Charnwood Forest onto the Dome terminating at Ballidon. The third and most recent survey was an intensive study of the structure of the Derbyshire Dome (Rogers 1983). The various seismic refraction lines with their interpretations are shown in Figure 1.5.

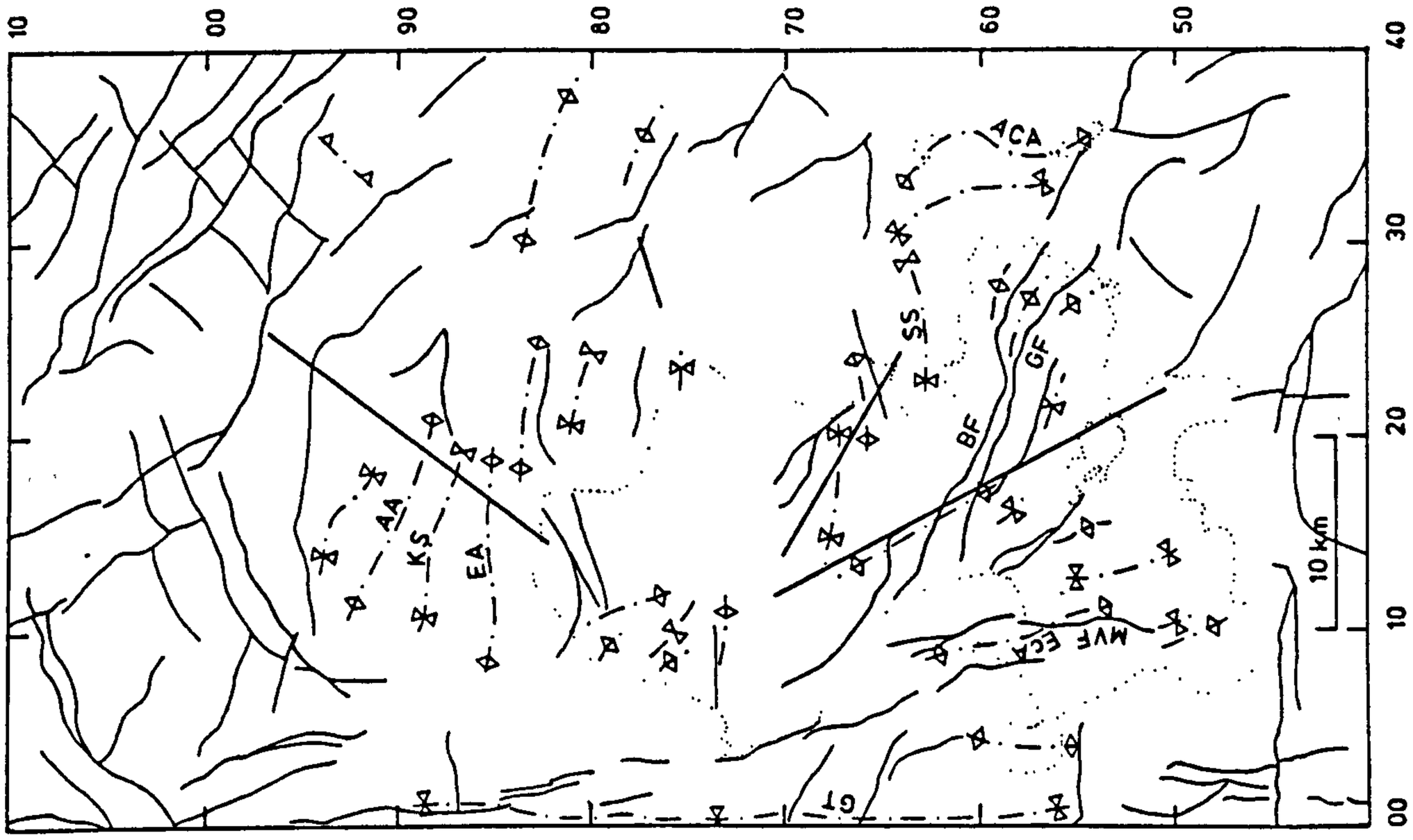

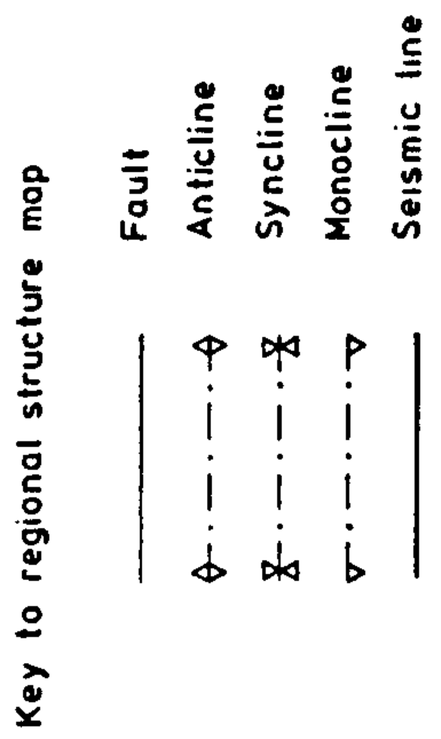

Figure 1.4 Simplified map of the major structures of the region.
(Carboniferous Limestone outcrop indicated.)

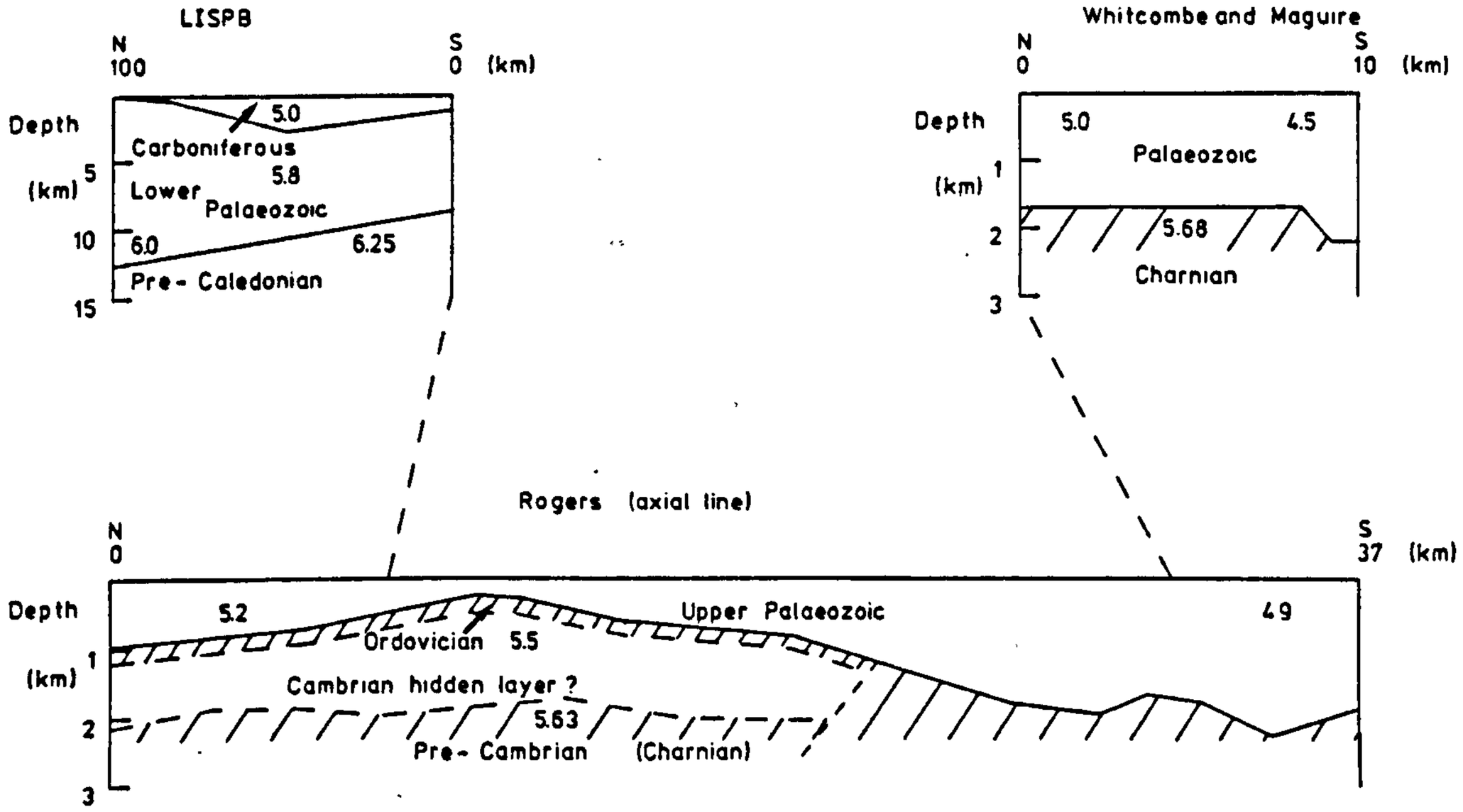

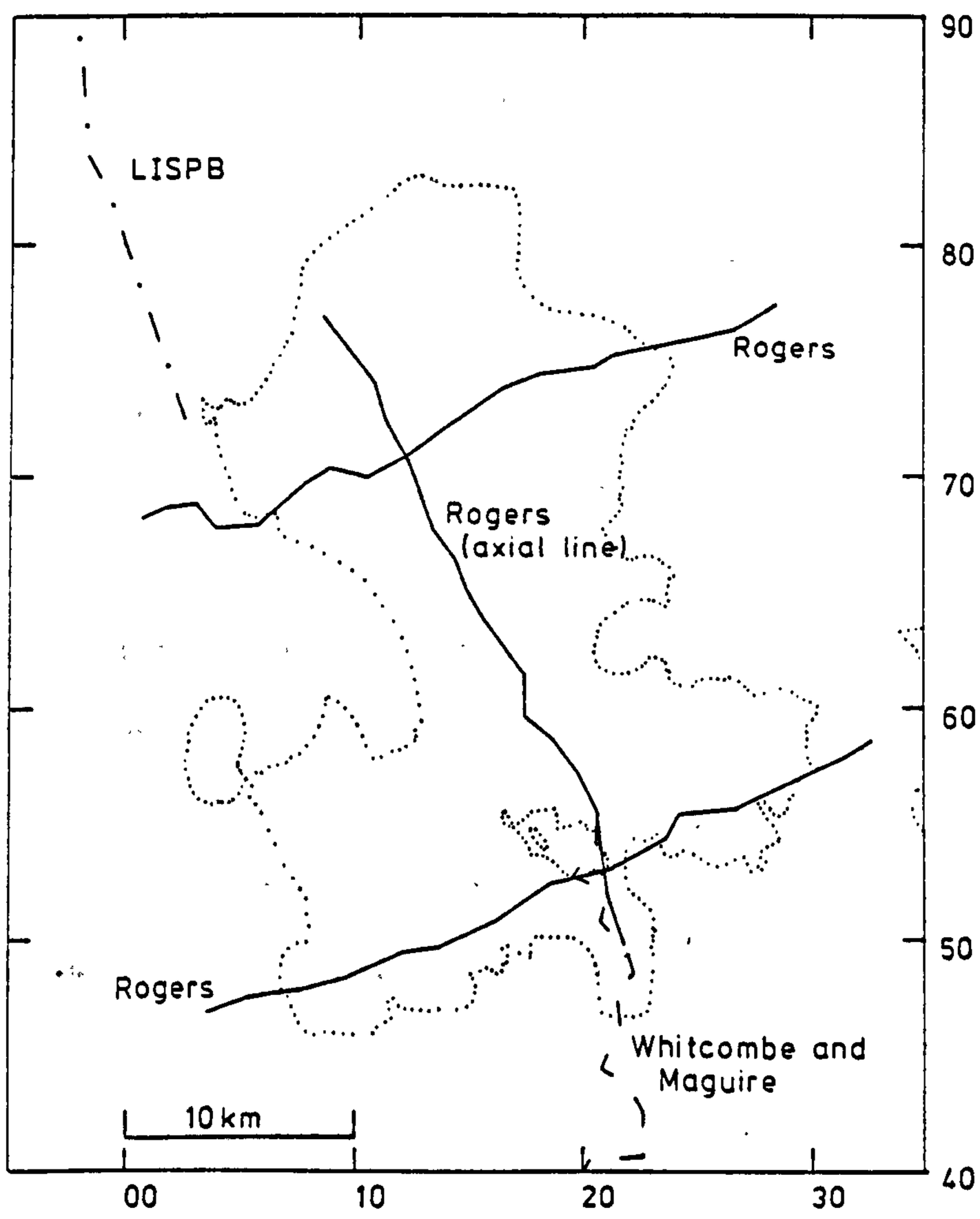

Figure 1.5 Disposition and velocity models of previous seismic surveys in the region. Numbers in the velocity models refer to compressional wave velocities in km s^{-1}. (Note the changes of scale for the various models.)

The LISPB experiment (Bamford et al. 1978) using a series of land shots to provide a number of overlapping, reversed profiles yielded a three layer structure overlying a Moho and upper mantle of rather interdeterminate nature. These three layers correspond to:

a) sediments with α 5.0 km s^{-1} and thickness 1.2 km

b) Lower Palaeozoic rocks with α 5.8-6.0 km s^{-1} and thickness 7.4 km

c) pre-Caledonian basement with α 6.25-6.3 km s^{-1} extending to the Moho at depths between 30 km and 35 km.

The survey of Whitcombe & Maguire (1981) utilised quarry blasts as a convenient seismic source and identified a two layer model corresponding to:

a) sediments with α 5.0 km s^{-1} in the north and 4.5 km s^{-1} in the south

b) basement with α 5.68 km s^{-1} at a depth of 1.75 km at Ballidon.

This basement is believed to be of Pre-Cambrian age forming a ridge of Charnian type rocks, which have been shown to exhibit similar velocities (Whitcombe & Maguire 1980), extending from the Charnwood Forest under the southern part of the Dome.

Comparing the two surveys above we find that whilst the depths to and velocities above and below the first refractor are similar they have been interpreted differently. The LISPB experimenters give a Lower Palaeozoic age to this refractor whilst Whitcombe & Maguire give a Pre-Cambrian one. It may be that the Lower Palaeozoic pinches out against the Pre-Cambrian at a point along the profile but because of the similar velocities this case is indistinguishable seismically from the produced interpretations.

The study of the Derbyshire Dome by Rogers (1983) attempted to

resolve this problem by linking the two earlier surveys with a further seismic line. Two other lines were deployed to examine more fully the nature of the Dome. Taken as a whole Rogers' results indicate that the structure of the Dome is much more complex than indicated by the surface geology.

Rogers finds, along the axial line, that the Dome is cut into two provinces by a basement fault to which the Bonsall Fault may be related. To the north of this fault two sub-Carboniferous refractors are identified; the upper one corresponding to Ordovician mudstones and pyroclastics, as seen in the northern bore holes, and the lower one to a Charnian basement. To the south of the fault only the lower refractor is seen.

The delay between the first and later arrivals in the northern province has been taken to infer a further layer of lower velocity below the Ordovician and is tentatively correlated with the Cambrian. A velocity inversion in the southern province, caused by the Devonian sandstones, is believed to exist and results in the lower velocities assigned to the sediments to the south of the fault.

This model would then seem to resolve the discrepancy between the earlier studies with the Lower Palaeozoic being absent south of the fault line. The depths to the supposed Charnian are, however, still much less than the depth to the pre-Caledonian basement as defined by LISPB. It may be, therefore, that the LISPB Lower Palaeozoic refractor is partially Pre-Cambrian or that the lower basement of Rogers is not of Charnian age.

Interpretations for the northern transverse line and the short surface wave experiment line (see chapter 2) support the model of the northern province and mirror the eastward deepening of the

basement indicated by the Eyam bore hole. The basement appears to dip below the sediments (Millstone Grit and limestone) at the southern end of the short line under the Stanton Syncline.

The southern transverse line shows the Charnian basement to have a much more variable topography than in the northern province. There is also an indication that this refractor dips below another Lower Palaeozoic refractor to the west of this line. The Devonian sandstones have been assumed to underlie the entire southern province. Rogers states that the basement shows no systematic deepening across the transition between shelf and basinal limestone facies. He explains this rather surprising observation by suggesting that the basinal facies were deposited in a series of small basins within a region of tectonic complication between the shelf and the Widmerpool Gulf.

Cox (1983) has analysed the body wave first arrivals recorded over the Millstone Grit district by the northern seismic line of this study. Interpretation of the reduced travel times gives a model consisting of a basin of Millstone Grit deepening northwards to a maximum thickness of 1.1 km. The Carboniferous Limestone is believed to everywhere underlie the Millstone Grit. This line, however, is unreversed and consequently true velocities or dips cannot be determined. Velocities of 3.8 km s^{-1} and 5.2 km s^{-1} were assumed for the Millstone Grit and Carboniferous Limestone respectively to calculate depths to the refractor. A complication in the refractor depth below the northernmost stations may arise from an arrival from a dolomitic horizon not clearly identified but possibly within the limestone.

1.5.5ii Gravity and Magnetic Surveys.

Features within the gravity field have been modelled by Maroof (1976) and also by Rogers (1983) along his seismic profiles. Maroof (1976) modelled the Bouguer anomaly by a shallow high density, Pre-Cambrian basement. The model at 0.5 km depth at Woo Dale dips away sharply to the east to be overlain by the Ordovician mudstones in the Eyam area. For his southern profile the basement high is shallower being at 0.2 km depth with a similar eastward dip. Both models indicate a shallower dip in the basement to the west than to the east.

The models produced by Rogers (1983) correspond closely to his interpretation of the seismic data. He requires that Lower Palaeozoic rocks everywhere overlie the Pre-Cambrian basement which is now deeper than that given by Maroof. A model of the profile along the axial seismic line again supports Rogers' seismic interpretation but shows considerable differences to Maroof's (1976) axial section.

A qualitative interpretation of the gravity and magnetic fields has been provided by Cornwell (pers. com.). A sub-circular Bouguer anomaly low near Bakewell has been interpreted as a small sedimentary basin, possibly of Devonian age, below the Carboniferous. On a broader scale, two distinct basement types are delineated; a high density basement and a strongly magnetic one discordant to the first. Whilst it would be reasonable to assign a Charnian type lithology to this basement calculations of maximum depth from the observed anomalies (Grant & West 1965, p263) do not preclude a causative body at deeper levels, perhaps the pre-Caledonian basement of LISPB. Further, the Pre-Cambrian outcrop at Charnwood Forest does not produce such a large amplitude positive

Bouguer anomaly and may be additional evidence that the observed field over the Dome is not caused by the shallow density distibutions of Rogers (1983) and Maroof (1976).

Similar maximum depth considerations for the anomaly in the magnetic field indicate that the depth to the magnetic basement is the same as or slightly greater than that to the high density basement.

Small scale surveys have also been conducted to investigate zones of mineralisation (Brown & Ogilvy 1982) or the extent of igneous bodies (IGS Ann. Rep. 1981/1982) but due to their limited extent these investigations are not considered further.

1.6 SUMMARY.

The research reported in this thesis is an investigation of the anelastic properties of the shallow, upper crust from the inversion of high frequency Rayleigh wave data. The work involves the measurement of the group velocity dispersion, $U(\nu)$, and the specific attenuation factor, $Q_\gamma^{-1}(\nu)$, for Rayleigh waves in the frequency band 0.5-5 Hz.

An essential part of the project was the design and execution of field experiments, described later, to record Rayleigh waves from quarry blast sources within the Derbyshire Dome and adjacent areas of central England. Previous studies of shallow, crustal anelasticity have been conducted in Scotland utilising existing refraction data which were not fully appropriate for the purpose. Surface wave investigations are also well suited to regions where refraction processing methods are not ideal due to the nature of the

underlying velocity structure.

Most laboratory measurements of attenuation have been conducted at frequencies that are unrealistic geophysically. Estimates of intrinsic attenuation from field observations for different lithologies should have, therefore, important implications for the elucidation of the physical nature of the shallow, upper crust.

The acquisition and preparation of the data which form the basis of this research are now described in chapter 2 together with some preliminary observations and deductions from the time domain.

CHAPTER TWO

EXPERIMENTAL DESIGN, ACQUISITION and PREPARATION of the DATA and PRELIMINARY TIME DOMAIN OBSERVATIONS.

2.1 INTRODUCTION.

To achieve the specific aims of this project a high quality data set had to be acquired. Few experiments have been designed specifically to record high frequency Rayleigh waves at short ranges and none has been conducted previously in England. Earlier seismic work within the field area was designed for the application of refraction techniques and was not fully suitable for the study of surface waves. The design and implementation of field experiments to obtain the best appropriate data was, therefore, essential to this study of anelasticity.

Within this chapter we shall discuss the resulting field experiments and the various stages required to prepare the raw data for computer analysis. Finally, a number of time domain observations are made prior to the frequency domain analyses given in the subsequent chapters.

2.2 FIELD EXPERIMENTS.

2.2.1 Experiment Design.

Since the source radiation pattern for quarry blasts is unknown it was necessary to establish a line of seismometers which was ideally

co-linear with the source thereby reducing the effect of any azimuthal variations in the source. The stations should be sited preferably within a single geologic province to eliminate lateral refractions or reflections, phase conversions and other anomalous amplitude variations produced at the boundaries between such provinces.

The line would have to be long enough to record a measurable decay in amplitude with distance and sufficient instruments deployed to give a good statistical basis to and a knowledge of the uncertainty in the results. Further, more mundane restrictions on the siting of stations were the necessity of having reasonable access to the sites and that radio telemetry was feasible by having a line-of-sight between outstations and recording sites.

Four sub-experiments were, therefore, designed to radiate from Tunstead Quarry near Buxton. This quarry was chosen as the main source quarry as it was known to blast regularly with large amounts of explosive. These surface wave experiments are given the mnemonics LST 1, LST 2, MG 1, MGAR. The first two were concerned with the anelastic properties of the southern limestone district and the latter being used to investigate the northern Millstone Grit district.

Line LST 1 re-occupied some of the sites from the earlier refraction study (Rogers 1983) and followed the axial region of the Dome where the near surface is least complicated (Fig 2.1). This line, whilst being entirely in the limestone district, crossed unavoidably a major fault system, the Bonsall Fault zone, and the transition between shelf and basinal facies limestones.

Running simultaneously with the main line was a shorter line, LST 2, again mainly in the limestone district. At an angle of 30^{o}

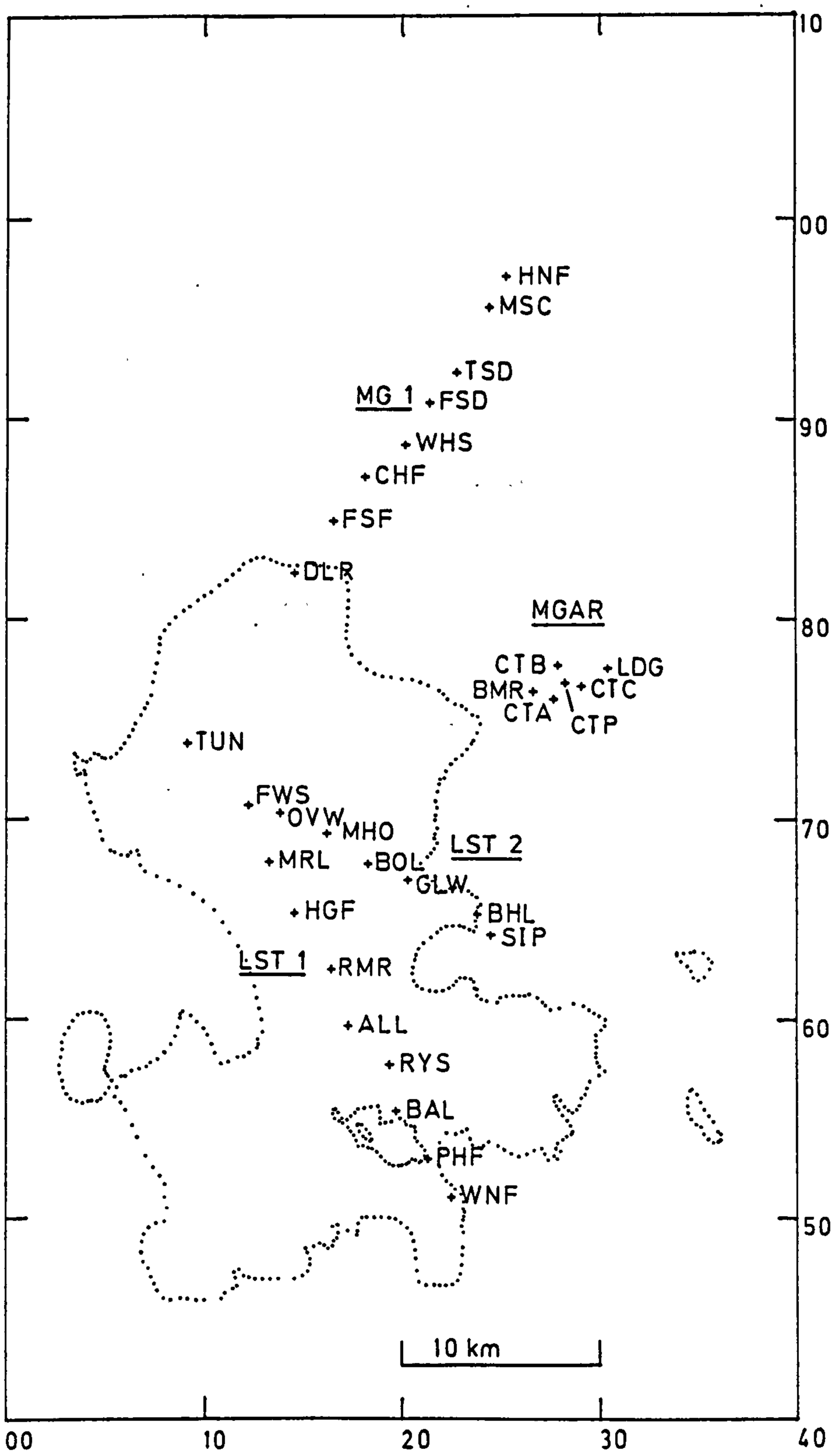

Figure 2.1 Location of stations with identifying experiment mnemonics for the surface wave study.

to LST 1 this line would provide further information on the structure of the Dome and indicate any azimuthal variation in anelastic parameters. The choice of sites forming this line was governed mainly by the amount of available equipment. Its southernmost stations were, by necessity, placed on a small area of Millstone Grit at Stanton-in-Peak; the dominant path length, however, being in the limestone.

Close to the southern ends of both lines were smaller quarries, Ballidon and Shining Bank (Alport), which would facilitate standard refraction processing by providing reversal of the lines (Rogers 1983) and potential reversal of the lines for Rayleigh waves. A dipping interface or surface can produce differences in the dispersion observed at the stations depending on the distance of the stations from the source and the sense and amount of dip (Tryggvason 1962).

The siting of line MG 1 over the Millstone Grit district to obtain estimates of anelasticity for a different lithology was further restricted due to the source quarries all being within the limestone district. To minimise the extent of lateral refraction caused by the change in lithology and topography associated with the limestone/Millstone Grit boundary the station line had to be near normal to this boundary.

Therefore, sub-experiment MG 1 consisted of a line of instruments extending to the north east from Tunstead. A secondary experiment, MGAR, running simultaneously with MG 1, comprised a small seismometer array on the Millstone Grit to the east of the Dome. This cluster array would permit the assessment of any possible lateral refraction and directionality of the signal together with studies of anelasticity.

The individual station details are given in Table 2.1.

2.2.2 Instrumentation.

The equipment used throughout this study consisted of Willmore MkIII seismometers together with the Geostore frequency modulated, analogue recording system belonging to the Seismological Equipment Pool of the Natural Environment Research Council.

The basic field unit comprised a three component set linked directly to the Geostore recorder typically with two vertical seismometers as outstations linked to the recorder by UHF radio telemetry. By deploying a number of these units lines of up to 30 km could be installed with an average station separation of 2.5 km (Fig 2.2).

The three component sets were deployed to help in the identification of the fundamental mode Rayleigh wave which exhibits distinctive retrograde elliptical motion in the vertical plane of propagation. To fulfil the design criteria using the available equipment three component sets were placed, where possible, at either end and in the centre of the lines.

The output from the seismometers was amplified and frequency modulated by an amplifier-modulator (amp-mod) unit connected to each seismometer prior to transmission and recording. During previous refraction experiments the gain settings of the amp-mods were fixed at a constant high gain. This produces excellent recordings of the low amplitude first arrivals but overloads the system when the high amplitude surface waves arrive. Such clipped signals are not a faithful record of signal amplitude and thus cannot be used in any study of anelasticity.

Table 2.1 Station Details

Name	Abbreviation	Grid Reference	Elevation	Instru-mentation
LST 1				
Tunstead	TUN	40942 37372	330 m	ZHS10
Five Wells	FWS	41226 37082	432	3W,ZBB,G
Moor Lane	MRL	41336 36771	310	ZW
Highlow Farm	HGF	41470 36507	352	ZW
Roman Road	RMR	41650 36234	340	ZW
Aleck Low	ALL	41733 35957	395	3W,ZBB,G
Roystone Grange	RYS	41944 35750	327	ZW
Ballidon	BAL	41973 35506	240	ZW
Park House Farm	PHF	42136 35295	221	ZW
Winn Farm	WNF	42265 35095	291	3W,ZBB,G
LST 2				
Over Wheal	OVW	41543 37017	356 m	ZW
Manor House	MHO	41675 36929	331	ZW
Bole Hill	BOL	41836 36760	354	3W,G
Grind Low	GLW	42042 36678	253	ZW
Haddon Fields	HDF	42170 36614	206	ZW *
Bowers Hall	BHL	42378 36505	113	ZW
Stanton-in-Peak	SIP	42453 36440	263	ZW,G
MG 1				
Dirtlow Rake	DLR	41514 38212	349 m	ZW
Fullwood Stile Farm	FSF	41708 38481	206	3W,G
Crookhill Farm	CHF	41873 38707	283	ZW,G
Wheel Stones	WHS	42023 38860	466	ZW *
Foulstone Delf	FSD	42145 39097	383	ZW
Thornseat Delf	TSD	42284 39223	400	3W,G
Moorside Cottage	MSC	42446 39555	290	ZW
Hunger Hill Farm	HNF	42538 39707	343	3W,G
MGAR				
Big Moor	BMR	42665 37634	364 m	ZW
Carr Top	CTP	42825 37676	312	3W,G
Lidgate	LDG	43047 37748	280	ZW
	CTA	42762 37595	297	ZW
	CTB	42787 37763	335	ZW
	CTC	42915 37667	260	ZW

Notes: Instrumentation. ZHS10 - vertical HS10 geophone, ZW - vertical Willmore MkIIIa seismometer, 3W - three component set of Wilmore MkIIIa seismometers, ZBB - vertical Willmore MkIIIc broad band seismometer, G - Geostore.

* - station inoperative or poor quality records for the major part of the experiment.

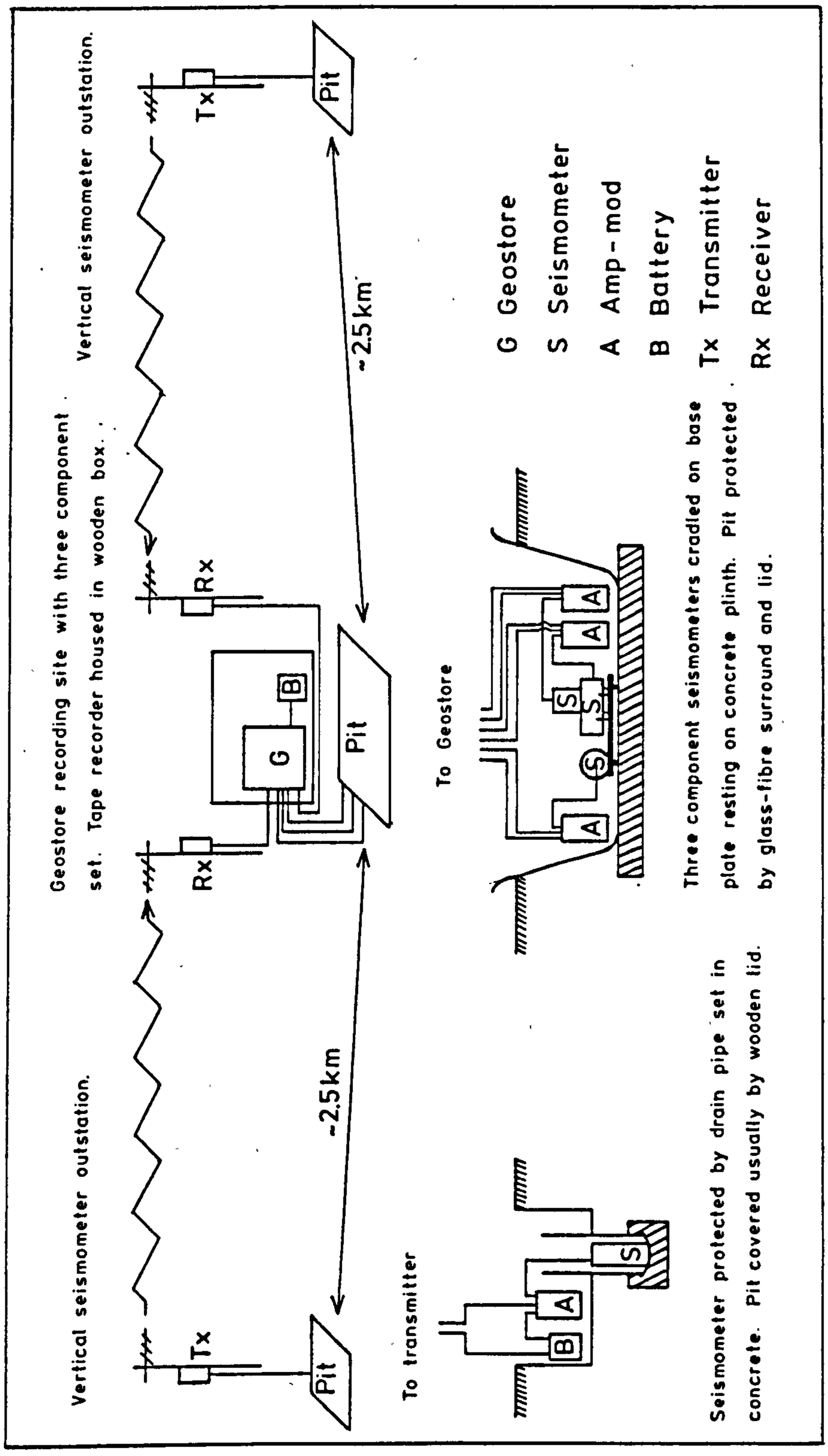

Figure 2.2 Schematic diagram of the field deployment of the basic equipment unit.

Examination of the records from the first field season (the second stage of the refraction study of Rogers (1983)) and especially from the more distant stations enabled the determination of a relation between amp-mod gain setting and distance from a source to maximise the amplitude of the signal without overloading the system. By measuring the maximum particle velocity in unclipped signals from blasts of known origin the output voltage from the seismometer could be calculated. The optimum gain setting was then found from the amp-mod specifications. (The gain settings correspond to the seismometer output voltage required to give the full frequency deviation of ±40% output from the amp-mod.) Correlating the source to station distance with the optimum gain provided the required relation. As the distance from the main source quarry to each station was known this relation, given in Figure 2.3 together with the correspondence between signal gain and gain setting, could then be used to determine the gain setting of each station in the field to yield unclipped signals of maximum amplitude.

It was suggested that seismometers having a longer natural period would provide enhanced recordings of the low frequency phases within the surface wave signal which contain valuable information about deeper levels in the crust (Burton pers. com., Evans 1981). Extending the period theoretically should increase the frequency bandwidth of the instrument and improve the signal-to-noise ratio for the low frequencies. The natural period of the seismometers was, therefore, extended from the usual 1.0 s to 1.5 s. For comparison purposes three Willmore MkIIIc force balance seismometers with a broad band response were deployed at stations FWS, ALL and WNF of experiment LST 1. The response of these instruments may be

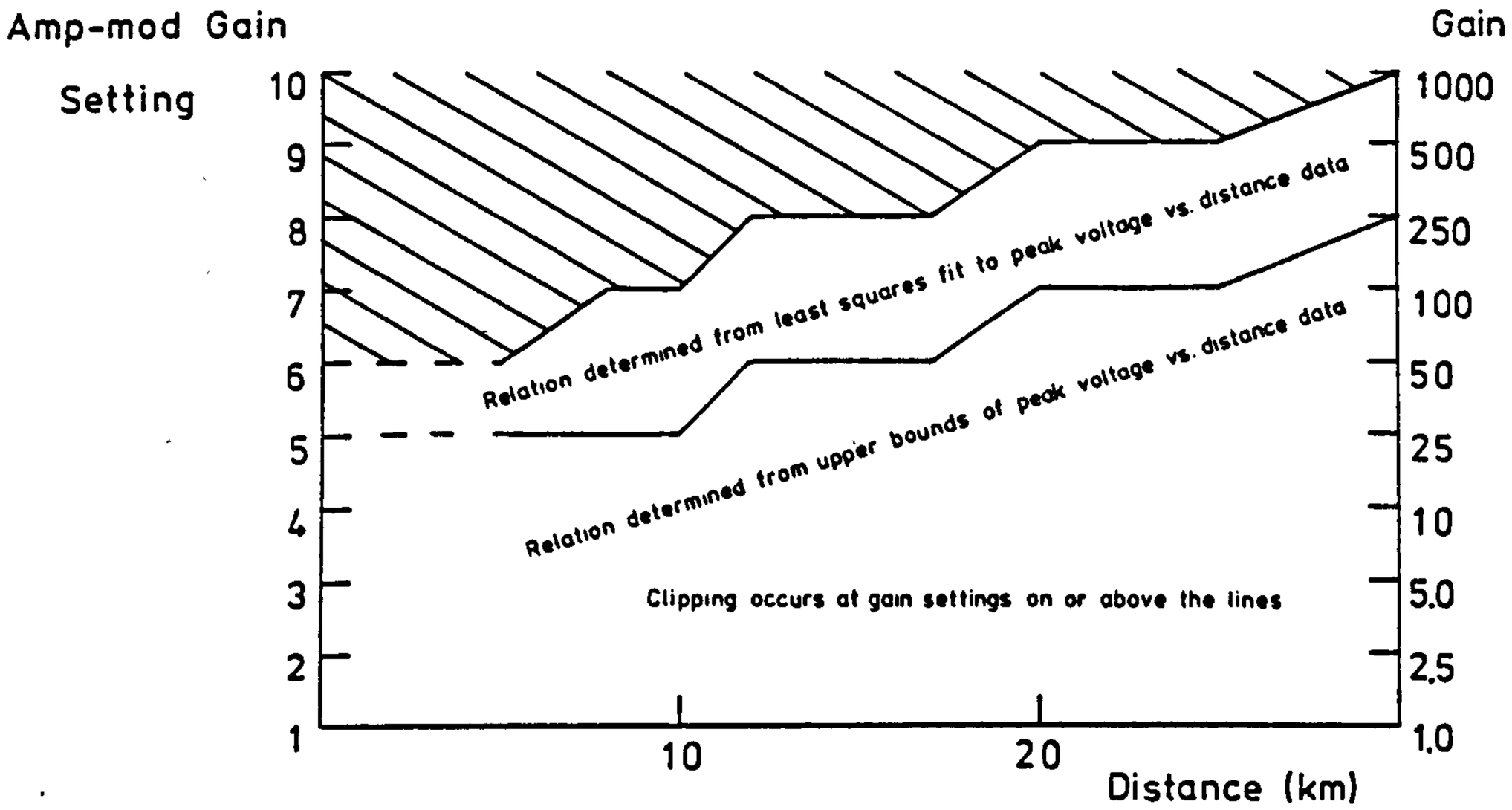

Figure 2.3 Empirically determined relation between amplifier-modulator (amp-mod) gain setting with distance to produce unclipped signals of optimum amplitude.

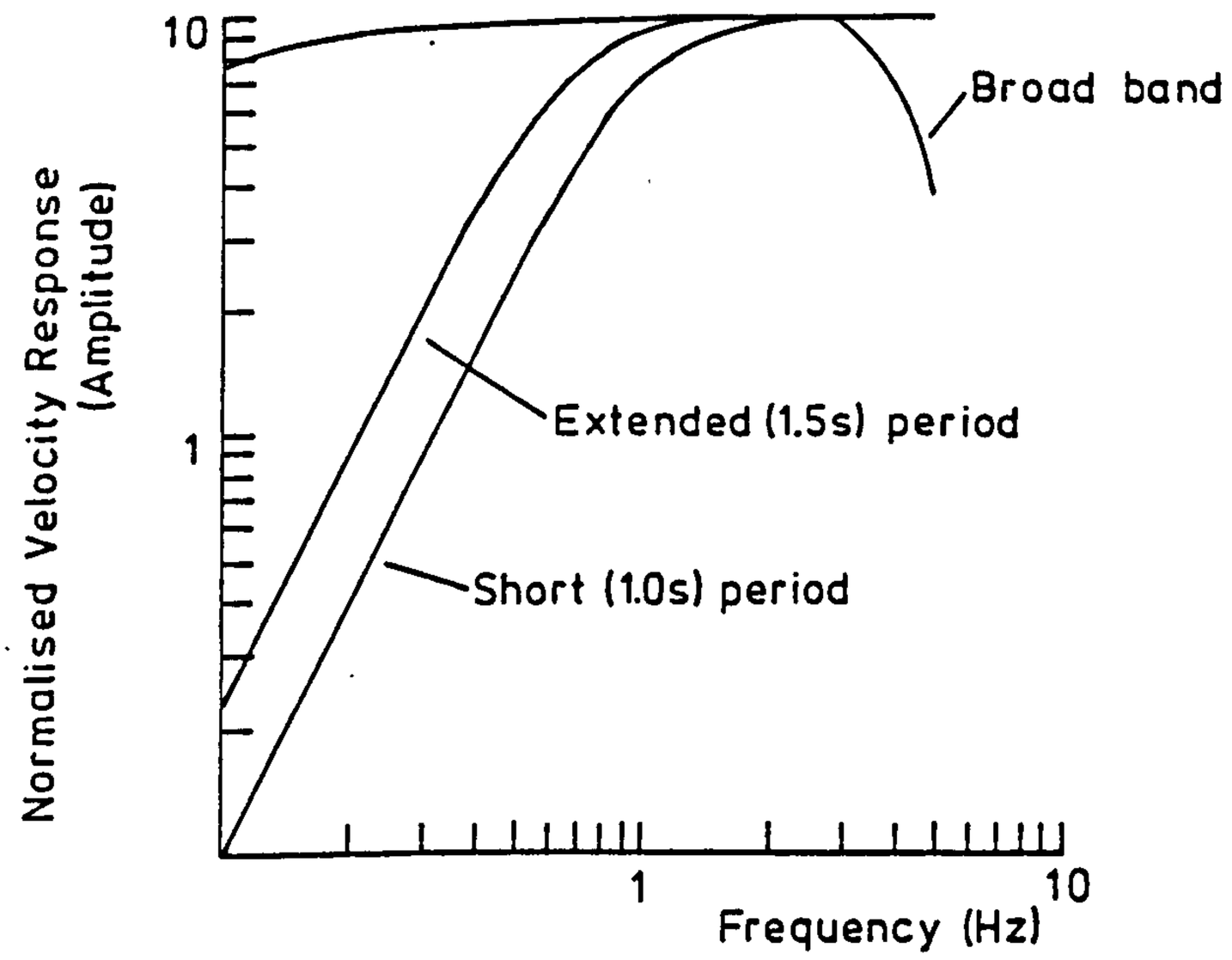

Figure 2.4 Normalised amplitude response for velocity for the three seismometer types deployed in this study.

adjusted to suit experimental requirements and were set to be flat to velocity between 0-5 Hz (Burch pers. com.). The velocity amplitude responses for the different instrument types are given in Figure 2.4.

The re-occupation of certain sites along LST 1 has allowed signals recorded by the different instruments to be compared. This comparison is discussed in greater detail in Appendix A. The signals recorded from quarry blasts by the extended period (1.5 s) and broad band seismometers were very similar after the longer period microseismic component is removed from the broad band record. The lowest frequency present in the signal is about 0.4 Hz in both cases. The records from the short period (1.0 s) instruments are noticeably different to those from the extended period seismometers. In this case the surface wave group is less well defined and the lowest frequency with amplitudes above the noise level is 0.6 Hz. Enhanced recordings of high frequency surface waves with an increased bandwidth accrue from the use of extended period or broad band instruments. For the present study, however, there was no advantage in deploying broad band seismometers in preference to extended period instruments.

Knowledge of the instrument transfer function allows the true spectrum to be obtained from the spectrum of the recorded signal. By calibrating the seismometers the response can be determined and standardised over the network. Two main parameters, the period and damping, are required to specify the response of the Willmore MkIII seismometer. A third parameter, the coupling factor, is usually assumed to be constant. In the laboratory calibration was achieved by driving the seismometer with a secondary input sinusoidal current and comparing this with the output. The instruments were then

standardised to a natural period of 1.50±0.08 s and damping factor of 0.70±0.01 of critical damping. Impulse calibration was conducted in the field following deployment and whenever a station was serviced to monitor the instrumental drift. Analysis of the recorded pulses showed little variation in the instrument parameters once the seismometers had settled into their working environment.

The complete recording system was assembled in the laboratory following calibration. By recording overnight in one location (the basement of Murchison House, BGS Edinburgh) any faults in the system could be identified and information on the relative gains of the instruments obtained. It did not always prove possible to conduct similar checks at the end of each experiment. Results obtained prior to the limestone district experiment are given in Table 2.2.

2.2.3 Field Work.

The field work for each experiment was divided into two parts separated by a period of a few weeks during which time the equipment was readied for field use and the instrumentation calibrated.

A period of site reconnaissance and preparation comprised the first part of the field work. Each proposed site was visited to assess the line-of-sight and ambient noise level. Alternative sites were chosen where necessary.

To prepare a low noise station at each site a pit was dug and a base of concrete laid to afford good contact with the ground. By making the pits similar variations in the seismometer 'plant' could be reduced hence lowering the variations in amplitude caused by poor coupling (O'Brien 1967). The larger, three component pits could

Table 2.2 Empirical Measurements of the Relative Gains of the Seismometers

Prior to the experiment to investigate the anelastic properties of the Carboniferous Limestone district the entire recording system was assembled in the basement of Murchison House, BGS Edinburgh. The system was left to record the ambient night time noise. These recorded data were then digitised at 100 Sps and the average amplitude level calculated from the spectral co-efficients given by the Fast Fourier Transform of the signals. The results of this investigation are given below; the individual instruments being identified by the mnemonic of the station at which they were installed in the field.

Vertical Components

Station	Relative Gain
FWS	1.13
MRL	1.01
HGF	0.87
RMR	0.85
ALL	1.23
RYS	1.04
BAL	no information
PHF	0.93
WNF	1.13
OVW	5.52
MHO	no information
BOL	0.88
GLW	8.57
HDF	0.79
BHL	0.92
SIP	1.16

Horizontal Components

Station		Relative Gain
FWS	N/S	1.10
	E/W	0.98
ALL	N/S	1.22
	E/W	1.26
WNF	N/S	3.02
	E/W	1.00
BOL	N/S	11.07
	E/W	0.78

Note: The instruments at stations OVW, GLW show large gains compared to the other seismometers. The north-south horizontal component for station BOL also has a high gain. In general, the horizontal components, appeared to be more sensitive than the vertical components and overall had a slightly higher average gain than the vertical instruments.

accommodate the additional broad band instrumentation whilst the outstations housed a vertical seismometer only.

The second phase of field work consisted of the installation and operation of the network. The three component sets were mounted on machined base plates ensuring, as far as possible, that the component seismometers were mutually perpendicular. The two horizontal instruments were orientated to give positive motion in the north and east directions.

Timing for the experiment was provided by recording the absolute time standard broadcast from MSF, Rugby (Wireless World 1978). All time measurements were made against this standard. A second, less accurate, level of timing was recorded from clocks internal to each Geostore recorder.

Of the 14 channels available for recording on the Geostore two were used to record the time standards. The flutter of the Geostore was recorded on two further channels enabling the fluctuations in recorder speed to be corrected for later. Of the remaining 10 channels available for seismic data recording the typical number utilised on one Geostore was five but in more exceptional cases (eg. MGAR) eight channels were used.

The network was maintained by weekly servicing and calibration visits to each site. Further additional inspection visits were made when convenient. The quality of the recorded data was also monitored each week as the Geostore tapes became available following their weekly change thereby ensuring maximum data retrieval.

2.2.4 The Source.

The many quarrying operations located in the limestone district

provide a convenient source of seismic energy. They have been utilised on a number of occasions during refraction studies (Whitcombe & Maguire 1981, Rogers 1983). Their repetitious nature enables a series of recordings over the same path to be made thereby reducing random errors in group velocity and attenuation analysis.

The larger primary blasts are used to obtain stone for processing and adhere usually to a fixed geometrical pattern. A line of drill holes is made parallel to the face extending below the floor of the next bench (lift) up to a depth of 10% of the height of the face. The distance back from the face (burden) and spacing are variables which determine the fragmentation of the stone.

For efficiency and environmental reasons these shots are usually ripple fired, that is there is a time delay of 1-25 ms between the detonation of each hole, Plate 1. By delaying each hole the explosion gases produced by the preceeding hole have a chance to rupture the rock before being vented and so assist those produced by the next hole. In this manner the efficiency of rock fracture is increased (Leet 1954).

The amount of vibration produced from a ripple fired shot is much less than an instantaneous blast of the same dimensions, with the maximum acceleration corresponding to the maximum loaded hole and not the sum of the holes. From a seismologists viewpoint, therefore, a ripple fired blast is less desirable than a single shot (Leet 1954). This observation is confirmed by Willis (1963) who also shows that there is no appreciable change in frequency bandwidth between instantaneous and ripple fired shots and that the reduction in amplitude is less for surface waves than for compressional waves.

The periodic nature of quarry blasts invites an analysis by

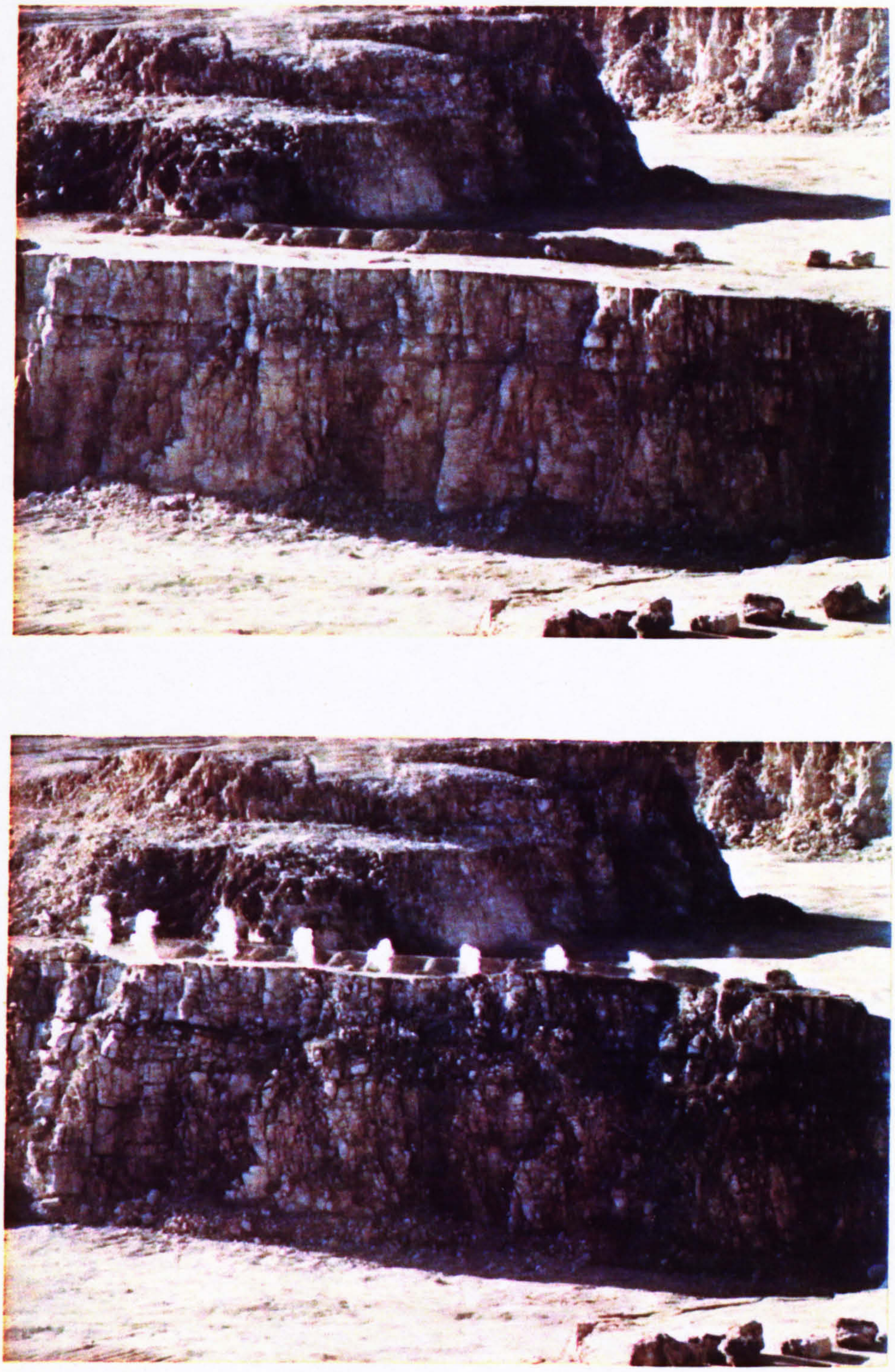

Plate 1 The Source - a quarry blast in Ballidon Quarry.

Total charge size	1252 kg
Number of holes	10
Delay interval	25 ms
Height of face	15 m

Top: Quarry face prior to blast.

Bottom: During blast - firing sequence from right to left.

Fourier techniques (Pollack 1963). If the number of holes or the time delay is large then the theoretical spectrum (body wave) will exhibit a series of peaks and troughs eventually becoming a harmonic sequence at frequencies which are multiples of the delay time reciprocal. If the number of holes or the delay time is small then the spectrum approaches a scaled version of that for a single hole. In either case quarry blasts cannot be considered as point sources and may, therefore, show an azimuthal variation in amplitude.

Accurate phase travel times, and hence velocities, to the recording stations were determined by visiting as many quarry blasts as possible whilst in the field. A small, portable recording system was used to obtain the shot instant using a geophone placed close to the centre of the shot and recording the signal against the MSF time standard. Bearings were then taken on fixed objects to locate the position of the geophone.

The recorded events could then be played back in the laboratory onto high speed paper records enabling the origin time to be picked to an accuracy of ±0.01 s. The location was determined usually to ±150 m by plotting the bearings on the relevant 1:10 000 scale maps.

During field operations it was not always possible to be present at every blast. The stations TUN, BAL for the limestone experiment and DLR for the Millstone Grit experiment, however, were placed sufficiently close to Tunstead, Ballidon and Hope quarries to act as continuous telemetred shot recorders. Estimates of the origin time of any untimed blast in these quarries could then be made by subtracting a delay time from the time of the first arrival. This delay time could be determined from other timed and located blasts. Records from these stations were also used to highlight location inaccuracies or gross errors mistyped into the

seismogram data sets held in computer files.

Where necessary further locations were obtained from the first arrival refraction study (Rogers 1983). These locations were also compared to solutions given by a least squares location programme (Global Seismology Research Group programme RLOC, R. Lilwall) using a number of simple compressional wave velocity structures.

The locations of the quarries used in this study are given in Figure 2.5.

2.3 DATA PREPARATION.

2.3.1 Data Replay.

The data were replayed on a system consisting of a Store 14 tape recorder linked to a stereo amplifier and headphones, an internal clock time decoder and a 16 channel jet-pen chart recorder.

A set of master tapes from one Geostore was selected using information from the weekly check on the data quality. These tapes, chosen for the reliability of the recorder and outstations over the duration of the experiment and that two separated stations had a high signal-to-noise ratio, were then replayed at a higher speed than that at which they were recorded producing an audible signal when played through the amplifier and headphones. Coherent energy recorded at two sites from a seismic source could be distinguished from site specific noise events in this manner (a passing vehicle for example) and the time logged from the decoder. A paper record was made for each event enabling a library of events containing details of recording time, size and possible source type to be generated.

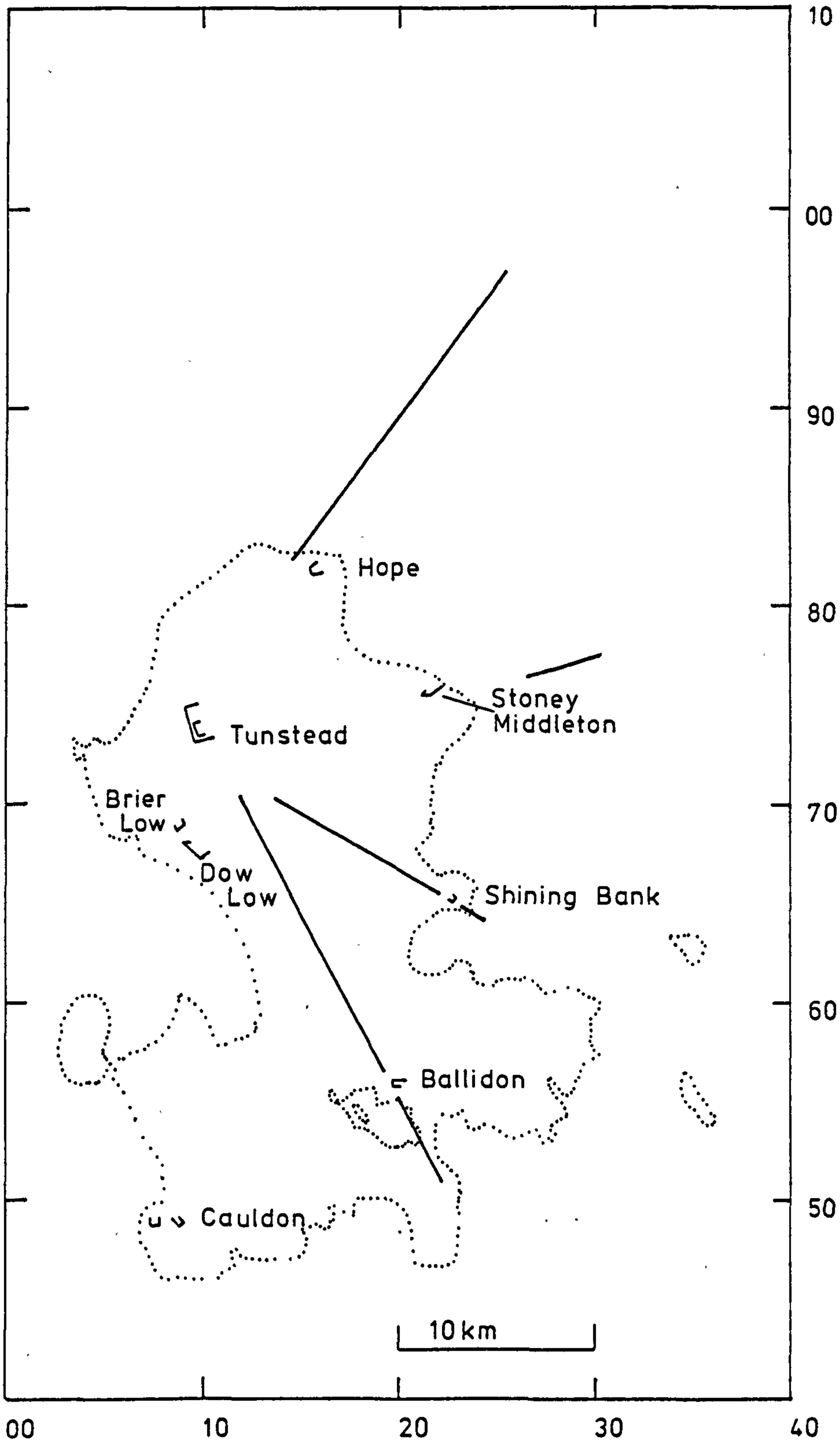

Figure 2.5 Location of principal quarries in the region in relation to the seismic station lines. (Carboniferous Limestone outcrop indicated.)

This library was examined to find all events of interest which included timed and untimed quarry blasts, large local events and teleseisms. To reduce the time spent in preparation of the data from the Millstone Grit experiment only timed quarry blasts were considered. Paper records of these events were then produced from tapes from the other Geostores deployed during the experiments.

Following this a catalogue was created giving details of the status of each station for every event. This catalogue was then used to further prune the data leaving only those events recorded well down the major part of any line. This constituted the final catalogue of event data prior to its digitisation to facilitate detailed analysis.

The analogue data and catalogues are held in archive by the Global Seismology Research Group.

2.3.2 Digitisation.

To facilitate analysis by computer the data have to be digitised. Digitisation is the process of sampling an analogue record at a number of points equally spaced, preferably, in time at an interval δt s. The magnitude of each sample is given by the value of the analogue signal at that instant in time.

Digital representations of the data allow the use of the Fast Fourier Transform (FFT: Cooley & Tukey 1965) whereby time domain seismograms are transformed into frequency domain spectra. These spectra can then be used to analyse the frequency dependent characteristics of the signal.

The complex spectrum may be split into two parts, the amplitude and phase spectra which are expressed at a series of harmonic

frequencies ν_i where

$$\nu_i = \frac{i}{2^N \delta t} \qquad i = 0,1,\ldots,2^{N-1} . \tag{2.1}$$

The highest harmonic, the Nyquist frequency ν_N, arises from the fact that two time samples are required to define a wave of a given period and must necessarily be limited by the sample interval. Above the Nyquist frequency aliasing may occur with any higher frequency signals, for example noise, being 'folded back' onto ones of lower frequency thereby adversely affecting the spectrum of the digital seismogram. The sampling interval and hence the Nyquist frequency should, therefore, be chosen to be greater than the maximum frequency of interest in the seismogram.

The data recorded for this project were digitised using the PDP11/50 and Store 14 replay system of the GSRG utilising standard programmes (Fyfe 1982). To retain compatability with the earlier refraction data format (Rogers 1983) a sample rate of 50 samples per second (Sps) was used giving a Nyquist frequency of 25 Hz.

Prior to being input to the digitiser the signals (excluding the time channels) were passed through wide bandpass filters whose action was merely to remove any shift in dc level between the various channels from the Store 14 replay tape recorder. No filters were used to remove the effects of aliasing.

A Nyquist frequency of 25 Hz is excessive when considering surface waves in the frequency band 0.5-5 Hz. For this reason and to reduce later computational effort it was decided to reduce the sampling rate to 25 Sps by removing alternate samples from the tapes sampled at 50 Sps. Each digital seismogram was now in a standard

format with a Nyquist frequency of 12.5 Hz.

The recorded calibration pulses were also digitised but at the higher sampling rate of 100 Sps. These pulses were not filtered prior to digitisation as it was found that the filters did not respond well to the transient nature of the pulse when set to pass a wide frequency band.

Each digital seismogram was identified uniquely by the addition of an information header block containing the instrument parameters, source origin time, distance and azimuth to the source and the absolute time of the first sample of the time series. These standard format seismograms were then held as computer files which formed the data base for this project.

2.3.3 Errors Produced During Data Preparation.

The accuracy of subsequent analysis could be affected severely by systematic errors produced during the recording and preparation of the data. By careful attention to the sources of such error their effect can be minimised.

Errors in timing may be produced by the record/replay system. The 14 channels recorded by a field Geostore are written to magnetic tape via two recording heads. The head assembly is manufactured so that the heads are a fixed distance apart and perpendicular to the tape transport direction. It is likely, however, that the heads are not perfectly aligned following their use in the field. The skew and displacement of the heads on various recorders will, therefore, be different. By replaying the tapes on a second machine, a Store 14 which uses a similar head assembly, a cumulative timing error can be produced due to the relative displacement and skew between the

record and replay heads (Fig 2.6a).

On digitising, the corresponding samples between each channel will have slightly different absolute times because of this head misalignment. Such time shifts may produce systematic variations in velocity or phase shifts when two channels are compared in particle motion studies for example.

To determine the time shifts a square wave signal was recorded simultaneously on all channels excluding the internal clock and flutter channels which continued to record time and recorder flutter. These tapes were then replayed on the Store 14 used for digitising and paper records obtained. Time delays to the leading edge of a given cycle of the signal were measured for all channels from a fixed line, usually a given time on the internal clock (Fig 2.6b). Repeated measurements provided an average time shift relative to channel 2. These average time shifts relative to the internal clock were then corrected to be relative to channel 14 upon which absolute time had been recorded in the field. In this way the first sample of any digital seismogram could be assigned its true absolute time irrespective of recording channel.

The maximum shift relative to absolute time was 43 ms but was more typically 10 ms. The major component of the time shift was caused by the relative displacement of the record/replay heads. This effect could be minimised by recording fewer seismic channels on one head only. This was achieved along the line MG 1 where the average relative time shift was reduced to about 4 ms.

During digitising the data are multiplexed introducing a small time shift between the samples of each channel and the size of this depends on the sampling rate and number of channels sampled. To estimate this time shift a record of the internal clock was input as

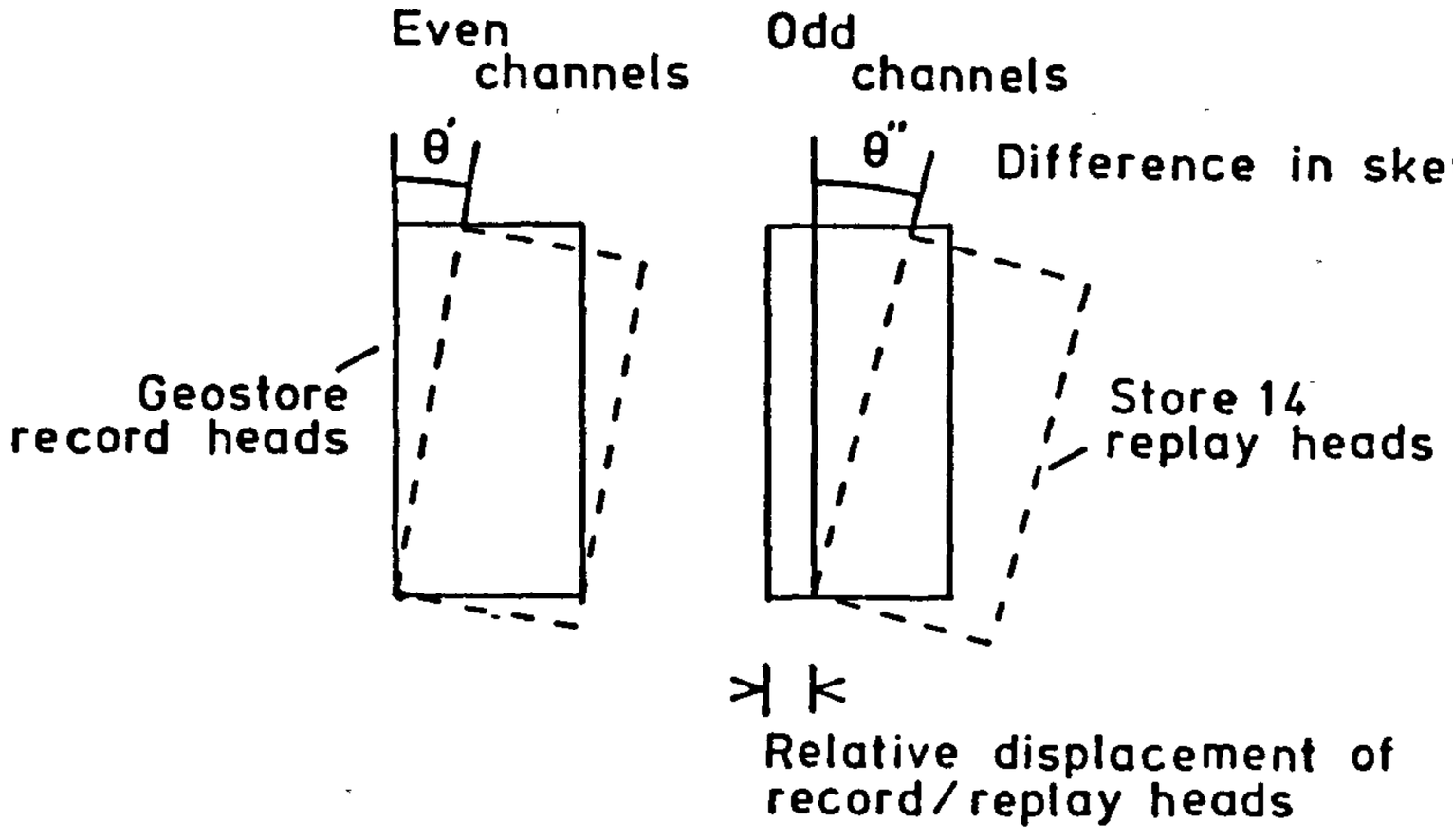

Figure 2.6a Schematic diagram of the possible mis-alignment between the recording and replay magnetic heads.

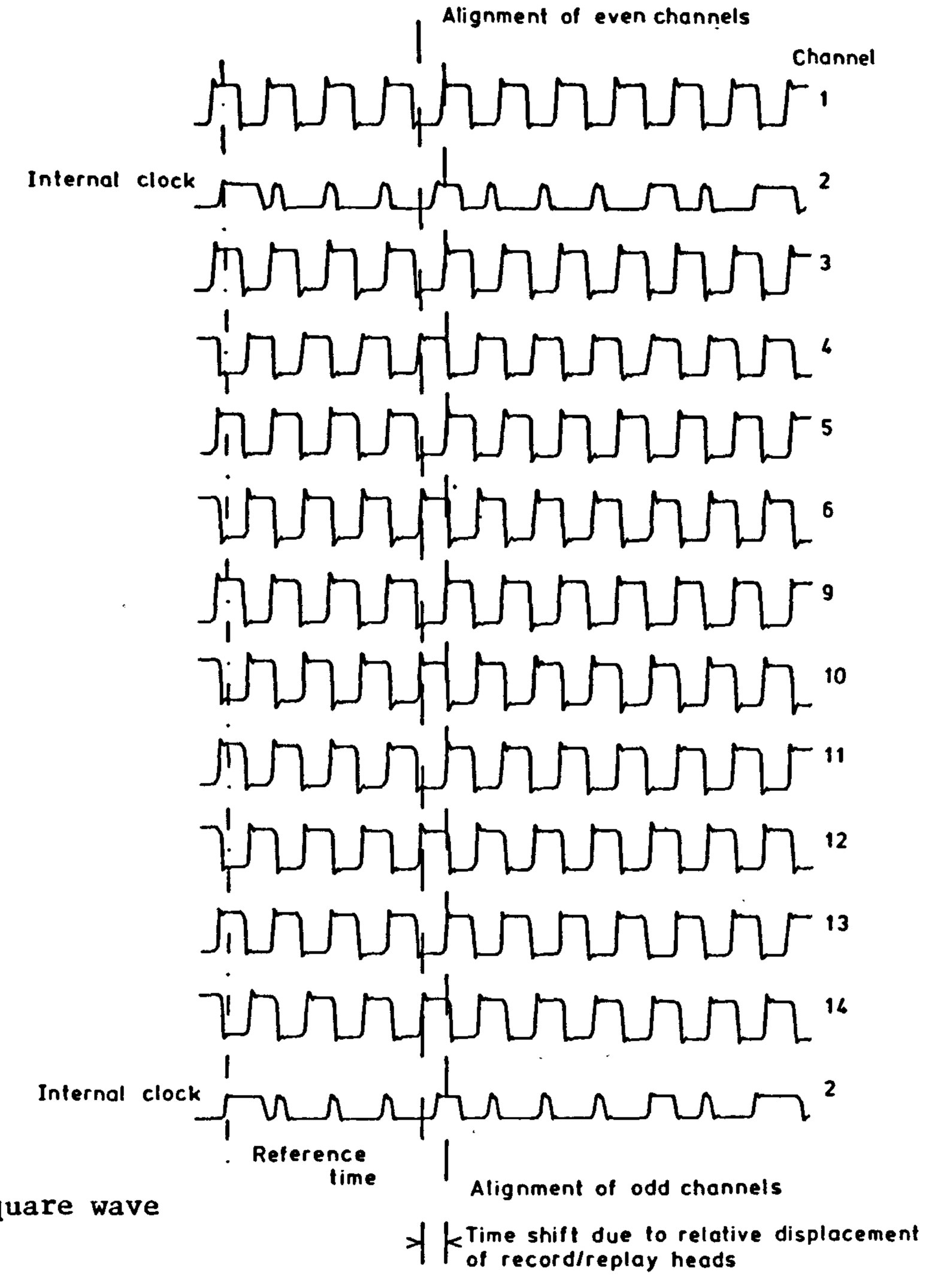

Figure 2.6b Time shifts induced by record/replay head mis-alignment shown from the replay of a square wave recorded simultaneously on all channels.

five channels into the digitiser and digitised at a high sampling rate of 200 Sps. The size of each sample was compared between the first and subsequent channels and the time shift required to equate the values taken to be the multiplexing interval. Throughout this study, therefore, a value of 800 μs was used. The highest number of channels digitised from one analogue tape was 10 resulting in a maximum time shift of 7.2 ms which is small compared to the sampling interval of 40 ms.

It was noted during the replay of the calibration pulses that for the three component sets a second signal had been induced in the two passive instruments not being calibrated. A distorted record and errors in amplitude could be produced, therefore, by the cross-talk between the individual instruments comprising the three component sets. The phase and amplitude of the induced signal varied depending upon which seismometer was being calibrated. The induced signal was usually in phase or in anti-phase with the calibration pulse and always of a lower amplitude. The source of this cross-talk was shown to be magnetic coupling between the instruments when they were placed in close proximity, as they were on the base plates used during the experiment. Measurements on the magnitude of the cross-talk, however, showed that for the typical quarry blast considered within this thesis the amplitude of the cross-talk was less than the ambient noise at the stations and could be ignored. For a large teleseismic signal, however, this effect may not be negligible because of the increased relative motion between the magnet-mass and the seismometer coils.

A second source of error in the signal amplitude could be caused by aliasing. The wide bandpass analogue filters used to remove any variations in dc level between the channels prior to

digitisation did not act in any way as anti-aliasing filters. On digitising any signal or noise between 20-24.5 Hz in the analogue record could be folded back about the Nyquist frequency of 12.5 Hz thereby contributing to the digital seismogram in the frequency band of interest, 0.5-5 Hz. To assess the degree of amplitude contamination caused by aliasing certain events were redigitised at 50 Sps using anti-aliasing filters and the recorded amplitudes measured between 12.5-25 Hz. These events were also digitised at 25 Sps with anti-aliasing filters. (The analogue filters used were set to have 3 dB points at 25 Hz and 12.5 Hz respectively having a roll-off of 24 dB/octave after this point). The anti-aliased seismograms at 25 Sps and their spectra were then compared with the 'aliased' standard format signals (Fig 2.7). For most events the degree of contamination was shown to be less than 5% of the anti-aliased amplitude and certainly never more than 10%. Aliasing, therefore, was considered to be within the experimental errors inherent in amplitude measurements and so not considered further. This low degree of aliasing is attributed to the filtering internal to the Store 14 (see Appendix A), and the low amplitudes of noise in the analogue record above 12.5 Hz.

A further possible error due to digitising could occur if the sampling rate was not the same for each seismogram. The variation in δt may be random or systematic and will affect the results of the Fourier transformation. When the variation in δt is random the spectral co-efficients, quoted at the standard harmonic frequencies, will contain random errors which may be included in the total error of the experiment. For a systematic variation in δt, however, the spectral co-efficients will be given at the standard harmonic frequencies and not at the correct ones pertaining to the actual

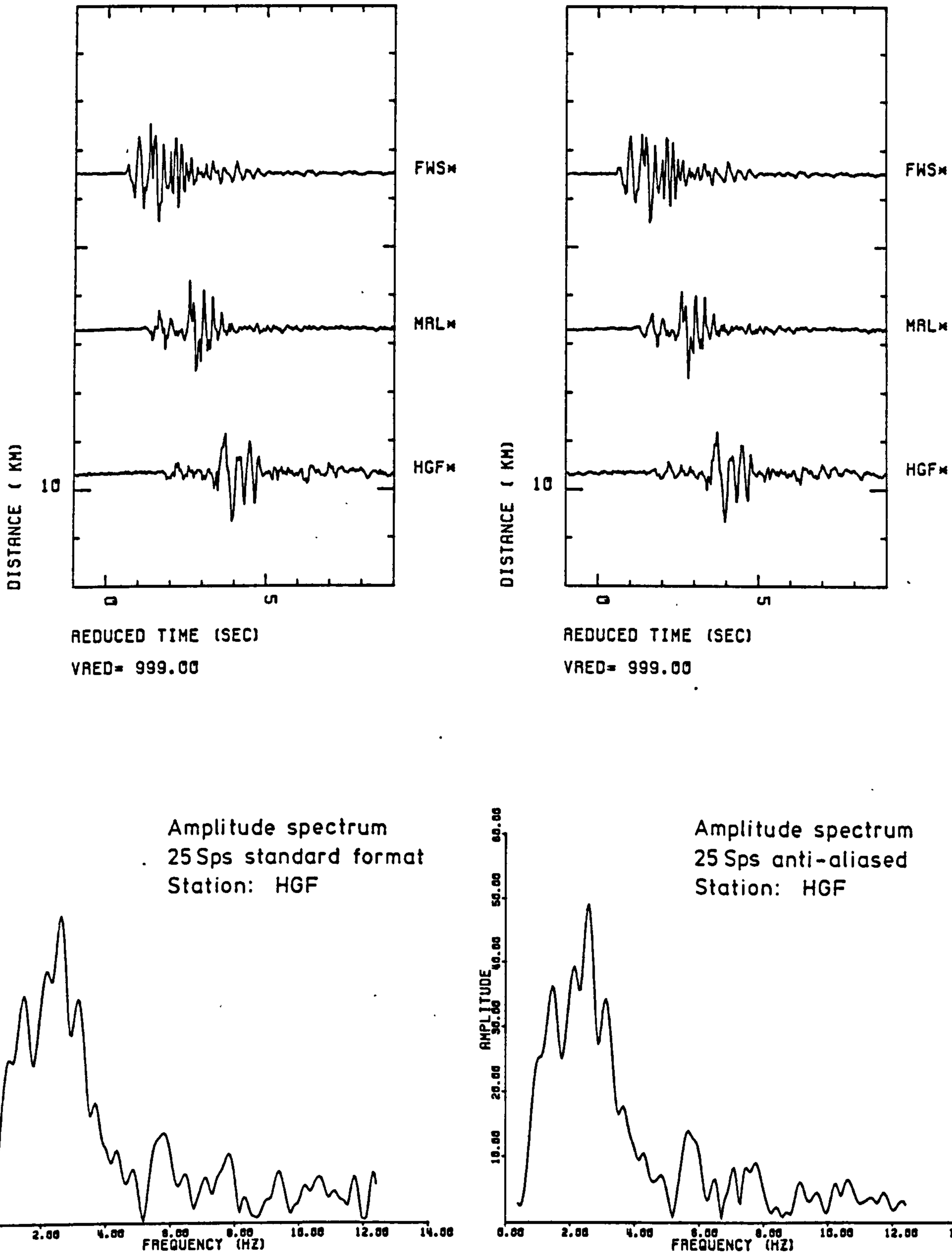

Figure 2.7 Comparison of seismograms and amplitude spectra for signals digitised at 25 samples per second (Sps) without anti-aliasing filters (standard format) and with anti-aliasing filters having a 3 dB point at 12.5 Hz.

sampling rate. This may result in a false stretching or compression of the frequency range from dc for the amplitude spectrum.

The accuracy of the sampling rate was assessed by counting the number of samples from the leading edge of one second mark to another 30 s later. In all cases the measured sampling rate was either 24.97 Sps or 25 Sps indicating that the sampling rate was accurately controlled by the digitiser; the difference in value being caused by the accuracy of determining the leading edge to ±1 sample. No errors, therefore, could be attributed to a variable sampling rate.

The final source of error due to the digitiser was the accuracy of its gain settings (ie. the voltages required from the Store 14 to yield ±1024 digitiser units, d.u.). Warner (pers. com.) showed that considerable variation from the nominal, documented values existed. To calibrate the digitiser, signals of known voltage were digitised and the pertinent gain settings determined. The digitiser was then re-adjusted to the nominal values. The gain setting of the digitiser is required to obtain true ground motion amplitudes (see Appendix A). All events digitised prior to the re-adjustment employed the settings given by the calibration exercise whilst those following the re-adjustment used the nominal, set values.

2.4 TIME DOMAIN OBSERVATIONS.

Geophysically significant results have been obtained from direct time domain measurements on the seismograms in the standard digital format given above. Such observations were used to assist and guide the frequency domain analysis discussed in subsequent chapters.

The standard refraction practice of plotting the data as reduced time seismic sections enables estimates of apparent velocity to be made (Telford et al. 1978, p368). For surface wave studies an approximate measure of group velocity can be obtained by correlating the maximum of the amplitude envelope. This point should represent the maximum energy in the wave packet but will depend on the group velocity dispersion function and the shape of the amplitude spectrum (Evans 1981). Reduction velocities of 6 km s^{-1} and 8 km s^{-1} have been used in studies investigating crustal or mantle compressional head waves respectively. In contrast, the lower reduction velocity of 3 km s^{-1} is more appropriate to shallow crustal, surface wave experiments.

Individual phases within the signal can be identified from their particle motions using the three component set data. Evidence for lateral refraction or reflection may also be obtained from the particle motion studies or from the seismic sections.

The true azimuth of propagation of a signal may be assessed using an array of seismometers. Array processing methods include sophisticated frequency domain techniques (Capon 1969, Bungum & Capon 1974) or, as employed here, methods using the arrival times of given phases (Jacob 1969b). Phase velocity and direction of propagation across the array can be determined provided the stations are less than one half wavelength apart enabling the peaks in the surface wave signal to be correlated unambiguously.

2.4.1 The Carboniferous Limestone District.

Seismograms from the co-linear source quarry at Tunstead showed considerable variations in signal character between events. Two

dominant signal types were observed, examples of which are given in Figure 2.8. Signal type 1 exhibits a prominent arrival of one and one half cycles which can be correlated along the line south of station RMR. In the type 2 signals this phase is absent, being replaced by a shorter period group. A low amplitude phase of one and one half cycles duration is, however, seen to arrive later in the signal. The details of each blast in Tunstead Quarry recorded whilst in the field reveal a correlation between the orientation of the shot line to the station line and the type of signal observed. Type 1 signals were recorded when the shot line was perpendicular to the station line but when both lines were parallel signal type 2 was recorded. This observation shows that whilst quarry blasts give reproducible signals they cannot be regarded as a simple source with little azimuthal variation. These differences in signal type were also manifest in preliminary frequency domain analysis for group velocities where consistent dispersion curves were difficult to determine.

Only surface wave signals having a low signal-to-noise ratio were recorded from the southern co-linear quarries of Ballidon and Shining Bank. This was attributable directly to the smaller total amounts of explosive used in these quarries. As a consequence no reversal of the lines for surface waves was achieved with the result that variations in dispersion curves due to a non-plane layered structure could not be investigated. For example, the differences in group velocity caused by an interface dipping at 5^{o} compared to an averaged, horizontally layered model may range approximately from 0.50 - 0.02 km s^{-1} over the frequency range of interest between 0.5 - 5 Hz given a reasonable velocity distribution with depth in the shallow upper crust.

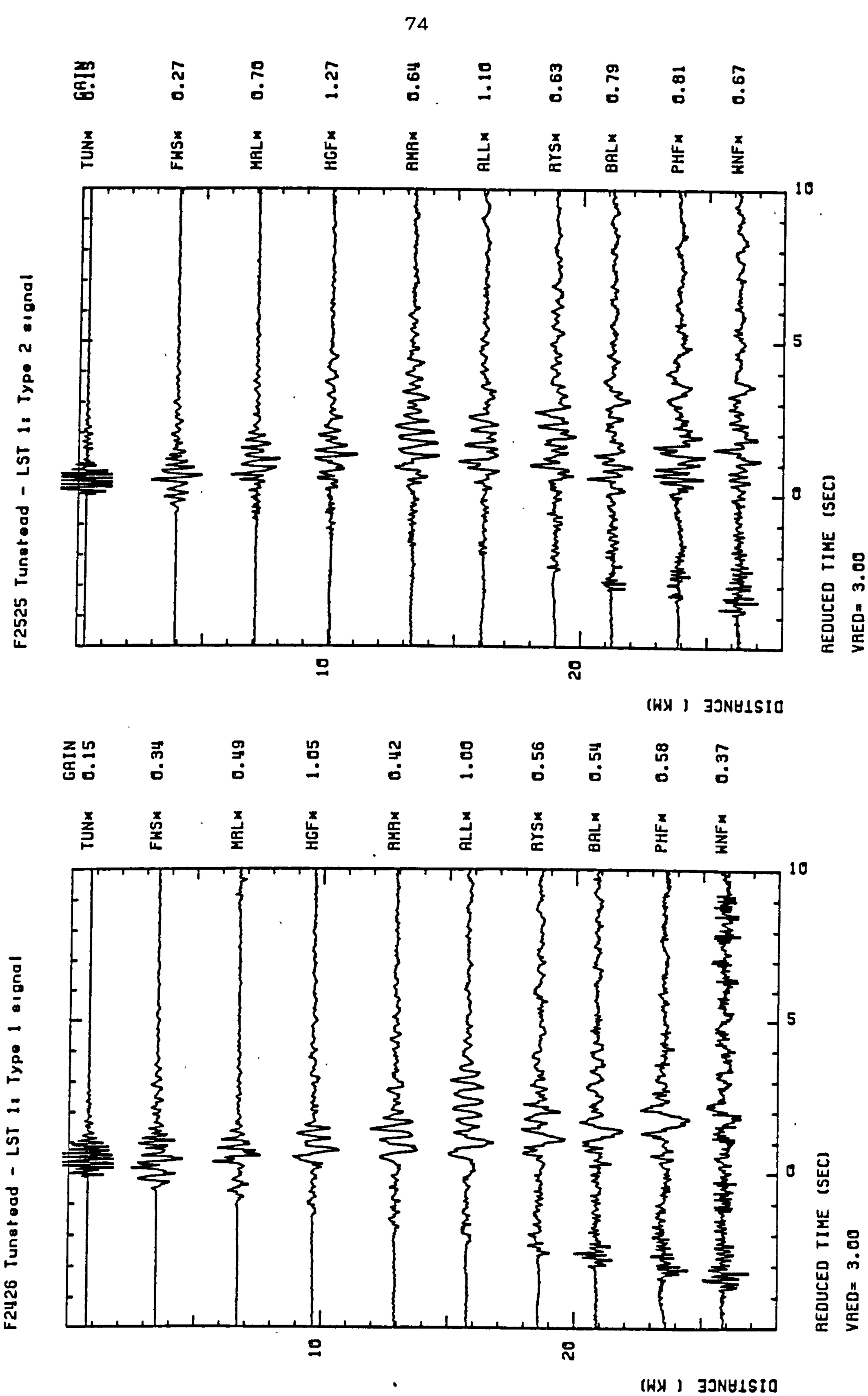

Figure 2.8 Comparison of seismic sections for two events (F2426, F2525) in Tunstead Quarry recorded along station line LST 1. Signal types 1 and 2 are repeatable and depend on the orientation of the blast to the station.

In contrast, a group of similar signals with a high signal-to-noise ratio and exhibiting dispersed surface waves were observed along lines LST 1 and LST 2 from a source in the north. These events did not correspond to any of the blasts visited and located whilst in the field.

Locations from the refraction study placed five of these events in Brier Low Quarry, south of Buxton (Rogers 1983). A further event was also located by Rogers in Brier Low Quarry but was subsequently rejected for two reasons. Firstly, the signals displayed a lack of consistency with those from the former group of events and secondly, the event was the only one to yield a different location when the events were checked using the least squares location programme, RLOC. The anomalous event was re-located to Dow Low Quarry further south; this location being confirmed later by the quarry manager.

The five events in Brier Low Quarry did not satisfy the requirement of co-linearity between the source and station line. The clarity and similarity of the signals compared to events from Tunstead Quarry were considered sufficient reason to proceed with the analysis. The possible consequences of removing the absolute azimuthal restriction could not be disregarded. The range of azimuths, however, was slight being about $\pm 15^{o}$ from the mean direction.

Phase identifications were confirmed from one of the three component sets deployed along LST 1; the records from the other two three component sets usually not being of sufficient quality for this purpose. Little dispersion was indicated at the low gain station FWS being close to the source and station WNF had a low signal-to-noise ratio for most events. In contrast, the three component set at station ALL was suited ideally to this purpose,

recording well dispersed signals with a high signal-to-noise ratio.

Retrograde elliptical particle motion in the vertical plane of propagation is exhibited by the main wave group in the signal (phase (1), Fig 2.9). The assumption that this high amplitude phase was the fundamental mode Rayleigh wave was, therefore, verified. For this wave the ratio of vertical to radial amplitude is, in theory, approximately 3:2 (Bullen 1979, p90). In all cases, the vertical component was shown to have amplitudes that were smaller than or similar to those of the horizontal components. The increased relative gain of the seismometers in the horizontal mode was not sufficient to account for this discrepancy between theory and observation (see Table 2.2). Other observations of quarry blasts have also shown large horizontal amplitudes (Habberjam & Whetton 1952, Leet 1954, Gupta & Hartenberger 1981).

Dispersed shots, such as quarry blasts, have also been shown to generate significant amounts of shear energy (Gupta & Kisslinger 1966). Consequently, phase (2) of Figure 2.9 is believed to be the shear wave and phase (4) on the transverse component a Love wave arrival. The short period arrival, phase (3), immediately preceeding the Love wave may be a higher mode. Phase (5) consists entirely of horizontal motion of lower wave velocity than the fundamental mode Rayleigh wave. Lateral refraction or reflection of the Love wave may explain this phase. Alternatively, mode conversion at some lithologic or topographic feature may have occurred. These features are common to all signals at station ALL from Brier Low Quarry.

Additional confirmation of the phase identifications was given by an analogue signal correlator (Houliston 1975). The correlator output was formed by the product of the vertical component signal

Figure 2.9 Particle motion plot for event F2441 in Brier Low Quarry recorded at station ALL. The seismograms are interpolated to give the same start time; filtered by a Gaussian filter of centre frequency 2.5 Hz and bandwidth ± 2.5 Hz. The horizontal seismograms rotated to give radial (R), transverse (T) components. The vertical (Z) component is retained. The identified phases are discussed in the text. (Positive motion is away from the source for the radial component, upwards for the vertical component and given by a right handed convention for the transverse component. Start of motion in each window marked by *.)

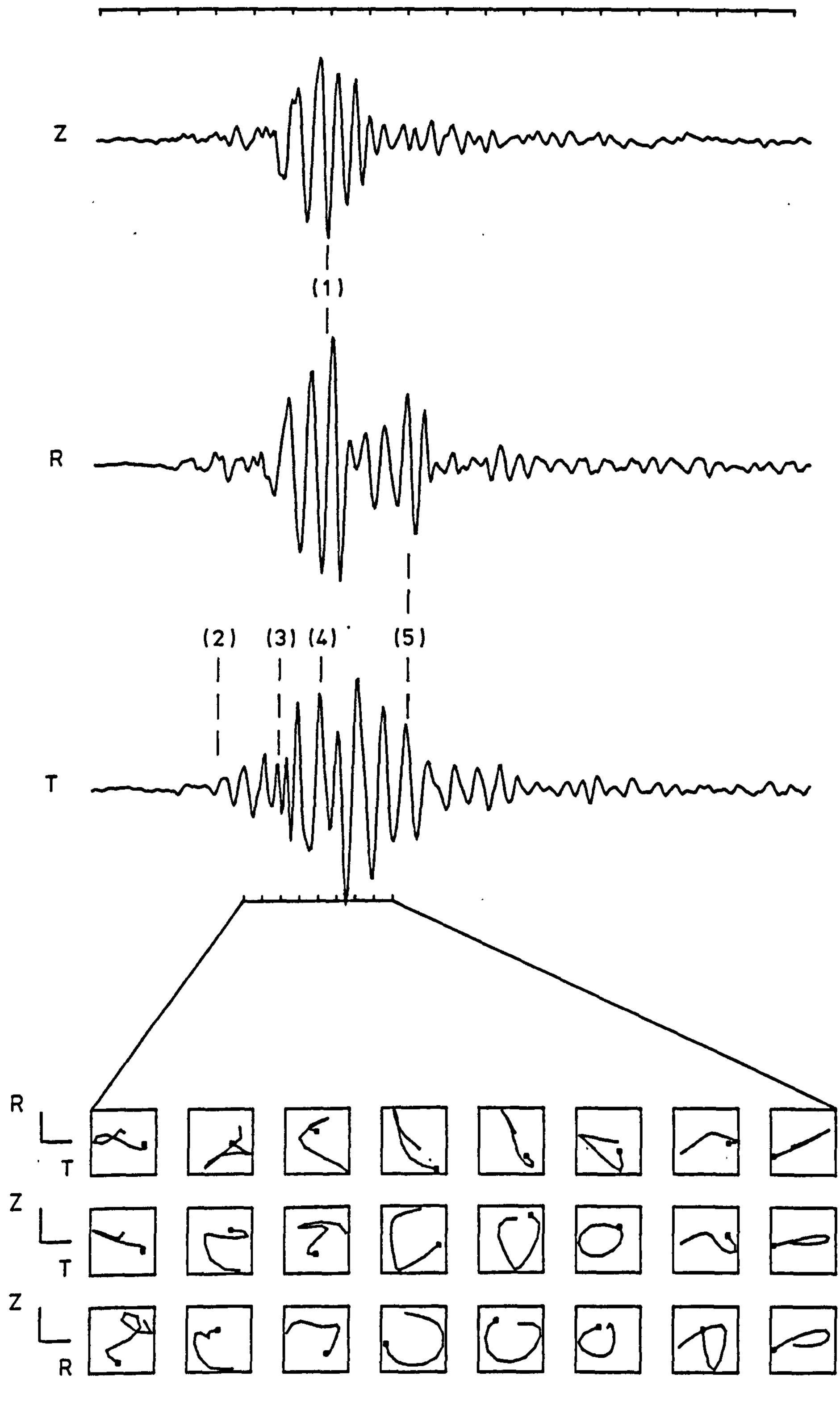
Z
(1)
R
(2)
(3)
(4)
(5)
T
R
T
Z
T
Z
R

with either of the radial or transverse components. Consequently, no information was given regarding purely horizontal motion, for example phase (5). This method confirmed the identification of phases (1) and (2) as the fundamental mode Rayleigh wave and the shear wave respectively. The directionality of the signal was also investigated using the correlator which showed that there was no lateral refraction of the Rayleigh wave at station ALL. The correlator is also useful in cases of a low signal-to-noise ratio where the noise on the individual components is random such as, for example, at station WNF. Again the identification of the Rayleigh wave was confirmed and no lateral refraction indicated.

Representative seismic sections from Brier Low Quarry are given in Figures 2.10, 2.11. Along the line LST 1 the surface wave packet consists of about five cycles and shows normal dispersion. The nature of the signal begins to change at RYS where it becomes extended in time. The southern stations show a high amplitude, short period arrival of velocity 2.9 km s^{-1} becoming prominant prior to the surface wave group. The change in signal between BAL and PHF is marked by the complete removal of the surface wave group at PHF. At WNF, however, the surface wave group can be discerned albeit with a low signal-to-noise ratio.

These observations would imply that the path traversed by the surface waves is not homogeneous with variations occurring between ALL/RYS and BAL/PHF. These changes in signal character correlate with mapped surface features; the Bonsall Fault zone and the change in facies from shelf to basinal limestones respectively.

Correlating the signal envelope maximum provides group velocities of 1.7 km s^{-1} and 2.5 km s^{-1} to the north and south of RYS respectively. The wave packet envelope also shows a shift to an

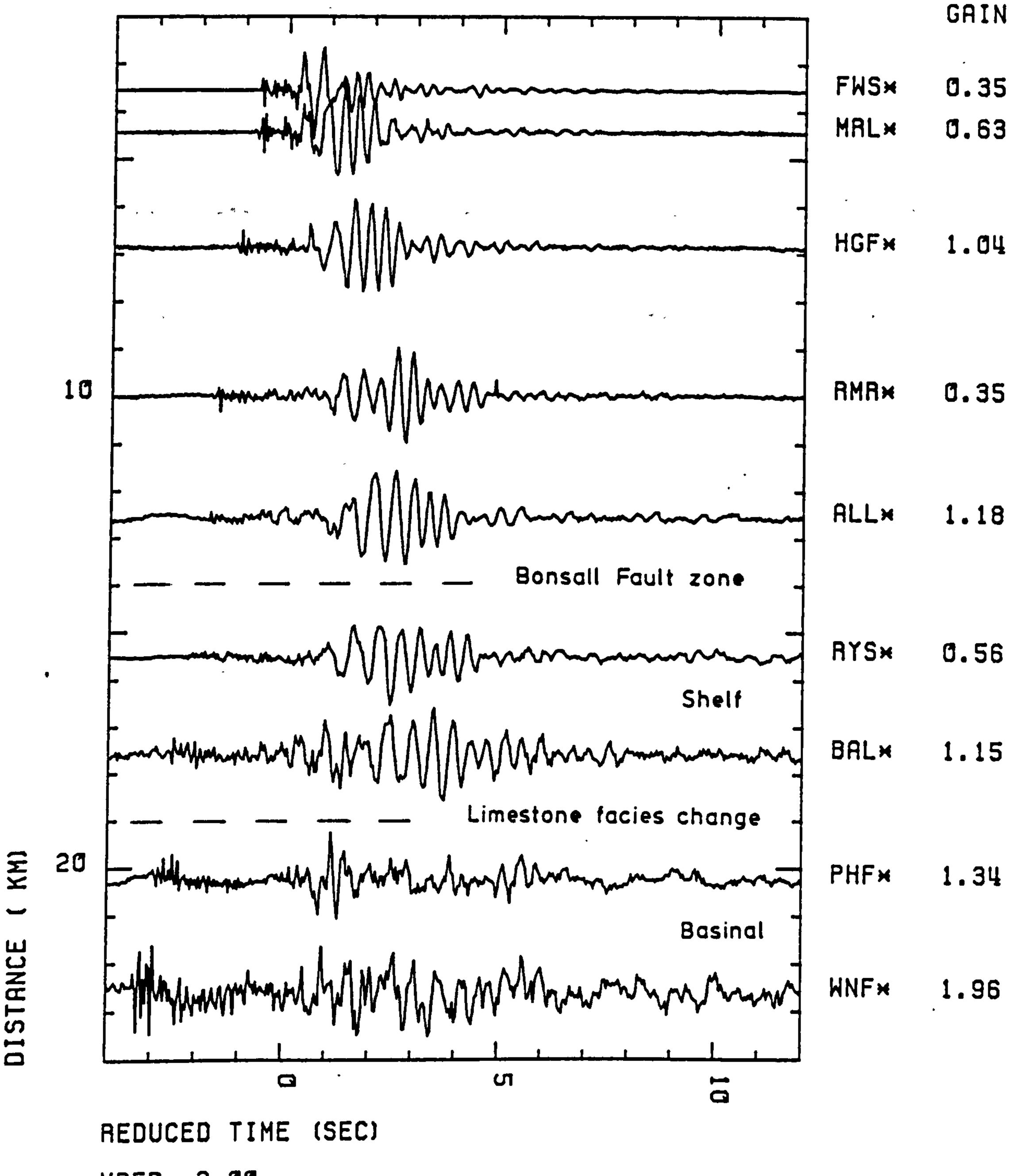

Figure 2.10 Reduced time seismic section for event F2522 in Brier Low Quarry recodred along LST 1. (Amplitudes for all seismic sections are normalised for display purposes.)

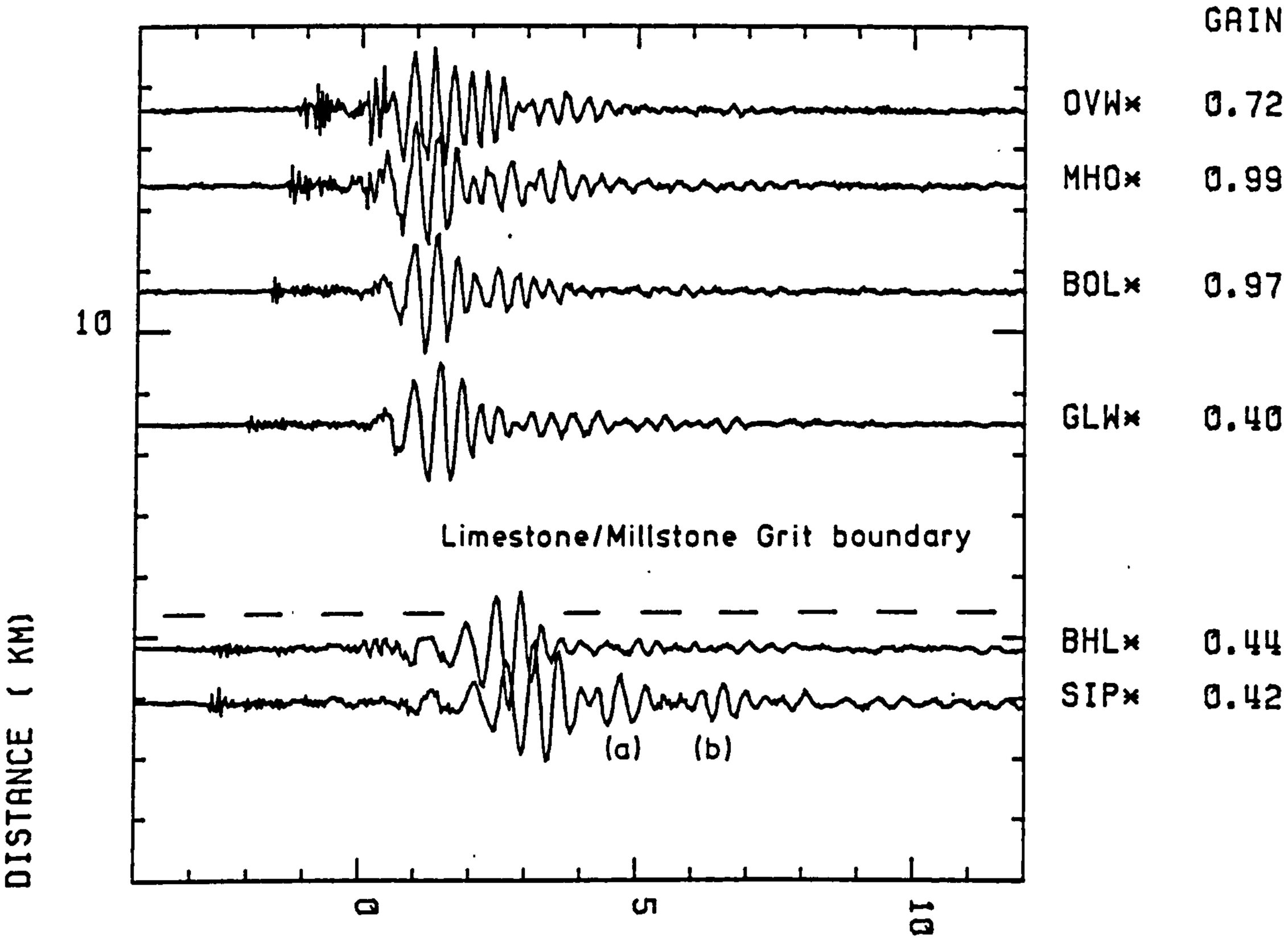

Figure 2.11 Reduced time seismic section for events F2522 in Brier Low Quarry recorded along LST 2. (The arrivals identified are discussed in the text.)

earlier arrival time at RYS.

The suite of seismograms for line LST 2 (Fig 2.11) shows a more consistent wave packet again displaying normal dispersion. Each packet consists of two or three cycles usually preceeded by a short period phase of lower amplitude. The shift in arrival time for stations BHL and SIP is marked and is a result of crossing the limestone/Millstone Grit boundary. Two later arrivals a) and b) identified on the record for SIP are possible lateral refractions.

Rayleigh wave group velocity estimates obtained from correlating the envelope peak are 2.6 km s^{-1} for the limestone and 1.1 km s^{-1} between the sites in the Millstone Grit at the southern end of the line. The velocity in the limestone is comparable to that given for the limestone of the southern part of line LST 1. Lithologically, however, the limestone of LST 2 is the same as that of the northern section of LST 1. The discrepancy between the surface lithologic units and corresponding velocities could indicate a change in sub-surface structure between the sections.

The consistency of the Brier Low events is shown in Figure 2.12 where signals from two events are compared.

2.4.2 The Millstone Grit District.

The design of the line MG 1 included two co-linear source quarries at the south of the line. Positioned on the boundary of the limestone shelf with the Millstone Grit, Hope Quarry was situated ideally to reduce the effects of lateral refraction caused by the change in lithology to a minimum. Very poor surface waves, however, were exhibited from events in this quarry (Fig 2.13). This may have been due to the short (1 ms) delays between holes or the smaller

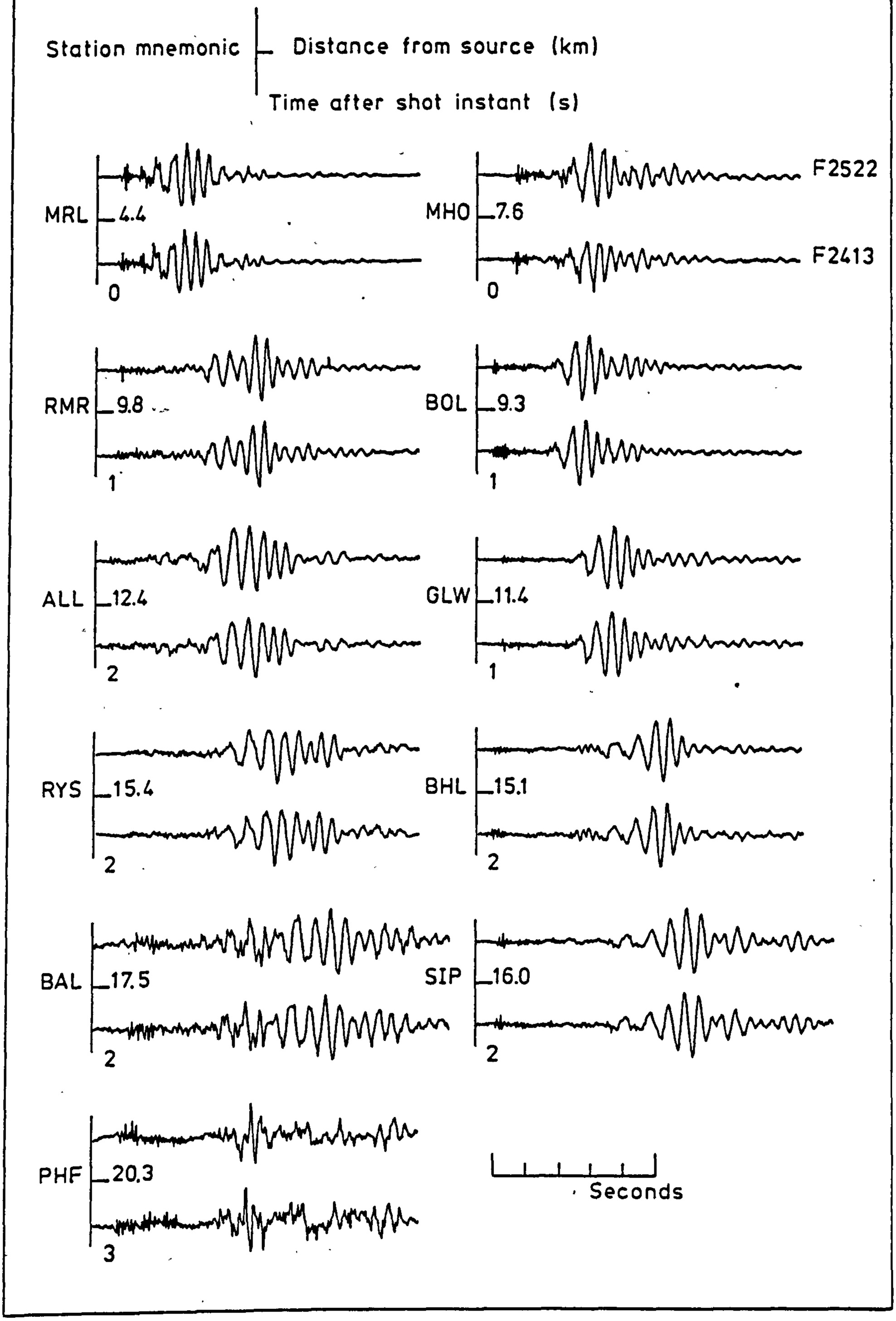

Figure 2.12 Comparison of the signals from two events in Brier Low Quarry recorded along LST 1 and LST 2 indicating the consistency of the records.

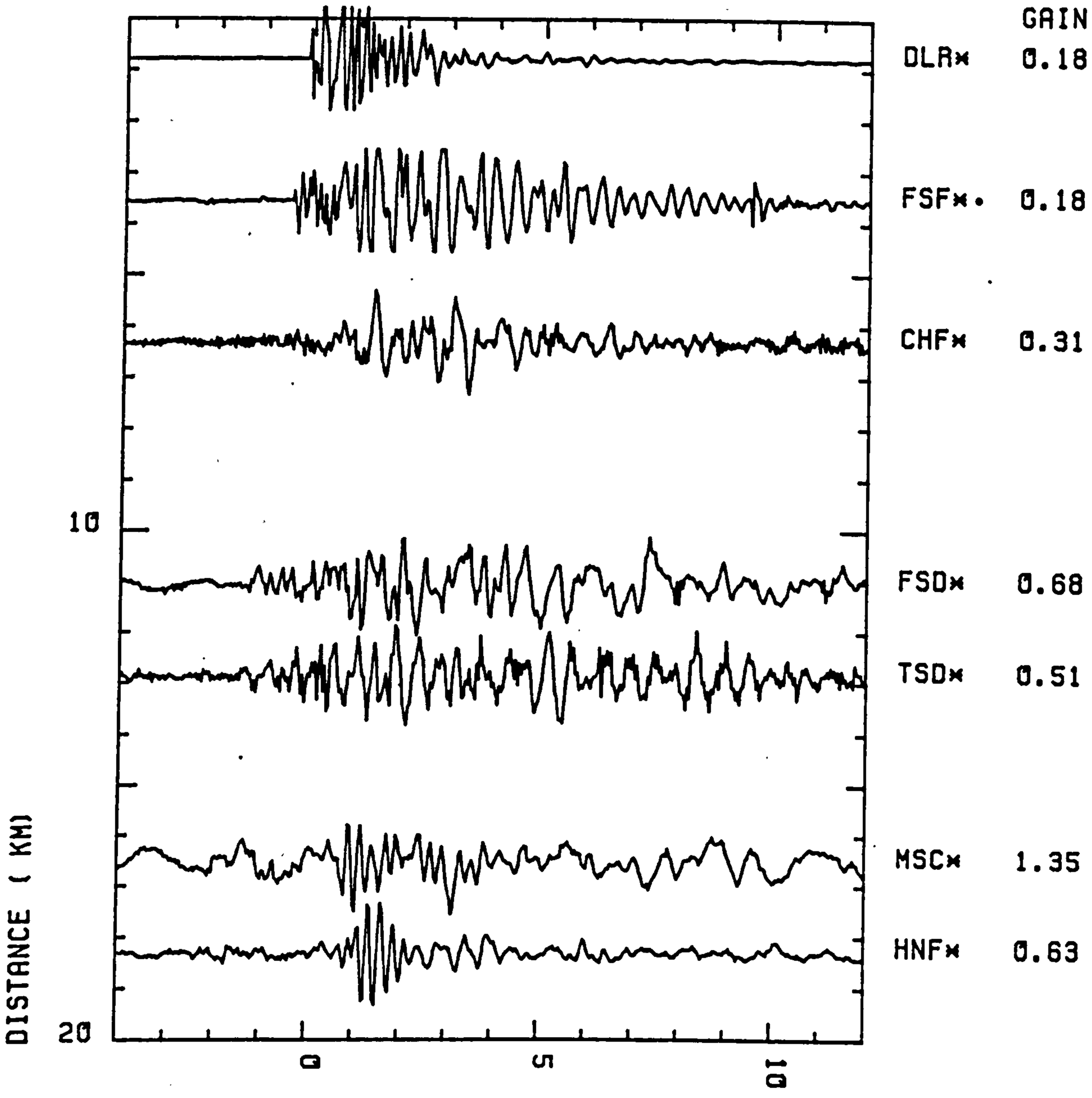

Figure 2.13 Reduced time seismic section for event F3617 in Hope Quarry recorded along MG 1 showing poor surface wave development.

overall size of the blasts. No events from Hope have been analysed in the investigation of anelasticity in the Millstone Grit district.

In contrast, seismograms recorded from events in Tunstead Quarry at stations along MG 1 showed similar characteristics irrespective of the nature of the individual blasts. These signals imply a consistency in the generation of surface waves at the source and also indicate the homogeneous nature of the Millstone Grit district. The main wavetrain was identified as the fundamental mode Rayleigh wave from particle motion studies (phase(1), Fig 2.14). The source used for the study of anelasticity in the Millstone Grit district was, therefore, Tunstead Quarry.

Shear and Love wave motion, phases (2) and (3) respectively (Fig 2.14), are shown on the transverse component. The slow, mainly horizontal motion seen previously in the signals over the limestone (phase (5), Fig 2.9) is absent from these records. The short period group on the radial component corresponding to phase (2) is a local or instrumental effect peculiar to the east-west horizontal instrument at station TSD; the vertical component is unaffected.

The particular combination of source character and transmission path through the Millstone Grit has resulted in longer periods within the wavetrain being more apparent than in signals from Tunstead over the limestone district (Fig 2.15). At the longest ranges a short period group preceeding the fundamental mode Rayleigh wave dominates the seismogram. This arrival may be a shear wave arrival or a higher mode Rayleigh wave. The body wave arrivals showed an increased short period component compared to signals in the shelf limestones and may indicate the response to a number of thin layers.

Rayleigh waves were more evident across MGAR (Fig 2.16). Two

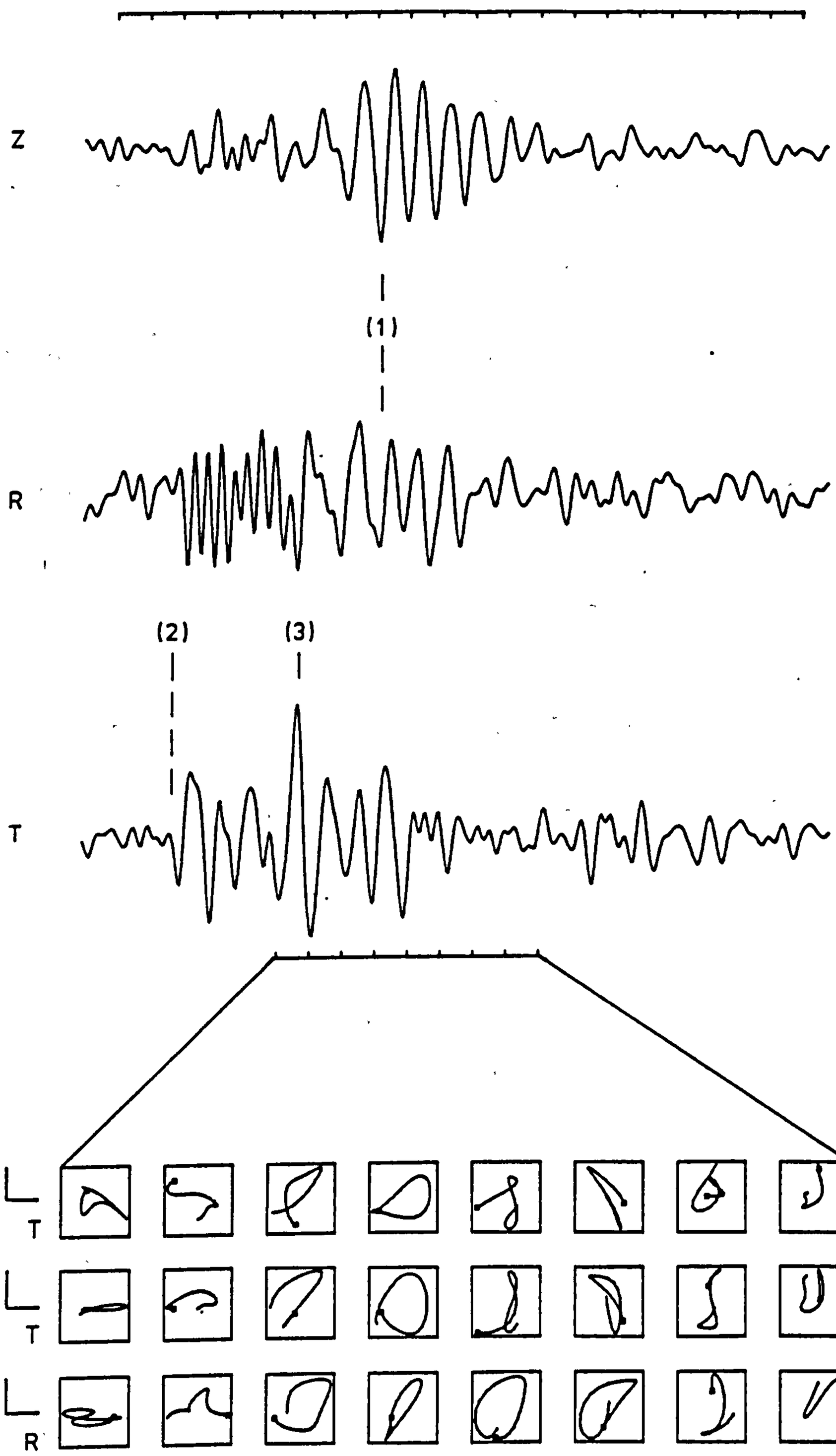

Figure 2.14 Particle motion plot for event F3418 in Tunstead Quarry recorded at station TSD. Gaussian filter has centre frequency 1.5 Hz and bandwidth ± 1.5 Hz. (Other characteristics of particle motion plot are as given in Figure 2.9.)

Figure 2.16 Comparisons of reduced time seismic sections for two events (F3230, F3223) in Tunstead Quarry recorded over MGAR. Signal types 1 and 2 depend on the position of the blast in the quarry.

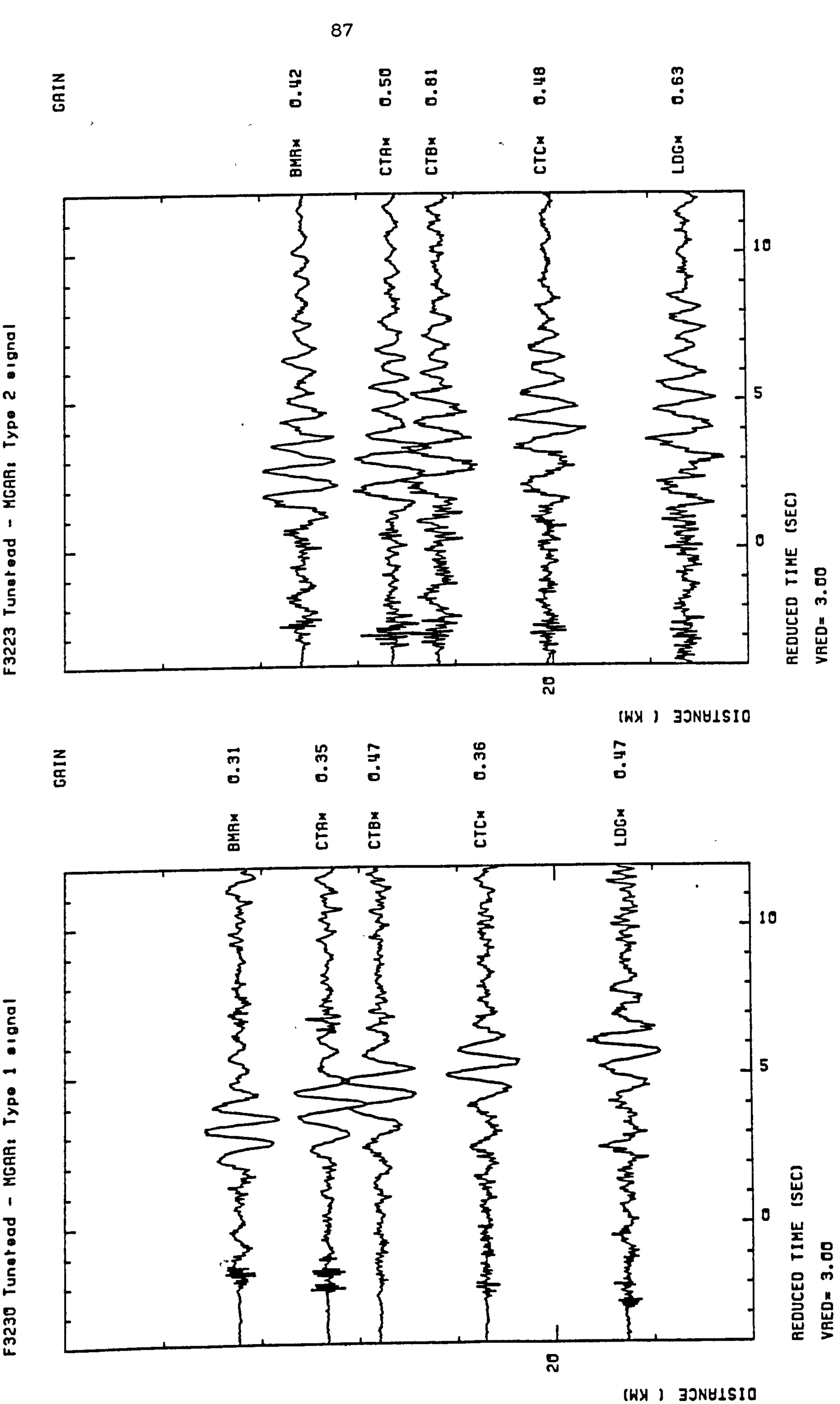
F3223 Tunehead - MGAR: Type 2 signal
GAIN
BMR× 0.42
CTA× 0.50
CTB× 0.81
CTC× 0.48
LDG× 0.63
0
5
10
20
DISTANCE (KM)
REDUCED TIME (SEC)
VRED= 3.00
F3230 Tunehead - MGAR: Type 1 signal
GAIN
BMR× 0.31
CTA× 0.35
CTB× 0.47
CTC× 0.36
LDG× 0.47
0
5
10
20
DISTANCE (KM)
REDUCED TIME (SEC)
VRED= 3.00

signal types were observed from events in Tunstead Quarry. A short group of three cycles and well shaped amplitude envelope, type 1, and a longer group containing four cycles showing less variation in amplitude, type 2. This contrasts with the signal similarity between events from Tunstead along MG 1. Details of the blasts indicated little correlation between signal type and size, orientation or firing sequence of the shot. The signal type, however, appears to have been influenced by the depth of the shot holes or the level in the quarry, the two being interrelated. The three cycle signal group was produced by shots fired at deep levels in the quarry in short 20 m holes. In contrast the longer wave group signals were generated by blasts at the quarry top (first lift) in 40 m holes.

Due to the nature of the signal it was not possible to correlate the peak in the amplitude envelope between the stations of MG 1. The observed wavetrain lay between velocities of 2.1 - 1.2 km s^{-1} being approximately 1.6 km s^{-1} at 1 s period. Over the cluster array, MGAR, a group velocity of 1.2 km s^{-1} was determined.

The stations of the array were, generally, less than one half wavelength apart permitting phase velocity to be estimated by correlation of the peaks in the signal. Circular wavefronts centred on the shot position were assumed. Phase velocity was then estimated by fitting a straight line to the arrival time against distance plot. For waves of approximately 1 s period a phase velocity of 1.65 km s^{-1} was determined.

The residuals between observed and calculated travel times show that the assumption of circular wavefronts centred on the shot point was invalid. A method has been given by Jacob (1969b) to obtain the phase velocity and azimuth of circular wavefronts over an array by

solving the linearised travel time problem using an iterative least squares method.

This technique yielded a phase velocity of 1.5 km s^{-1} over the array, lower than that given previously. The solution azimuth (station to source) was 250° which compares to the direct azimuth of 261° to Tunstead Quarry from station CTP. The arrivals have, therefore, been refracted into the array. The most likely cause is the boundary between the limestone and Millstone Grit which constitutes a lateral variation in velocity. A geometric ray construction indicated that the boundary near Stoney Middleton (GR 42360 37510) produced the refraction. Using Snell's law and angles measured from the construction gave a not unreasonable phase velocity of 2.0 km s^{-1} for the limestone when a phase velocity of 1.5 km s^{-1} for the Millstone Grit was assumed (Fig 2.17). Signals from the three component set at CTP were examined using the analogue signal correlator. Lateral refraction of both body and surface waves was indicated. The amplitude of the output signal corresponding to the Rayleigh wave was maximised for an azimuth of 240°, not too dissimilar from the value returned by the array processing method.

2.5 SUMMARY.

Within this chapter the rationale of the experiment design has been discussed together with the ensuing field experiments. The use of extended period (1.5 s) seismometers having gains increasing with distance from the source facilitated the recording of unclipped surface wave signals of good signal-to-noise ratio and of a maximum

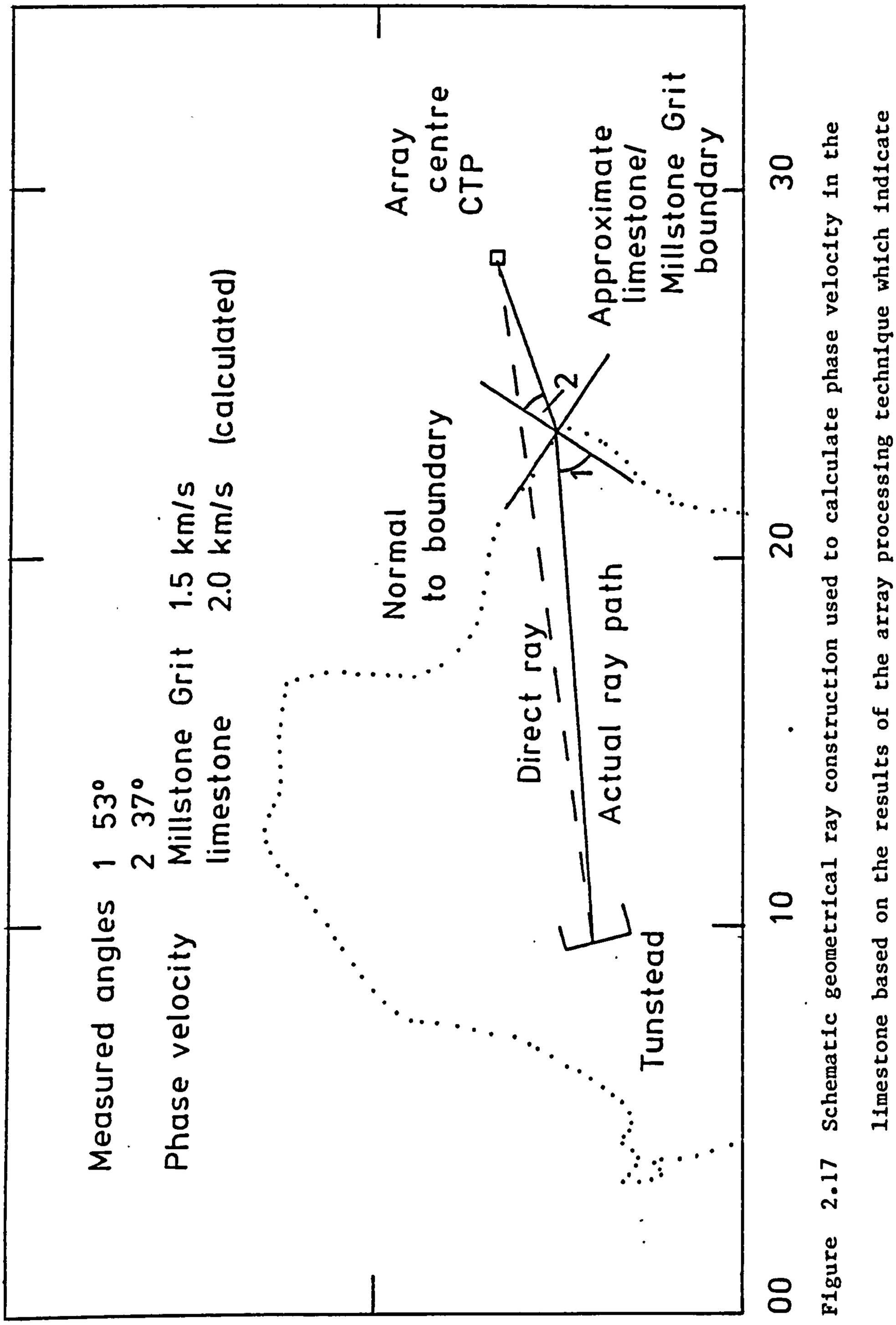

Figure 2.17 Schematic geometrical ray construction used to calculate phase velocity in the limestone based on the results of the array processing technique which indicate lateral refraction at the limestone/Millstone Grit boundary.

bandwidth.

Possible errors in timing and amplitude induced by the recording system or during data preparation have been investigated and corrections applied when necessary.

Observations and direct time domain measurements on the seismograms have provided results of geophysical significance. Events from Tunstead Quarry over the limestone district have indicated the dependence of the character of the recorded signal on the orientation of the source line to the main station line LST 1. Identification of the fundamental mode Rayleigh wave was confirmed by particle motion studies on a group of consistent signals from Brier Low Quarry. These signals also showed the limestone district to be less homogeneous than had been presupposed with changes in structure evinced by the change in Rayleigh wave signal character as it progressed across the Bonsall Fault zone and through the transition between shelf and basinal facies limestones. The change in signal was also manifest in the approximate measure of group velocity given as 1.7 km s^{-1} at 0.5 s period north of the Bonsall Fault zone and 2.5 km s^{-1} at 0.6 s period to the south.

Consistent signals showing no abrupt changes in character were observed from events in Tunstead Quarry over the Millstone Grit district. This indicates little structural variation over the district. The Rayleigh waves, again confirmed by particle motion studies, showed the Millstone Grit district to be essentially homogeneous having a typical group velocity of 1.6 km s^{-1} at a period of about 1.0 s.

These observations were used as an aid to the more detailed frequency domain analysis for group velocity dispersion and attenuation which is discussed in the following chapter.

CHAPTER THREE

ESTIMATES of DISPERSION and ATTENUATION from HIGH FREQUENCY RAYLIEGH WAVES

3.1 INTRODUCTION.

The advantages of analysing surface waves in the frequency domain have been mentioned in chapter 1. In particular, the failure of the stationary phase method at turning points in the group velocity dispersion curve is no longer a restriction on the analysis. Further, the anelastic parameters can be determined for a fixed series of harmonic frequencies rather than at the apparent periods seen on the seismograms. The correction for the instrument response is also facilitated more easily in the frequency domain.

The fundamental mode Rayleigh wave has been shown to penetrate the crust to an approximate depth of one wavelength. For a dispersed wave, then, each frequency will sample a slightly different average structure depending on the wavelength. A suite of observations of dispersion and attenuation for a range of frequencies will, therefore, contain information pertaining to different depths with different weights at particular levels.

Within this chapter we shall consider the methods used to obtain the anelastic parameters as functions of frequency. The time domain data presented in the previous chapter are transformed into the frequency domain by the Fast Fourier Transform (FFT: Cooley & Tukey 1965). A multiple filter technique is then applied to obtain group velocity dispersion (Dziewonski *et al*. 1969). Interstation

techniques are described and used to obtain the provincialised estimates of dispersion and attenuation presented; the analysis being guided by the earlier time domain observations.

3.2 DETERMINATION of ANELASTIC PARAMETERS.

3.2.1 The Determination of Group Velocity by the Multiple Filter Technique and the Calculation of Rayleigh Wave Spectra.

The multiple filter technique, reviewed by Dziewonski & Hales (1972), was used to determine group velocity dispersion from single seismograms. A computer programme, Time Series Analysis Programme (TSAP: Burton & Blamey 1972) which accomplishes the transformation of the seismogram into the frequency domain and the determination of group velocity has been modified by Evans (1981) to work with high frequency surface waves.

The multiple filter technique (Dziewonski et al. 1969) consists of filtering the signal by a number of narrow bandpass filters at pre-determined centre frequencies. It has been shown that the maximum of the filtered seismogram corresponds to the arrival time of the wave group with frequency equal to the filter centre frequency (Dziewonski & Hales 1972).

The group arrival time as a function of frequency can be determined using filters at a number of centre frequencies. Group velocity dispersion is computed from the arrival times if the event time and source to station distance are known.

The maximum of an oscillating waveform is more readily obtained from the maximum of the signal envelope. The chosen form of the envelope of the filtered seismogram is that used by Burton & Blamey

(1972) given by the instantaneous amplitudes determined from the modulus of the inverse Fourier transform of the filtered spectrum having first zeroed the negative frequency components (Fig 3.1).

Good resolution in the time domain can be achieved only at the expense of resolution in the frequency domain and vice versa; analogous to the uncertainty principle. The two domain problem of determining the group arrival time by filtering the spectrum at specific frequencies requires optimum resolution in both domains. To achieve this Gaussian filters of the form

$$\exp\left[-\alpha\left(\frac{\omega - \omega_n}{\omega_n}\right)^2\right], \qquad (3.1)$$

were used where α describes the filter roll-off

ω_n is the centre frequency.

These filters were of constant quality factor (the ratio of peak frequency to bandwidth) and therefore had different pass bands for each centre frequency. Dziewonski et al. (1969) stepped in constant intervals of logarithmic period between successive centre frequencies assigning the group velocities to the harmonic frequency nearest to the centre frequency. Burton (1973, 1974), however, introduced a linear step in frequency which sets the filter centre frequencies to be multiples of the fundamental frequency at which the spectral amplitudes are determined. Evans (1981) has indicated that this change in frequency step should be accompanied by a change in the form of the filter. The appropriate form is, however, inconvenient as it would attempt to include negative frequencies and so the Gaussian was retained introducing a variation in the frequency resolution with centre frequency.

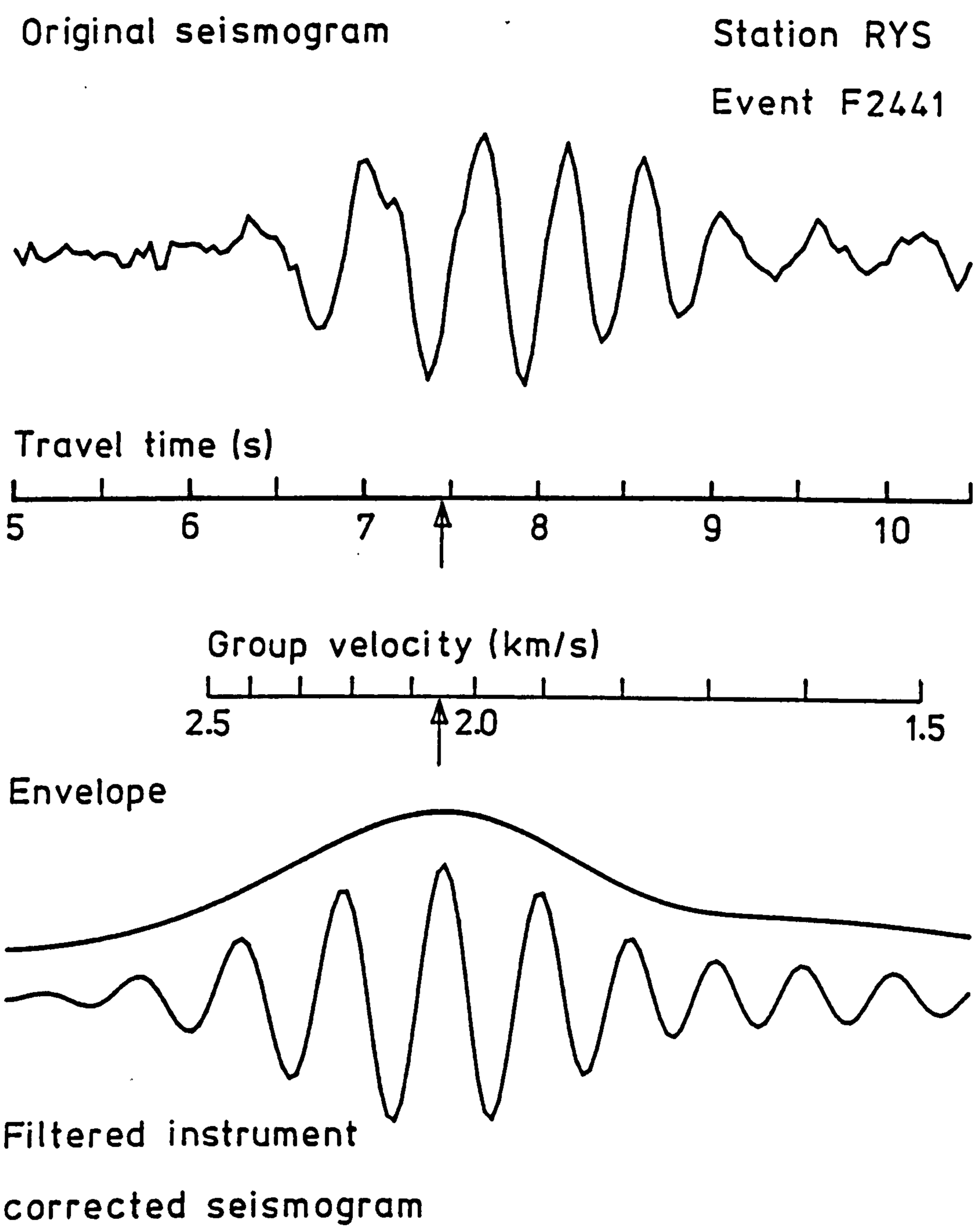

Figure 3.1 An example of narrow bandpass filtering to obtain group arrival time and hence group velocity. (The determination of the chosen envelope is described in the text.)

Prior to the multiple filter analysis the seismogram, in a suitable form had to be transformed into the frequency domain. Initially, a time window having broad velocity limits was used to separate the Rayleigh wave from the seismogram. This signal was then baselined to a zero mean. Eight points at either end were cosine tapered to reduce the Gibb's phenomenon and square wave effect (Båth 1974, p31, Burton & Blamey 1972). To fulfil a requirement of the Fast Fourier Transform (FFT: Cooley & Tukey 1965) the signal length was increased to 2^L points where L is an integer. For all the seismograms used L = 9 giving 512 points. By keeping L constant all the spectra were quoted at the same harmonic frequency points which were integer multiples of the fundamental frequency $\Delta\nu$

$$\Delta\nu = \frac{1}{2^L \, \delta t} = 0.049 \text{ Hz.} \qquad (3.2)$$

The adjusted signal was then transformed into the frequency domain and the instrument response removed by complex division. At low frequencies the apparent instrument magnification, calculated theoretically, was very small producing a false increase in the amplitude of low frequency harmonics. To limit this effect frequencies below 0.39 Hz were removed from the spectrum by assuming the spectral harmonic amplitudes to be zero below this frequency.

Possible filter parameters were investigated by examining the effects of varying them on a number of typical seismograms, the objective being to obtain the best resolution. The roll-off, α, was set to 31 with the band-limits of 0.62 ω_n - 1.38 ω_n. At these limits the Gaussian filter is at 1/85 of its peak value and

for ease of computation was assumed to be zero outside these limits.

The instantaneous amplitudes of the filtered signal envelope as a function of group velocity rather than time are stored as one column of a two dimensional matrix with each column corresponding to a different filter centre frequency. To regularise the grid formed by this matrix the envelopes were sampled by interpolation at intervals of 0.05 km s^{-1} between the upper and lower velocity limits of the seismogram. This energy matrix forms the basis of the frequency-time analysis (FTAN) diagram of Levshin et al. (1972). To produce the FTAN diagram the energy matrix is normalised to 99 dB and contoured between 60 dB and 95 dB with an interval of 5 dB. The noise and component phases in the signal may be separated on the basis of frequency content and velocity by this frequency-time analysis. This separation cannot be achieved only by analysis in either of the domains separately. Although the physical observables are the arrival times at different distances, group velocity was used in the FTAN diagrams to enable the direct comparison of the dispersion observed at different stations for the various propagation paths.

For a noise free signal consisting of only Rayleigh wave energy there is usually a single maximum of instantaneous amplitude for each frequency. This would be indicated by a simple ridge in the contours of the FTAN diagram. To obtain the group velocity, in this case, it would be sufficient to search each column of the energy matrix for the maximum value and to assign its corresponding velocity to be the group velocity of that frequency. A more robust approach, however, is required when considering real data. Evans (1981) employed a ridge seeking procedure to ensure that a continuous ridge of local maxima was chosen to be the dispersion

curve. For each frequency a parabola was fitted to the point of maximum energy and the velocity point on either side of it; the maximum of this parabola was then taken to be the group velocity. The search then moved to the point with equal velocity at the adjacent frequency. This procedure was also used in this study but because it proved not to be totally reliable the FTAN diagram was always examined to confirm the dispersion analysis.

Increasing each seismogram to 512 points, by the addition of zeros to the trailing end of the seismogram, overdefines the resulting spectrum. This implies that the number of frequency values could be reduced with no loss of information from the Rayleigh wave frequency content. The input signal was approximately 1/4 x 512 points in length, although this varied with distance from the source, and consequently the spectrum was smoothed to provide the amplitude at every fourth frequency value, that is at integer multiples of 0.195 Hz. The complete range of frequencies used was from 0.59 - 5.9 Hz yielding 28 spectral amplitude points. Reliable group velocities were not obtained over this entire bandwidth which was designed to extend beyond the Rayleigh wave frequency content.

Systematic errors in the group velocities determined by the multiple filter technique can be caused by a significant amplitude spectral gradient which invalidates the assumption that the amplitude and wave-number of the signal within the filter bandwidth can be described by a first order Taylor expansion (Dziewonski & Hales 1972). To reduce the effect of spectral gradients Dziewonski et al. (1972) introduced a 'residual dispersion technique' whilst Godlewski & West (1977) pre-whitened the spectrum prior to analysis. In this study no such modifications were made. Evans (1981) shows, however, that the systematic errors in velocity introduced by the

multiple filter technique may amount to 2% approximately. Other systematic errors caused by timing, instrument correction and location, for example, were minimised during data preparation.

A further source of error may be caused by the interference of other phases with the fundamental mode Rayleigh wave. At close ranges the separation between the shear wave, higher mode surface waves (if present) and the fundamental mode Rayleigh wave arrivals is small. A condition for the resolution of two arrivals on a FTAN diagram has been given by Herrmann (1973). This condition together with reported values of first higher and fundamental mode velocities in the Carboniferous of the Midland Valley of Scotland (MacBeth 1983) show the two modes are separated adequately at distances greater than 12 km. This distance was within the range of the experiments described here implying some degree of interference was possible which was assessed by considering distant records and comparing them with closer stations. Both shear wave and higher mode arrivals may be distinguished on the FTAN diagram by their velocity and frequency content; the shear wave appears as a high velocity, non-dispersed ridge with broad frequency limits whilst higher modes are frequency limited but of higher velocity than the fundamental.

For some frequencies arrivals preceeding the fundamental may be of higher energy levels than the Rayleigh wave resulting in the ridge seeking procedure returning a false dispersion curve. In this case a large scale plot of the FTAN diagram with posted energy values was obtained. The preferred dispersion curve was then drawn by hand and the corresponding group velocities picked for each frequency.

To ensure the choice of the true dispersion curve particle motion plots were used to determine the extent of the Rayleigh wave

motion. Comparison with dispersion curves at adjacent stations provided additional information for the choice of the preferred ridge. By using distant stations and progressing to closer records the effects of interference were reduced. The ridge search was restricted to a closed pattern of contours or to contours having a similar trend to a closed pattern to further reduce the effects of noise and unwanted phases.

Major discontinuities in the phase spectrum can indicate the presence of lateral refractions in the signal. The existence of multi-pathed arrivals can also be assessed from the FTAN diagram. These appear as ridges of similar trend to that of the fundamental mode arrival but at lower overall velocities. Comparison of adjacent station analyses can assist in the removal of lateral refractions.

With perfect data it would be sufficient to use the instrument corrected spectrum, determined prior to the multiple filter analysis for group velocities, as the amplitude spectrum of the fundamental mode Rayleigh wave. During the determination of group velocities an extended signal was used to eliminate edge effects in the FTAN diagram contouring. The amplitude spectrum of this extended signal does not represent the true spectrum because of the inclusion of extraneous phases and noise.

To isolate the Rayleigh wave and hence obtain the true spectrum a window with revised velocity limits was used. The group velocity dispersion curve was used to define the time window of the revised signal. The velocity limits were taken to be the minimum and maximum velocities at the 85 dB contour level enclosing the dispersion curve. The corrected, smoothed amplitude spectrum of this revised signal was taken to be that of the fundamental mode

Rayleigh wave. Group velocities were also calculated as a check on the repeatability of the mid-portion of the preferred dispersion curve away from edge effects.

Alternatively, spectral amplitudes could be obtained by using time variable filtering (Dziewonski & Hales 1972). Filters, applied to time windows symmetric about the dispersion curve, are used to improve estimates of the true spectral amplitude by removing the effects of interfering phases or noise at frequencies not expected for a dispersed Rayleigh wave in a particular time window. This method was not used, however, in this study; the isolation of the fundamental mode Rayleigh wave and its spectrum being achieved adequately by the use of the revised window about the signal having first determined the group velocities.

To ensure that no data were lost by prejudgement of the signal bandwidth all the analyses discussed above were conducted between 0.59 Hz and 5.9 Hz. The true bandwidth of the signal was determined from the analysis of the revised signal. The low frequency effect produced by removing the instrument response imposed the lower limit. The true upper frequency limit was determine by assessing the onset of incoherent noise. In many cases this is marked by a distinct 'kink' in the phase spectrum (Burton 1973). Where this criterion could not be applied the frequency at which the amplitude dropped to the obvious noise level was taken to be the upper limit.

3.2.2 Determination of Provincial Rayleigh Wave Dispersion and Attenuation.

The true physical quantity measured from seismograms is that of group arrival time rather than velocity. Further, Knopoff (1969)

states that the apparent group slowness is the distance weighted average of the group slownesses of the individual provinces comprising the propagation path. The quantity slowness which is linear in time should, therefore, be determined in preference to velocity.

By utilising blasts at repeated positions within a given quarry averaged observations of dispersion and attenuation could be obtained together with their empirical standard deviation over what is essentially the same path between each station and the quarry.

Group slowness at each frequency for the individual source to station paths was obtained by taking the arithmetic mean of the reciprocal of group velocity over the number of events observed at the particular station.

The number of observations contributing to a particular average group slowness value could vary between frequency points because of the change in signal bandwidth or instrument malfunction. This may produce steps in the dispersion curve. These were removed by a two stage process after Evans (1981). For the point where the step occurred a small correction was added to the slowness to make the slope between it and adjacent points the average of the gradients immediately above and below the step. The second stage consisted of applying a weighted, five point running mean to the entire curve. This smoothing removes any residual corners left by the first stage removal of steps in the curve.

These smoothed, average group slowness curves were taken to be the best estimates of the dispersion caused by the individual source to station propagation paths.

These individual curves were then used to determine the average slowness over the provinces traversed by the station lines. This

was achieved by an interstation technique. For each frequency the relative group arrival times were calculated and plotted against distance. For each station the arrival time was calculated from the averaged source to station slowness using the distance to the station averaged over the number of events. The gradients from a least squares fit to the relative arrival time-distance data gave the average slowness at that frequency together with its statistical uncertainty. Circular wavefronts were assumed and corrected for by the use of direct source to station distances rather than interstation distances.

This technique required data from at least three stations to give reliable estimates of the group slowness together with the uncertainties. The resulting group slowness curves were again smoothed according to the scheme above and were taken to be the best estimates of group slowness over the different provinces.

Amplitude data alone are sufficient to provide estimates of $\gamma(\nu)$. The dimensionless specific attenuation factor Q_γ^{-1} is, however, a more meaningful quantity in the present context as it allows direct comparison of the anelastic properties of different geologic provinces by correcting for their varying velocity structures.

Consider the instrument corrected form of equation (1.23). By restricting the azimuthal variation the source term may be reduced to a constant such that

$$A(r,\nu) = K\, r^{-1/2} \exp\left[\frac{-\pi\nu r}{U(\nu)}\, Q_\gamma^{-1}(\nu)\right], \tag{3.3}$$

or in logarithmic form (Burton 1974)

$$\log A + \tfrac{1}{2}\log r = -Q_\gamma^{-1}(\nu)\left[\frac{\pi\nu r}{U(\nu)}\right] + \log K', \qquad (3.4)$$

which is a straight line of gradient $-Q_\gamma^{-1}$ for each frequency. A similar expression has been used by Tryggvason (1965) and Tsai & Aki (1969) in earlier determinations of attenuation.

A least-squares straight line fit to the observed data for each frequency point provides estimates of Q_γ^{-1} as a function of frequency together with statistical uncertainties. (A similar relation for γ may be obtained by substituting for Q_γ^{-1} from equation (1.21) in equation (3.4)).

The simple linear regression used to estimate the gradients to give either group slowness or $Q_\gamma^{-1}(\nu)$ assumes that the ordinate contains all the error. This is a reasonable assumption if (Burton 1973)

$$a^2 e(X_i) \ll e(Y_i), \qquad (3.5)$$

where a is the gradient of the straight line

$e(X_i)$ is the relative error in the abscissae

$e(Y_i)$ is the relative error in the ordinate.

For the estimates of group slowness

$$e(X_i) \sim \frac{\delta r}{r} \quad \text{and} \quad e(Y_i) \sim \frac{\delta t}{t} \sim \frac{\delta U}{U}.$$

The accuracy of location of ±0.5 km (max) and distances of the order of 15 km gives $e(X_i) \sim 0.03$. Timing errors due to processing have been minimised but errors in velocity from the multiple filter technique give $e(Y_i) \sim 0.05$. As the slowness is in general less

than one, expression (3.5) is satisfield during the dispersion analysis. For Q_γ^{-1} the expression is satisfied since a < 0.1, that is Q_γ^{-1} is unlikely to exceed 0.1, and $e(X_i) < e(Y_i)$ since the group arrival times are measured to greater accuracy than the amplitudes.

Repeated events in one quarry can also be used to provide average values of $Q_\gamma^{-1}(\nu)$ with statistical uncertainties over each province. The varying size of the blasts produces different absolute amplitudes recorded at a given station. The amplitude-distance data for each event had, therefore, to be treated individually in contrast to the group slowness curves which were averaged prior to the arrival time-distance analysis. Provided that the azimuthal variation can be limited and assuming similar propagation paths then individual estimates of $Q_\gamma^{-1}(\nu)$ can be combined because Q_γ^{-1} is given by the gradient of the amplitude-distance analysis as shown by equation (3.4) and not by the overall level of the regression line. The Q_γ^{-1} at a given frequency for all events, therefore, were averaged following a scheme which uses the regression co-efficients of the individual lines and given as the computer programme QBAR by Burton (1973). The data were smoothed according to the scheme described earlier for the group slowness estimates to reduce the effects of variations in the number of events used to obtain any given Q_γ^{-1} datum.

3.3 ESTIMATES of OBSERVED DISPERSION and ATTENUATION.

3.3.1 The Carboniferous Limestone District.

The frequency domain analysis described above was used to obtain

estimates of the anelastic parameters over the Carboniferous Limestone district from events in Brier Low Quarry. A total of 55 seismograms, having a high signal-to-noise ratio, recorded by the lines LST 1 and LST 2 were analysed to provide these estimates (see section 2.4.1).

Two stations of LST 1 have not been included in the analysis. Station FWS was too close to the source to display adequate dispersion of the phases. The anomalous signals recorded at station PHF (see section 2.4.1) resulted in this station also being excluded from the analysis. The frequency-time analysis exhibited a narrow, high energy ridge extending across the frequency bandwidth (Fig 3.2). The ridge seeking algorithm followed this ridge returning a velocity of 2.5 km s^{-1}. (In this section values of velocity refer to manipulations of the multiple filter analysis or direct measurements from the frequency-time analysis. Group slowness, however, is reserved exclusively for estimates of dispersion over the provincial propagation paths.) Only at frequencies below 2.5 Hz does the ridge broaden to a plateau of energy level 90 dB. No dispersion curve consistent between events could, however, be determined. The frequency bandwidth and sharpness of the ridge are a consequence of the pulse-like high amplitude arrival which corresponds to the shear wave.

In comparison the FTAN diagram for station RYS shows a well defined ridge of energy levels 80 dB to 95 dB with normal dispersion between 0.75 Hz and 4.0 Hz (Fig 3.3). This ridge has been traced successfully by the search procedure. The lowest frequency point is distorted by edge effects and at higher frequencies the algorithm has moved onto a higher velocity ridge which has larger values of instantaneous amplitude at these frequencies. Inspection of the

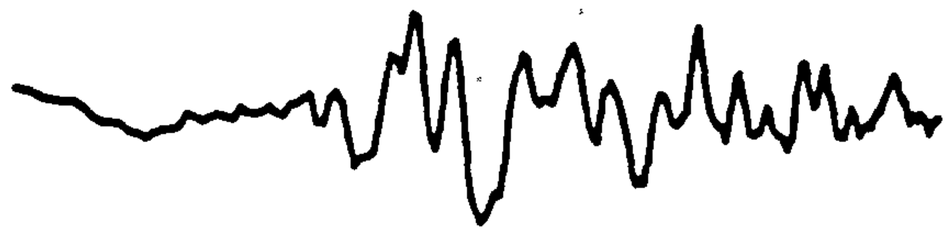

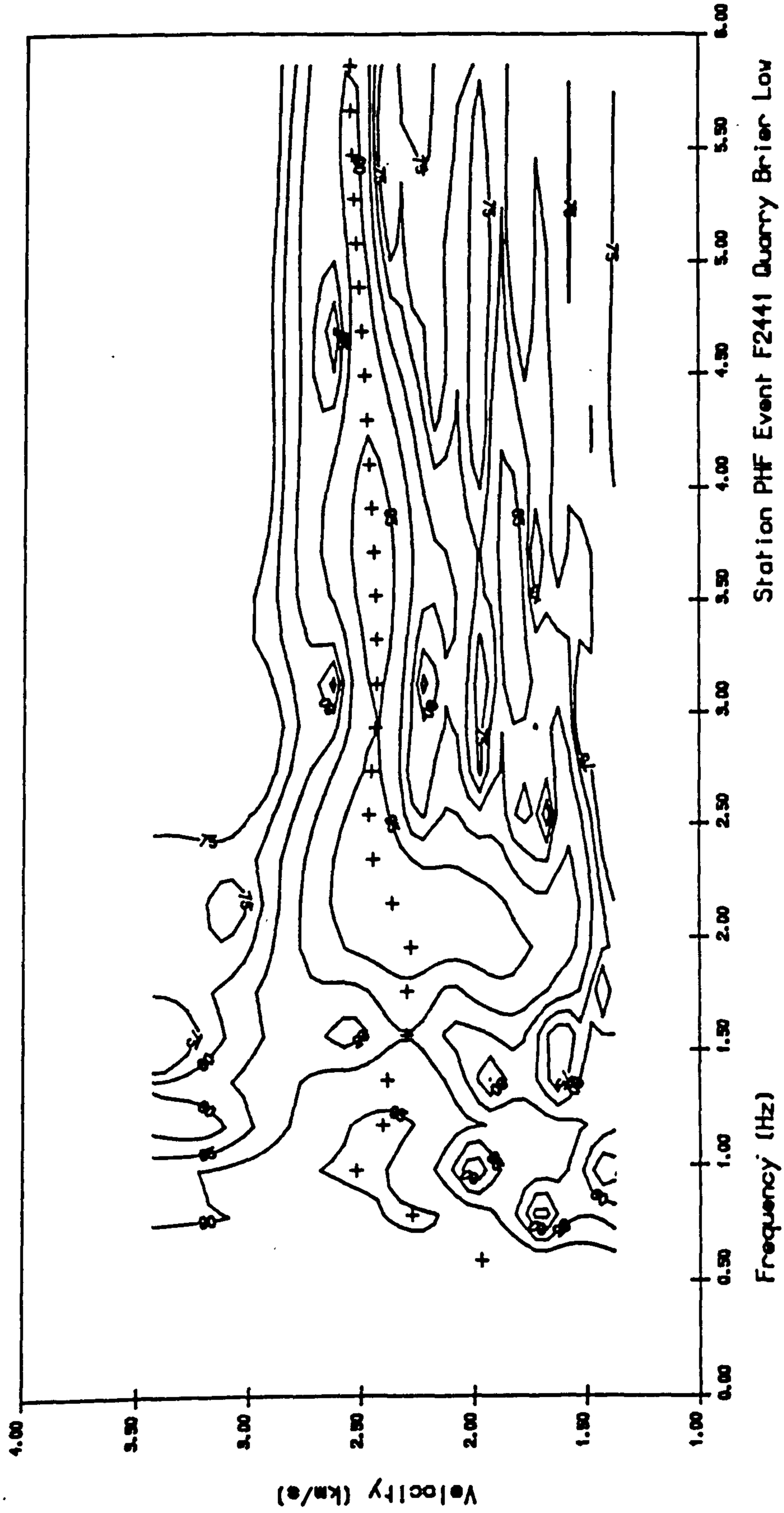

Figure 3.2 Frequency-time analysis diagram for the signal recorded at PHF from event F2441 in Brier Low Quarry. (Contoured between 75 - 95 dB at 5 dB intervals.)

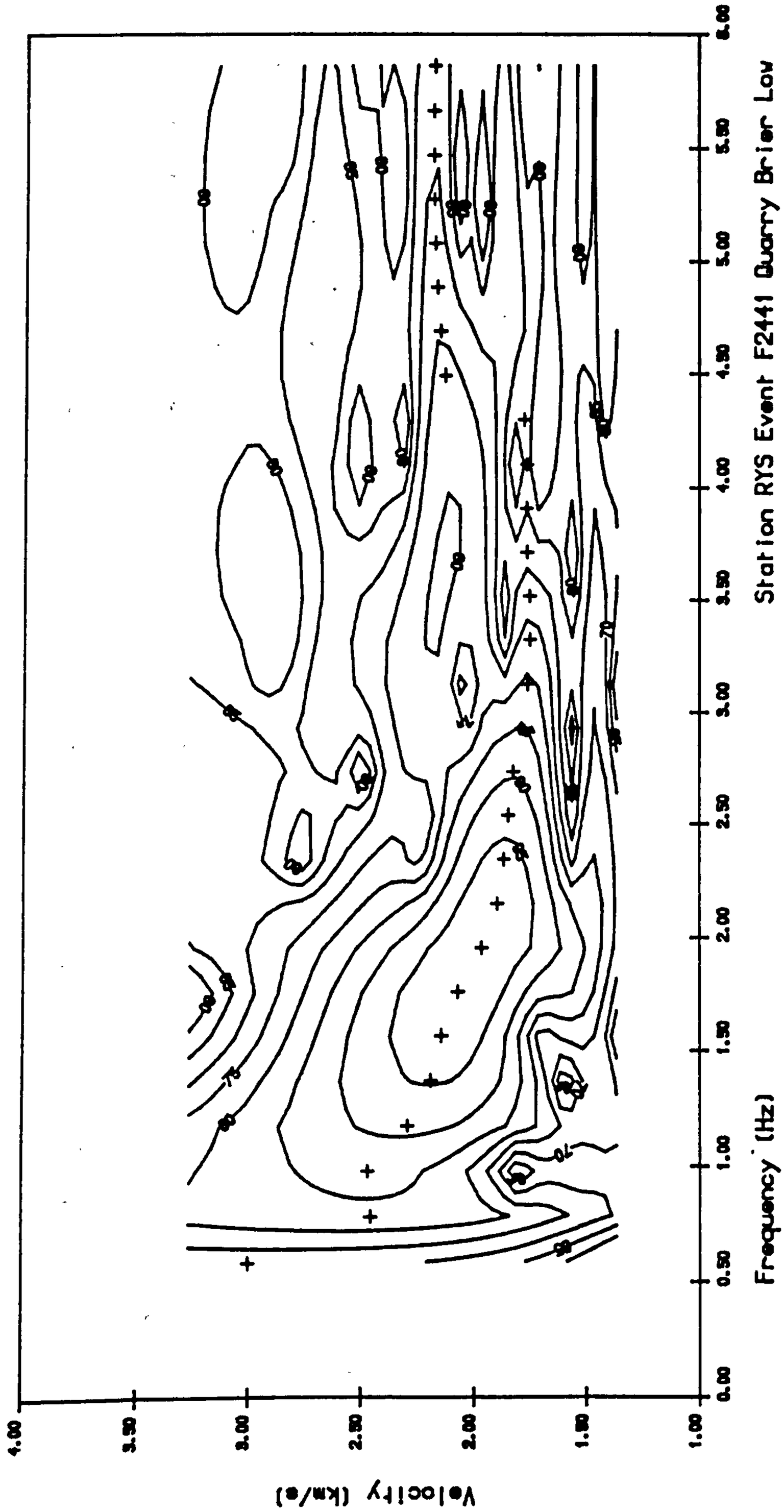

Frequency-time analysis diagram for the signal recorded at RYS from event F2441 in Brier Low Quarry. (Contoured between 60 - 95 dB at 5 dB intervals.)

Figure 3.3

individual energy values enabled a continuous, undistorted curve to be followed.

For most frequency-time analyses the individual energy values had to be inspected to determine reliable dispersion curves undistorted by interfering phases or edge effects. The resulting suite of prefered dispersion curves were examined to obtain the revised signal time windows from which the amplitude spectra of the Rayleigh waves were calculated. By this method phases preceeding or following the fundamental mode were excluded from contributing to the spectrum. Interfering phases within the Rayleigh wave signal could not be removed by this method. Such phases, including lateral refractions, have been shown not to be prevalent in the Rayleigh wave signal implying that the use of revised time windows does not increase the error in subsequent amplitude determinations.

The choice of window varied between stations and events depending on the signal-to-noise ratio. For LST 1 the maximum velocity used was 2.8 km s^{-1} with a minimium of 1.1 km s^{-1}. For LST 2 higher values of 3.1 km s^{-1} and 1.5 km s^{-1} respectively were used reflecting the higher velocities observed in the time domain along LST 2.

It was found that the averaged, individual source to station dispersion curves grouped into discrete families exhibiting similar dispersive characteristics. The differences between the family groups correlated directly with certain geologic features and corroborated the division of the district into smaller provinces suggested by the time domain observations of section 2.4.1.

These differences were also indicated by the arrival time-distance analysis where perturbations in the trend of the arrival times with distance were shown (Fig 3.4). For LST 1 a

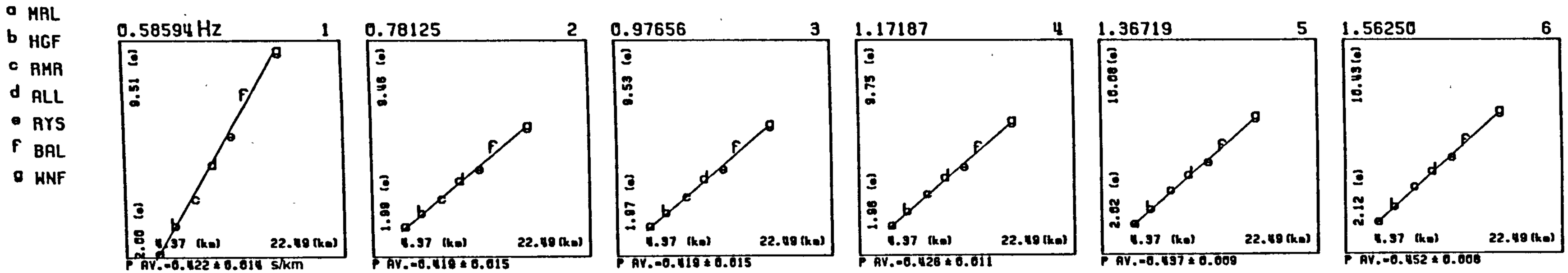

Figure 3.4 Group arrival time against distance for representative frequencies along lines LST 1 and LST 2. Note especially the perturbation in the arrival time at RYS of LST 1 and BHL of LST 2.

perturbation was seen between stations ALL and RYS correlating with the Bonsall Fault zone. Along LST 2 the marked change in slope for stations BHL and SIP is a direct result of crossing the boundary between the limestone and the Millstone Grit of the Stanton Syncline.

As a consequence the limestone district, assumed previously to be homogeneous, was divided into smaller provinces of different dispersive character and geologic structure. For both lines therefore, three estimates of group slowness have been made using the arrival time-distance technique. An average curve was determined along the entire length of each line with secondary curves being obtained for each province contributing to the line. The complete station groupings together with their identifying mnemonics are given in Table 3.1.

The observed group slownesses are given in Figures 3.5, 3.6 and tabulated together with the other estimates of anelastic parameters for the individual provinces in Appendix B. Slowness varies between 0.42 s km^{-1} to 0.49 s km^{-1} for the district average PLST 1 with normal dispersion indicated between 0.6-2.7 Hz. For PLST 2, the values exhibit a greater range between 0.39 s km^{-1} and 0.56 s km^{-1} again indicating normal dispersion.

The provincial curves show considerable differences to the district averages although the low frequency estimates of slowness for the three curves of LST 1 are similar being between 0.41-0.43 s km^{-1} at 0.6 Hz. The standard deviations on the slowness estimates for the provinces closer to the source are, in general, smaller than for the district averages indicating an improved fit to the observations when the lines are divided into discrete geologic provinces. For PLST 2S no estimates of the error in the dispersion

TABLE 3.1 Staion Groupings and Mnemonics

Group mnemonic	LST 1	LST 1N	LST 1S	LST 2	LST 2N	LST 2S
Station	MRL	MRL	RYS	OVW	OVW	BHL
	HGF	HGF	BAL	MHO	MHO	SIP
	RMR	RMR	WNF	BOL	BOL	
	ALL	ALL		GLW	GLW	
	RYS			BHL		
	BAL			SIP		
	WNF					

Group mnemonic	MG 1	MGAR	BMR
Station	FSF	LDG	BMR
	CHF	CTP	
	FSD	CTA	
	TSD	CTB	
	MSC	CTC	
	HNF		

LST 1 Carboniferous Limestone district line 1
LST 1N Carboniferous Limestone district line 1 northern province
LST 1S Carboniferous Limestone district line 1 southern province
LST 2 Carboniferous Limestone district line 2
LST 2N Carboniferous Limestone district line 2 northern province
LST 2S Carboniferous Limestone district line 2 southern province

All observations made over the limestone district are from sources in Brier Low Quarry

MG 1 Millstone Grit district main line
MGAR Millstone Grit district cluster array
BMR Single station observations from station BMR

All observations made over the Millstone Grit district are from sources in Tunstead Quarry

Parameter prefixes: P observed group slowness data (s km^{-1})
Q observed specific attenuation factor for Rayleigh waves, $Q_\gamma^{-1}(\nu)$, data.

Hence PLST 1N is the group slowness data set from the northern province of line 1 over the Carboniferous Limestone.

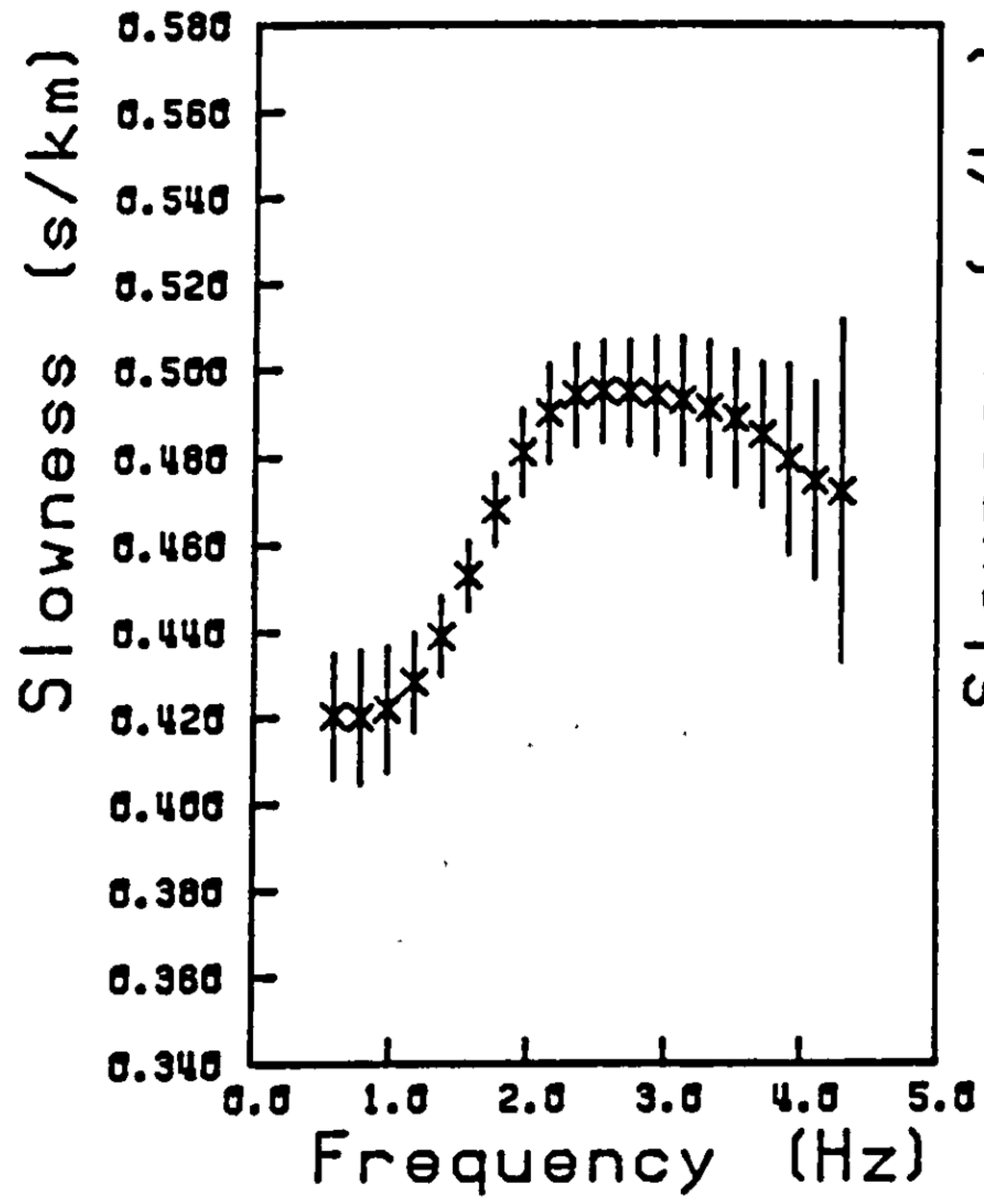

PLST 1

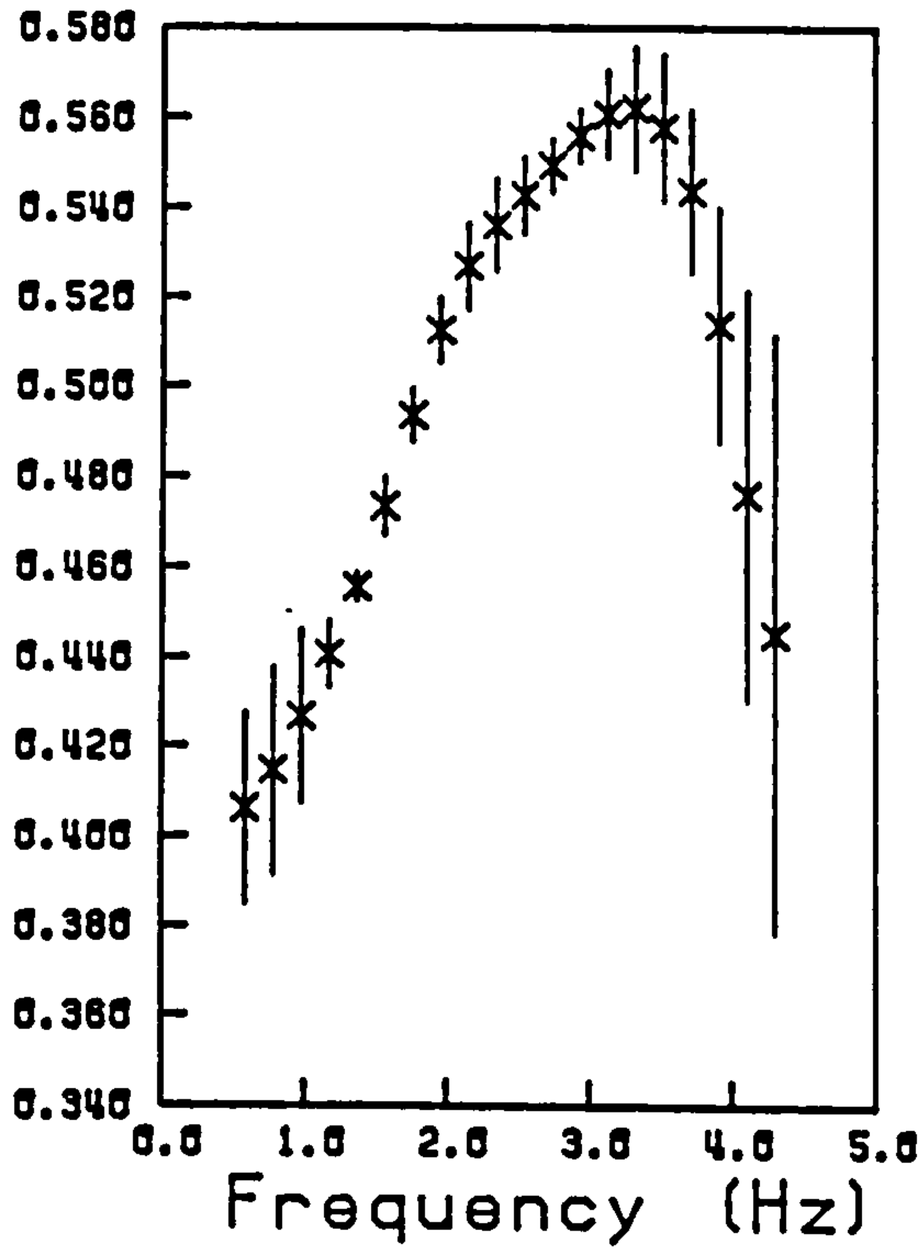

PLST 1N

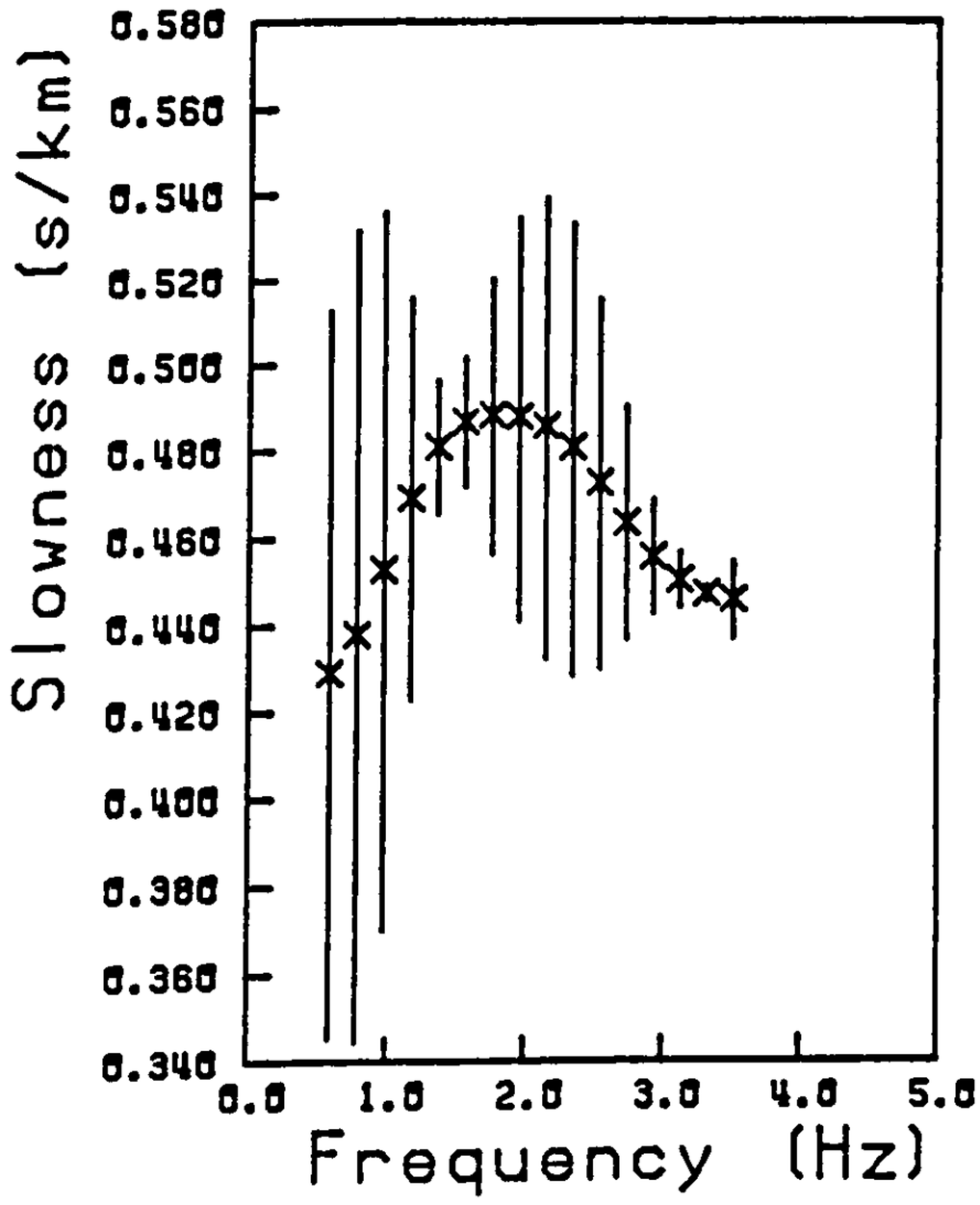

PLST 1S

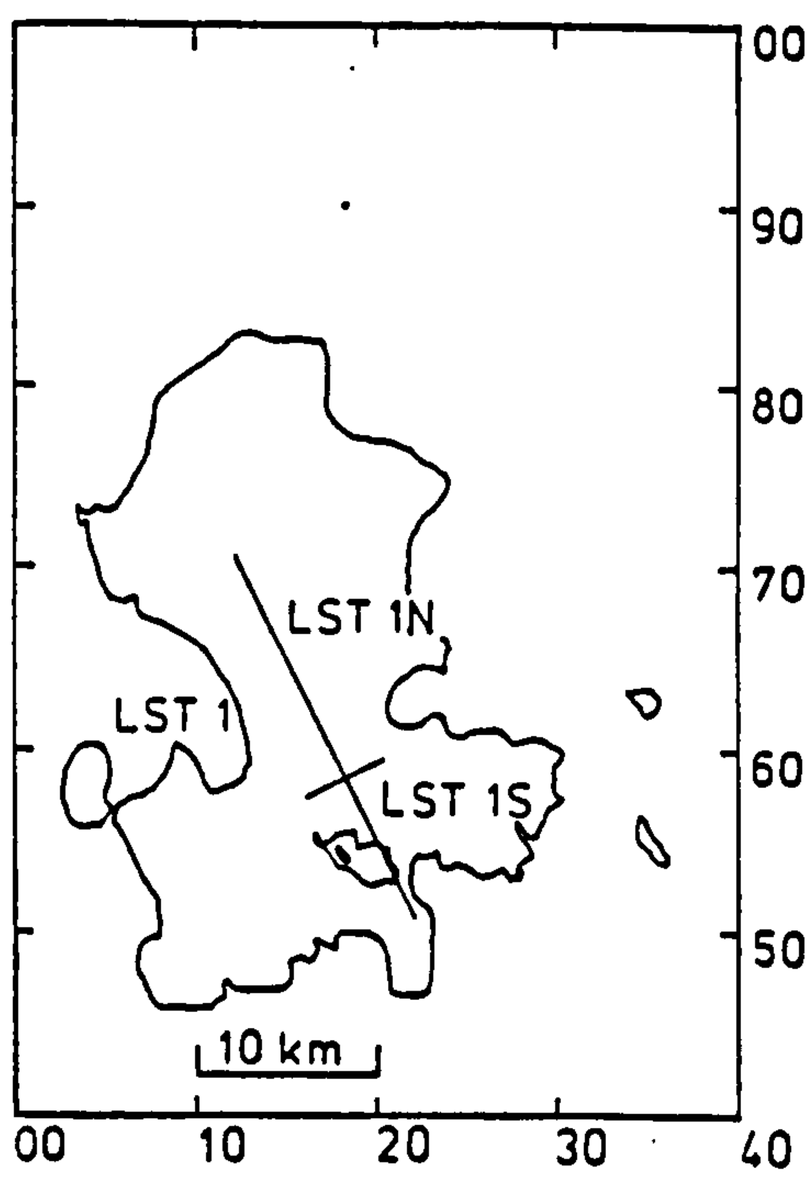

Figure 3.5 Rayleigh wave group slowness determined along the entire line LST 1 and for the component provinces LST 1N and LST 1S.

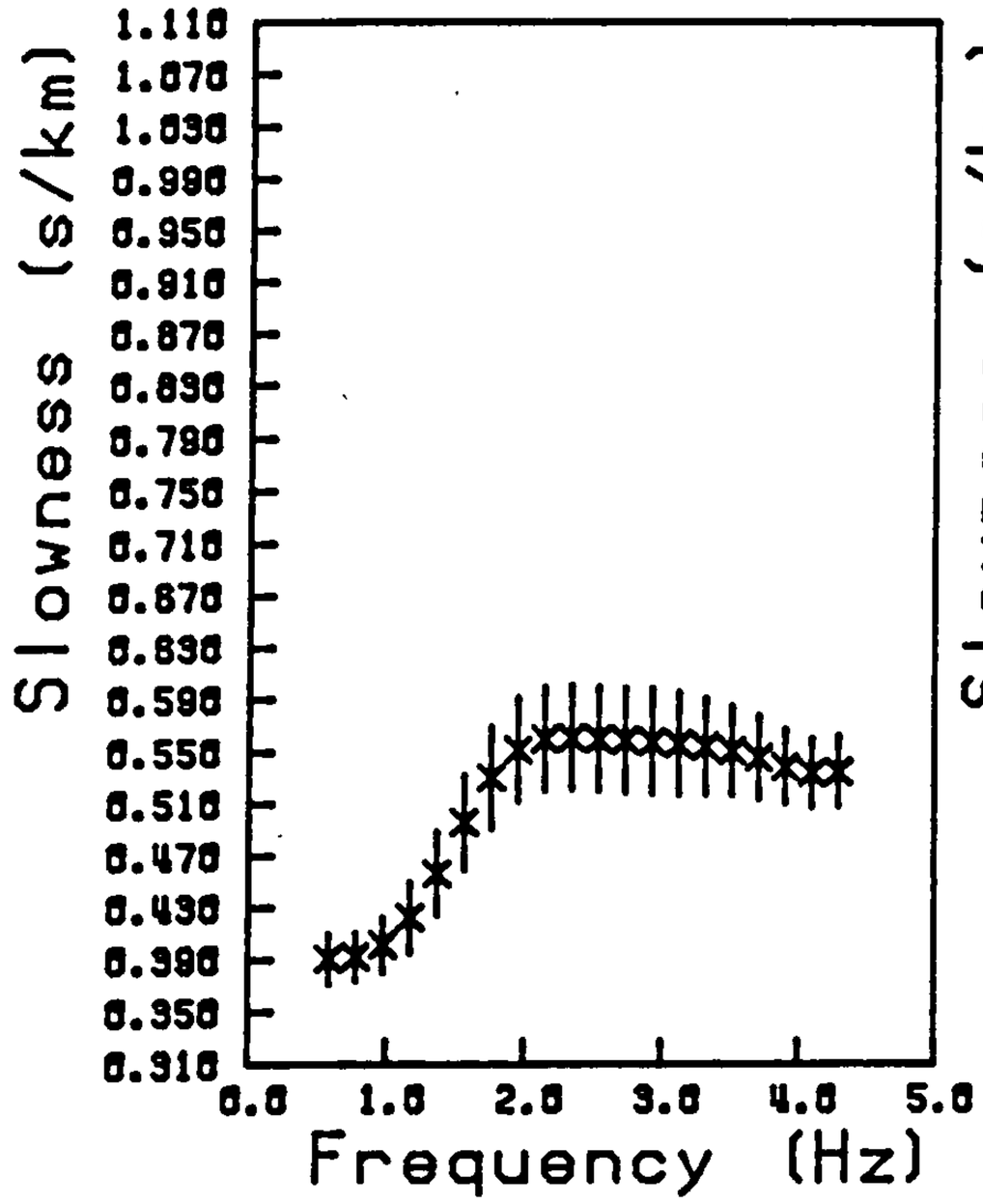

PLST 2

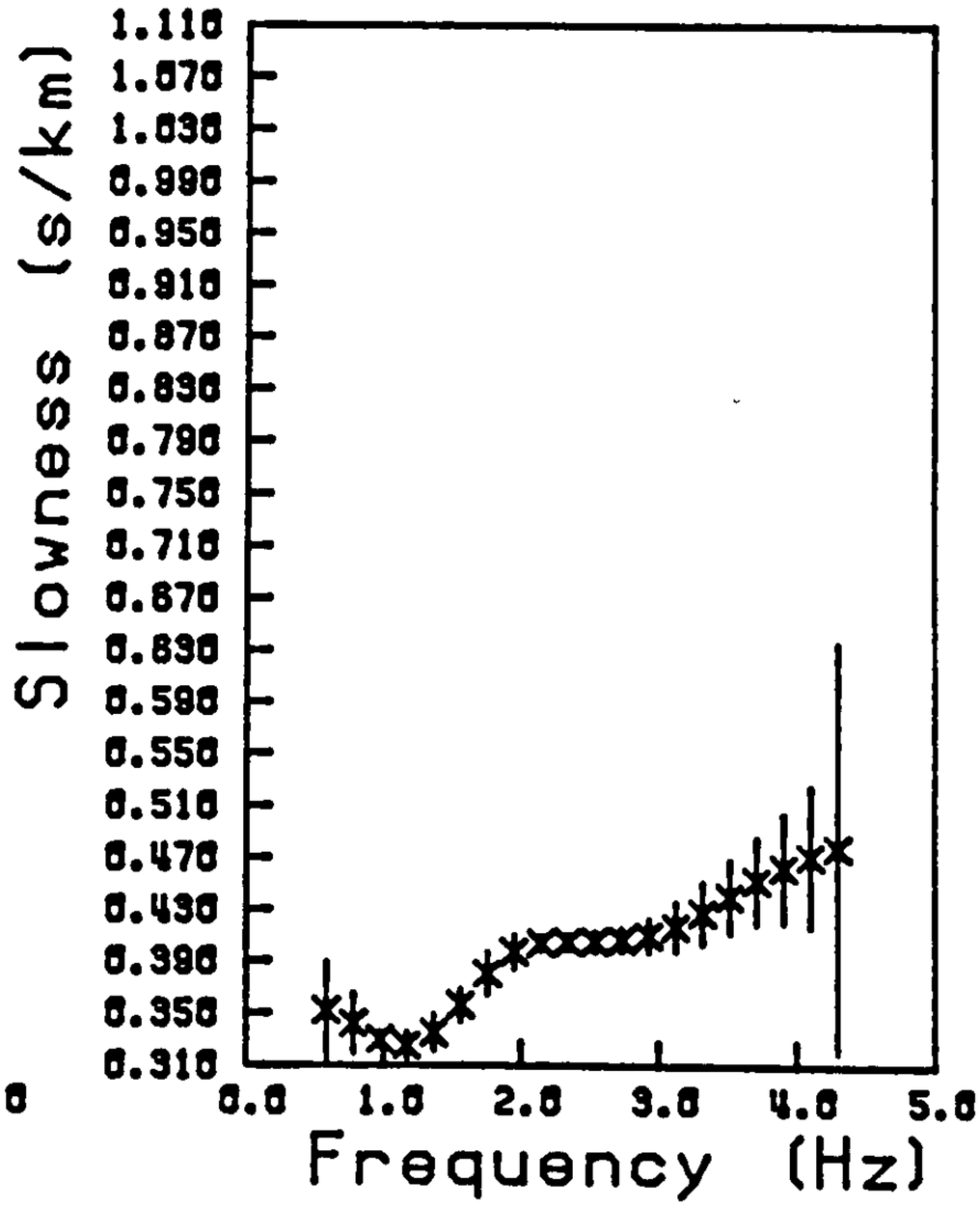

PLST 2N

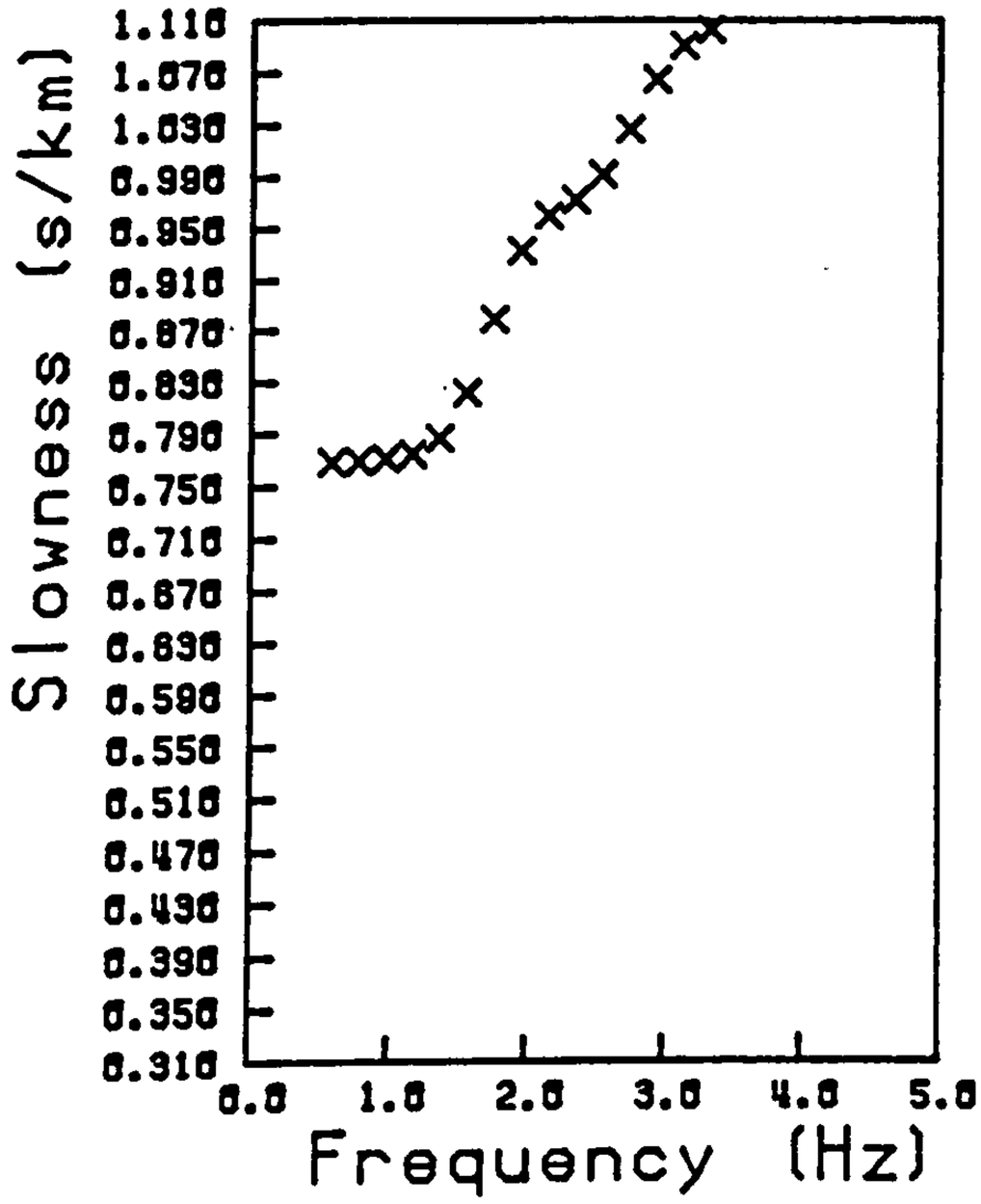

PLST 2S

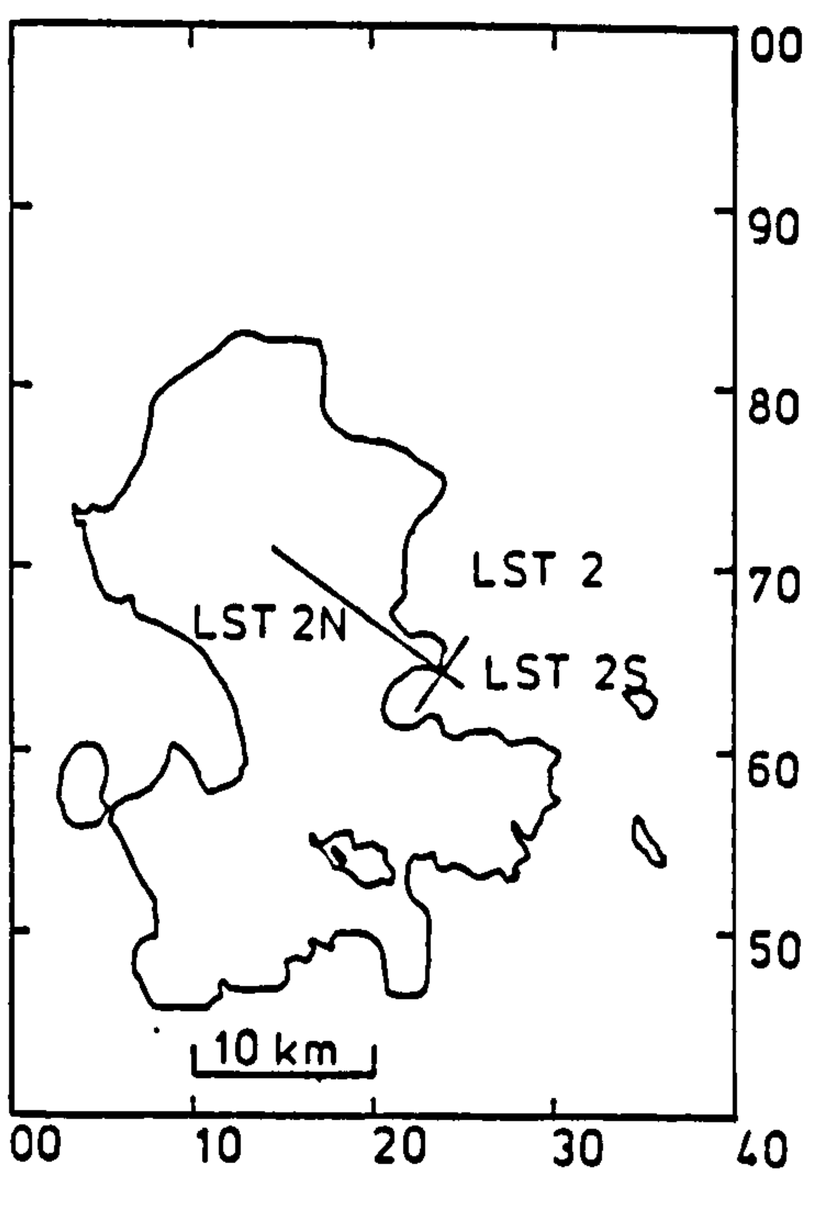

Figure 3.6 Rayleigh wave group slowness determined along the entire line LST 2 and for the component provinces LST 2N and LST 2S.

curve were obtained from the arrival time-distance analysis as this province contained only two stations.

Observations in the two southern provinces could have been affected seriously by the occurrence of lateral refractions caused by propagation across either the Bonsall Fault zone or the limestone/Millstone Grit boundary. No evidence for such effects was found in signals over LST 1S from the particle motion analysis, analogue signal correlation methods or from the existence of major discontinuities in their phase spectra. The opportunity of using particle motion studies did not exist in LST 2S as no three component set was available in that province. The arrivals identified earlier (Fig 2.11) as lateral refractions were excluded from any analysis and no discontinuities were observed in the phase spectra implying that there was no lateral refraction present in the signals analysed to obtain PLST 2S.

The maximum frequency in the signal was shown to decrease with distance along the line LST 1 from 4.5 Hz at station MRL to 3.5 Hz at the furthest station WNF. In contrast, the upper frequency observed along line LST 2 remained reasonably constant at 4.5 Hz dropping only slightly at stations BHL, SIP. The shorter length of LST 2 compared to LST 1 may account for this almost constant bandwidth. These values of maximum frequency varied slightly from event to event indicating some dependence on the nature of the source but the decrease in the highest frequency exhibited along LST 1 was always shown. Representative amplitude spectra for LST 1 and LST 2 are given in Figures 3.7, 3.8.

Along LST 1 the frequency and magnitude of the peak in the amplitude spectra, in general, decreases with distance. At the lower frequencies, however, the amplitudes are of similar

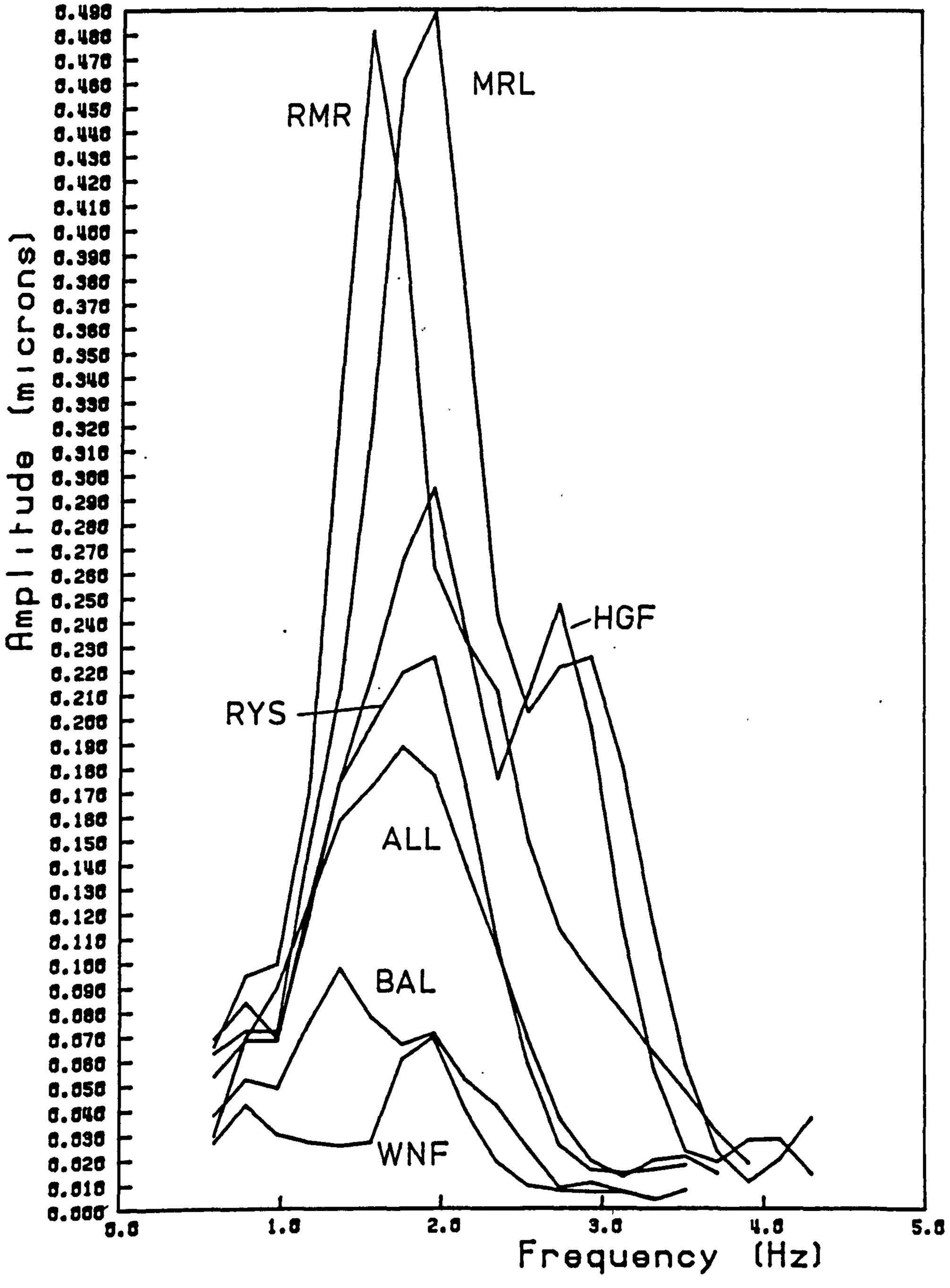

Instrument corrected amplitude spectra

Figure 3.7 Instrument corrected, smoothed amplitude spectra for stations of LST 1 from event F2441 in Brier Low Quarry.

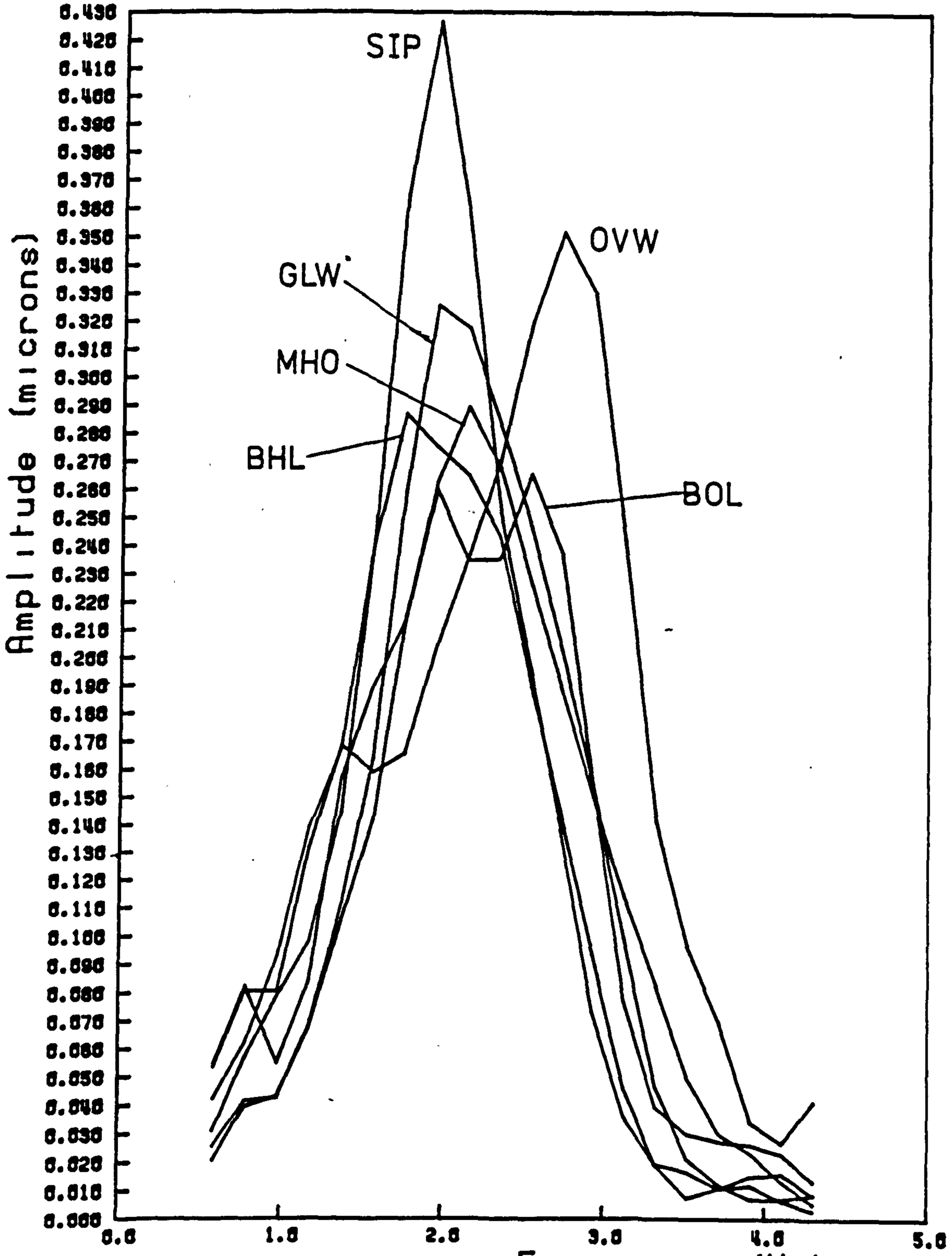

Figure 3.8 Instrument corrected, smoothed amplitude spectra for stations of LST 2 from event F2522 in Brier Low Quarry.

dimensions. If the anelastic structure of the propagation path produces a Q_γ^{-1} which is constant with frequency then the amplitudes of the higher frequencies will decay more rapidly with distance than those at the lower frequencies because of the shorter wavelengths inherent to the higher frequency phases. At short distances from the source, the small decrease in amplitude with distance of the lower frequencies, together with variations in the observed amplitudes produced by the effect of noise on the individual records and measurement errors, implies that any low frequency estimate of Q_γ^{-1} may have little physical meaning. This necessitates a careful assessment of the significance of any Q_γ^{-1} datum.

A similar decrease in the frequency and magnitude of the peak amplitude was not exhibited along the line LST 2 (Fig 3.8). Amplitude spectra of similar shape and amplitudes were returned consistently along this line. Further, for LST 2N, the largest amplitudes were always given at station GLW and not at the station closest to the source. These observations indicate a marked departure from the predicted decay in amplitude with distance given by equation (1.18).

Examination of the empirically determined relative gains of the instruments comprising LST 2 and given previously in Table 2.2 showed a considerable variation. Indeed, the gain of the seismometer at GLW was the highest for the entire experiment. During the correction for the instrument response too small a calculated gain was assumed for GLW producing the high spectral amplitudes discussed above. The variation in the relative gains of the seismometers along LST 2 accounts for most of the anomalous amplitude attenuation.

The southern stations BHL, SIP, however, had gains which were

consistent with the majority of the other instruments along LST 1 for example. The relative amplification of the signal for these stations must, therefore, be due to effects peculiar to these sites.

For the reasons given above no amplification could be attributed to focussing or constructive interference caused by lateral refraction. Alluvium filled valleys have been shown, both theoretically and from observation, to amplify the incident body waves (Sanchez-Sesma & Esquival 1979, Gutenberg 1957, Joyner et al. 1981, King & Tucker 1984). Amplitudes of quarry blast signals at close distances have also been shown to be higher for sites on alluvium (Thoenen & Wildes 1937). It is possible that the large amplitudes at BHL are due to the alluvial deposits in the valley of the River Lathkill. The large amplitudes observed at station SIP could be caused by the abrupt change in slope produced by the Stanton Syncline. This effect has been observed for Rayleigh waves in the laboratory and the field (Martel et al. 1977, Griffiths & Bollinger 1979); the observations corresponding well with the theory of propagation past a step change in topography given by Mal & Knopoff (1965). The amplification produced as the wave propagates past the step is due to interference effects between the incident and scattered waves producing a frequency dependent group delay.

Examples of the amplitude - distance analysis for the lines LST 1 and LST 2 are given in Figure 3.9. The wide scatter in the data along LST 2 as shown in Figure 3.9 is thought to be a result of the anomalous amplitude effects discussed above. Consequently, reliable estimates of $Q_\gamma^{-1}(\nu)$ in the limestone district could only be achieved along the line LST 1. Estimates of $Q_\gamma^{-1}(\nu)$ over the entire line and for the individual provinces are presented in Figure 3.10.

To obtain estimates of $Q_\gamma^{-1}(\nu)$ with their statistical

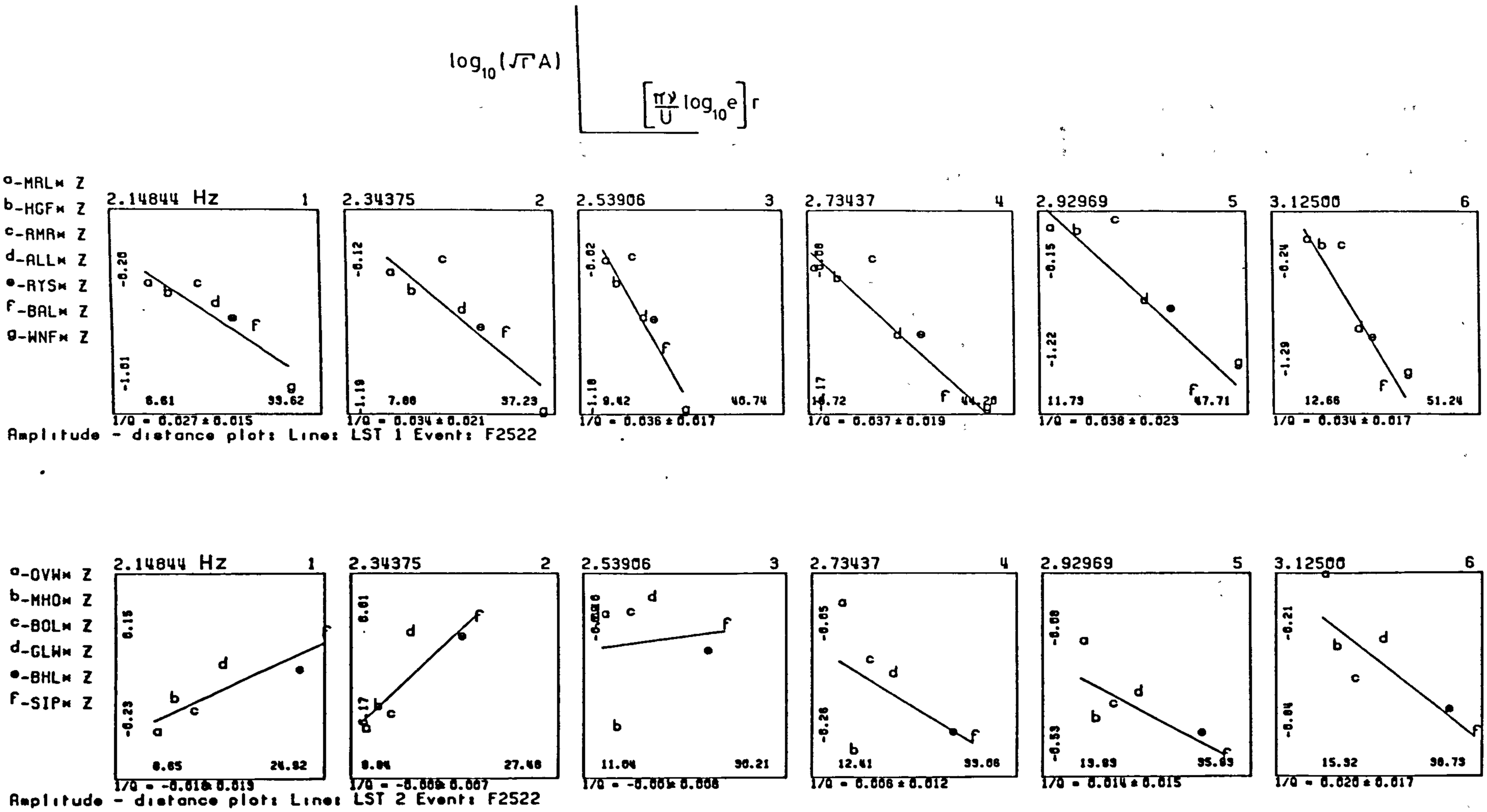

Figure 3.9 Amplitude - distance analysis for a selection of representative frequencies along LST 1 and LST 2 for event F2522 in Brier Low Quarry. Note the wide scatter of amplitude data for LST 2 producing unrealistic values of Q_γ^{-1} (thought to be caused by anomalous instrumental and site effects).

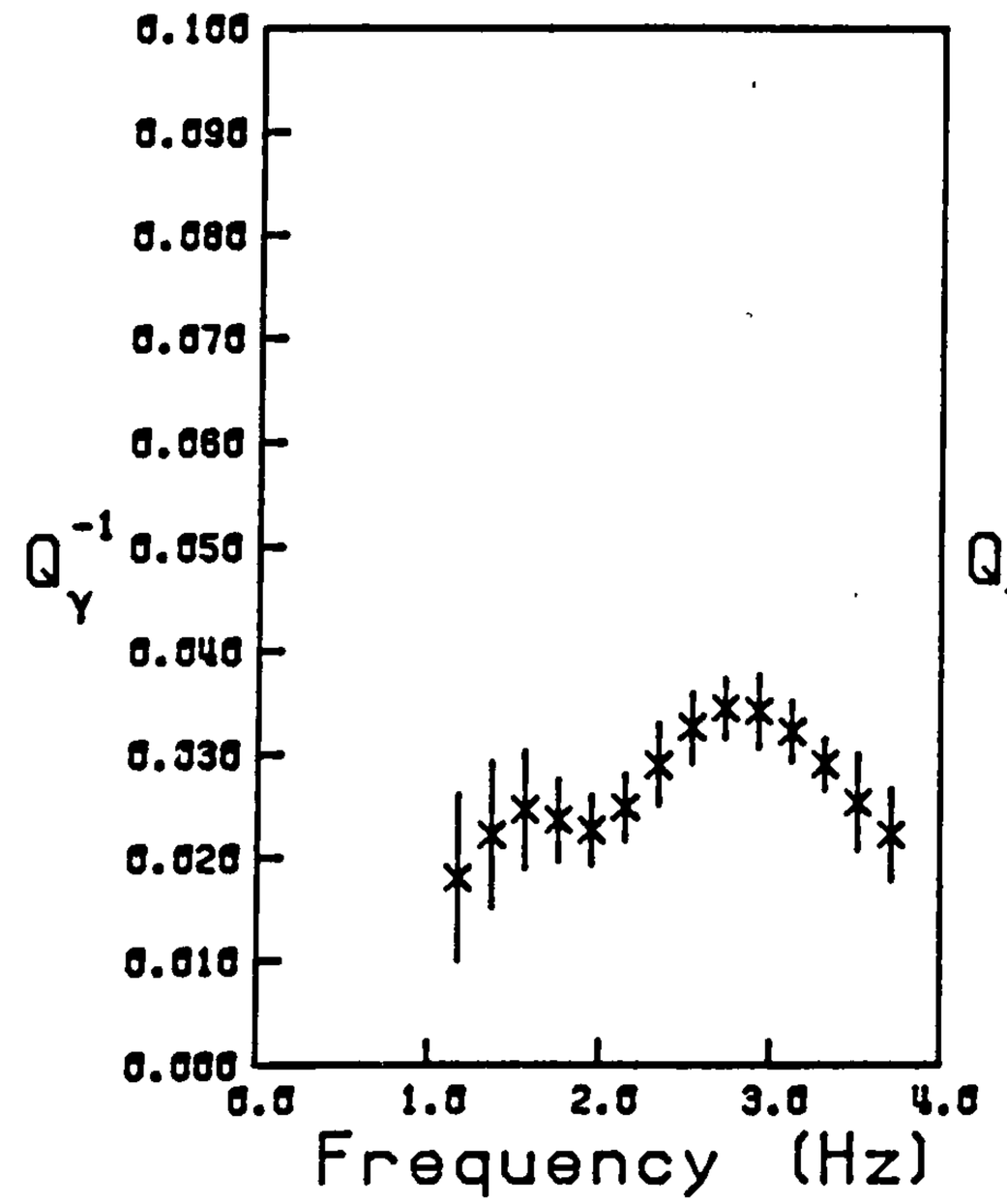

QLST 1

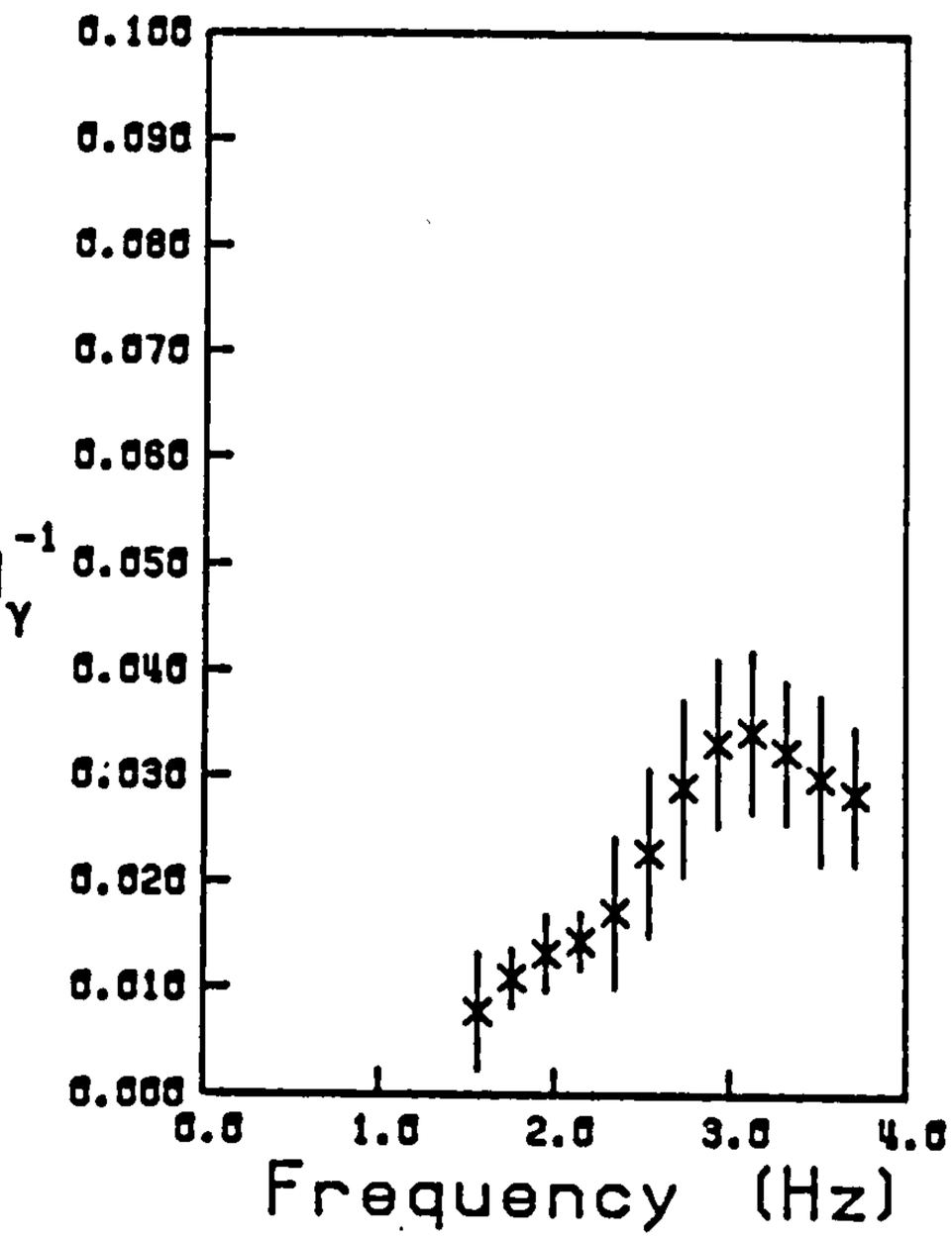

QLST 1N

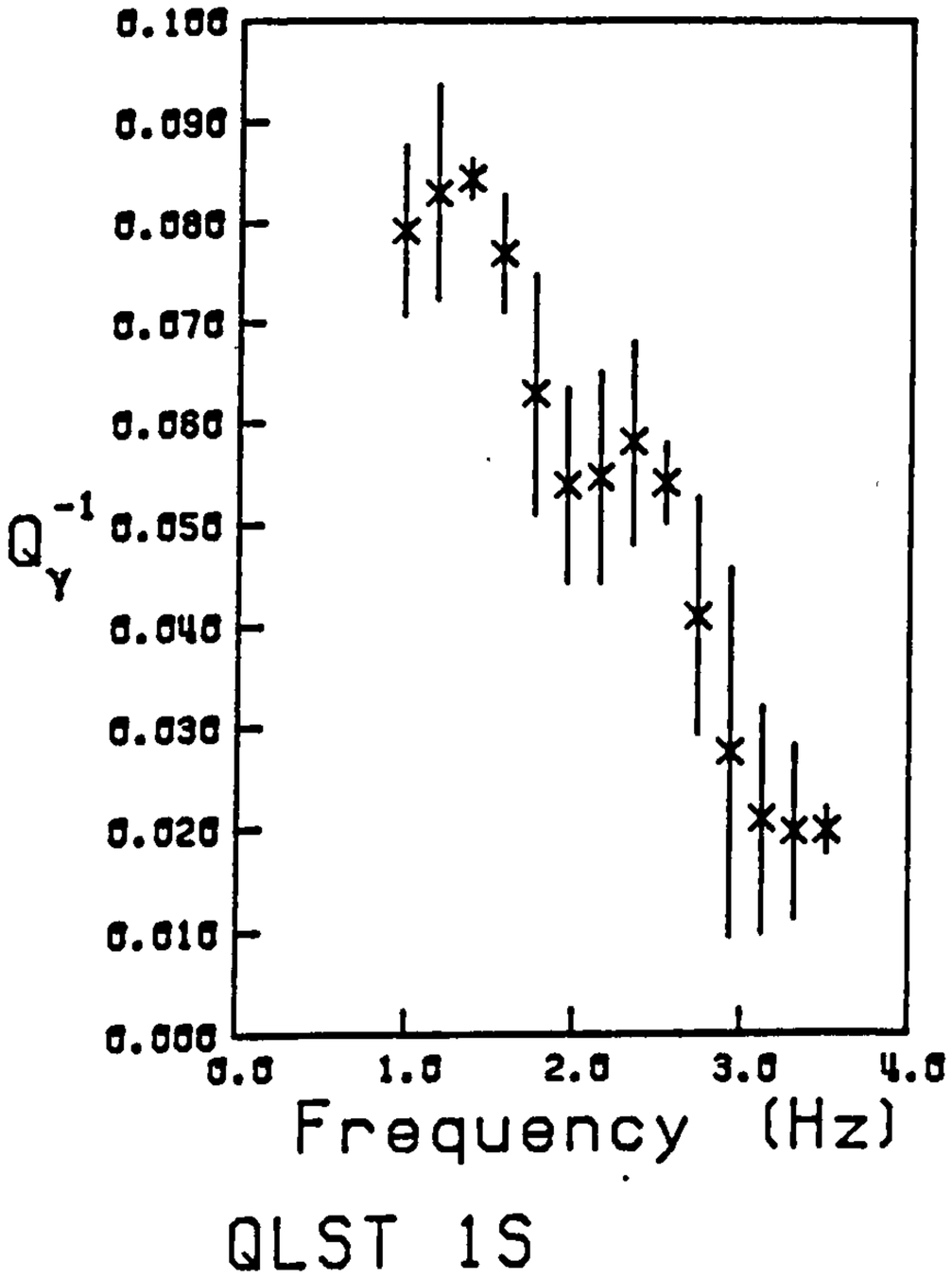

QLST 1S

Figure 3.10 Specific attenuation factor for Rayleigh waves, $Q_\gamma^{-1}(\nu)$, determined for the entire line line LST 1 and the component provinces LST 1N and LST 1S.

uncertainties a minimum of three stations were required. Because of changes in the signal bandwith, together with the effects of high frequency noise and the lack of amplitude differences at low frequencies, the frequency range over which reliable estimates are determined is smaller than that of the corresponding group slowness data set.

Both QLST 1 and QLST 1N show a general increase in $Q_\gamma^{-1}(\nu)$ to a maximum of 0.034 at 2.7 Hz for the district average and 3.1 Hz within the smaller province LST 1N. In comparison, higher overall values of the Rayleigh wave specific attenuation factor, decreasing with frequency, are given for the southern province LST 1S. The estimates of $Q_\gamma^{-1}(\nu)$ with their large uncertainties for QLST 1S reflect the poorer quality of the data at these greater distances and the fact that amplitudes from only three stations were used in the determination of the specific attenuation factor. High values of Q_γ^{-1} may also be produced partially by scattering of the Rayleigh wave energy. Features in the propagation path having similar dimensions to the wavelengths in the signal could produce scattering. For example, the transition between the shelf and basinal limestones or the deposit of Namurian shales near station PHF could be such features. The increase in the relief of the basement south of the Bonsall Fault inferred from the refraction experiment (Rogers 1983) could also produce scattering particularly at the lower frequencies.

3.3.2 The Millstone Grit District.

A total of 98 seismograms from ten events in Tunstead Quarry have been analysed to obtain estimates of group slowness and $Q_\gamma^{-1}(\nu)$

in the Millstone Grit district to the north and east of the Derbyshire Dome.

Some stations have been omitted from the analysis. The southern station, DLR of line MG 1, sited on the edge of the limestone plateau obviously recorded no information on the nature of the Millstone Grit. It should have been possible, however, to obtain estimates of group slowness over the limestone to the north east of Tunstead. The signal observed at DLR was very similar to the type 1 signals (Figs 2.15, 2.8) from Tunstead Quarry recorded over the limestone district to the south. As a consequence of the nature of this signal no consistent dispersion curve was determined.

Records from station WHS suffered from a high degree of noise contamination due to its exposed position and the character of the local drift deposits. No useful surface wave data were returned from this station.

Only limited data sets were available from stations CTP and LDG of the cluster array. Station CTP was affected severely by noise for the early part of the experiment. Some data were recorded after the station was repositioned. A transmission fault, undetectable in the field, resulted in the loss of recorded data from LDG. Unfortunately, these stations did not work simultaneously at any time; as one became operational the other ceased to function.

An FTAN diagram representative of signals along line MG 1 is given in Figure 3.11. The high frequency arrival from a second shot in Tunstead Quarry can be seen as a ridge in the contours at low velocities. The separation in frequency between the fundamental mode Rayleigh wave and the later arrival shows that the distortion of the dispersion curve and amplitude spectrum is minimal. At a velocity of 2.6 km s^{-1} a high energy ridge is indicated above

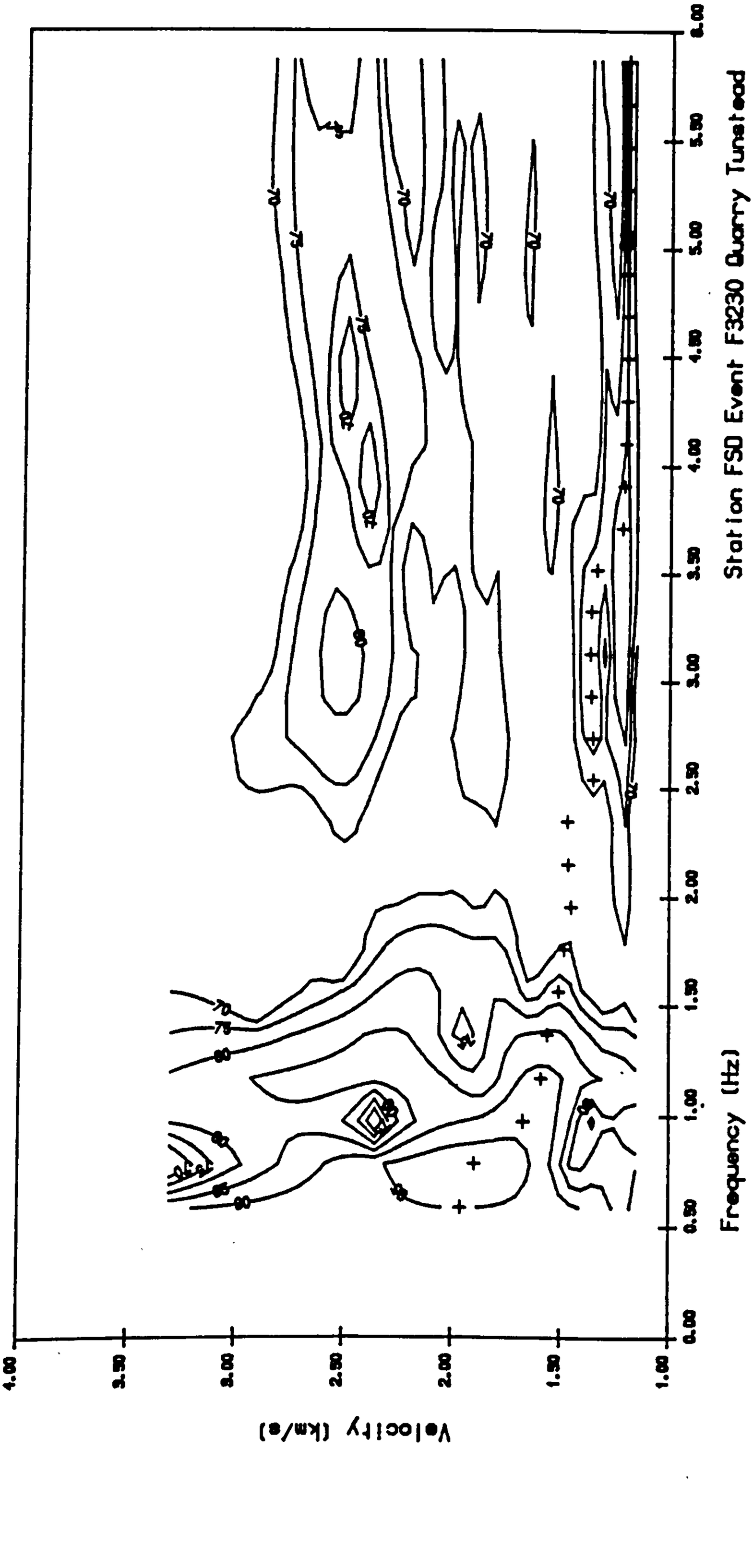

Figure 3.11 Frequency-time analysis diagram for the signal recorded at FSD from event F3230 in Tunstead Quarry. (Contoured between 70 - 95 dB at 5 dB intervals.)

2.2 Hz and is identified as a shear wave arrival.

In general, the FTAN diagrams exhibited a reduced bandwidth compared with similar diagrams for the limestone district. Further, the peak energy corresponding to the Rayleigh waves occurs at lower frequencies and velocities than in the limestone. In common with the limestone frequency-time analyses, individual energy values had to be examined to obtain reliable dispersion curves.

The simpler character of the signals over the cluster array is highlighted by Figure 3.12. The well defined region of high energy contrasts with the smaller high energy regions indicated for events recorded along MG 1 (Fig 3.11). The effect of the second event is less obvious and there is little evidence of a strong shear wave arrival.

The revised velocity windows used to isolate the fundamental mode Rayleigh wave had limits which varied from a maximum of 2.8 km s^{-1} to a minimum of 1.1 km s^{-1} for MG 1. These velocity limits were coincidently the same as those used for LST 1 but for most events lay well between these extreme values. The range for MGAR varied between 3.0 km s^{-1} and 1.2 km s^{-1}.

The individual source to station dispersion curves for stations of line MG 1 were, on the whole, consistent. The arrival time-distance analysis showed that for some higher frequencies arrivals at CHF and HNF were consistently late being above the determined regression line (Fig 3.13). The line could, therefore, have been divided into two provinces. The resulting provincial dispersion for the northern stations, however, was the same as the district average dispersion and hence the late arrivals at CHF must be due to errors in the individual dispersion curve and not due to a significant change in geologic structure. The late arrivals at HNF

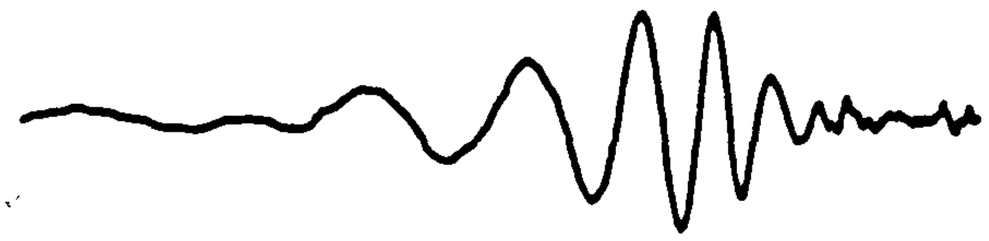

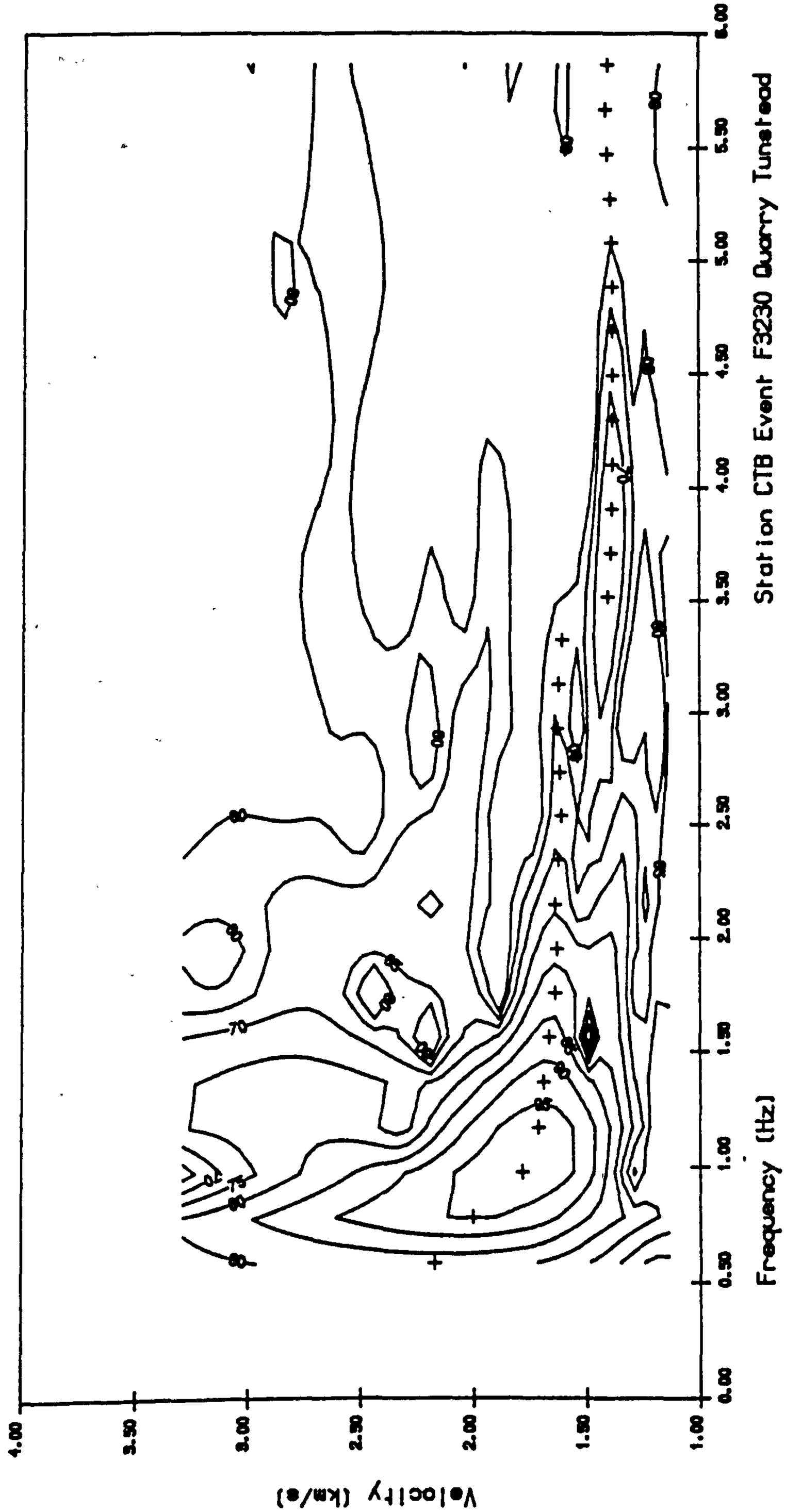

Figure 3.12 Frequency-time analysis diagram for the signal recorded at CTB from event F3230 in Tunstead Quarry. (Contoured between 60 - 95 dB at 5 dB intervals.)

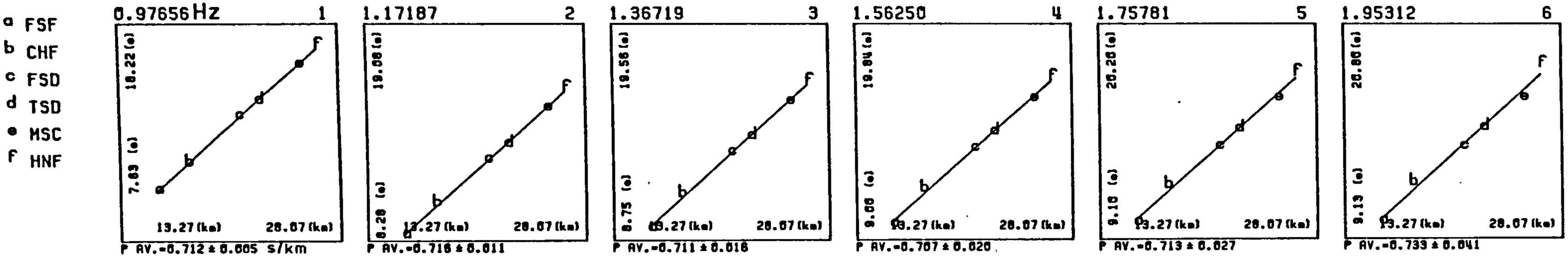

Figure 3.13 Group arrival time against distance for representative frequencies along MG 1 and over MGAR. Note especially the perturbations at CHF and HNF of MG 1 and the wide scatter of the data about the regression line for MGAR.

may indicate a complication in the structure implied previously during the study of compressional wave arrivals along MG 1 (Cox 1983).

A least squares fit to arrival time-distance data has been shown to be inappropriate over the cluster array due to lateral refraction (Fig 3.13 and section 2.4.2). The individual source to station dispersion curves were very similar for all stations except BMR which consistently gave lower slownesses for all frequencies. An average dispersion curve for the array, excluding station BMR, was obtained by taking a simple arithmetic mean of the individual slowness. This procedure, whilst not returning estimates of true provincial slowness, was more appropriate for stations close together and showing similar individual dispersion curves.

The estimates of group slowness dispersion over the Millstone Grit district are shown in Figure 3.14. Normal dispersion is indicated over the district. Group slowness varies from 0.67-0.75 s km^{-1} between 0.6 Hz and 3.1 Hz along MG 1. Lower values of slowness, 0.49-0.66 s km^{-1}, are observed for MGAR over a reduced frequency range of 0.6-2.3 Hz. These values must reflect the contribution of the limestone structure on the dispersion.

The lower overall values of slowness observed at BMR from Tunstead Quarry would be indicative, normally, of a mis-location or timing error. Such errors have been found to be minimal and insufficient to produce the observed difference. The conclusion must be that a marked change in structure occurs over the short distance between BMR and the rest of the array.

The maximum frequency in the signals along MG 1 was seen to decrease from 3.2 Hz at station FSF to 1.6 Hz at station HNF. This decrease in bandwidth was displayed consistently along MG 1 for each

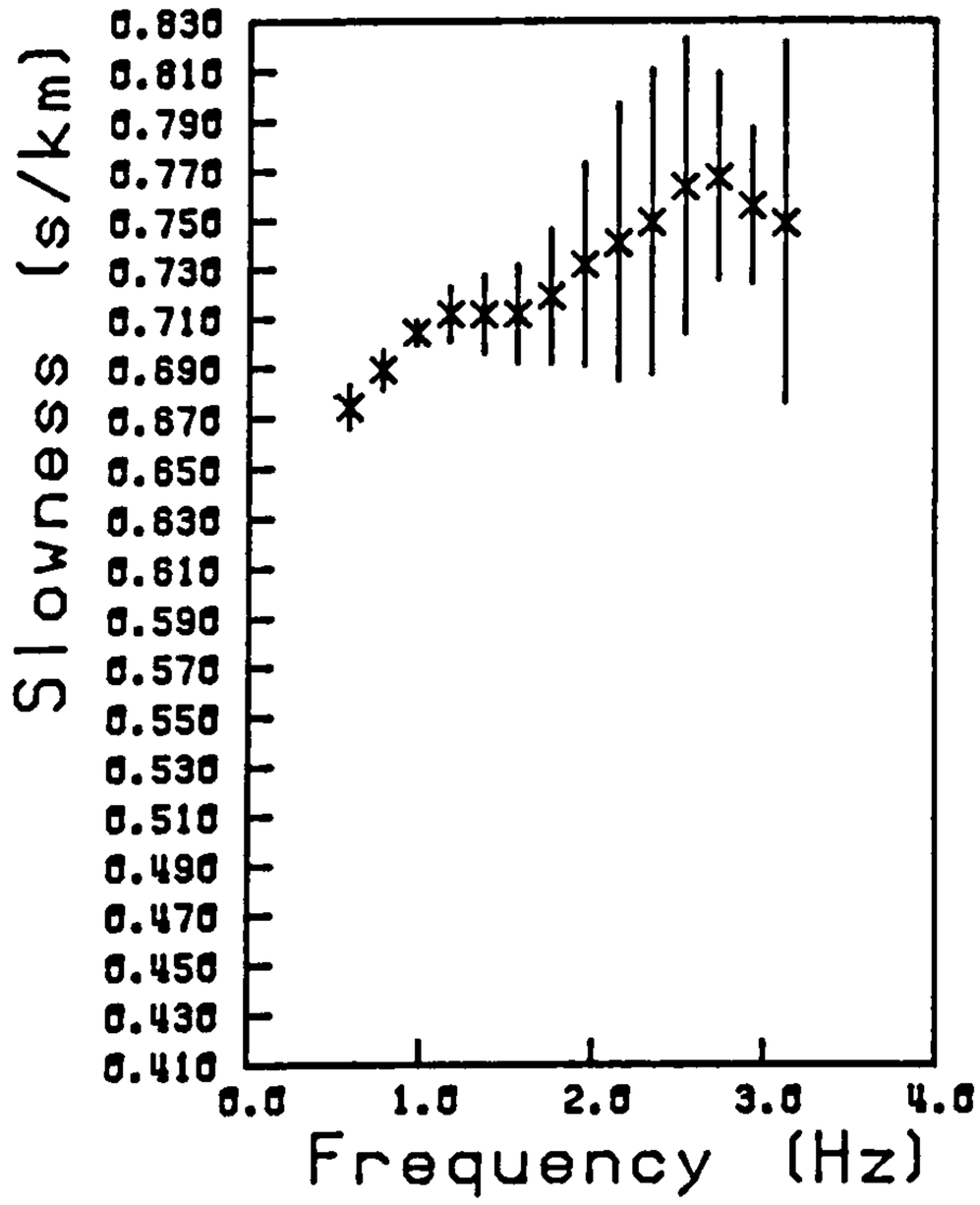

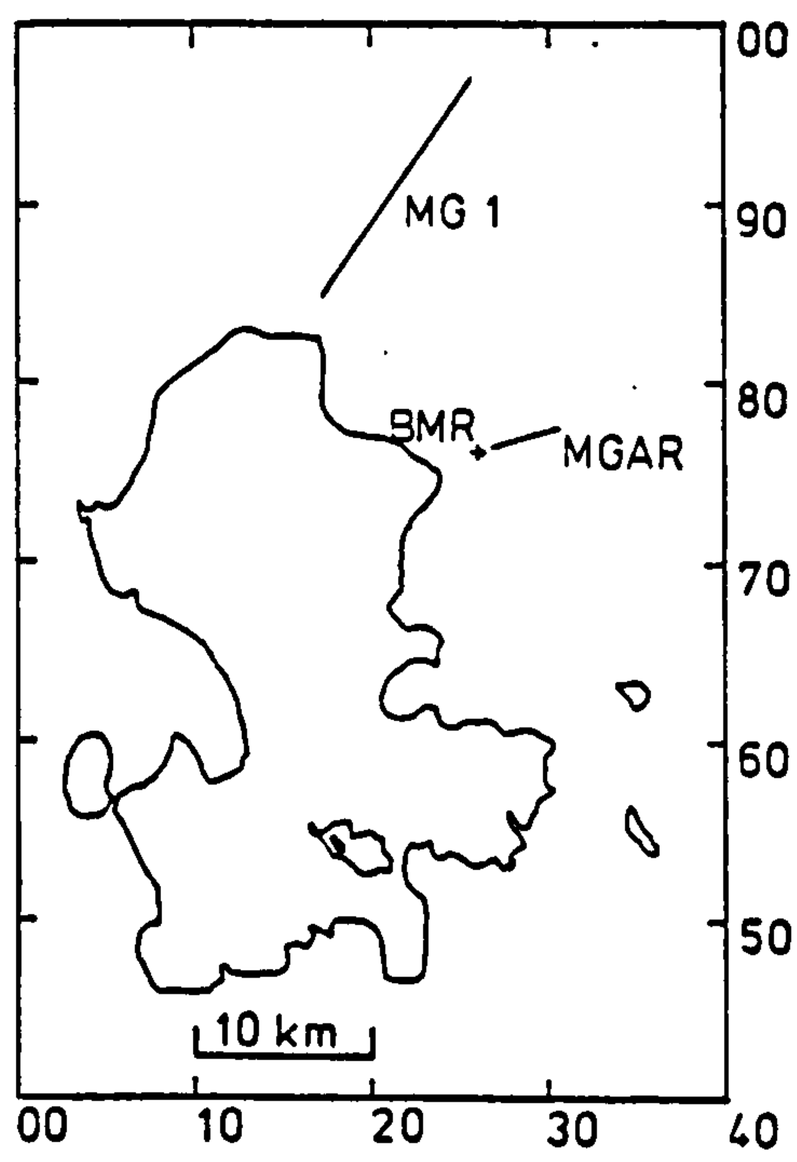

PMG 1

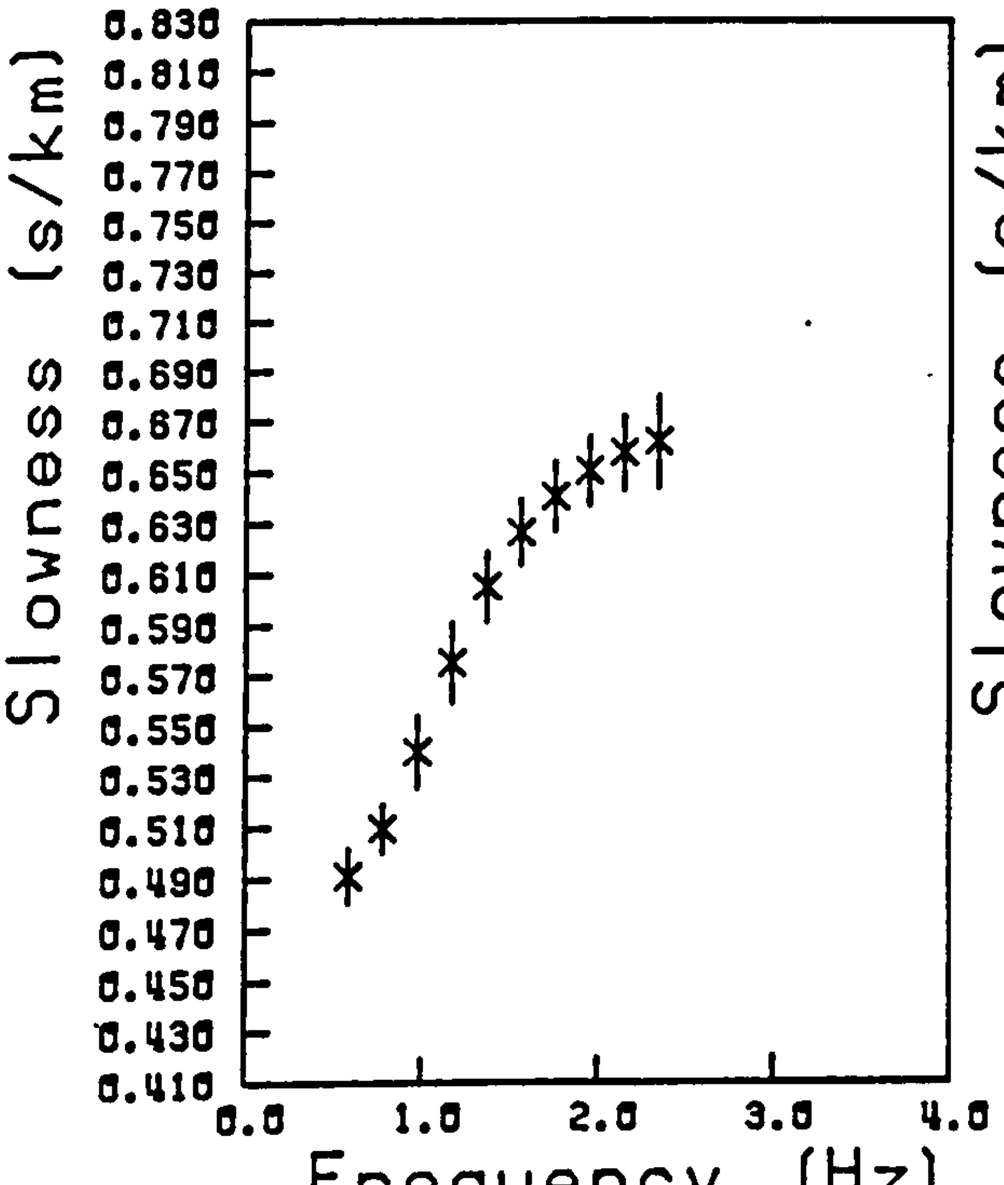

PMGAR

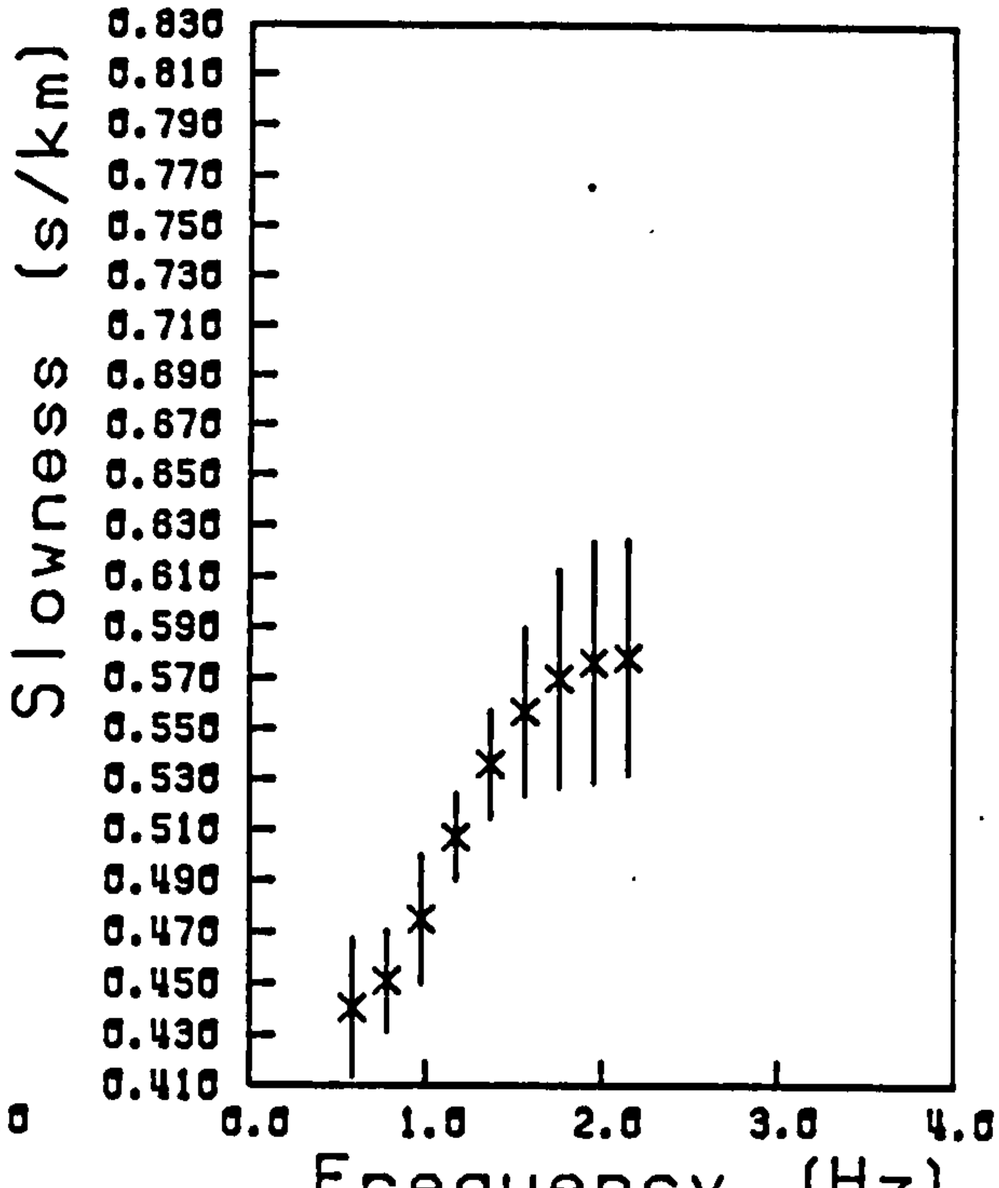

PBMR

Figure 3.14 Rayleigh wave group slowness dispersion determined along MG 1 and from multiple events over the mixed province paths to BMR and MGAR.

event although the absolute values varied slightly depending on the signal-to-noise ratio. The bandwidth of signals crossing the cluster array is constant as would be expected from stations separated only by short distances. The upper frequency limit was 1.9-2.3 Hz for all events. For both experiments in the Millstone Grit district the lowest frequency available was 0.6 Hz, imposed by the effect of the instrumentation at lower frequencies.

The amplitude spectra along MG 1 (Fig 3.15) were peaked sharply at 0.8 Hz for the entire line; no decrease in peak frequency with distance was observed. The magnitude of this peak did, however, decrease with distance. Such an invariant peak frequency is a result of the combination of the source spectrum with an appropriate medium response. In general, the spectra returned from station FSF showed a less steep roll-off in amplitude at the upper frequencies. Amplitude spectra from the cluster array are slightly broader and also show an invariant peak frequency due in part to the smaller differences in path length (Fig 3.16).

Amplitude - distance plots for representative frequencies and the quarry blasts given are presented for the Millstone Grit district in Figure 3.17. The results from the amplitude - distance analysis for every event where then averaged to give reliable estimates of $Q_\gamma^{-1}(\nu)$ in the Millstone Grit district (Figure 3.18). The data sets are again comprised of fewer points than their corresponding group slowness data sets for the reasons given previously. For the array, values from station BMR have been omitted because of the anomalous dispersion. $Q_\gamma^{-1}(\nu)$ for MG 1 varies from 0.015 to 0.022 between the frequencies of 0.8 Hz and 2.5 Hz. The estimates of observed attenuation over the array show a reduced variation being 0.016 at 0.8 Hz and 0.011 at 2.0 Hz. The standard

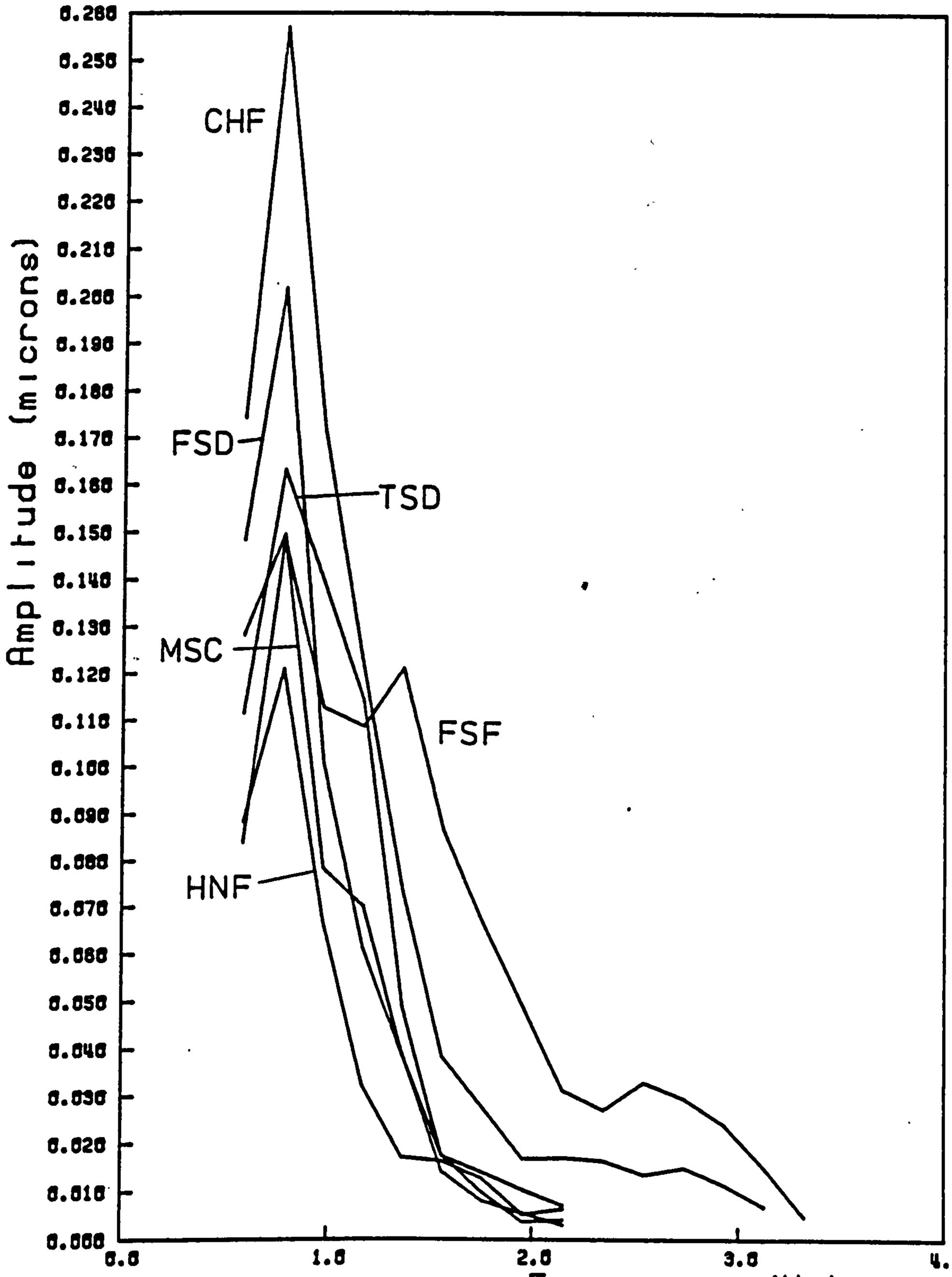

Instrument corrected amplitude spectra

Figure 3.15 Instrument corrected, smoothed amplitude spectra for stations of MG 1 from event F3230 in Tunstead Quarry.

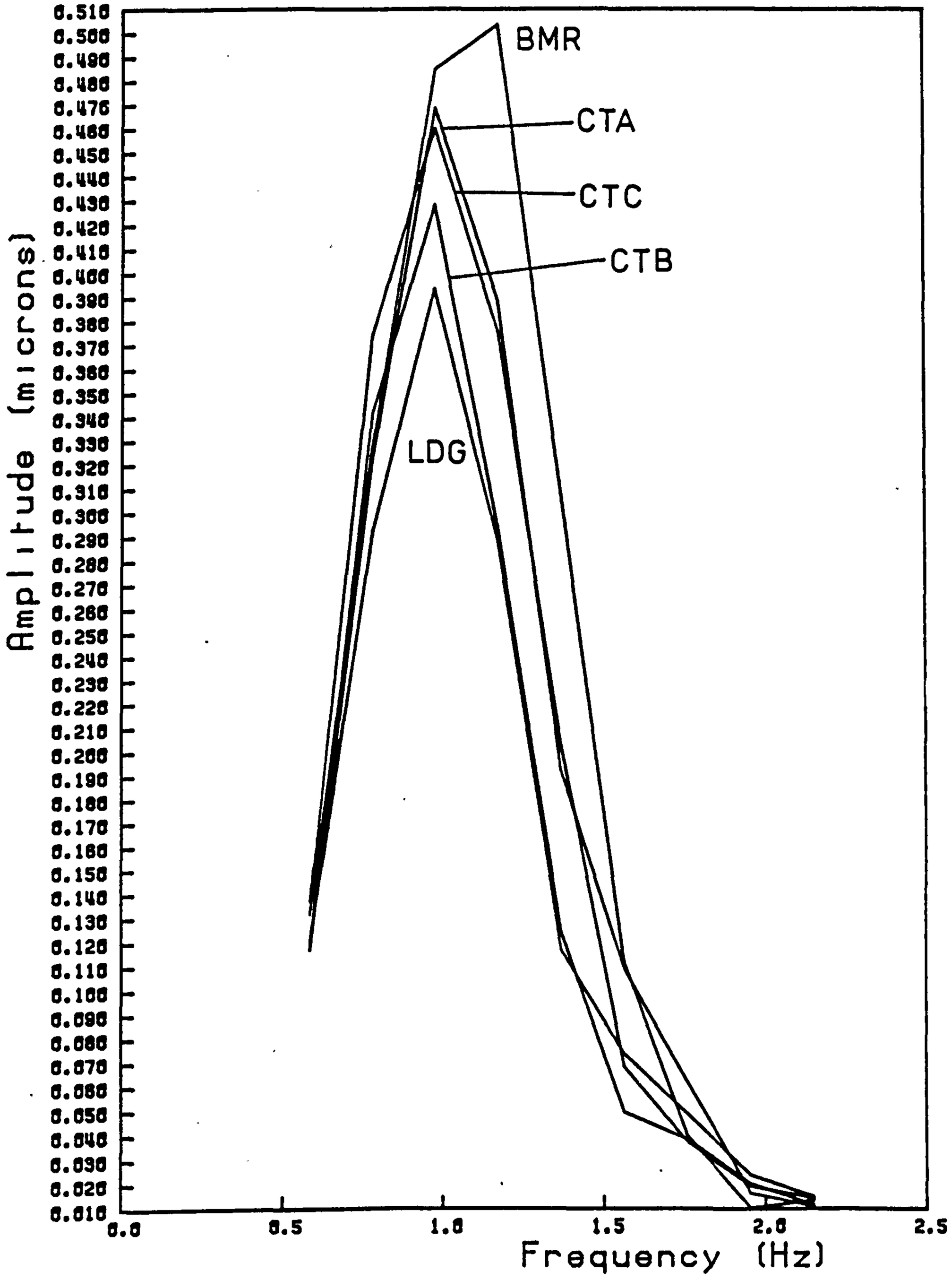

Instrument corrected amplitude spectra

Figure 3.16 Instrument corrected, smoothed amplitude spectra for all the stations of the cluster array from event F3230 in Tunstead Quarry.

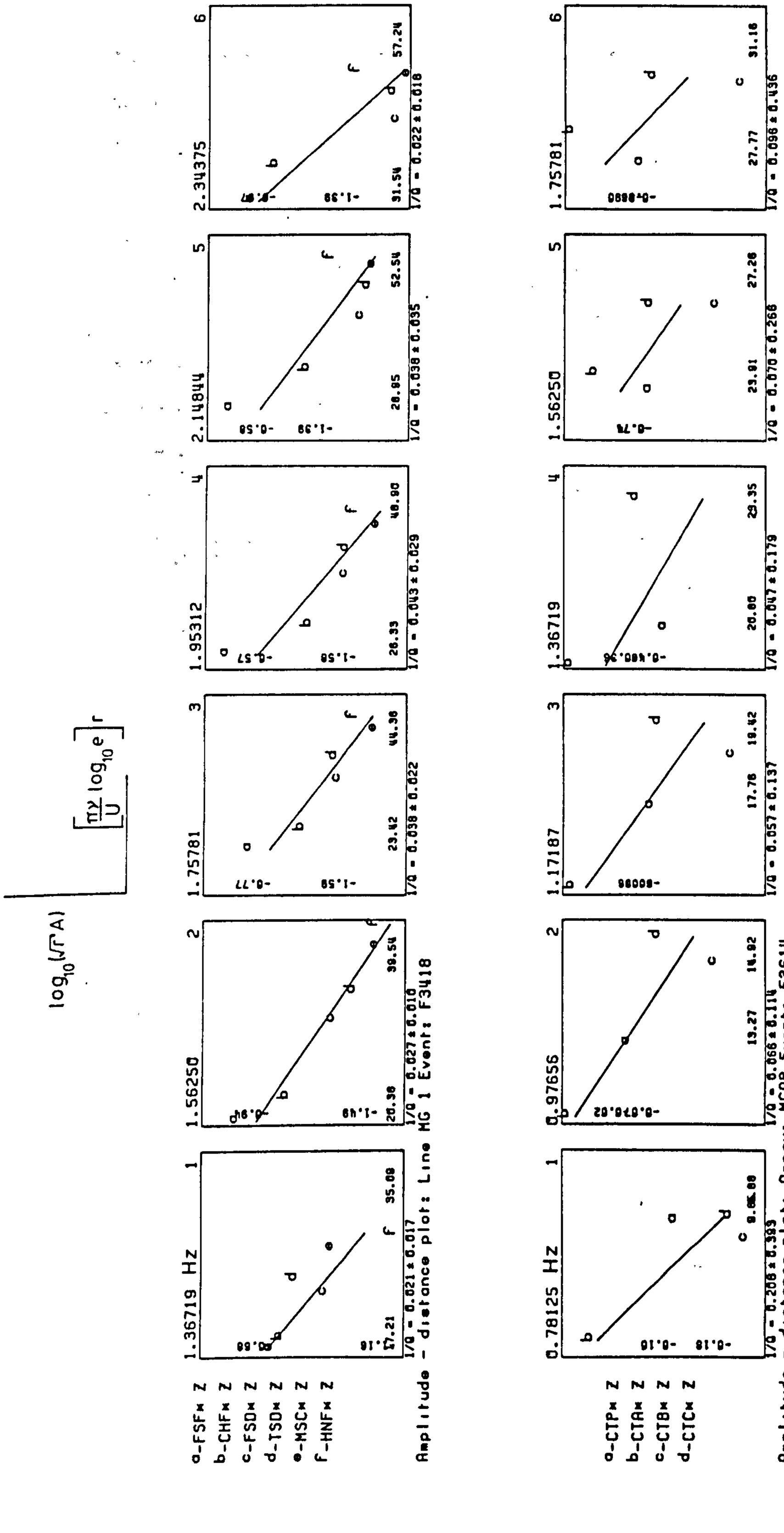

Figure 3.17 Amplitude - distance analysis for a selection of representative frequencies along MG 1 from event F3418 and over MGAR from event F3614, both events being in Tunstead Quarry.

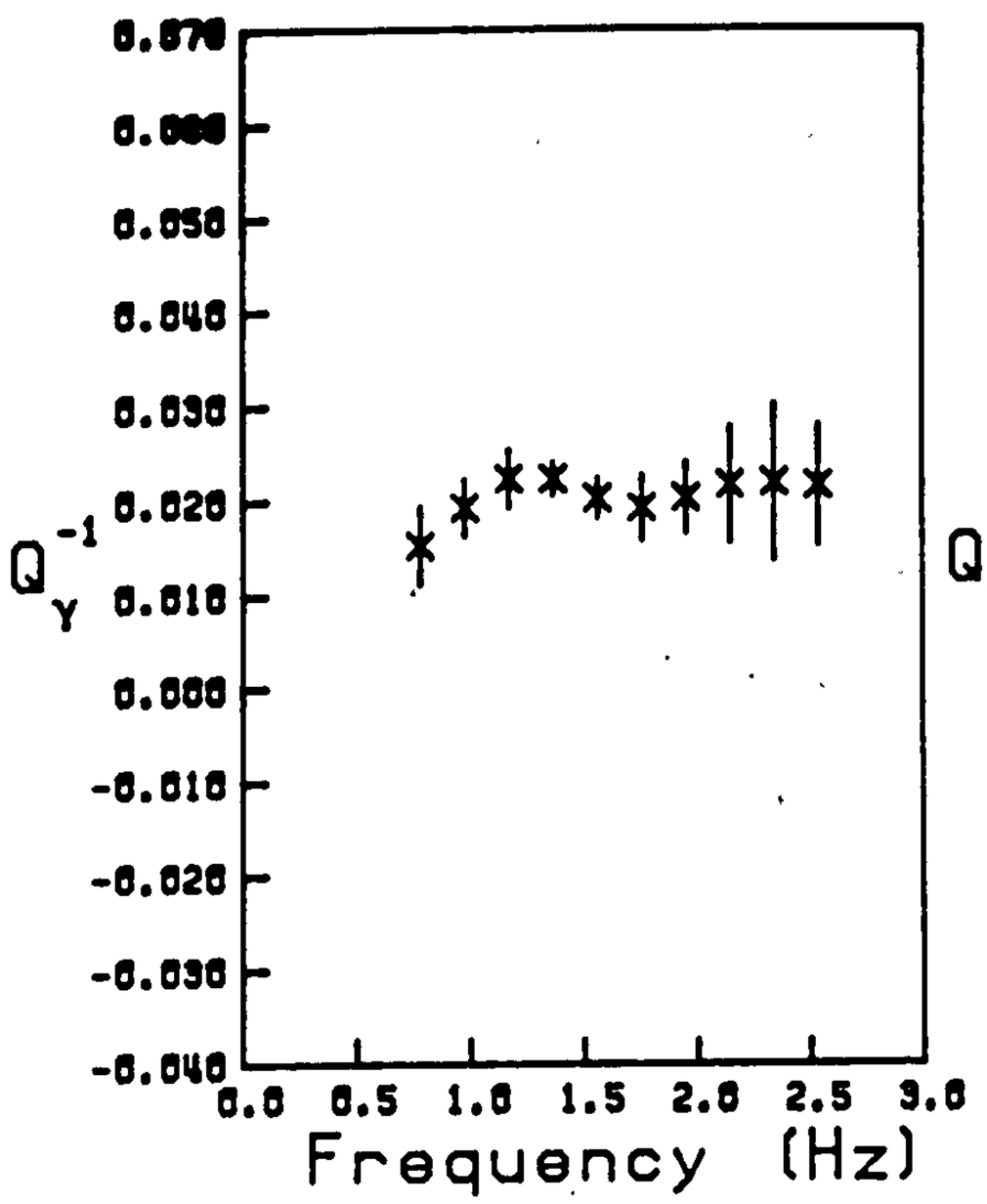

QMG 1

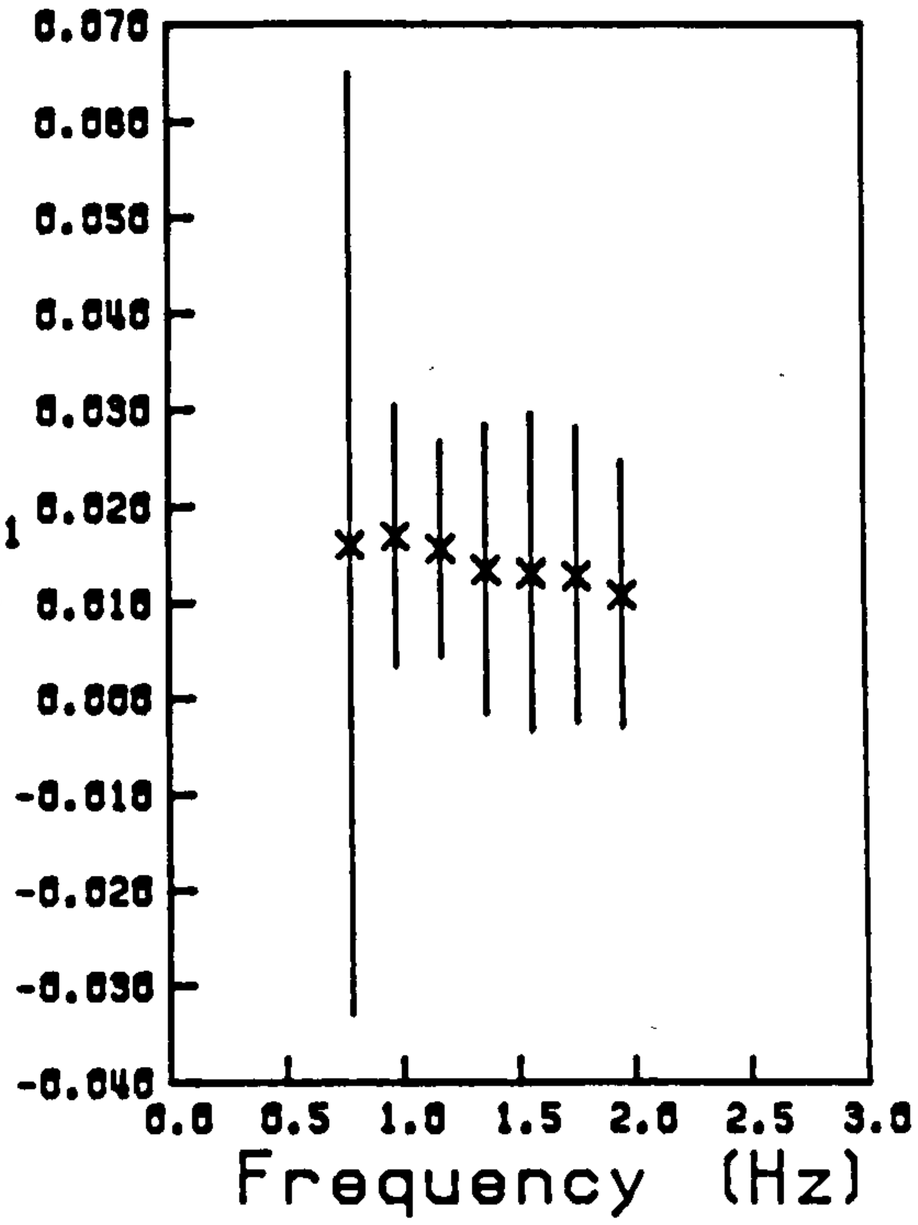

QMGAR

Figure 3.18 Specific attenuation factor for Rayleigh waves, $Q_\gamma^{-1}(\nu)$, determined for the line MG 1 and MGAR.

deviations, however, are much larger indicating a greater scatter in the amplitude measurements. This scatter could be caused by the greater azimuthal variation or, as is more probable, the amplitudes may be scattered about a mean value, an effect compounded by the shorter differences in path length.

The array processing technique of section 2.4.2 has been modified to investigate changes in azimuth with frequency over the array. By using the determined group slowness data to provide estimates of travel time the procedure is no longer restricted to stations in close proximity where a given peak can be correlated unambigously between stations.

Application of this method to the cluster array showed that the azimuth of propagation varied with frequency; the lowest frequencies showing the maximum deviation of 18^{o} from the direct azimuth (Fig 3.19). The higher frequencies were close to the direct azimuth which lay within their errors. The boundary between the Millstone Grit and limestone close to Eyam is the probable cause of this lateral refraction and the variation in azimuth with frequency must be related to the nature of this boundary. The variation in velocity must be most pronounced at deeper levels which requires the structure to be more complex than a simple change in velocity for all depths. A wedge of low velocity material, the Millstone Grit, overlying a steeply dipping layer, the Carboniferous Limestone, having an increase in velocity with depth could be envisaged to account for the observed variations in azimuth.

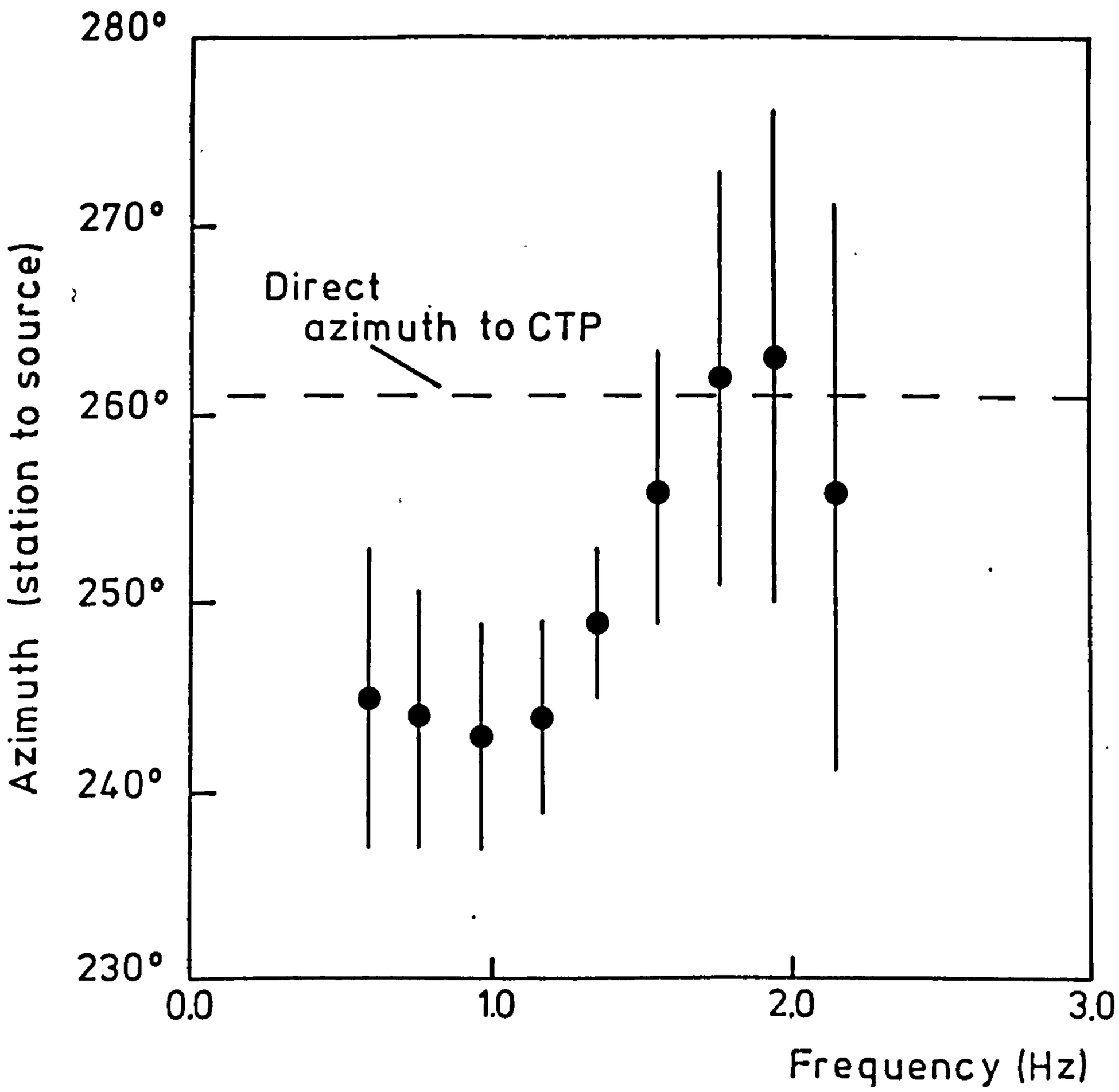

Figure 3.19 The variation with frequency of the azimuth of propagation of Rayleigh waves from Tunstead Quarry over the cluster array .

3.4 COMPARISON of OBSERVED DISPERSION and ATTENUATION.

The nine group slowness dispersion curves, determined from high frequency Rayleigh waves recorded over the Derbyshire Dome and adjacent areas, which were discussed in the previous section have been drawn together in Figure 3.20 for comparison. Normal dispersion is indicated by all the curves at the lower frequencies. The dispersion curves representative of the limestone district are different and show slowness which decreases or remains constant at the higher frequencies.

Figure 3.20 also indicates that a simple correlation between group slowness and surface lithology exists with the slowness in the Millstone Grit district being higher than in the Carboniferous Limestone district for all frequencies. The effect of increasing slowness due to propagation within the Millstone Grit is demonstrated elegantly by the observed dispersion for the mixed province data sets PMGAR and PBMR. The observed dispersion PBMR is similar to the limestone dispersion curves because the station BMR was sited close to the limestone/Millstone Grit boundary. As the proportion of the path comprised of Millstone Grit increases, however, the observed slowness for PMGAR also increases overall. This helps substantiate the important conclusion that group slowness can be considered as a sensitive indicator of changes in propagation path and a diagnostic parameter of surface geology.

For Rayleigh waves at high frequencies the crustal structure approximates to a half-space having the average properties of the upper layers and in which the group slowness approaches the phase slowness asymptotically. As phase slowness is related to the shear wave velocity by Poisson's ratio, σ, estimates of shear wave

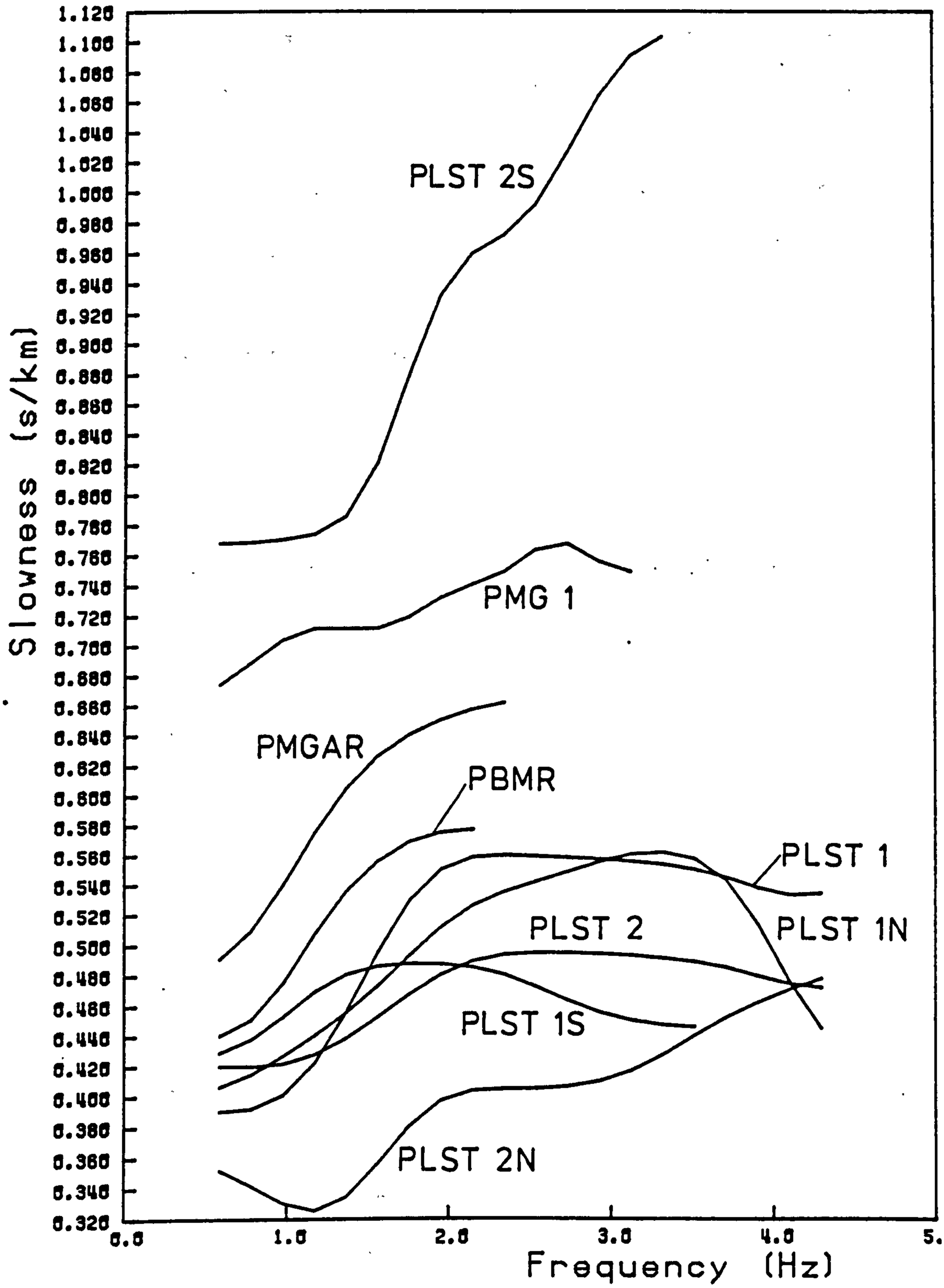

Comparison of observed dispersion

Figure 3.20 Comparison of the observed Rayleigh wave group slowness dispersion curves.

velocity of the surface layer can be obtained from the observed dispersion by assuming a Poisson's ratio and that group velocity equals the phase velocity at high frequencies.

Over the limestone district the shear wave velocity from the surface to approximately 500 m ranges between 1.6-1.9 km s^{-1} for an assumed Poisson's ratio of 0.25. A higher value of σ may be more appropriate in the shallow crust (Assumpcao & Bamford 1978) and would provide higher estimates of shear wave velocity. The refraction study of Rogers (1983) gives a compressional wave velocity of 5.2 km s^{-1} for the limestone which would correspond to a shear wave velocity of 3.0 km s^{-1} for the Poisson's ratio of 0.25. This estimate is higher than that obtained from the Rayleigh wave dispersion and may indicate that Poisson's ratio is indeed higher than 0.25 in the upper crust, perhaps being around $\sigma = 0.3$.

Within the Millstone Grit district the shear wave velocity estimated from the observed dispersion ranges from 1.2 km s^{-1} to 1.6 km s^{-1}, the higher values being determined from the mixed province propagation paths. The compressional wave velocity measured from direct waves in the Millstone Grit of 3.5-4.0 km s^{-1} (Rogers 1983) yields a shear wave velocity of 2.0-2.3 km s^{-1}, which is again higher than the estimates calculated from the observed dispersion.

The five $Q_\gamma^{-1}(\nu)$ curves determined for the individual provinces within the limestone and Millstone Grit districts are compared in Figure 3.21. $Q_\gamma^{-1}(\nu)$ ranges from 0.008 to 0.084 comparing favourably with previous determinations of the specific attenuation factor for Rayleigh waves in the upper crust (Evans 1981) although the estimates of attenuation QLST 1S are high. The curves of $Q_\gamma^{-1}(\nu)$ do not display a common trend although QLST 1, QLST 1N and QMG 1, to a

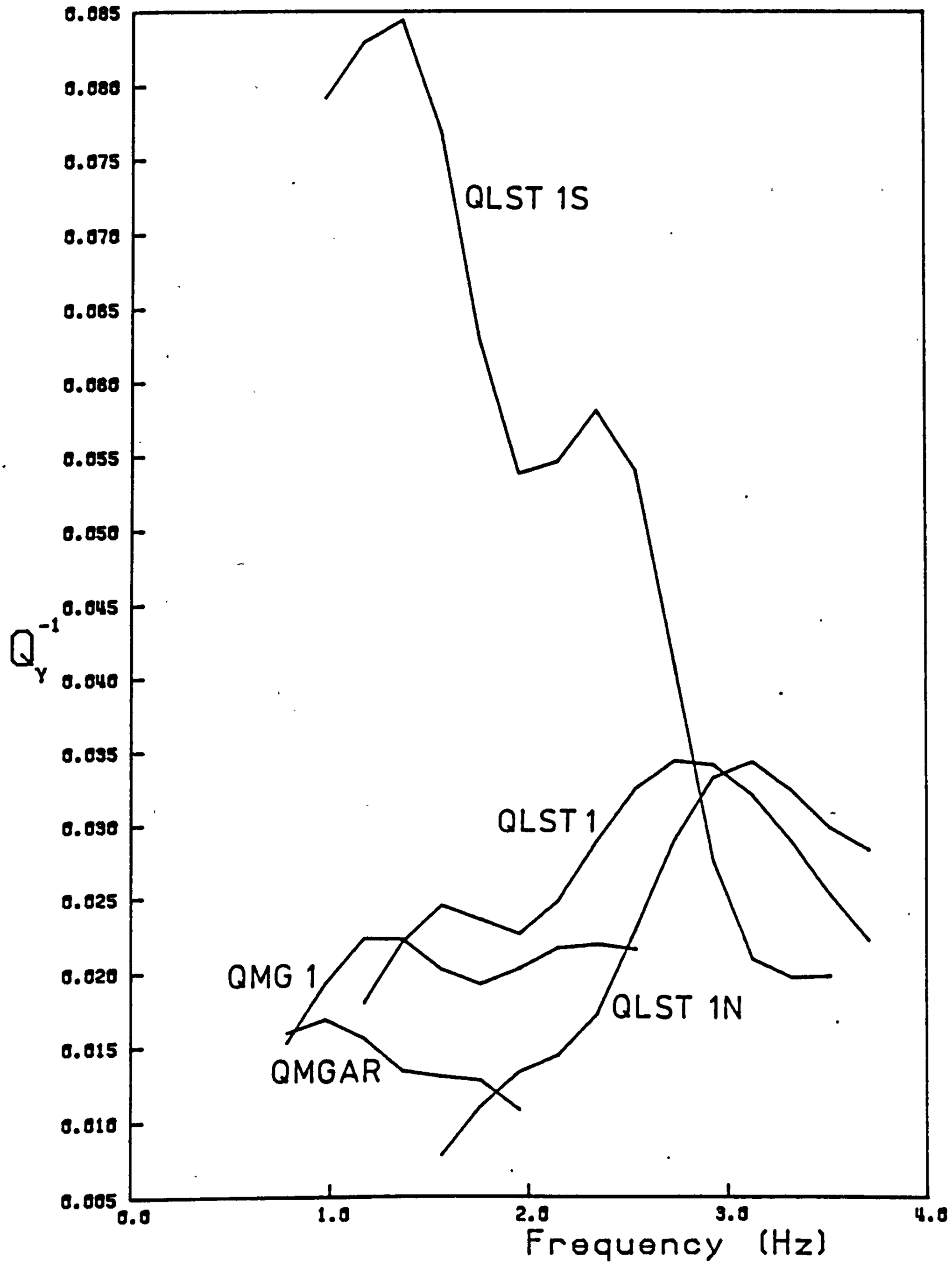

Comparison of observed attenuation

Figure 3.21 Comparison of the observed Rayleigh wave specific attenuation fator, $Q_\gamma^{-1}(\nu)$, curves.

lesser degree, do indicate an increase with frequency.

In contrast to group slowness, there is no apparent correlation between Q_γ^{-1} and the main lithology of each province. This observation implies that the composition of the rock is not the only factor contributing to the anelasticity and hence to the observed Rayleigh wave attenuation.

Estimates of intrinsic shear wave specific attenuation factor have been calculated from the observed attenuation data in a manner similar to that used to estimate shear wave velocity from observed group slowness. At high frequencies the structure approximates to a half-space in which the intrinsic body wave attenuation factors can be related to the observed attenuation by (Burton 1973)

$$Q_\gamma^{-1} \approx Q_\alpha^{-1} + Q_\beta^{-1}. \qquad (3.6)$$

The intrinsic attenuation factors may be related by (Anderson et al. 1965, Burton & Kennet 1972),

$$Q_\alpha^{-1} = \frac{4}{3}\left(\frac{\beta}{\alpha}\right)^2 Q_\beta^{-1}, \qquad (3.7)$$

which gives

$$Q_\beta^{-1} = \frac{3\alpha^2}{3\alpha^2 + 4\beta^2}\, Q_\gamma^{-1}. \qquad (3.8)$$

For a Poisson solid with $\sigma = 0.25$ then

$$Q_\beta^{-1} = \frac{9}{13}\, Q_\gamma^{-1}. \qquad (3.9)$$

The shear wave specific attenuation factor in the near surface of the limestone district is estimated to be 0.022 north of the Bonsall Fault zone and 0.37 to the south. A lower value of Q_β^{-1} of 0.015 is given for the Millstone Grit district. These estimates were calculated from observed $Q_\gamma^{-1}(\nu)$ at the same frequency. As a consequence of the group slowness dispersion, however, the estimate for the Millstone Grit district pertains to a thinner surface layer than for the limestone district. The higher intrinsic attenuation in the limestone district could possibly be the result of higher dissipation at lower levels. These estimates of Q_β^{-1} for the surface layer compare well with the half-space models for discrete geologic provinces in Scotland in which $\bar{Q}_\beta^1$ varies between 0.011 and 0.030 (Evans 1981).

Laboratory observations have shown Q^{-1} to be essentially independent of frequency. For some crustal studies (Mitchell 1980, Souriau *et al.* 1980) a frequency dependence has been exhibited by Q_β^{-1}. Mitchell (1980) considered relations of the form

$$Q_\beta^{-1} = Q_{\beta_o}^{-1} \nu^{-\eta} . \qquad (3.10)$$

Using the half-space relations between intrinsic body wave attenuation factors and Q_γ^{-1} given by Anderson *et al.* (1965), Burton & Kennet (1972) permits Q_β^{-1} to be replaced by Q_γ^{-1} in equation (3.10). In logarithmic form we now have

$$\log Q_\gamma^{-1} = \log Q_{\gamma_o}^{-1} - \eta \log \nu . \qquad (3.11)$$

Estimates of $Q_{\gamma_o}^{-1}$ and η can be made from a least square fit to

the data using equation (3.11). The results are given below:

Data set	$Q_{\gamma_o}^{-1} \times 10^{-5}$	η
QLST 1	12.3	-0.324 ± 0.122
QLST 1N	0.4	-1.681 ± 0.188
QLST 1S	613.8	1.127 ± 0.193
QMG 1	10.5	-0.184 ± 0.080
QMGAR	6.9	0.355 ± 0.089

Mitchell (1980) finds $\eta = 0.5$ at 1 Hz in North America; noticeably different to the values above. The correlation co-efficient and the Student's t statistic for the individual regression lines indicate that the values of η are only significant for the data sets QLST 1N and QLST 1S. These inconsistent values of η are insufficient to confirm that a frequency dependence exists for Q_γ^{-1} and hence for the intrinsic Q_β^{-1}.

3.5 SUMMARY.

Within this chapter we have described the methods by which the dispersion and attenuation of Rayleigh waves can be obtained as functions of frequency. These methods were then employed to provide reliable estimates of group slowness and $Q_\gamma^{-1}(\nu)$ for provinces within the field work area. Group slowness over the limestone district varies between 0.33-0.56 s km^{-1} and between 0.67-0.77 s km^{-1} for the Millstone Grit district. Variations in group slowness were shown to correlate directly with geologic features such as changes

in surface lithology and structure. The limestone district, assumed earlier to be homogeneous, had to be divided into two provinces separated by the Bonsall Fault zone on the basis of dispersion evidence. Estimates of $Q_\gamma^{-1}(\nu)$ range from 0.01 to 0.08 in the limestone district and between 0.01 to 0.02 within the Millstone Grit district. In contrast to the estimates of group slowness, no correlation between the observed specific attenuation factor of Rayleigh waves and surface lithology can be shown to exist.

In the following chapters mathematical inversion techniques are used to obtain the anelastic structure of the field-work area from the observed dispersion and attenuation presented above. This improves on the approximate half-space modelling employed previously to estimate shear wave velocity and intrinsic attenuation by utilising the entire frequency bandwidth of the observed group slowness and Q_γ^{-1} data.

CHAPTER FOUR

INVERSION of OBSERVED RAYLEIGH WAVE DISPERSION

4.1 INTRODUCTION.

Models of earth structure may be obtained from surface observations through the application of mathematical inversion techniques. Within this chapter we shall use such techniques to determine the distribution of shear wave velocity with depth implied by the observed group slowness dispersion presented in the previous chapter.

The forward problem of calculating group velocity for a given model has been solved using the Thomson-Haskell matrix formulation (Thomson 1950, Haskell 1953). A more efficient alternative is given by Knopoff (1964b) and presented in FORTRAN code by Schwab & Knopoff (1972). A dispersion function is formulated for a model defined by the compressional and shear wave velocities, density and thickness of isotropic, horizontal plane layers overlying, and including, a half-space. The fundamental mode Rayleigh wave phase velocity dispersion curve is determined by finding the zeros of the dispersion function having a minimum phase velocity for each frequency. Slowness is given by the reciprocal of the velocity thus obtained.

Group velocities are then calculated from a numerical approximation to equation (1.15) such that

$$U(\nu_i) = \left[\frac{(\nu_i + \delta\nu)p_1 - (\nu_i - \delta\nu)p_2}{2\delta\nu} \right]^{-1} \qquad (4.1)$$

where p_1 is phase slowness at frequency $\nu_i + \delta\nu$

p_2 is phase slowness at frequency $\nu_i - \delta\nu$

$\delta\nu$ is a small change in frequency.

Numerical overflow can occur within the FORTRAN routine when the ratio of layer thickness to wavelength exceeds a given value. This effect is most pronounced for high frequency studies with models comprised of thin layers. This problem can be overcome by employing a modification of the routine given by Abo-Zena (1979).

Throughout the inversion procedure the dispersion function has been calculated for models consisting of elastic media. The effects of the anelastic Earth is to introduce a dispersion which is related causally to the attenuation in addition to the geometric dispersion (Futterman 1962). The magnitude of this causal dispersion may alter the phase velocities by about 1% (Carpenter & Davies 1966, Kanamori & Anderson 1977) and could be corrected for in the matrix formulation (Schwab & Knopoff 1972). The resulting error is smaller than the standard deviations on the observations and so has been ignored.

Whilst the forward problem shows one-to-one mapping of model to observable parameter curve the inverse problem contains an inherent non-uniqueness with one observed parameter corresponding to many possible models (Backus & Gilbert 1967, Parker 1977).

In early studies of surface waves (Oliver & Ewing 1958, Tryggvason, 1962, Hermann 1969) acceptable models were obtained by trial-and-error matching of theoretical dispersion curves to the

observed data. This forward modelling technique by itself gives no information on the reliability of the model.

The aim of inversion is, therefore, to provide the range of suitable models which will fit the observed data to within their uncertainties. Furthermore, the degree to which the individual layers within the models can be resolved is estimated. Two inversion techniques have been utilised to obtain shear wave velocity distributions with depth; the resulting solution models being compared. A linearised inversion technique (Wiggins 1972) employs a matrix formulism whilst the Hedgehog method (Keilis-Borok & Yanovskaja 1967) is an extension of the forward modelling process designed to map out the region of acceptable models. Both schemes are discussed below.

4.2 TECHNIQUES for the INVERSION of OBSERVED DISPERSION DATA.

4.2.1 Linearised Inversion Method.

The non-linearity of the forward problem to obtain group velocities from a given model implies that the inverse problem is also non-linear. By explanding the functionals as a Taylor's series and discarding all terms of second or higher order the inversion process can be linearised (Wiggins 1972). We have then that

$$O_i - C_i = \sum_{i=1}^{n} \frac{\partial C_i}{\partial P_i} \Delta P_i, \qquad (4.2)$$

where O_i is the i^{th} observation

C_i is the corresponding i^{th} calculated functional

value

ΔP_i is the i^{th} parameter correction to the starting model parameter P_i

$\partial C_i/\partial P_i$ is the partial derivative of C_i with respect to the i^{th} parameter.

In our case we have

$$U_{obs_i} - U_{cal_i} = \sum_{j=1}^{n} \frac{\partial U_{cal_i}}{\partial \beta_j} \delta\beta_j, \qquad (4.3)$$

where i is the frequency index; i=1,...m

and j is the parameter (layer) index; j=1,...n.

This may be represented as a system of linear equations in matrix form as

$$\underline{A}\delta\underline{x} = \delta\underline{b} \ , \qquad (4.4)$$

where $\underline{A}$ is an m x n matrix of partial derivatives

$\delta\underline{x}$ is an n x 1 matrix of parameter corrections

$\delta\underline{b}$ is an m x 1 matrix of differences between observed and calculated group velocities.

If an inverse of $\underline{A}$ can be found then the parameter corrections $\delta\underline{x}$ can be found and applied to the starting model used to provide the calculated group velocities and partial derivatives. In this linearised scheme, therefore, we do not obtain the shear wave velocity model directly but small corrections to be applied to an initial model. The inversion can be repeated for each corrected model until a satisfactory fit is obtained. Because of this the

resulting models can be dependent on the initial starting model.

The inverse of matrix $\underline{A}$ may be calculated from its singular value decomposition (Lanczos 1961) and exists for any m x n matrix. This inverse is constructed of two matrices of orthogonal eigen-vectors and a third, the inverse of the square diagonal matrix of singular values. Small non-zero singular values in the square diagonal matrix can effect the stability of the solution. Small errors in matrix $\delta\underline{b}$ are magnified greatly in the solution resulting in dramatically varying or poorly resolved parameters.

One method to reduce the effect of small singular values is to employ a cut-off strategy. Small singular values and their corresponding eigen-vectors are removed until the ratio of maximum to minimum singular value, the condition number, reaches a satisfactory level (Lanczos 1961) or the variances of the model parameters fall below a given value (Wiggins 1972). An alternative method of damping an unstable linear inversion, and that employed here, is to modify the singular value matrix by a smoothing parameter. The Levenberg-Marquardt method (Levenberg 1944, Marquardt 1963) employs the smoothing parameter, θ, which has the following properties. As θ tends to infinity the solution is damped out and as θ tends to zero the modified inverse approaches the Lanczos inverse. For finite θ as a given singular value tends to zero (that is its reciprocal would approach infinity) the corresponding element of the modified diagonal inverse matrix tends zero and the effect of the singular value is damped out. A succinct review of the matrix formulation of linear inverse problems has been given by Evans (1981).

The degree of resolution of individual layers may be expressed in terms of the resolution matrix which is produced by the

multiplication of the matrix $\underline{A}$ with its calculated inverse (Jackson 1972). The j^{th} row of this matrix expresses the extent to which the estimate $\bar{x}_j$ is an average of the true parameters x_j, j=1,n. Perfect resolution obtains if the resolution matrix is the identity matrix. The rows of the matrix have been called resolution kernels (Der et al. 1970) and are, therefore, delta functions for perfect resolution. Resolving kernels may be plotted against depth and regarded as windows through which we view the true solution (Braile & Keller 1975). For non-zero θ the parameter corrections are no longer independent with the result that the resolution can at best only approximate delta functions.

Estimates of the variance of each parameter are also obtained and indicate the spread of acceptable models. There exists a trade-off between the estimates of the variance and the resolution of parameters with one improving only at the expense of the other (Braile & Keller 1975).

The dimensions of the elements of matrices $\delta\underline{x}$ and $\delta\underline{b}$ can affect the inversions by favouring changes in thick layers. Therefore, an n x n weighting matrix is introduced which divides each layer parameter by the thickness of that layer. A similar matrix is used to weight the observations by their standard deviations (Wiggins 1972). In the following inversions the half-space of each model has been weighted arbitrarily at twice the thickness of the layer immediately above.

4.2.2 Hedgehog Inversion Method.

The second inversion method employed forms an improvement on the trial-and-error forward modelling techniques of earlier workers. In

the Hedgehog method the forward problem is solved for models within parameter space and the resultant dispersion curve tested against the observed data (Keilis-Borok & Yanovskaja 1967).

Initially, a Monte-Carlo random search within a defined sub-space of parameter space is used to find a point, that is a preliminary model, which satisfies the test criteria. This random search could be continued but would not indicate efficiently the measure of the goodness of fit because many of the random points tested would not yield acceptable or realisable models.

The Hedgehog method improves on this by using a network of discrete points to span the parameter sub-space. Having found a successful random point the model defined by the discrete point, or knot of the network nearest to the random point, is tested. If this model satisfies the tests then the search continues by testing the models from neighbouring knots on the discrete mesh. In this manner a singly connected region of acceptable knots is constructed. Having completed this region the Monte-Carlo search is resumed to find further acceptable regions outwith the existing ones.

The accceptance of a point or knot from the parameter sub-space was assessed using two test criteria applied to the forward solution. Following Burton & Kennet (1972) tests were made between observed and calculated slowness at individual frequencies and on the complete dispersion curve such that

$$a_i = \frac{p_{ti} - p_{oi}}{\sigma_{pi}} < a_{max} \quad \text{for all } i, \tag{4.5}$$

$$s = \frac{1}{m}\left[\sum_{i=1}^{m}\left(\frac{p_{ti} - p_{oi}}{\sigma_{pi}}\right)^2\right]^{\frac{1}{2}} < s_{max}, \qquad (4.6)$$

where σ_{pi} is the standard deviation of the observation.

The choice of a_{max}, s_{max} and the size of the mesh spanning the parameter sub-space control the nature of the final solution. The confidence limit to which the model solution fits the observed data is governed by a_{max} and s_{max}. If the criteria used in the tests were too strict no acceptable models would be found whilst a region with little physical meaning would result if the test criteria were too lenient. Similarly for too large a mesh size all the acceptable models could lie between adjacent knots and so not be located whilst too small a mesh size would result in a large number of redundant knots. Optimum values for the test criteria and mesh size may be determined from preliminary inversion runs.

4.3 INVERSION of OBSERVED RAYLEIGH WAVE DISPERSION DATA.

The theoretical group velocities and partial derivatives required by the inversion techniques above have been obtained by the solution of the forward problem for a model specified by the parameters α_j, β_j, ρ_j and h_j, j=1,n for n-1 layers overlying a half-space.

For the linearised inversion method a system of equations could be established to solve for each of these parameters for a number of layers provided the number of observations were greater than or equal to the total number of parameters. Stability of the inversion could then be achieved by a suitable choice of θ. Many of the model parameters, however, would not be adequately resolved. Similarly,

in the Hedgehog technique any attempt to invert for the 4 x n parameters of the model would, in general, be outside the resolution capabilities of the observed data. Further, the computational effort required for such inversions would be prohibitive. It is necessary, therefore, to place constraints on some parameters thereby reducing the number of independently variable parameters in the inversion.

Partial derivatives of velocity with respect to different parameters have been given by Takeuchi *et al.* (1964) and Bloch *et al.* (1969) and show that

$$\frac{\partial c_i}{\partial \beta_i} >> \frac{\partial c_i}{\partial \alpha_i} \quad \text{and} \quad \frac{\partial c_i}{\partial \beta_i} >> \frac{\partial c_i}{\partial \rho_i} . \tag{4.7}$$

These inequalities imply that α_i and ρ_i would be poorly determined by the inversion of Rayleigh wave dispersion data and are, therefore, constrained to be variables dependent on the shear wave velocity.

Compressional wave velocity is related to shear wave velocity by Poisson's ratio, σ. Assumpção & Bamford (1978) using shear wave observations along the LISPB profile give σ between 0.27 and 0.33 near the surface and from 0.23 to 0.26 at greater depth. These data apply only to the Scottish portion of the LISPB and no estimates of σ have been given for central England. A Poisson's ratio of 0.28 was found to yield the best fit between observed data and theoretical slowness calculated for simple models of two layers overlying a half-space using reported values of compressional wave velocity and density for the region. Further, $\sigma = 0.28$ was the median of the extremal values reported by Assumpção & Bamford (1978). A Poisson's ratio of 0.28 constant with depth was assumed

to constrain the compressional wave velocity to the shear wave velocity of each layer by the relation

$$\alpha = 1.81\beta. \qquad (4.8)$$

A relationship between rock density and compressional wave velocity has been established by Nafe & Drake (1965) empirically. Approximating the low velocity portion of the curve by a straight line gives

$$\rho = 0.286\alpha + 1.736. \qquad (4.9)$$

The independently variable model parameters for each inversion are the shear wave velocity and the thickness of each layer. The number of layers is limited by the number of observational points.

The linearised inversions proceeded as follows. An initial model was obtained from the forward modelling described above. Such forward modelling to match the observed group slowness dispersion curve highlights a further cause of non-uniqueness in the inversion of group slowness data. Unlike phase slowness the shape of the curve for group slowness need not relate simply to the intrinsic shear wave velocity distribution with depth. It is possible to increase (decrease) the group slowness by increasing (decreasing) the shear wave velocity at the appropriate depth or by decreasing (increasing) the shear wave velocity at some other depth (Yu & Mitchell 1979).

For the first iteration of the starting model θ was set equal to the maximum singular value thus guaranteeing a stable solution (Evans 1981). At each subsequent step θ was halved, thereby

increasing the resolution, until the variance of any layer velocity was greater than 0.15 km s^{-1} after which θ was kept constant at this value.

Each iteration then continued until the reduced chi-squared

$$\chi_r^2 = \frac{1}{(m-n-1)} \sum_{i=1}^{m} \left[\frac{U_{obs_i} - U_{th_i}}{\sigma_{obs_i}} \right]^2 < 0.25, \qquad (4.10)$$

where U_{obs_i} is the observed group velocity

U_{th_i} is the theoretical group velocity

σ_{obs_i} the standard deviation of the i^{th} observed velocity

for m frequency observations, index i, and

n layers.

The resolution kernels and final solution of each inversion were then examined and the model modified by subdividing layers. The inversion procedure was then repeated, recalculating the partial derivatives for each new starting model, until the layer thickness reached a minimum width for resolution; thinner layers would add merely to computational effort whilst thicker layers would be resolved independently of the others and would not represent all the available information (Evans 1981). The depth to the half-space was fixed during early inversions by noting where deep layers were not resolved and had shear wave velocities, with small variances, close to those of the starting model.

The fit of the theoretical group velocity for the model to the observed is given by the residual

$$\delta U_i = U_{obs_i} - U_{th_i} , \qquad (4.11)$$

and the normalised residual

$$n_r = \frac{U_{obs_i} - U_{th_i}}{\sigma_{obs}} \quad , \tag{4.12}$$

for each frequency, index i.

The results from the linearised inversion method were used to assist the initial Hedgehog inversions. The starting bounds on the parameter sub-space were determined by inspection of the solution velocities and their variances from the linearised inversions. Layer thicknesses were fixed by combining layers of similar velocities. The variables in parameter space were, therefore, the shear wave velocity of the layers and the half-space; other parameters required to define the model being constrained as given above.

In these inversions the number of variable parameters was restricted to four or five. An attempt to invert for more parameters, suggesting finer resolution, would result in poorly defined models having little physical meaning. The reduction in the number of variable parameters is, therefore, similar to the use of the Levenberg-Marquardt parameter, in the linearised inversions, where a smoothing of the variable parameters results (Evans 1981).

For the final Hedgehog solution regions the mesh size varied between 0.05 km s^{-1} and 0.15 km s^{-1}. The test criteria were set with a_{max} and s_{max} equal and varying between 1.0 and 2.5 providing fits to the data between the 68% and 99% confidence levels.

4.3.1 The Carboniferous Limestone District.

The shear wave velocity-depth profile for LST 1 from the linearised inversion technique shows the velocity to decrease with depth from 2.5 km s^{-1} at the surface to 2.1 km s^{-1} at 300 m (Fig 4.1). The velocity then increases sharply to 2.5 km s^{-1} and shows a positive velocity gradient to a depth of 900 m. At deeper levels the solution velocity decreases with depth.

A negative velocity gradient at depth could be caused by forcing the inversion to depths below which there is little or no propagating Rayleigh wave energy. In the final models presented, however, the half-space has been fixed at levels above these depths (see above) and hence the lower velocity at depth cannot be a spurious facet of the inversion. The use of alternative inversion schemes, for example the Hedgehog method, could substantiate, or otherwise, the existence of a negative velocity-depth gradient.

The Hedgehog solution for LST 1 (Fig 4.2) shows the same trend as the linearised inversion solution with a maximum velocity at 1 km. A well defined region of lower velocity is given below 1 km implying that a velocity inversion at these depths does exist. The poorer definition of the velocity of the upper layer implies that the decrease in velocity within the top 300 m of the linearised solution could be replaced by a layer of velocity between 2.2 km s^{-1} and 2.4 km s^{-1}.

The 300 m discontinuity is also shown in the linear inversion solution for LST 2 (Fig 4.3). Below this the velocity increases with depth reaching a higher maximum of 3.1 km s^{-1} at 1.1 km. There is some evidence for a velocity inversion at depth. A velocity between 2.00 - 2.22 km s^{-1} is given for the upper layers of the model.

Key to the figures giving the results of the inversion of the observed Rayleigh wave group slowness dispersion for the distribution of shear wave velocity with depth.

Linearised Inversions: Figures 4.1, 4.3, 4.5, 4.7, 4.9, 4.11, 4.13, 4.15, 4.17.

Each figure shows:

1. Graph of shear wave velocity against depth giving mean solution shear wave velocity with its standard deviation for each layer.

2. Resolution kernels. The resolution kernel for each layer is shown from the surface layer on the left to the half-space on the right. Each resolution kernel is drawn against the same depth scale as in 1 above and are normalised to the same peak value. A small tick is drawn against each kernel showing the middle of the relevant layer. Positive values are shaded.

3. Residual and normalised residual. These graphs show the comparison of the theoretical dispersion for the layered model with the mean values of shear wave velocity given in 1 above and the observations.

The residual is calculated from

$$\delta U_i = U_{obs_i} - U_{th_i} \quad s\ km^{-1},$$

and the normalised residual from

$$n_r = \frac{U_{obs_i} - U_{th_i}}{\sigma_{obs_i}},$$

where U_{obs_i} is the observed group velocity
U_{th_i} is the theoretical group velocity
σ_{obs_i} is the standard deviation of the observation

at each frequency, index i.

The captions for the individual inversions give the values of the significance level and smoothing parameter, θ, of the solution.

Hedgehog Inversions: Figures 4.2, 4.4, 4.6, 4.8, 4.10, 4.12, 4.14, 4.16, 4.18.

Each figure gives the solution region (hatched) and the search region of parameter space (broken lines). The confidence level of the fit to the data is also given.

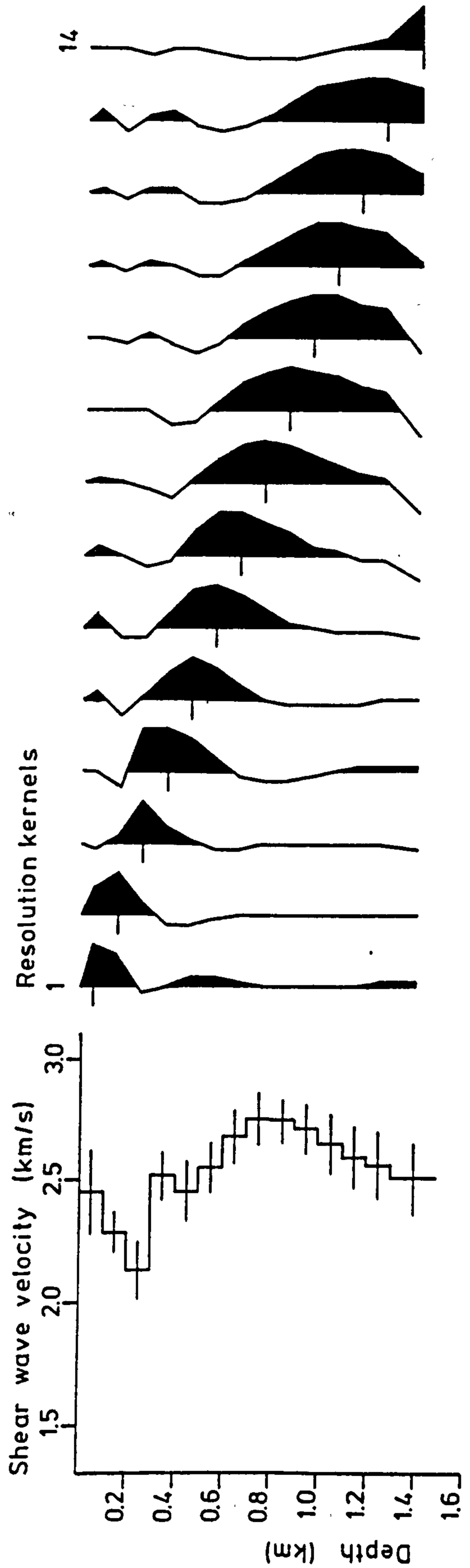

Linearised inversion of the observed Rayleigh wave group slowness dispersion for shear wave velocity with depth for LST 1. (Significance level 99%, θ = 14.7)

Figure 4.1

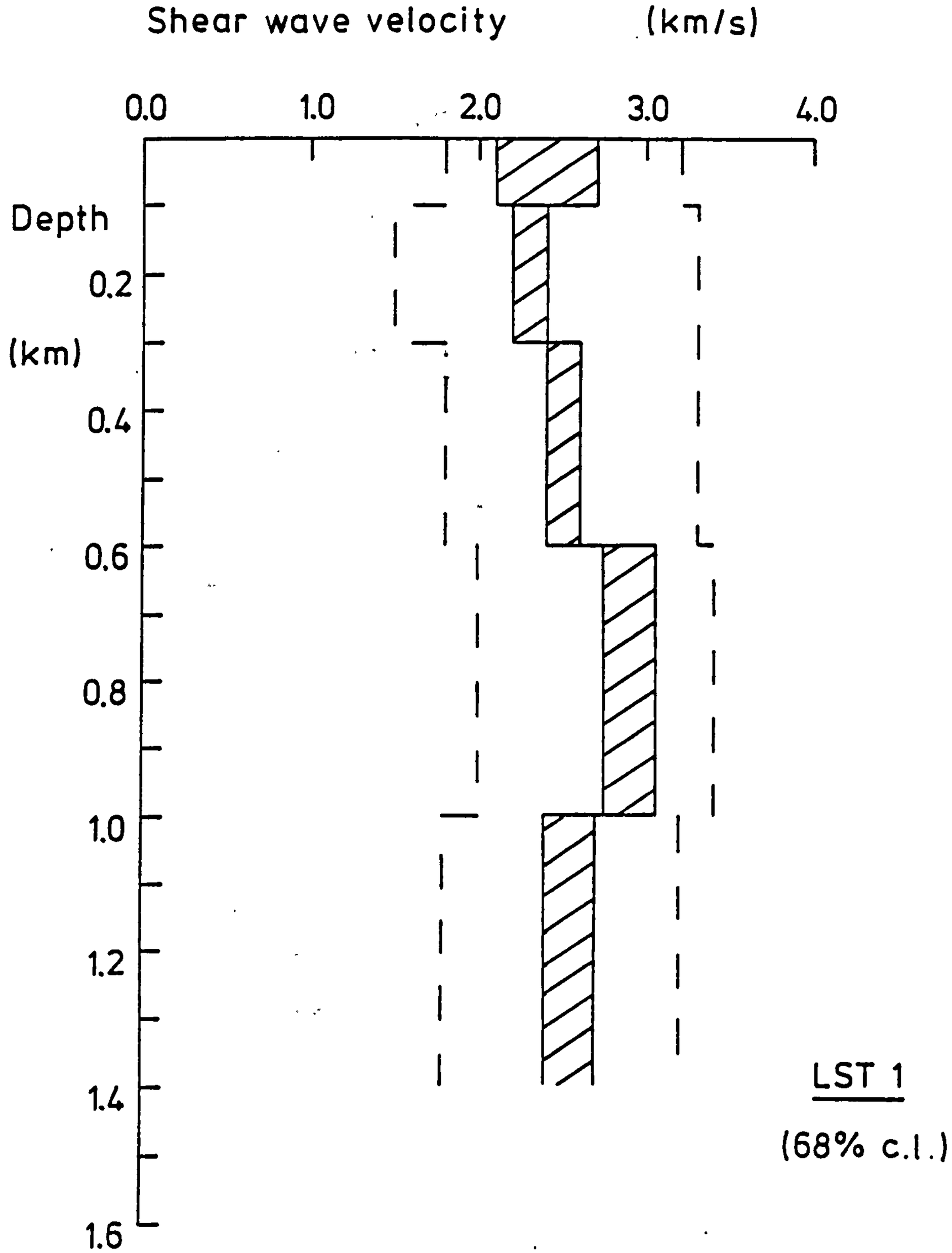

Figure 4.2 Hedgehog inversion of the observed Rayleigh wave group slowness dispersion for shear wave velocity with depth for LST 1.

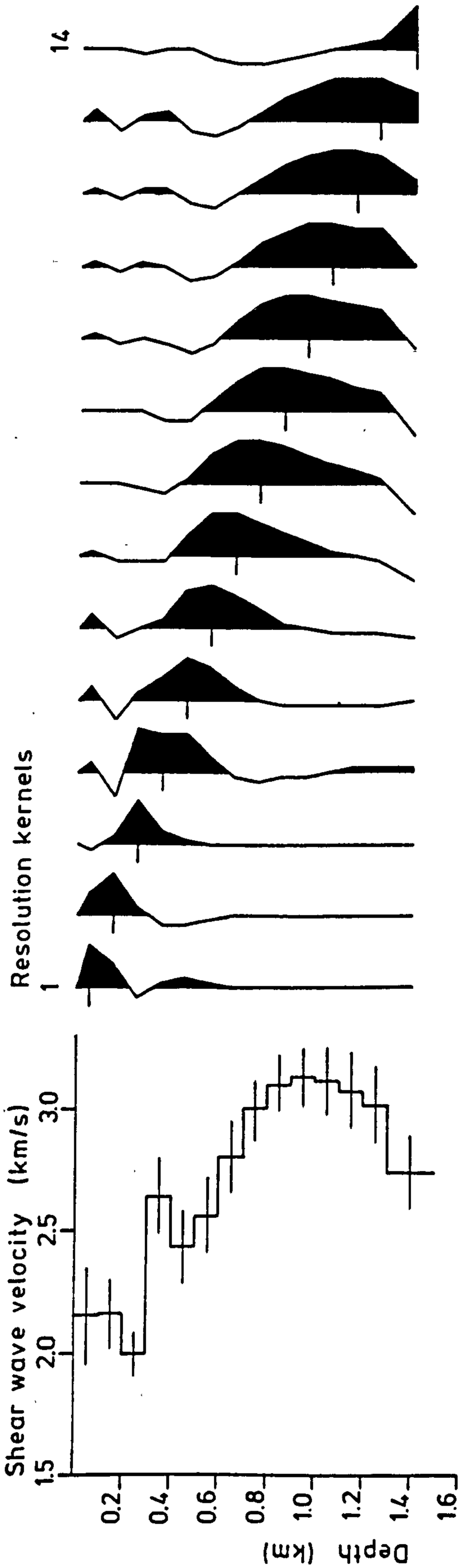

Linearised inversion of the observed Rayleigh wave group slowness dispersion for shear wave velocity with depth for LST 2. (Significance level 99%, θ = 13.3)

Figure 4.3

The Hedgehog solution model for LST 2 (Fig 4.4) reflects the general trend in velocity with depth. At depth the layer velocities are less well defined and the possibility of a constant velocity with depth below 1 km, rather than a velocity inversion, is not precluded.

The resolution kernels for the linearised inversion solutions (Fig 4.1, 4.3) are compact implying good resolution for most layers although the resolution kernels are not delta functions. Some kernels exhibit small negative side-lobes which could produce apparent low velocity zones in the solutions. These side-lobes could be removed by forcing the shape of the kernels to be a function other than the delta function. Braile & Keller (1975) modify their kernels by a cosine-bell function to remove the undesirable side-lobes. Within this thesis no such modification has been attempted and so care must be taken in interpreting any low velocity zones in the models which do not exhibit compact resolution. The resolution kernel for the half-space is, in all cases, peaked sharply; a distortion thought to be due to the arbitrary weighting imposed on the half-space (Evans 1981).

The model for LST 1 must represent an average of the structures implied by the different dispersion north and south of the Bonsall Fault zone. An attempt was made to invert the group slowness dispersion data PLST 1N over the entire frequency range. The resulting solution consisted of a series of layers with widely oscillating shear wave velocities and was considered, therefore, to be an unrealistic model. These oscillatory layer velocities were required by the inversion technique to model the steep decrease in group slowness above 3.7 Hz. A second, more acceptable model was determined by conducting the inversion on a sub-set of the observed

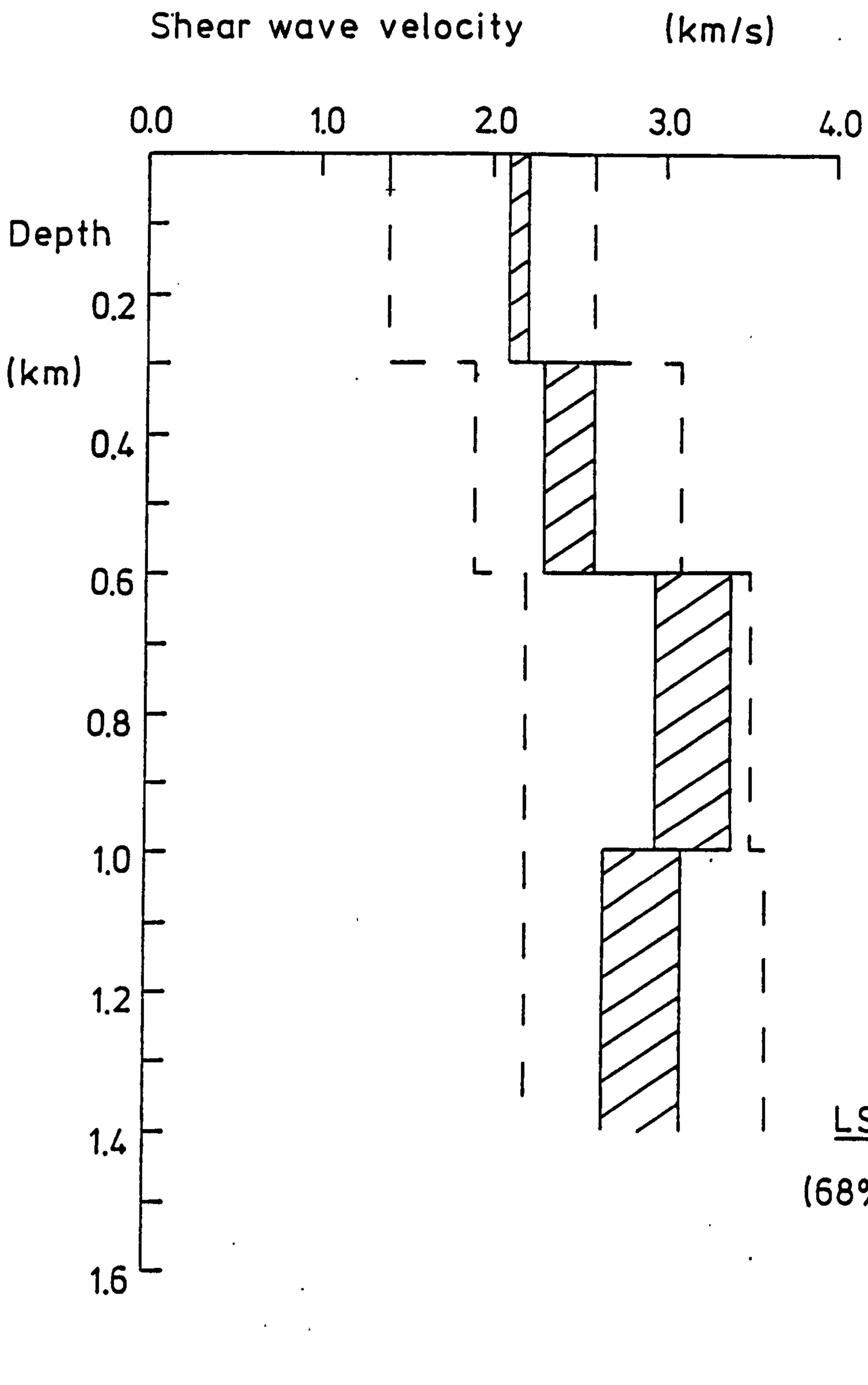

Figure 4.4 Hedgehog inversion of the observed Rayleigh wave group slowness dispersion for shear wave velocity with depth for LST 2

dispersion PLST 1N. Frequencies of 3.7 Hz and above were, therefore, excluded from the inversion. Only the shallowest layers of any model will be affected by the exclusion of higher frequency estimates of dispersion.

The resulting model (Fig 4.5) again shows the discontinuity in velocity at 300 m. Velocities of 2.0 - 2.2 km s^{-1} are given above this boundary; similar to those of LST 2. There is a general increase in velocity with depth to a maximum of 3.0 km s^{-1} at 800 m. A zone of lower velocity is defined at depth. A low velocity channel may also exist at higher levels between 400 - 500 m. Good resolution exists for all layers.

The Hedgehog solution regions for LST 1N (Fig 4.6) indicate that the velocity of the upper layers may be more variable than given by the linearised inversion solution. The 300 m discontinuity and increase in velocity with depth to 1 km is well substantiated. The presence of a low velocity layer at depth is not denied by the Hedgehog inversion which gives a solution region of only moderate definition below 1 km.

The solution model for LST 1S contrasts sharply with that of LST 1N (Fig 4.7). Whilst the resolution is good the standard deviations of the layer solution velocities are large and reflect the increased errors within the observed dispersion data PLST 1S. The upper layer of velocity 2.5 km s^{-1} is now only 200 m thick below which the velocity decreases with depth producing a low velocity channel between 200 - 600 m. Velocity increases to a maximum of 2.6 km s^{-1} at 1.1 km after which there may exist a small decrease in velocity.

The general trend in velocity between the surface and 800 m is supported by the Hedgehog inversion (Fig 4.8). The possibility of a

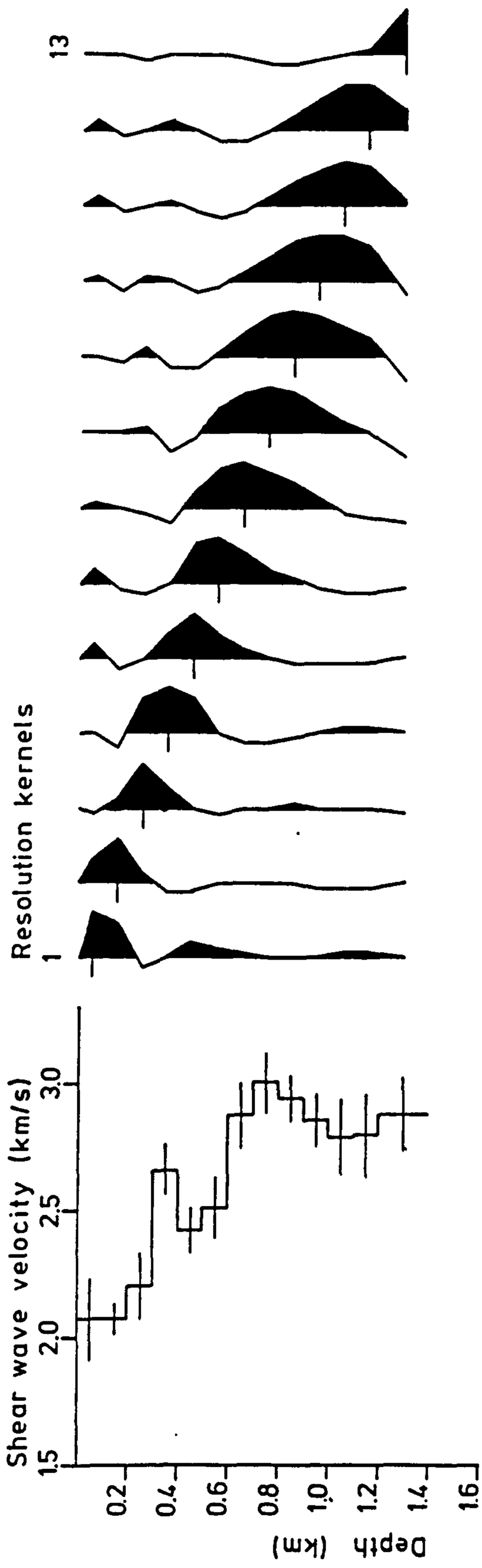

Figure 4.5 Linearised inversion of the observed Rayleigh wave group slowness dispersion for shear wave velocity with depth for LST 1N. (Significance level 80%, $\theta = 14.2$)

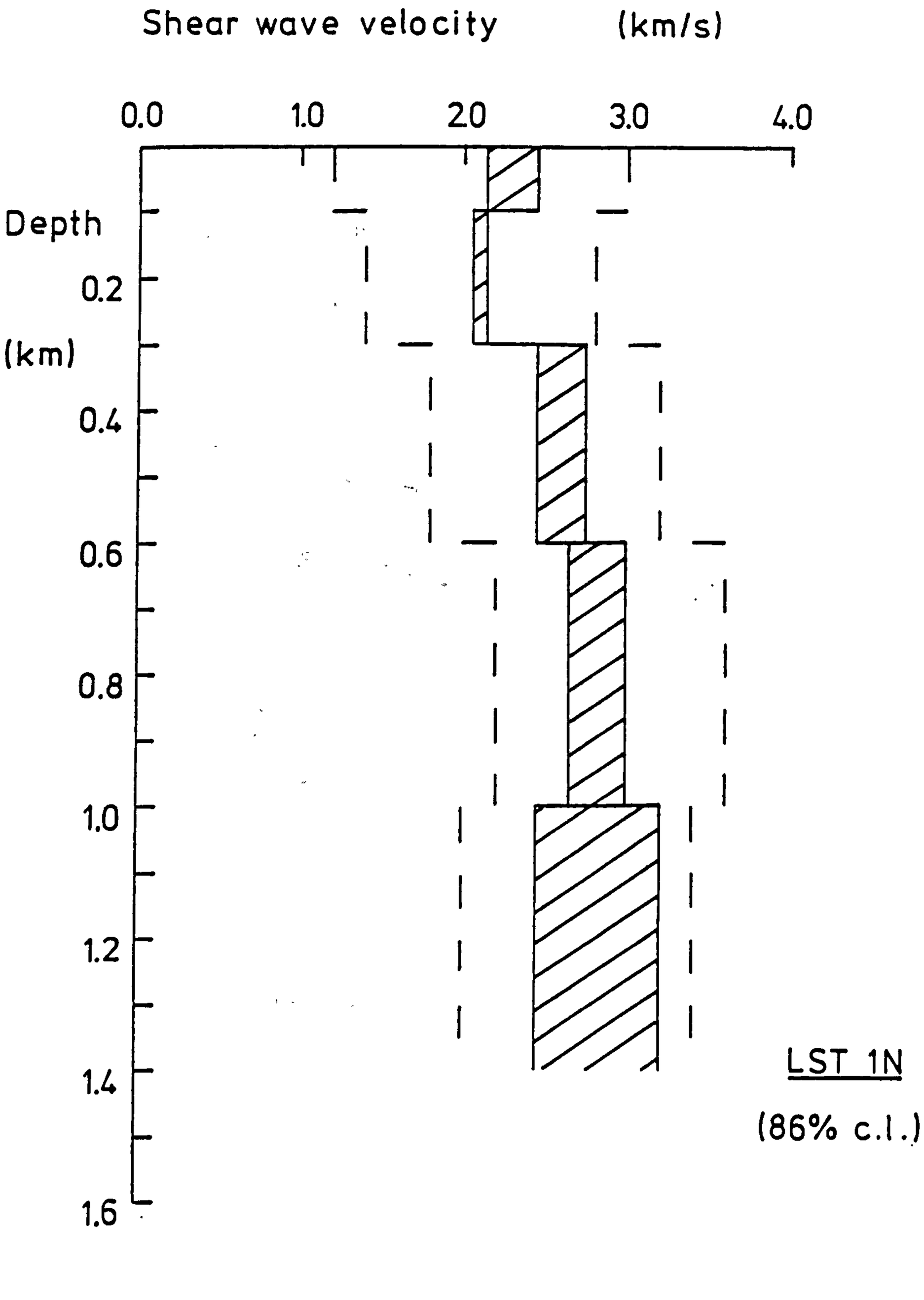

Figure 4.6 Hedgehog inversion of the observed Rayleigh wave group slowness dispersion for shear wave velocity with depth for LST 1N.

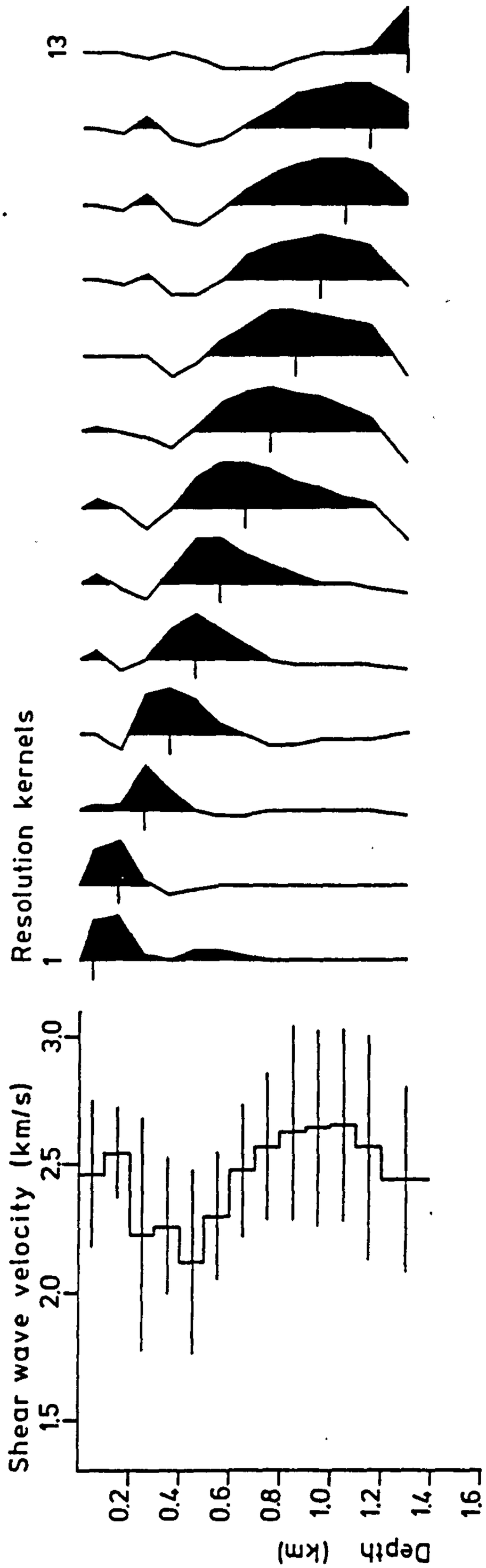

Figure 4.7 Linearised inversion of the observed Rayleigh wave group slowness dispersion for shear wave velocity with depth for LST 1S. (Significance level 90%, θ = 5.5)

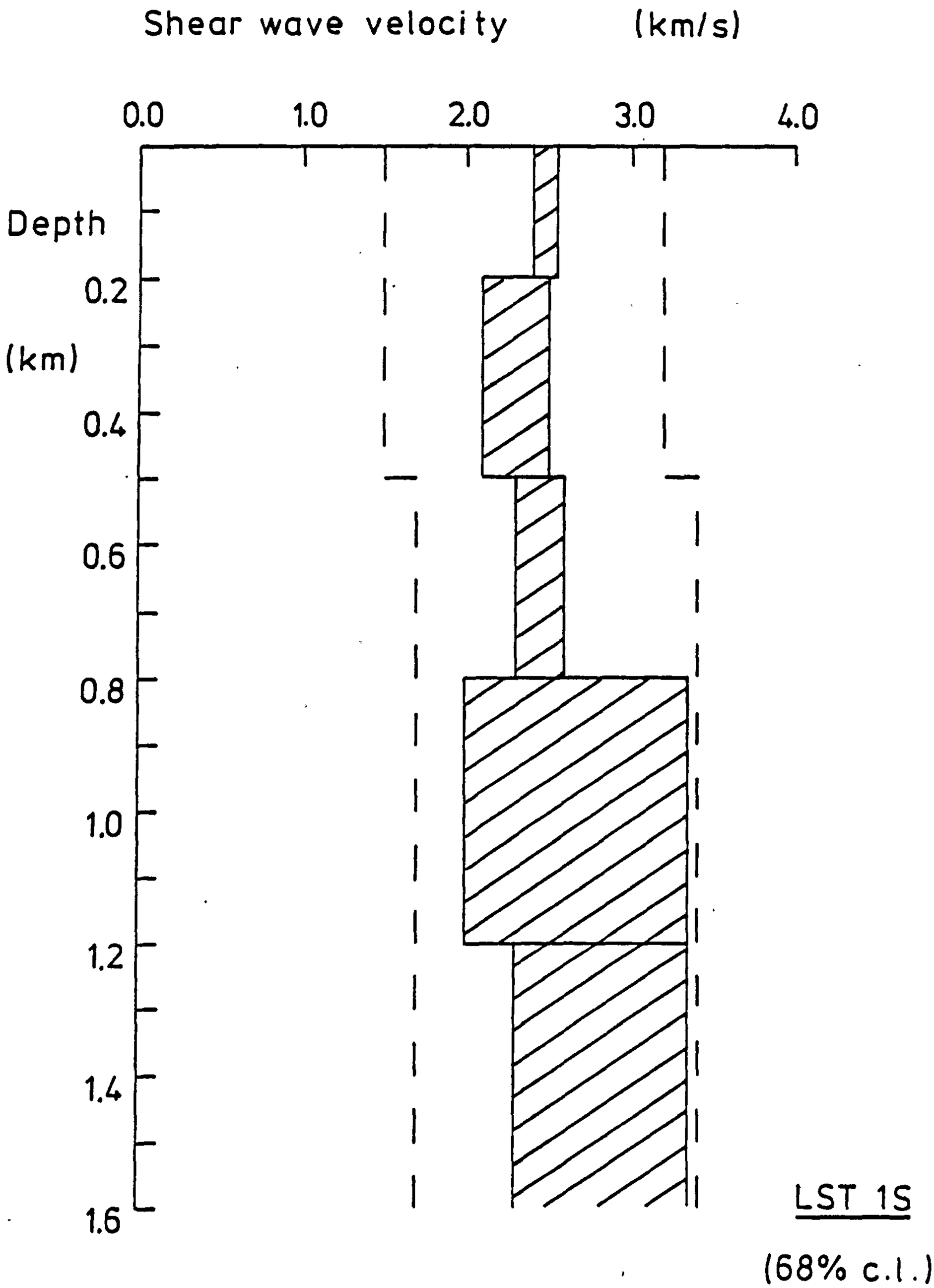

Figure 4.8 Hedgehog inversion of the observed Rayleigh wave group slowness dispersion for shear wave velocity with depth for LST 1S.

constant velocity with depth to 800 m is not precluded by the solution regions. At depths below 800 m little can be inferred about the velocity pertaining to those levels due to the poor definition of the solution regions.

Solution models were also determined for the provinces LST 2N, LST 2S. The shear wave velocity-depth profile for LST 2N (Fig 4.9) shows solution velocities which vary widely between layers. A high velocity of 4.6 km s^{-1} is given at a depth of 900 m. The resolution kernels, however, are no longer compact with a number of secondary peaks and large negative side-lobes. The fit between the observed dispersion and the forward solution for this model is poor in comparison to the previous provincial models, having a minimum χ_r^2 = 0.4. The oscillatory distribution is also shown in the Hedgehog solution (Fig 4.10). The solution regions are not well defined supporting the poor resolution given by the linearised inversion.

To facilitate the inversion of the group slowness data PLST 2S, which contained no estimates of error, each observation was assumed arbitrarily to be determined to an accuracy of ±10%. The solution indicates an increase in velocity from 1.2 km s^{-1} at the surface to 2.1 km s^{-1} at depths below 2.1 km. This solution, therefore, extends to greater depths than other models (Fig 4.11). The half-space, however, is not resolved. Attempts to improve the solution by limiting the inversion to levels comparable to those of other solutions failed; meaningful dispersion curves could not be generated for the resulting models. The fit to the observed data was very poor returning a χ_r^2 of 1.4. This solution for LST 2S cannot, therefore, be considered as meaningful implying that two stations are not sufficient to give reliable estimates of group

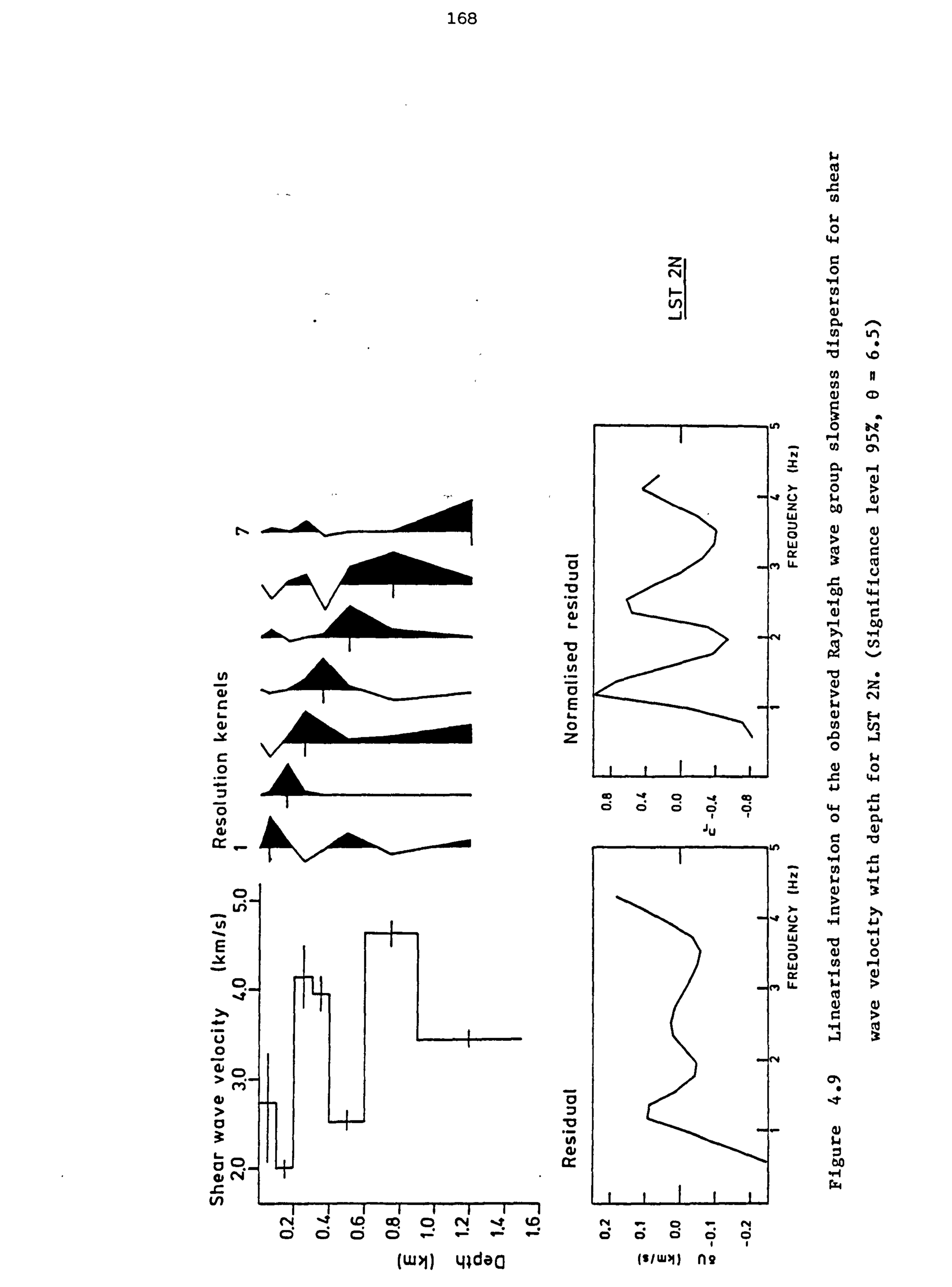
LST 2N
Linearised inversion of the observed Rayleigh wave group slowness dispersion for shear wave velocity with depth for LST 2N. (Significance level 95%, θ = 6.5)
Resolution kernels
Shear wave velocity (km/s)
Depth (km)
Normalised residual
Residual
FREQUENCY (Hz)
δu (km/s)

Figure 4.9

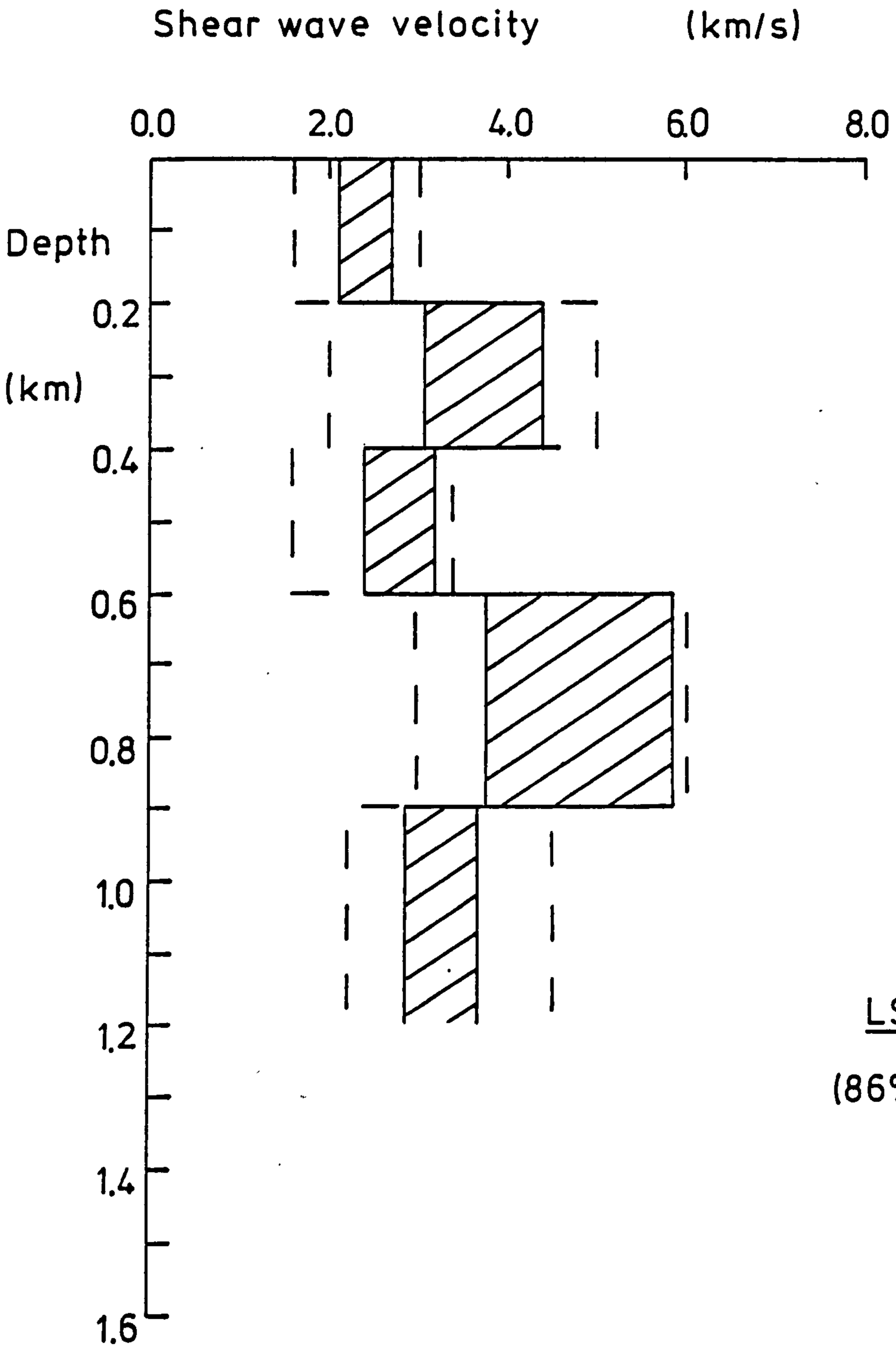

Figure 4.10 Hedgehog inversion of the observed Rayleigh wave group slowness dispersion for shear wave velocity with depth for LST 2N.

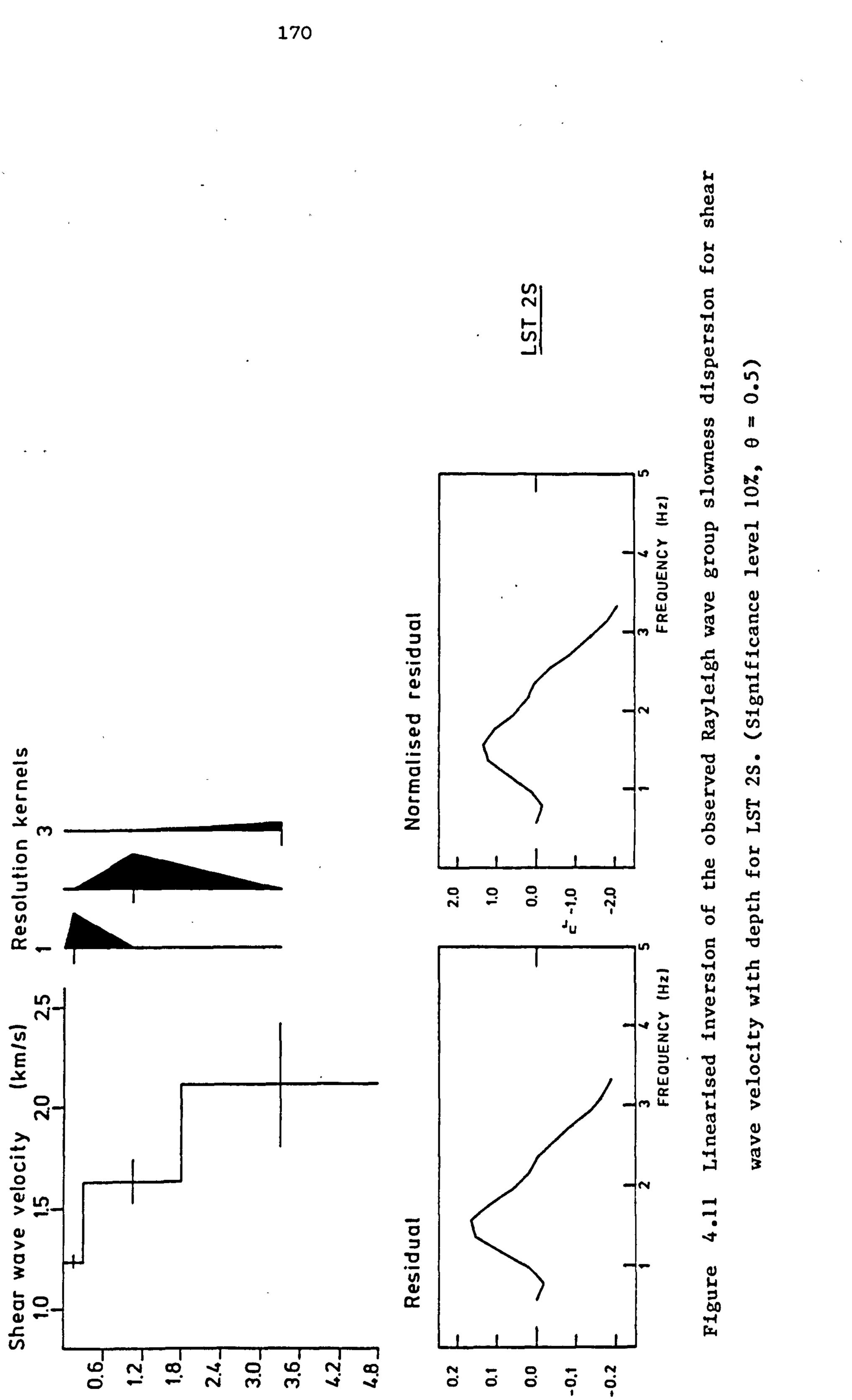

Figure 4.11 Linearised inversion of the observed Rayleigh wave group slowness dispersion for shear wave velocity with depth for LST 2S. (Significance level 10%, θ = 0.5)

slowness. Solution regions could only be obtained from the Hedgehog inversion scheme if the test criteria a_{max}, s_{max} were set to a high value of 2.5 (99% confidence limit) indicating that the acceptable models resulted in a poor fit to the observed dispersion (Fig 4.12).

4.3.2 The Millstone Grit District.

Of the three group slowness dispersion curves determined for the Millstone Grit district only PMG 1 represents a single province unaffected by the structure of the limestone district.

The model for MG 1 from the linearised inversion scheme exhibits shear wave velocities which are lower overall than in the limestone district (Fig 4.13). The profile consists of a number of layers with velocities varying from a minimum of 1.2 km s^{-1} at 200 m to a maximum of 2.0 km s^{-1} at a depth of 400 m. In contrast to the unstable solution for LST 2N the resolution kernels for MG 1 are compact and located well about the relevant layer. The fit to the observed data is good with a χ^2_r of 0.02. Whilst the solution model is oscillatory, therefore, this profile must be regarded as a reasonable model because of the good resolution and fit to the observed data.

For the Hedgehog inversion the general trend of the velocity variation is supported (Fig 4.14). The solution does not extend to the same depths as the linearised inversion because the maximum number of variables was restricted to five. The inversion could have been extended to deeper levels by combining the upper two layers and hence reducing further the definition of the velocity at the surface. The solution regions do not preclude a constant velocity of 1.6 km s^{-1} from the surface to a depth of 700 m

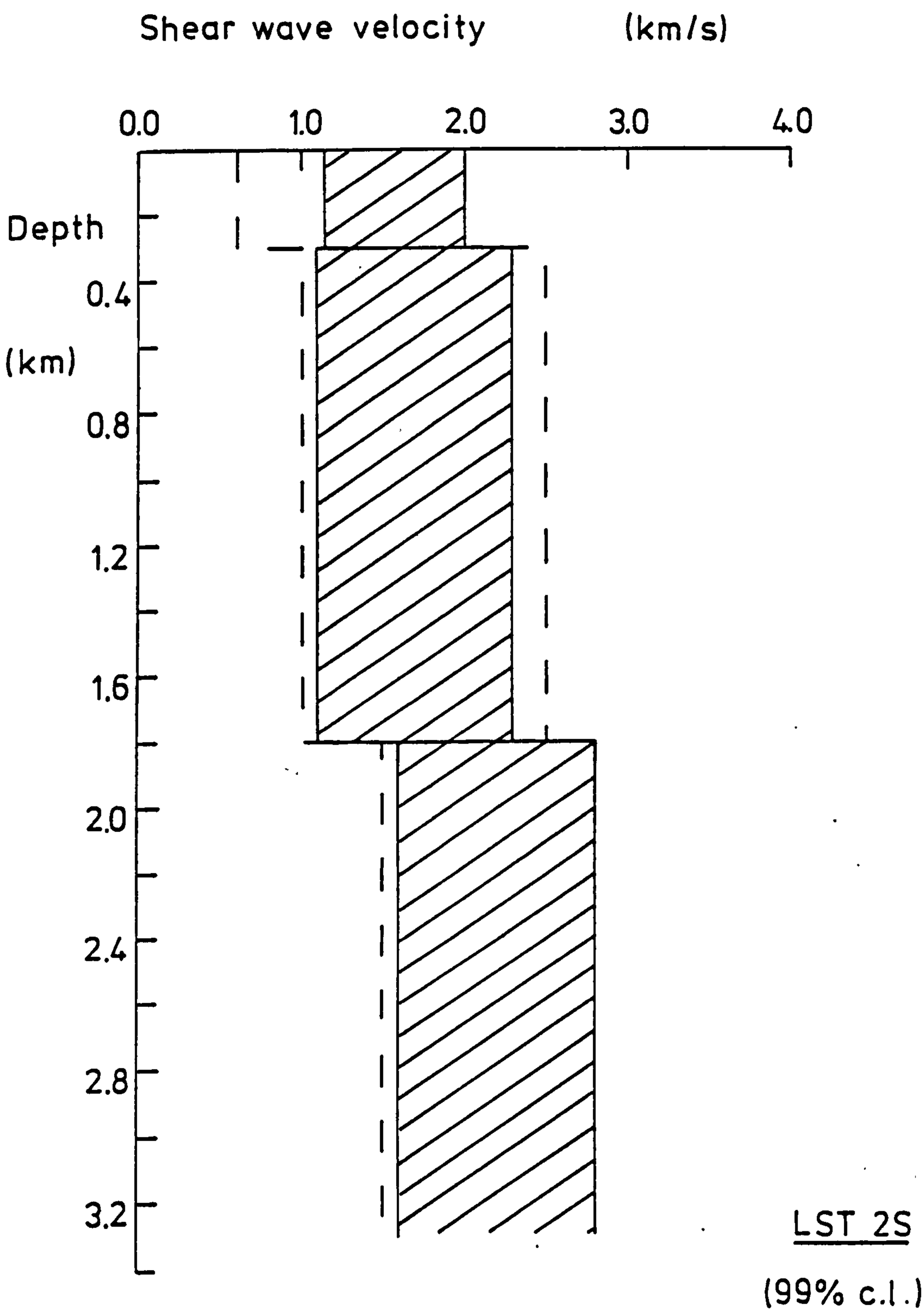

Figure 4.12 Hedgehog inversion of the observed Rayleigh wave group slowness dispersion for shear wave velocity with depth for LST 2S.

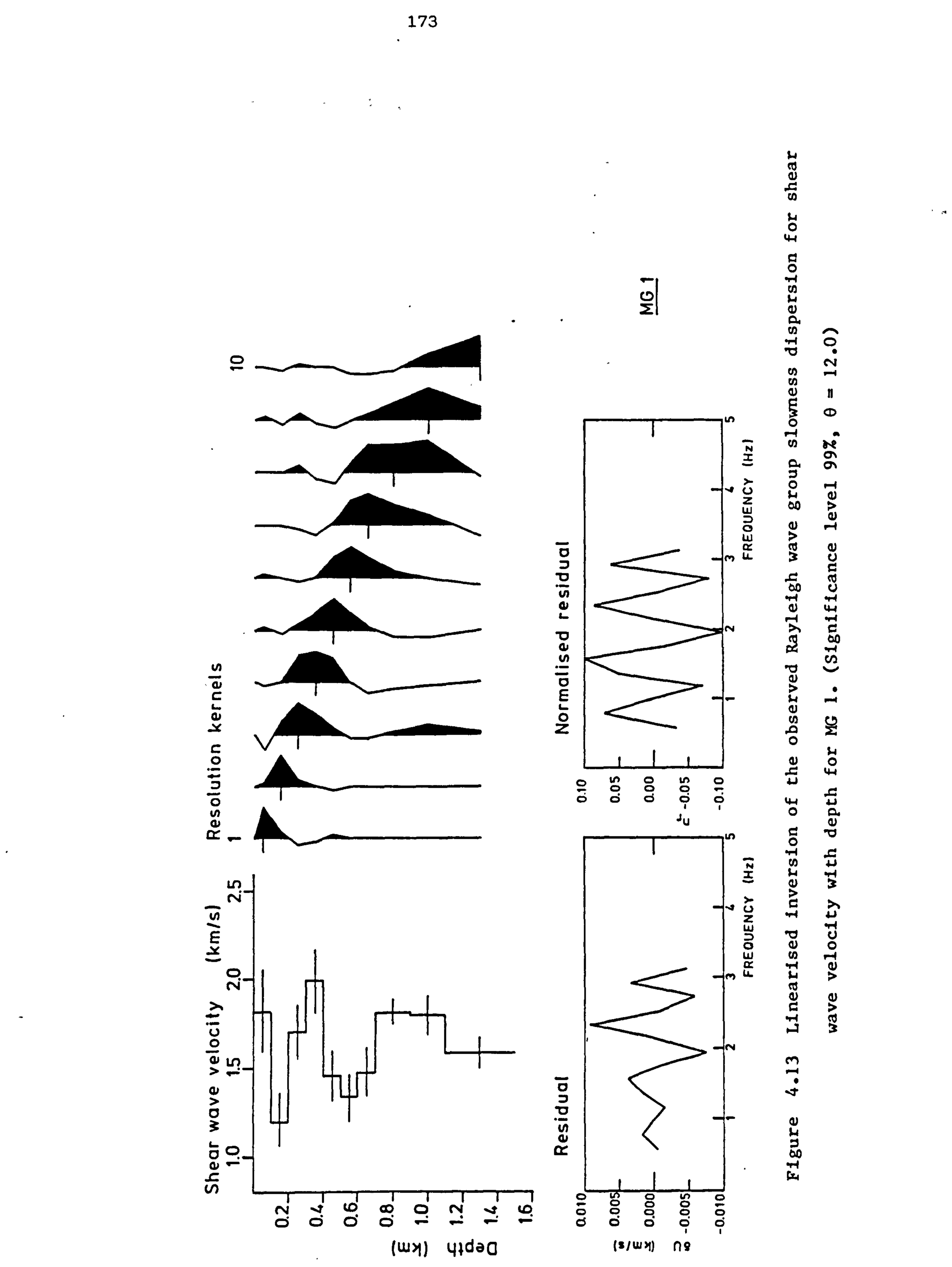

Figure 4.13 Linearised inversion of the observed Rayleigh wave group slowness dispersion for shear wave velocity with depth for MG 1. (Significance level 99%, θ = 12.0

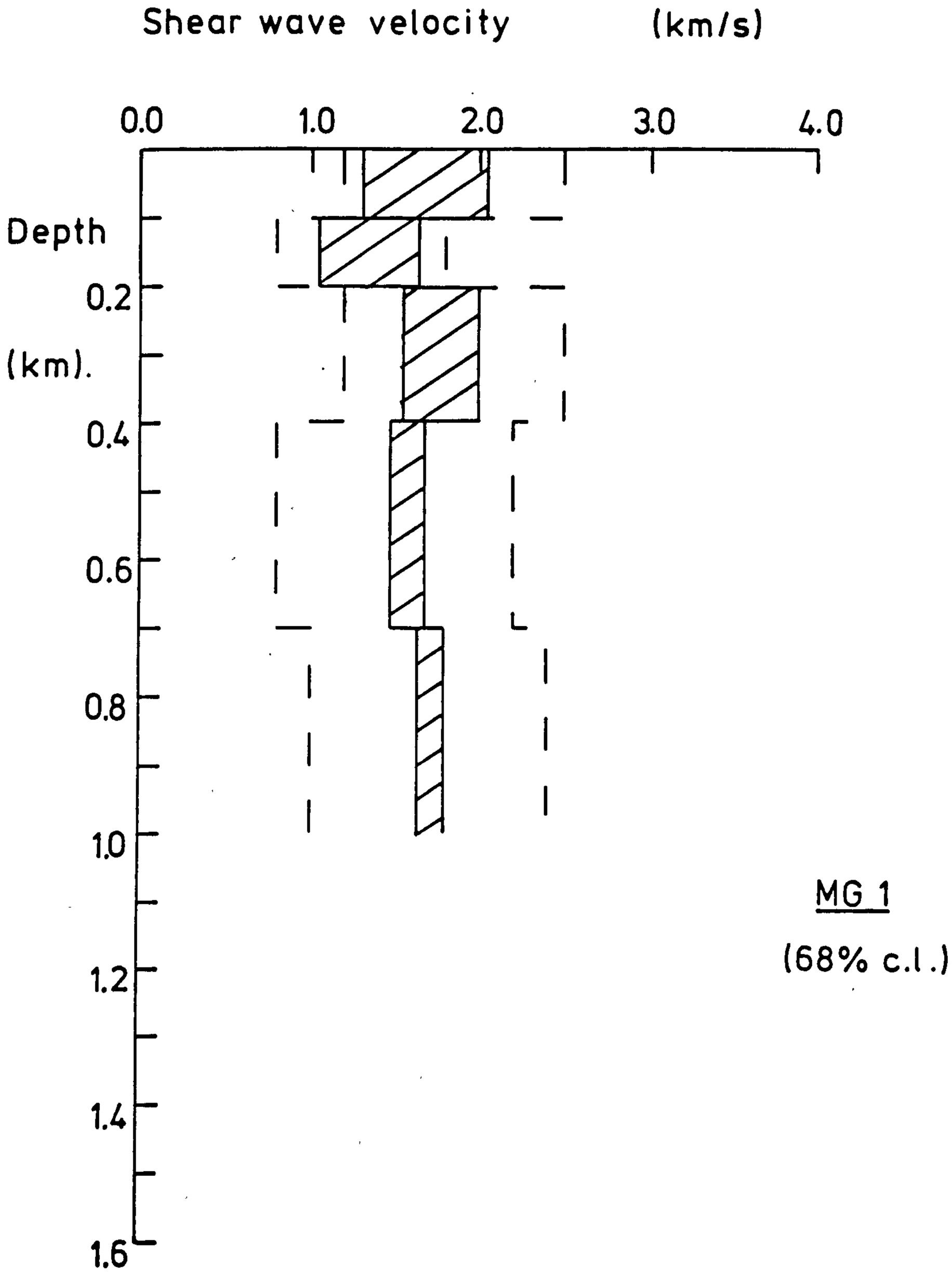

Figure 4.14 Hedgehog inversion of the observed Rayleigh wave group slowness dispersion for shear wave velocity with depth for MG 1.

increasing slightly below this.

Two models are furnished by each of the inversion schemes for the stations comprising the cluster array. These models are for mixed province propagation paths but that for BMR is affected only slightly by the Millstone Grit being close to the limestone/ Millstone Grit boundary.

The solution from the linearised inversion scheme for MGAR (Fig 4.15) shows a velocity gradient with velocities between 1.6 - 2.0 km s^{-1} from the surface to 0.5 km. A layer of velocity 2.3 km s^{-1} and thickness 200 m is followed by a further increase in velocity at 700 m. Poor resolution obtains for the surface layer with a broad kernel having significant components at depth.

The Hedgehog inversion provides a model indicating an increase in velocity with depth (Fig 4.16). The range of acceptable velocities is larger in the surface layer than the rest of the inversion. In general the solution regions have higher velocity limits than the profiles for MG 1.

The solution velocities for BMR from the linearised inversion are higher than for MGAR by 0.16 km s^{-1} (Fig 4.17). The surface layer, of greater thickness because of poor resolution, has a velocity of 2.2 km s^{-1} which contrasts with the average velocity of 1.7 km s^{-1} for the first 200 m of MGAR. Below the surface layer of BMR there exists a low velocity channel which is followed by a positive velocity gradient to a depth of 0.7 km. Below this depth the velocity is constant at 2.6 km s^{-1}.

The Hedgehog model is very poorly defined even at the confidence limit of 68% fit to the data (Fig 4.18). The low velocity channel at 300 m is not substantiated by the Hedgehog solution regions. The resolution of this model, therefore, is low

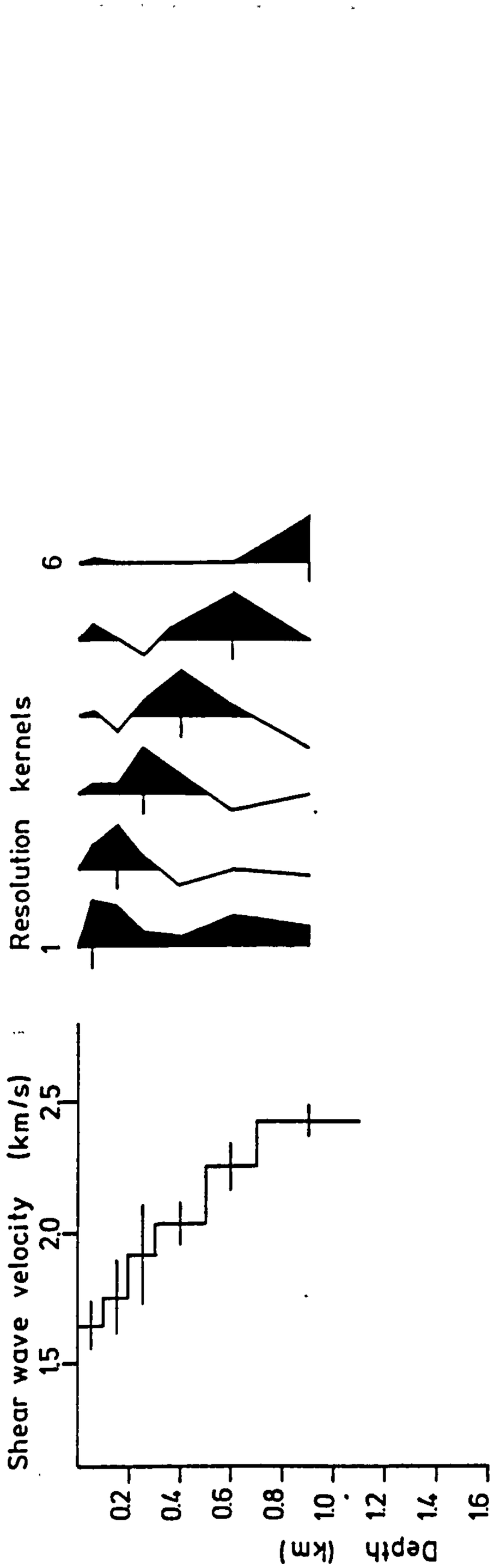

Figure 4.15 Linearised inversion of the observed Rayleigh wave group slowness dispersion for shear wave velocity with depth for MGAR. (Significance level 99%, θ = 12.5°)

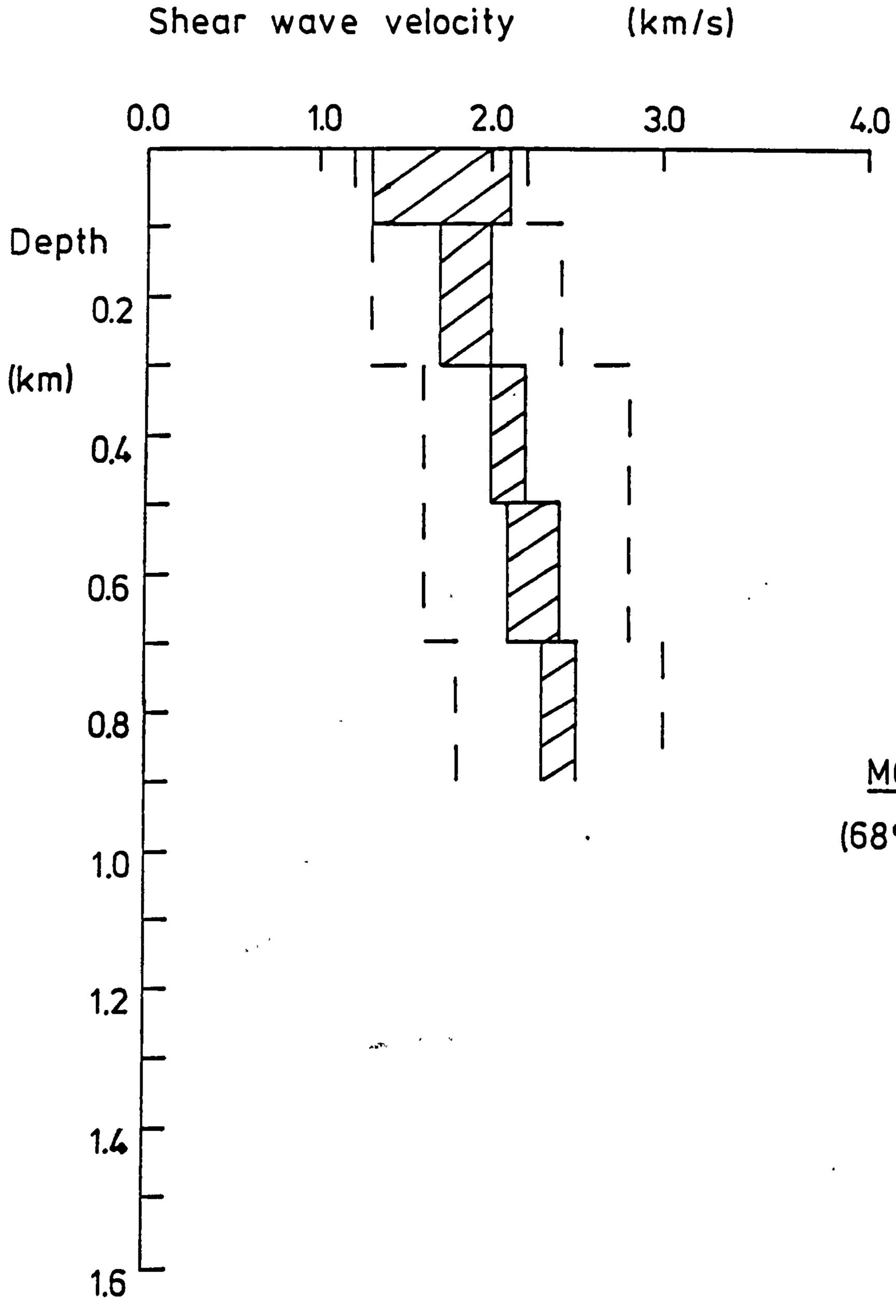

Figure 4.16 Hedgehog inversion of the observed Rayleigh wave group slowness dispersion for shear wave velocity with depth for MGAR.

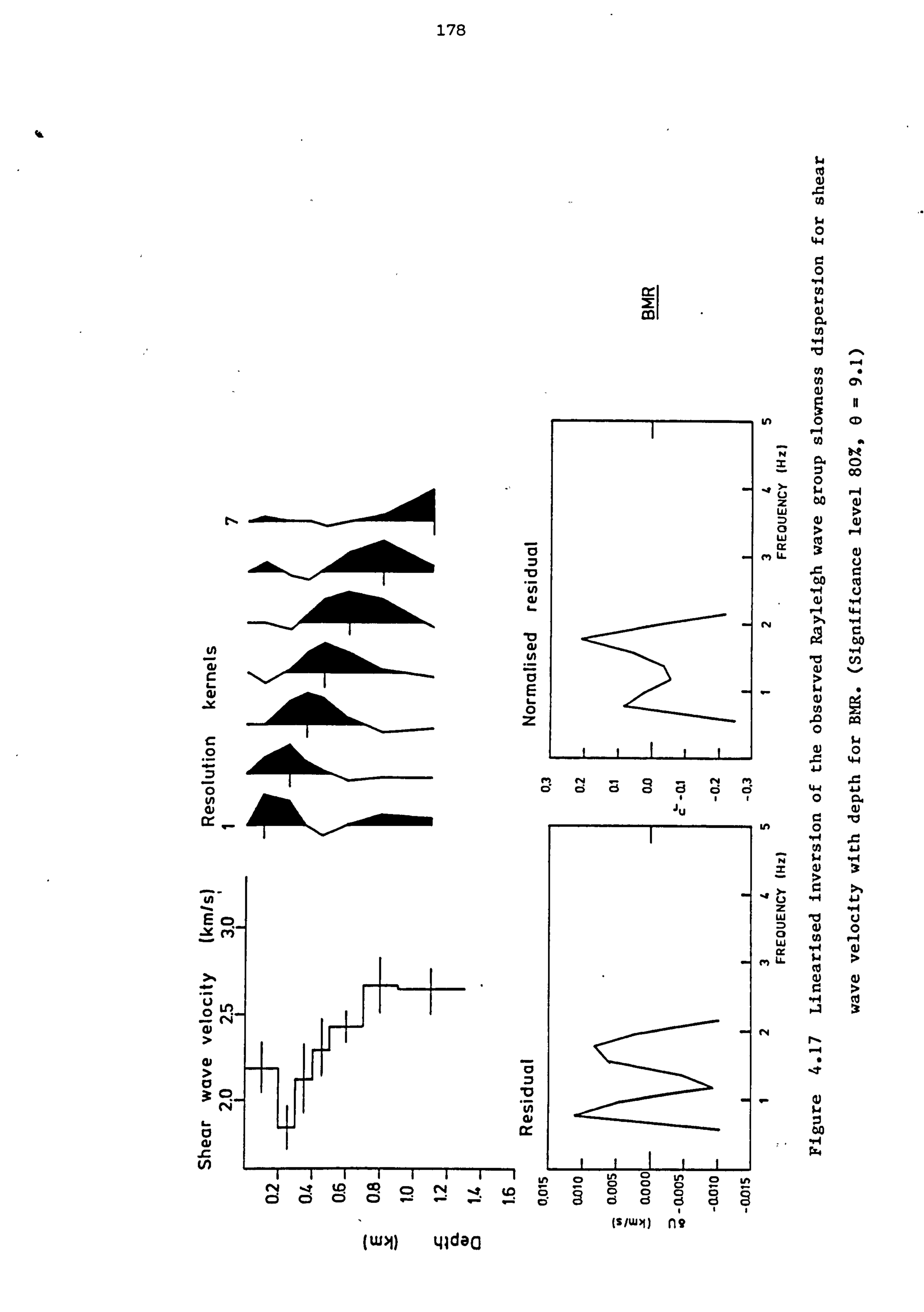

Figure 4.17 Linearised inversion of the observed Rayleigh wave group slowness dispersion for shear wave velocity with depth for BMR. (Significance level 80%, $\theta = 9.1$)

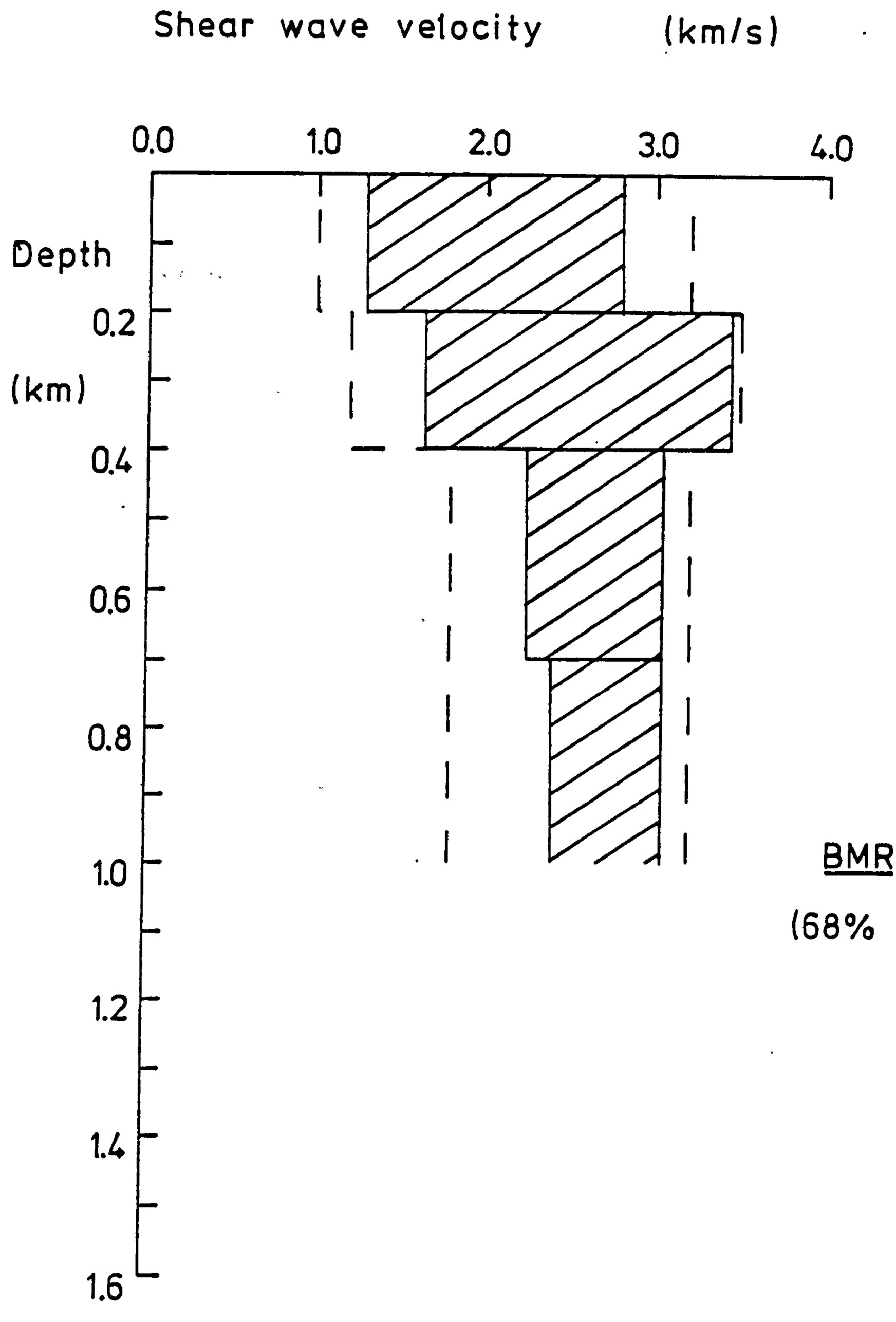

Figure 4.18 Hedgehog inversion of the observed Rayleigh wave group slowness dispersion for shear wave velocity with depth for BMR.

reflecting the higher standard deviations and limited bandwidth of the observed dispersion.

4.4 INTERPRETATION of the SHEAR WAVE VELOCITY-DEPTH PROFILES.

The salient features of the shear wave velocity-depth profiles obtained from the inversion of the observed group slowness dispersion data have been described in the previous section. We now attempt to furnish models of geological structure for the area by interpreting these profiles. The necessary geological and geophysical background has been given in section 1.5. The various profiles are compared in Figure 4.19.

No interpretation of the two profiles for LST 2N and LST 2S has been attempted. Shear wave velocities of 4 km s^{-1} and higher are considered, normally, to be representative of ultramafic or high grade metamorphic rocks. In the context of the regional geology, to infer the existence of such rocks in the shallow, upper crust of the Derbyshire Dome would be unrealistic. The unstable profile for LST 2N which exhibits high velocities and poor resolution can only be considered to be an arithmetic solution to the inverse problem and not a realistic geological model. Similarly, an attempt to interpret the solution for LST 2S would be erroneous due to the poor quality of the inversion.

The failure of the inversion techniques to yield realistic models may be caused by having to restrict the modelling to a series of horizontal, plane layers. Igneous rocks of significant areal extent have been found at sub-crop on the eastern side of the Dome. This suite of lavas and tuffs interdigitate with the limestones and

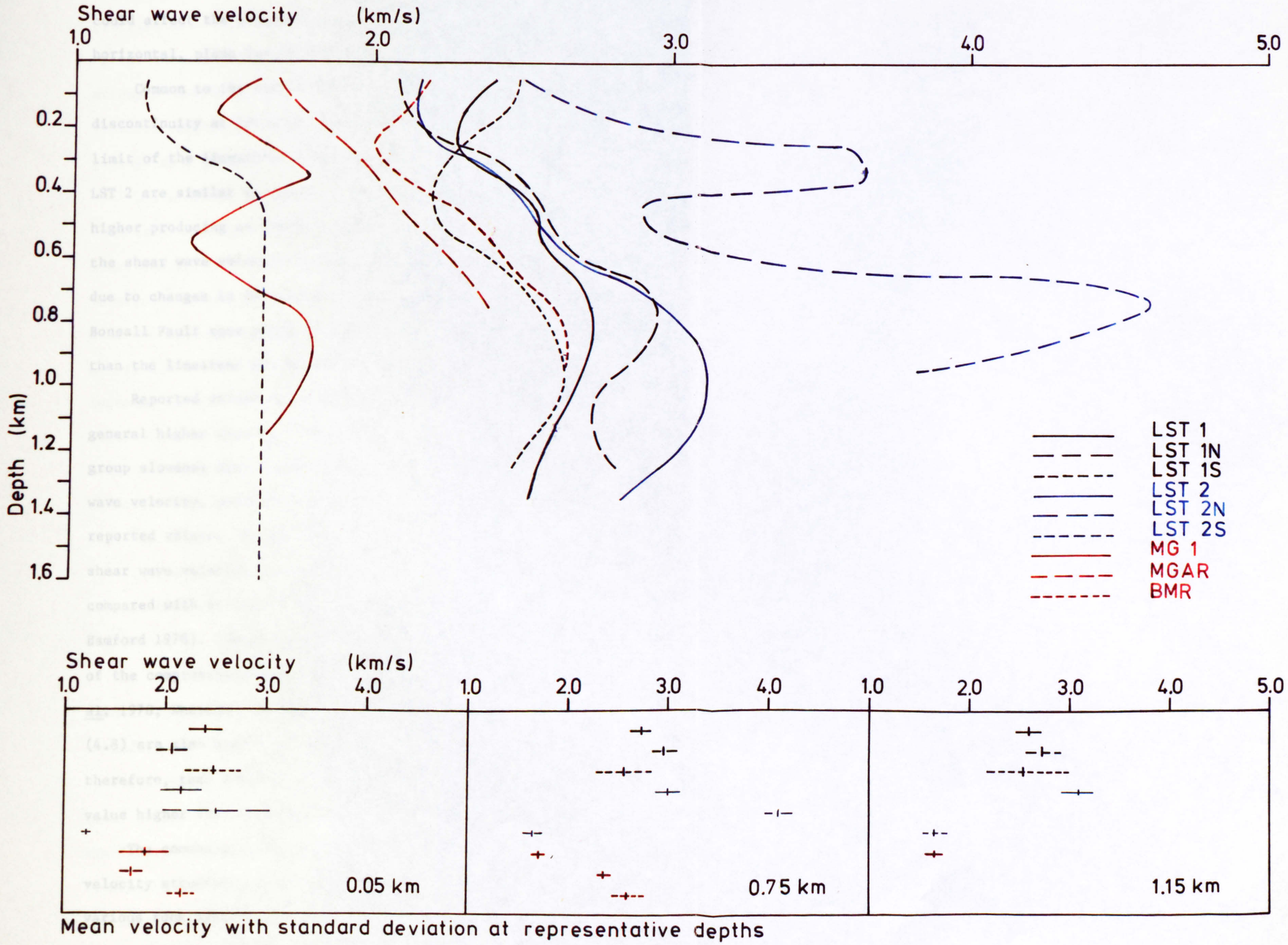

Figure 4.19 Comparison of the solution shear wave velocity profiles from the linearised inversion of the observed Rayleigh wave group slowness data. A weighted 300 m running mean was used to smooth each profile. Standard deviations about mean velocities are shown for a selection of representative depth in each profile.

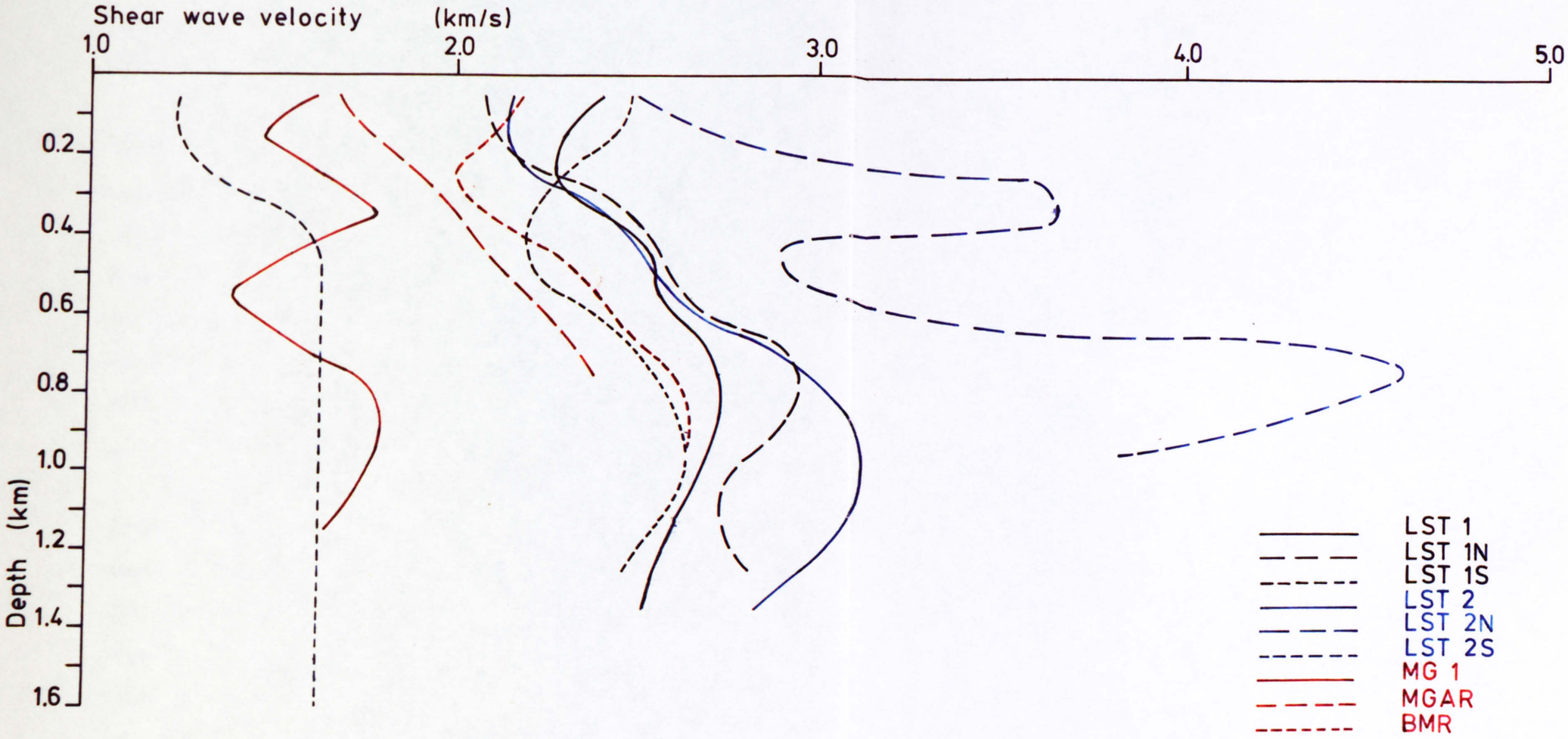

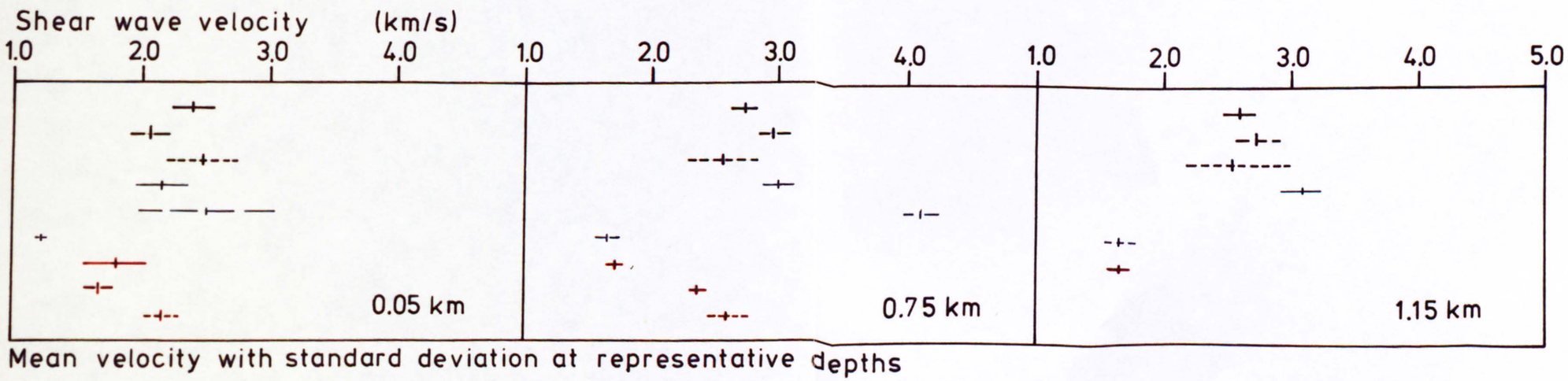

Figure 4.19 Comparison of the solution shear wave velocity profiles from the linearised inversion of the observed Rayleigh wave group slowness data. A weighted 300 m running mean was used to smooth each profile. Standard deviations about mean velocities are shown for a selection of representative depth in each profile.

could affect the structure sufficiently to make the assumption of horizontal, plane layers inappropriate.

Common to the models for the limestone district is a velocity discontinuity at 200 m or 300 m depth and is taken to be the lower limit of the limestone. The velocities for the upper layers of LST 2 are similar to those of LST 1N whilst those of LST 1S are higher producing an overall variation of 2.1 - 2.5 km s^{-1} for the shear wave velocity of the limestone. This variation could be due to changes in the nature of the limestone; those south of the Bonsall Fault zone being of higher purity with less mineralisation than the limestone of the northern provinces (Cox & Bridge 1977).

Reported values of shear wave velocity in limestone are in general higher than the values determined by the inversion of the group slowness data (Clark 1966). The present estimates of shear wave velocity, however, are not outside the overall range of reported values. Evans (1981) has also shown that low values of shear wave velocity are determined by the inversion process when compared with direct observations of shear waves (Assumpção & Bamford 1978). Shear wave velocities calculated from the top layer of the compressional wave velocity models of the region (Bamford et al. 1978, Whitcombe & Maguire 1981, Rogers 1983) using equation (4.8) are also higher than the values given here. It is probable, therefore, that Poisson's ratio is not constant with depth and has a value higher than 0.28 in the shallow, upper crust.

The common practice of assigning lithologies to a given velocity structure using velocities determined previously for various rock types could, clearly, produce unrealistic geologic models for the region because of the low overall shear wave velocities. For layers below the limestone the velocity-depth

profiles have been interpreted on the basis of changes in velocity rather than absolute values. To produce a unified interpretation attempts have been made to keep the assignation of lithology to velocity consistent between profiles using the known regional geology as a guide.

The profiles LST 1N and LST 1S indicate a marked change of structure. In the northern province, the 300 m of Carboniferous Limestone is underlain by a further 300 m of higher velocity material believed to consist of Ordovician pyroclastics in the north near Woo Dale but mainly of deformed mudstones and shales. Cambrian quartzites are thought to underlie the Ordovician producing the increase in velocity below 600 m. Rocks of Cambrian age have been proven in boreholes outside the area (Kent 1967) and inferred by Wills (1978) to underlie the Ordovician at Eyam. The possible reduction in velocity below 1 km suggests a change in lithology, possibly to mudstones and shales still of Cambrian age.

In the southern province the limestone layer is apparently thinner than in the north being only 200 m thick. This abrupt difference in thickness could be achieved by a fault down-throwing to the north. The Bonsall Fault itself has been mapped with a down-throw to the south. The overall effect of the fault zone including the Gulf Fault, however, could be to produce a down-throw to the north. The low velocity channel immediately below the top layer of LST 1S is interpreted as the Devonian sandstones proven in the Caldon Low borehole. Below these sands the increase in velocity is used to infer the existence of rocks similar to the Ordovician of LST 1N. This would imply the boundary fault between the provinces down-throws to the south contrary to the sense of the fault at higher levels. The surface fault, therefore, is believed to be a

younger structure produced along the line of an earlier zone of weakness in response to local stress. The inferred geological structure of the provinces north and south of the Bonsall Fault zone is given in Figure 4.20.

The profile for the district average LST 1 could be interpreted to provide a structure similar to that of LST 1N. Overall, the solution velocities lie between the shear wave velocities of the two component provinces. There would, however, be no evidence for the existence of the Devonian sandstones of the southern province.

The solution profiles for the district average LST 2 must be interpreted with care because of the possible problems in the structure evinced by the inversions of the individual provinces. A similar structure to LST 1N is proposed to a depth of 800 m. At deeper levels the velocities are higher than for LST 1N. This may indicate that the proposed Cambrian lithologies are more competent on the eastern side of the Dome.

The geologic evolution of the district is thought to conform to the following sequence. Sedimentation during the Cambrian resulted in the deposition of muds and later sands, now the quartzites of the wider region. Little can be inferred of the period between the Cambrian and Ordovician. During the Ordovician, localised volcanic activity was accompanied by mudstone deposition. Subsequent uplift of the region may account for the lack of Silurian rocks in the region. During the Devonian the deposition of the sandstones in the south may be accounted for by block uplift to the north together with a subsiding basin to the south. The boundary of this block would have been co-incident with the present surface expression of the Bonsall Fault zone. The district as a whole would then have been covered by the shallow shelf sea of the Carboniferous

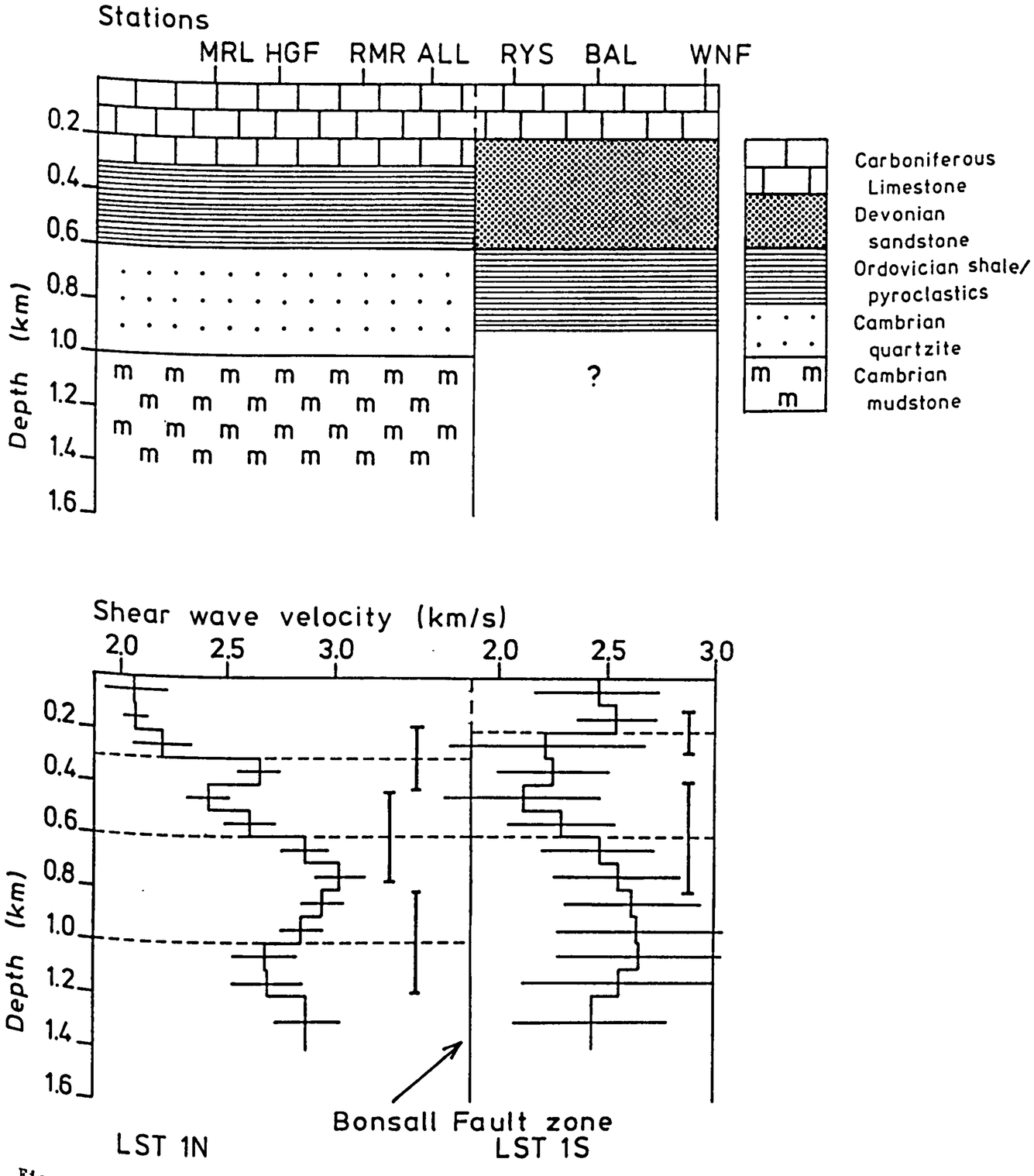

Figure 4.20 Schematic geological structure along LST 1 inferred from solution shear wave velocity profiles from the linearised inversion of the Rayleigh wave group slowness for LST 1N and LST 1S. Depth resolution of interfaces, indicated on velocity profiles, is given by the average spread of the resolution kernels immediately above and below the interface.

Basis of geological interpretation:

i) distinct changes in velocity used to indicate change in lithology

ii) assignation of lithology to a given velocity kept consistent between profiles

iii) information from known regional geology, previous geophysical surveys and bore hole data used to produce realistic model.

Notes:

i) low values of shear wave velocity are returned from the inversions as a possible consequence of assuming too low a value for σ. Any assignation of lithology based on the comparison of calculated velocities and reported values for given rock types would lead to an unrealistic model for the district

ii) the layer thicknesses used in the velocity profiles are a minimum for resolution

iii) depth resolution of interfaces given by the average spread of the resolution kernels immediately above and below the interface. Spread defined by Braile & Keller (1975)

iv) velocity discontinuity at 300 m or 200 m depth taken to indicate base of Carboniferous Limestone

v) wide range of velocity in limestone layer caused by different frequency ranges used in the inversions over LST 1N and LST 1S and the change to purer limestone south of the Bonsall Fault zone

vi) Bonsall Fault zone appears to be a near surface feature produced along the line of an earlier zone of weakness related to a major structure in the basement below the Derbyshire Dome.

vii) the geological model represents only the mean structure within each province because the observed dispersion is a physical average of the velocity structure from the source to each station and an arithmetic mean of the slownesses over all the stations in each province. The restriction of the inversions to layers of constant thickness also constrains the models to a series of horizontal interfaces.

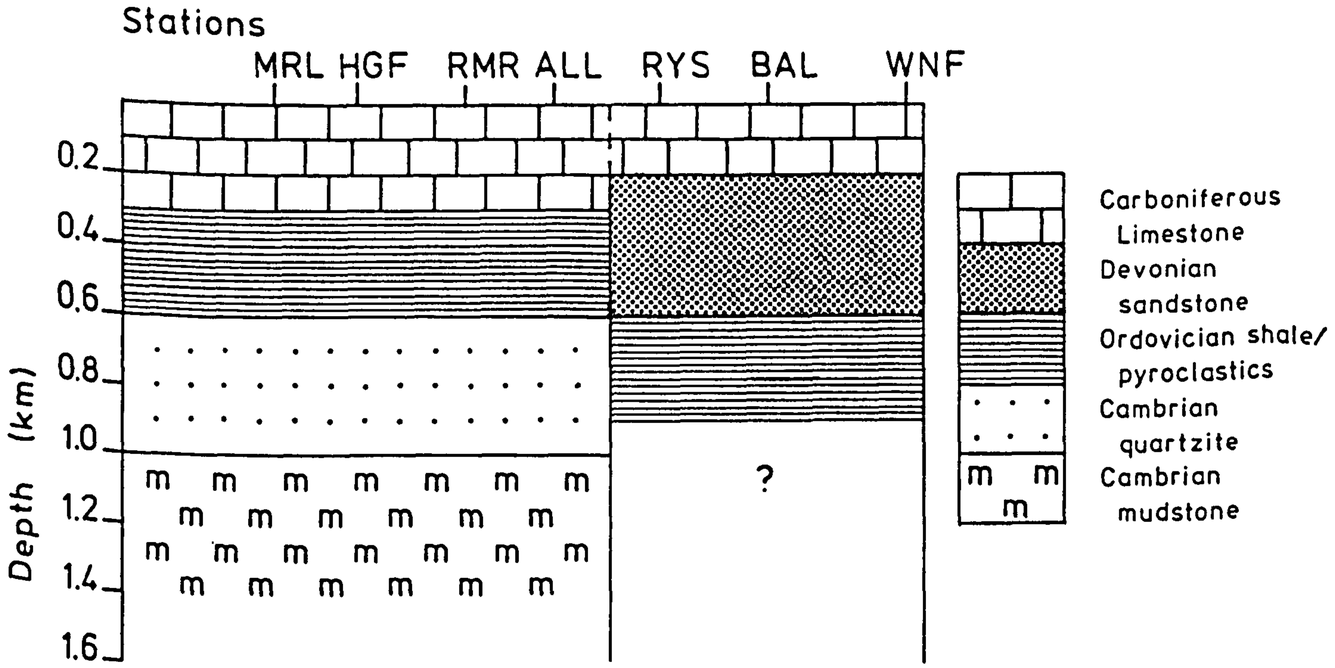

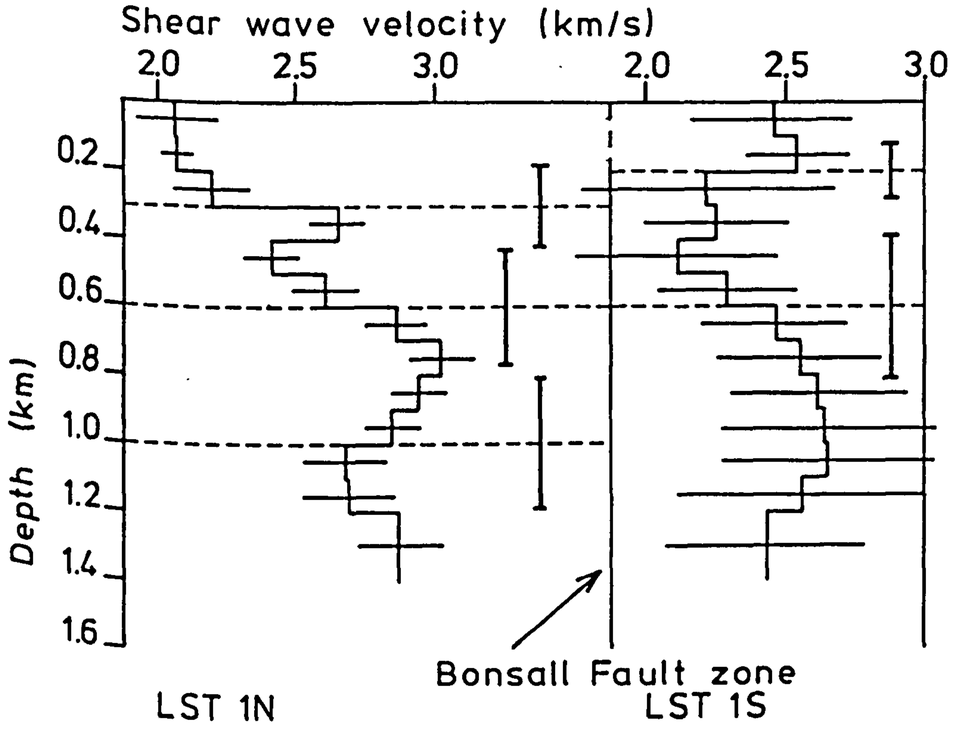

Figure 4.20 Schematic geological structure along LST 1 inferred from solution shear wave velocity profiles from the linearised inversion of the Rayleigh wave group slowness for LST 1N and LST 1S. Depth resolution of interfaces, indicated on velocity profiles, is given by the average spread of the resolution kernels immediately above and below the interface.

Basis of geological interpretation:

i) distinct changes in velocity used to indicate change in lithology

ii) assignation of lithology to a given velocity kept consistent between profiles

iii) information from known regional geology, previous geophysical surveys and bore hole data used to produce realistic model.

Notes:

i) low values of shear wave velocity are returned from the inversions as a possible consequence of assuming too low a value for σ. Any assignation of lithology based on the comparison of calculated velocities and reported values for given rock types would lead to an unrealistic model for the district

ii) the layer thicknesses used in the velocity profiles are a minimum for resolution

iii) depth resolution of interfaces given by the average spread of the resolution kernels immediately above and below the interface. Spread defined by Braile & Keller (1975)

iv) velocity discontinuity at 300 m or 200 m depth taken to indicate base of Carboniferous Limestone

v) wide range of velocity in limestone layer caused by different frequency ranges used in the inversions over LST 1N and LST 1S and the change to purer limestone south of the Bonsall Fault zone

vi) Bonsall Fault zone appears to be a near surface feature produced along the line of an earlier zone of weakness related to a major structure in the basement below the Derbyshire Dome.

vii) the geological model represents only the mean structure within each province because the observed dispersion is a physical average of the velocity structure from the source to each station and an arithmetic mean of the slownesses over all the stations in each province. The restriction of the inversions to layers of constant thickness also constrains the models to a series of horizontal interfaces.

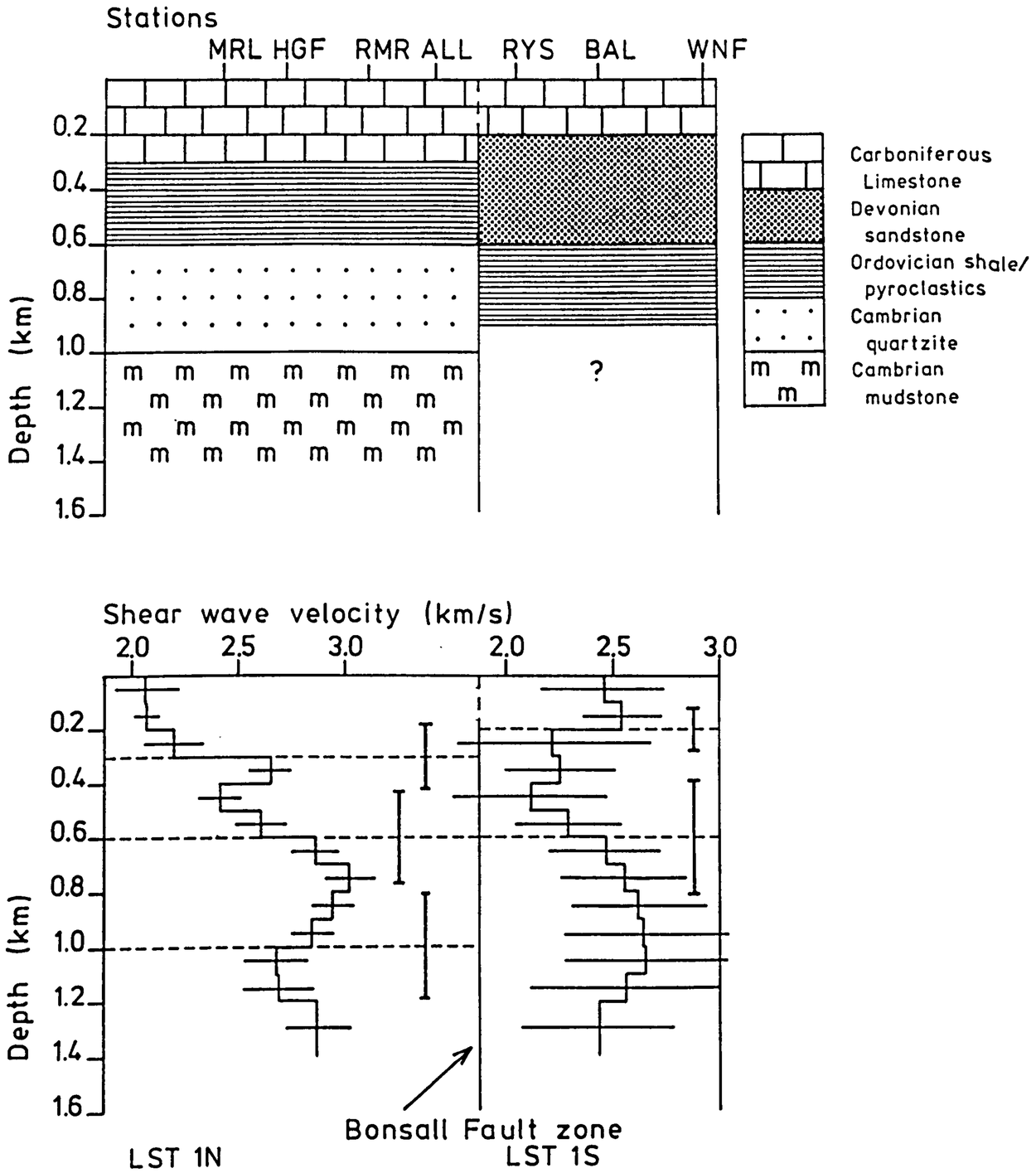

Figure 4.20 Schematic geological structure along LST 1 inferred from solution shear wave velocity profiles from the linearised inversion of the Rayleigh wave group slowness for LST 1N and LST 1S. Depth resolution of interfaces, indicated on velocity profiles, is given by the average spread of the resolution kernels immediately above and below the interface.

Basis of geological interpretation:

i) distinct changes in velocity used to indicate change in lithology

ii) assignation of lithology to a given velocity kept consistent between profiles

iii) information from known regional geology, previous geophysical surveys and bore hole data used to produce realistic model.

Notes:

i) low values of shear wave velocity are returned from the inversions as a possible consequence of assuming too low a value for σ. Any assignation of lithology based on the comparison of calculated velocities and reported values for given rock types would lead to an unrealistic model for the district

ii) the layer thicknesses used in the velocity profiles are a minimum for resolution

iii) depth resolution of interfaces given by the average spread of the resolution kernels immediately above and below the interface. Spread defined by Braile & Keller (1975)

iv) velocity discontinuity at 300 m or 200 m depth taken to indicate base of Carboniferous Limestone

v) wide range of velocity in limestone layer caused by different frequency ranges used in the inversions over LST 1N and LST 1S and the change to purer limestone south of the Bonsall Fault zone

vi) Bonsall Fault zone appears to be a near surface feature produced along the line of an earlier zone of weakness related to a major structure in the basement below the Derbyshire Dome.

vii) the geological model represents only the mean structure within each province because the observed dispersion is a physical average of the velocity structure from the source to each station and an arithmetic mean of the slownesses over all the stations in each province. The restriction of the inversions to layers of constant thickness also constrains the models to a series of horizontal interfaces.

facilitating the deposition of the limestone. Tilting of the northern block to the north east during this period would produce the thicker limestone sequence proven in the Eyam borehole. This tilting could have been accompanied by movement along the line of weakness created by the block boundary producing the Bonsall Fault zone showing a northerly down-throw within the limestone.

The proposed stratigraphic sequence is similar to that inferred by Whitcombe & Maguire (1981) above the Charnian basement postulated to the south of the Dome. The absence of Charnian rocks in the present interpretations is not incompatible with the models from the refraction data as the shear wave velocity-depth profiles do not extend to levels at which the Pre-Cambrian has been predicted. The restriction of the inversion process to a series of horizontal, plane layers can account for the differences in the depths to given horizons inferred from the shear wave velocity-depth profiles and the axial model of Rogers (1983). Further, the observed dispersion represents an average of the dispersive characteristics of the propagation path and hence any model will represent a structure which has averaged out any refractor topography. A major discrepancy exists, however, in the sense of motion on the basement fault. Rogers (1983) indicates the basement down-throws to the north whilst the inference from the surface wave model is that of a southerly down-throw. The proposed Charnian basement south of the fault has a similar compressional velocity to the Ordovician of the north (Roger 1983). Rather than a fault bringing up the Charnian basement the refractor to the south could be a continuous layer of Ordovician rocks dipping to the south. The provincialised shear wave velocity models would also be compatible with this interpretation. Further, Whitcombe & Maguire (1981) give limited

evidence for a second refractor at depth to the south of the Dome. This could be a Pre-Cambrian refractor against which the Ordovician pinches out further south towards Charnwood. The alternative is that the Ordovician proposed south of the basement fault from the surface wave data is in reality a Charnian basement. If this was the case, however, a more complex tectonic sequence would be required to explain the absence of the Ordovician in the southern province.

The shear wave velocity-depth profile for the line MG 1 whilst showing layer velocities which vary widely with depth has good resolution and must represent a realistic solution. The profile can be interpreted in terms of the cyclic sedimentation within the Namurian. Each change in velocity indicates a change in the bulk composition of the layer; the higher velocities representing more competent, sandstone units. The shear wave velocity is nowhere above 2.0 km s^{-1}. This would imply that the limestone, which is believed to underlie the Millstone Grit, must be at depths greater than 1.5 km. The thickness for this sedimentary basin has been calculated approximately from compressional wave first arrivals as 1.1 km (Cox 1983). This value, however, may be an underestimate because of the lack of reversal of the seismic line.

As expected the inversion for MGAR has yielded solution velocities intermediate to the models for the pure provincial data. Resolution is also poor for the upper layer and, hence, it would be erroneous to infer too much from this profile. From the solution velocities, however, it would appear that approximately 300 m of Millstone Grit sediments overlie a limestone sequence.

The solution profile for BMR represents a limestone path being affected little by the Millstone Grit. This model consists of a

thicker limestone sequence that shown by the pure limestone province profiles. Increased amounts of primary dolomite could produce the increase in velocity at depth.

In an area with little physical control on the deep geology the interpretation of geophysical models can be the result of much speculation. In the interpretations above we have attempted to use geophysical models to indicate changes in physical parameters with depth. Essentially, the interpretations show the limestone district to be flanked on the north and east by basins of terrigenous, clastic sediments. No information on the nature of the basement below the northern basin has been obtained although it is believed to be limestone and at depths greater than 1.5 km. On the eastern flank of the Derbyshire Dome a limestone layer dipping steeply eastwards is required to accommodate the inferred rapid increase in thickness of the Millstone Grit.

Over the limestone district two possible interpretations may be supported. Both, however, require structures more complex than suggested by the surface geology. The depth to a Pre-Cambrian basement can nowhere be less than 1.6 km as suitable shear wave velocities are not obtained above this level. Indeed, for deeper levels the decrease in velocity exhibited is believed to be caused by Cambrian sediments. This supports a low velocity layer postulated by Rogers (1983) using refraction techniques. Accepting this must require that the volcanoclastics in the Woo Dale borehole are of Ordovician to Carboniferous age and not Pre-Cambrian as given initially (Cope 1973).

Over the Derbyshire Dome the Ordovician may be overlain directly by Carboniferous Limestone or a layer of Devonian sandstones succeeded by a thinner layer of limestone. The boundary

between the two structural models is thought to be a fault formed by the edge of an uplifted block. The proposed interpretations require that considerable tectonic activity took place throughout the Palaeozoic with major changes in structure occuring over relatively short distances.

CHAPTER FIVE

INVERSION of OBSERVED RAYLEIGH WAVE ATTENUATION DATA

5.1 INTRODUCTION.

In the previous chapter two inversion techniques were utilised to provide shear wave velocity models with depth. Here, inversion methods are used to furnish models of Q_β^{-1} with depth from the observed attenuation data given in chapter 3.

The forward problem for attenuation has been formulated by Anderson & Archambeau (1964) and Anderson *et al.* (1965). This theory of anelasticity has been modified by Burton (1977) through the use of the causal relations between dissipation and dispersion given by Futterman (1962).

The expression for the amplitude of a travelling surface wave will contain a term of the form

$$\exp[i(\omega t - k_e r)], \tag{5.1}$$

where k_e is the elastic wavenumber with all other terms as defined previously (section 1.2).

For an anelastic medium in which the dissipation is small the Rayleigh wave amplitude may be calculated by replacing k_e by a complex wavenumber k_a such that

$$k_a(\omega) = k_e(\omega) + \delta k(\omega),$$

with (5.2)

$$\delta k(\omega) = \phi(\omega) + i\gamma(\omega).$$

The propagation term for the travelling wave in an anelastic medium is now

$$\exp[i(\omega t - \phi(\omega)r] \exp(\gamma(\omega)r). \quad (5.3)$$

Anelasticity, therefore, introduces amplitude attenuation and causal dispersion into the wave equation, given by $\gamma(\omega)$ and $\phi(\omega)$ respectively.

We have defined the relation between $\gamma(\nu)$ and $Q_\gamma^{-1}(\nu)$ previously in section 1.2 with

$$Q_\gamma^{-1}(\nu) = -\frac{2U(\nu)}{\pi\nu}\gamma(\nu) \quad (5.4)$$

An expression for $\delta k(\omega)$ in terms of a partial derivative summation of body wave parameters is given by Anderson et al. (1965). This was used by Burton (1977) to provide a statement of $\gamma(\omega)$ and $\phi(\omega)$, such that

$$\gamma(\omega) = \frac{1}{2}\sum_{j=i}^{n}\left[\frac{\partial k_e}{\partial \alpha_{ej}} Q_{\alpha j}^{-1}\alpha_{ej} + \frac{\partial k_e}{\partial \beta_{ej}} Q_\beta^{-1}\beta_{ej}\right] \quad (5.5)$$

and

$$\phi(\omega) = \frac{2}{\pi}\ln\left[\frac{\omega}{\omega_o}\right]\gamma(\omega) \quad (5.6)$$

where $\delta k_e / \delta \alpha_{ej}$ is the partial derivative of wavenumber with respect to compressional wave velocity in layer j for the fully elastic case

$Q_{\alpha j}^{-1}$ intrinsic specific attenuation factor for compressional waves in layer j

α_{ej} is the compressional wave velocity in layer j for the fully elastic case

$\partial k_e / \partial \beta_{ej}$ is the partial derivative of wavenumber with respect to shear wave velocity in layer j for the fully elastic case

$Q_{\beta j}^{-1}$ is the intrinsic specific attenuation factor for shear waves in layer j

β_{ej} is the shear wave velocity in layer j for the fully elastic case

and ω_o is a minimum cut off frequency.

From equation (5.5) we can see that the attenuation co-efficient, $\gamma(\omega)$, has been expressed in terms of physically obtainable quantities.

The two inversion techniques employed to obtain the distribution of Q_β^{-1} with depth are discussed below. The linear inversion technique uses a matrix method similar to that used in the velocity inversions. The second scheme used linear programming techniques to provide bounds on the acceptable models of $Q_\beta^{-1}(z)$.

5.2 TECHNIQUES for the INVERSION of OBSERVED ATTENUATION DATA.

5.2.1 Linear Inversion Method.

An individual layer or constituent of a medium has unique physical

constants describing its intrinsic properties. The combination of equations (5.4) and (5.5) for the several intrinsic attenuation factors or specific attenuation factors ($Q^{-1}_{\alpha,\beta}$) and body wave velocities (α,β), which together describe the physical properties of the layered medium, provides a relationship with the observed $Q^{-1}_{\gamma}(\nu)$. The latter is observed to be dependent on both the intrinsic properties of velocity and attenuation in the individual layers and on the arrangement of these layers. In the subsequent description of profiles of Q^{-1}_{β} against depth from the inversion of the observed $Q^{-1}_{\gamma}(\nu)$ data, intrinsic properties of anelasticity of the medium are often referred to as its intrinsic attenuation or more simply its attenuation. Relating Q^{-1}_{α} to Q^{-1}_{β} by equation (3.7) and dropping the suffix e gives

$$Q^{-1}_{\gamma_i} = \frac{-U_i}{2\pi\nu_i}\left[\sum_{j=i}^{n}\left(\frac{\partial k_i}{\partial \alpha_j}\,\frac{4}{3}\,\frac{\beta_j^2}{\alpha_j} + \frac{\partial k_i}{\partial_{\beta_j}}\,\beta_j\right) Q^{-1}_{\beta_j}\right], \qquad (5.7)$$

$$i = 1,2,\ldots m.$$

This system of equations may be represented in matrix form such that

$$\underline{Ax} = \underline{b}, \qquad (5.8)$$

where

$$a_{ij} = \frac{-U_i}{2\pi\nu_i}\left[\frac{\partial k_i}{\partial \alpha_j}\,\frac{4}{3}\,\frac{\beta_j^2}{\alpha_j} + \frac{\partial k_i}{\partial_{\beta_j}}\,\beta_j\right],$$

$$x_j = Q_{\beta_j}^{-1}, \qquad b_i = Q_{\gamma_i}^{-1} .$$

This is similar to equation (4.4). Note, however, that equation (5.8) is immediately linear whilst the forward problem for velocity is not so initially. The solutions for intrinsic Q_β^{-1} are, therefore, obtained in a single step compared to the iterative procedure to obtain shear wave perturbations to velocity-depth distributions (section 4.2.1).

Solution of equation (5.8) is again achieved by the singular value decomposition technique (Lanczos 1961) using the Levenberg-Marquardt smoothing parameter, θ, to reduce the effect of small singular values.

A model specifying α_j, β_j, ρ_j and h_j is required to enable the group velocity U_i and partial derivatives to be computed (see section 4.1). The partial derivatives, $\partial k_i / \partial \alpha_j$, $\partial k_i / \partial \beta_j$, are found by solving for the elastic wavenumber, perturbing the relevant layer velocity and using first order differences. The resulting models of Q_β^{-1}, therefore, are for a series of horizontal, plane layers over a half-space.

The arithmetic solution of equation (5.8) may require some Q_β^{-1} to be negative. Such solutions are undesirable as usually they have no physical basis. Only by using alternative schemes of inversion (q.v.) can the Q_β^{-1} be constrained to meaningful positive values.

5.2.2 Linear Programming Method.

Where a problem is governed by a set of linear equations it is possible to invert the observed data by using the technique of linear programming (Garvin 1960). The object of this technique is to build

an envelope of possible models subject to certain constraints. The results, therefore, are similar to the Hedgehog method which could also have been employed. The Hedgehog approach has been used in previous studies of anelasticity by Burton & Kennet (1972), Burton (1977) and Evans (1981). The linear programming technique has only been used in a comparative study of inversion techniques by Lee & Solomon (1975) and with single station Q_γ^{-1} data by MacBeth & Burton (1983).

The system of equations defined by (5.8) is constructed. The maximum and minimum bounds on each layer parameter is found by optimising the equations so that the observed and calculated parameters are within a given tolerance. Each datum restricts the possible solutions to the space between the hyperplanes defined by the equations

$$\sum_{j=i}^{n} a_{ij} Q_{\beta_{jmin}}^{-1} = Q_{\gamma_i}^{-1} - tol_i, \qquad i = 1,2,\ldots m,$$

$$\sum_{j=i}^{n} a_{ij} Q_{\beta_{jmax}}^{-1} = Q_{\gamma_i}^{-1} + tol_i, \qquad i = 1,2,\ldots m, \tag{5.9}$$

where a_{ij} are the matrix elements given in equation (5.8)

tol_i the tolerance between the observed $Q_{\gamma_i}^{-1}$ and calculated Q_γ^{-1}

$Q_{\beta_{jmin/jmax}}^{-1}$ extreme values of layer parameters $Q_{\beta_j}^{-1}$ to satisfy the constraints.

The Revised Simplex method (Garvin 1960) is used to solve the problem. The routine utilised (H01ADF, NAG 1980) also constrains the solution Q_β^{-1} the meaningful positive values unlike the solutions

returned by the linear inversions. A general theory for linear inverse problems which must be constrained to positive values is given by Sabatier (1977).

5.3 INVERSION of OBSERVED RAYLEIGH WAVE ATTENUATION DATA.

As with the inversions for shear wave velocity the number of independent variables within the inverse problem must be reduced to permit adequate resolution of the parameters.

Partial derivatives of wavenumber with respect to α are smaller than those with respect to β (Burton 1977). Inversions were, therefore, conducted to obtain the distribution of Q_β^{-1} with depth rather than Q_α^{-1}. The intrinsic specific attenuation factor for compressional waves was constrained using equation (3.7) in a similar way to which compressional wave velocity was related to shear wave velocity by Poisson's ratio in the velocity inversions. This relation has a physical basis that no dissipation may be ascribed to the bulk modulus, that is, no loss of energy is caused by compression. A constant Poisson's ratio of 0.28, as assumed in the velocity inversions, gives

$$Q_\alpha^{-1} = 0.41\ Q_\beta^{-1}. \qquad (5.10)$$

The group velocities and partial derivatives required by equation (5.8) were obtained by solving the forward problem using the appropriate shear wave velocity model determined by inversion of the observed dispersion data. The inaccuracy in layer velocity produced by ignoring the causal dispersion implied by equation (5.3)

produces an error in the Q_β^{-1} returned from the inversions of the observed attenuation data. Such errors are, however, small compared to the accuracy of the observed data. Schwab & Knopoff (1972) have developed a formulism for the computation of surface wave dispersion and attenuation in an anelastic earth. Lee & Solomon (1978) conducted simultaneous inversions from observations of phase velocity and attenuation of Love waves in North America. They found the resolution of Q_β^{-1} with depth to be improved whilst the general features of the models were left unchanged. In comparison the shear wave velocities were less well resolved suffering from varying degrees of causal dispersion depending upon the frequency dependence of Q_β^{-1}.

Consistency between the inversions of the observed data for shear wave velocity with depth and $Q_\beta^{-1}(z)$ was maintained by using the same number of layers with the same thicknesses in both cases. A given Rayleigh wave attenuation data set could have fewer observational points than its corresponding dispersion data set for the reasons given in section 3.3.1. This was a problem when the number of layers in the solution shear wave velocity model became greater than the number of points within the observed attenuation data set. When this occurred modifications in the structure were made by combining appropriate layers assigning the arithmetic mean of the velocities of the original layers to the new, thicker layer.

The linear inversions proceeded as follows. The smoothing parameter, θ, was set equal to the maximum singular value producing an over damped but stable solution. For each subsequent solution θ was halved, decreasing the damping, until the standard deviation on Q_β^{-1} was greater than 0.05 or that Q_β^{-1} was less than zero for any layer.

Following Evans (1981) the fit between the observed $Q_\gamma^{-1}(\nu)$ and

those calculated from the solution models of $Q_\beta^{-1}(z)$ was determined for each solution model and quantified by the chi-squared

$$\chi^2 = \frac{1}{m} \sum_{i=1}^{m} \left[\frac{Q_{\gamma_i}^{-1} - Q_{\gamma_{thi}}^{-1}}{\sigma_i} \right]^2 \qquad (5.11)$$

where $Q_{\gamma_i}^{-1}$ is the observed attenuation data

$Q_{\gamma_{thi}}^{-1}$ is the Q_γ^{-1} calculated from the solution Q_β^{-1} model

σ_i is the standard deviation of the observations

i is the frequency point index.

An acceptable fit between the observations and forward solution is indicated by a χ^2 less than one; that is the fit is, on average, within one standard deviation of the observations. Each linear inversion gives a solution model of $Q_\beta^{-1}(z)$ for a particular degree of damping. The preferred model was chosen using the criteria that the chi-squared was less than one and that the model had physical meaning with no values of Q_β^{-1} significantly less than zero.

For the inversion by linear programming the number of variable parameters was reduced by using a velocity model having the same layer boundaries as the Hedgehog velocity inversions. The layer velocities were obtained by taking the median velocity of each Hedgehog solution region. The number of parameters solved for, therefore, reduced to four or five.

The linear programming inversions proceeded by setting the tolerance to one standard deviation. If no feasible solution was found at this level the tolerance was increased until a solution envelope was given. The simplex inversions presented give, therefore,

the regions for the lowest confidence limit (closest fit to the data) which could support a feasible solution.

5.3.1 The Carboniferous Limestone District.

The inversion techniques described above have been used to determine the distribution with depth of the intrinsic shear wave attenuation factor $Q_\beta^{-1}(z)$, implied by the observed data sets QLST 1, QLST 1N and QLST 1S over the limestone district.

Application of the linear inversion scheme for LST 1 yielded six solution models, at different degrees of damping, of which the fifth is preferred (Fig 5.1). The solution models 1 and 2 are over damped with the values of Q_β^{-1} at depth being held close to zero. As the damping was decreased the Q_β^{-1} at deep levels were no longer forced to be close to zero until instability occurred in model 6 with some negative values of Q_β^{-1} being obtained.

Of the six solutions model 4 was first for which the fit between the calculated $Q_\gamma^{-1}(\nu)$ and the observed data gave a χ^2 less than one. Model 5 was chosen as the preferred solution because no decrease in Q_β^{-1} with depth could be attributed to over damping and the solution to the forward problem gave a χ^2 less than one. The calculated $Q_\gamma^{-1}(\nu)$ do not model all the features in the observed attenuation curve; in particular, the local maximum and minimum, between 1.5 - 2.0 Hz where the model exhibits a smoothed fit without a local turning point and the decrease in Q_γ^{-1} above 3.3 Hz where the model remains constant at a higher value of Q_γ^{-1}.

The preferred solution exhibits an upper layer which has a low Q_β^{-1} 0.005, with a thickness of 200 m. Below this the attenuation

Key to the figures giving the results of the inversion of the observed Rayleigh wave specific attenuation factor, $Q_\gamma^{-1}(\nu)$, data for the distribution of intrinsic shear wave specific attenuation factor, $Q_\beta^{-1}(z)$, with depth.

Linear Inversions: Figures 5.1, 5.3, 5.5, 5.7, 5.8, 5.9, 5.11

Each figure shows:

1. Graph of intrinsic shear wave specific attenuation factor against depth for the preferred solution model giving the mean solution $Q_\beta^{-1}(z)$ with its standard deviation for each layer.

2. Resolution kernels. The resolution kernel for each layer is shown from the surface layer on the left to the half-space on the right. Each resolution kernel is drawn against the same depth scale as in 1 above and are normalised to the same peak value. A small tick is drawn against each kernel showing the middle of the relevant layer. Positive values are shaded.

3. Alternative solution models of $Q_\beta^{-1}(z)$ without standard deviations at different degrees of damping.

4. Graph displaying the comparison of the observed Rayleigh wave specific attenuation factor data with values of $Q_\gamma^{-1}(\nu)$ calculated from the presented models of $Q_\beta^{-1}(z)$.

Figure 5.1 Linear inversion of the observed Rayleigh wave specific attenuation factor data for the intrinsic specific attenuation factor, $Q_\beta^{-1}(z)$, with depth for LST 1. (Smoothing parameter of preferred solution, $\theta = 231.9$)

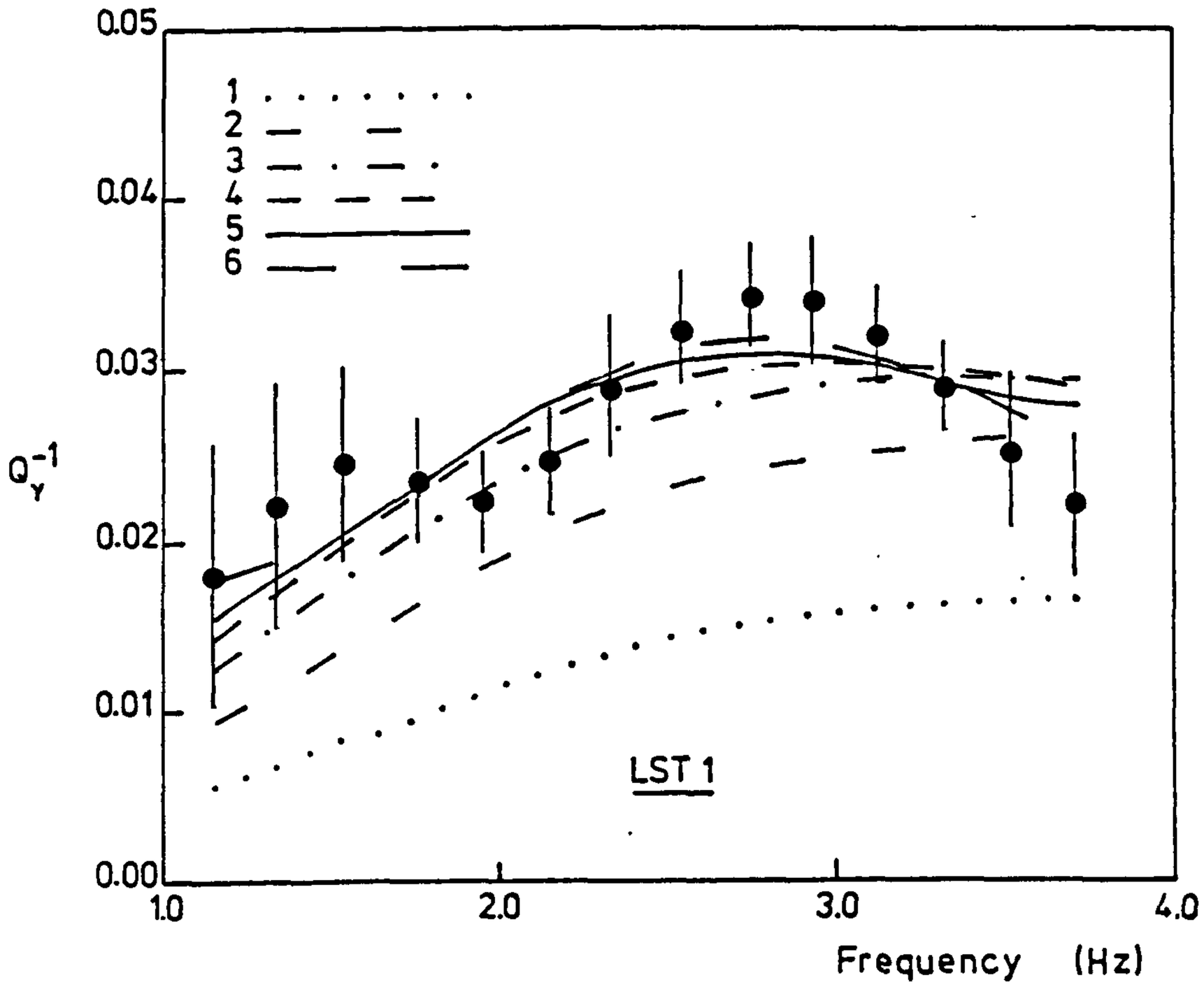
0.05
0.04
0.03
0.02
0.01
0.00
Q_γ^{-1}
1
2
3
4
5
6
LST 1
1.0
2.0
3.0
4.0
Frequency (Hz)

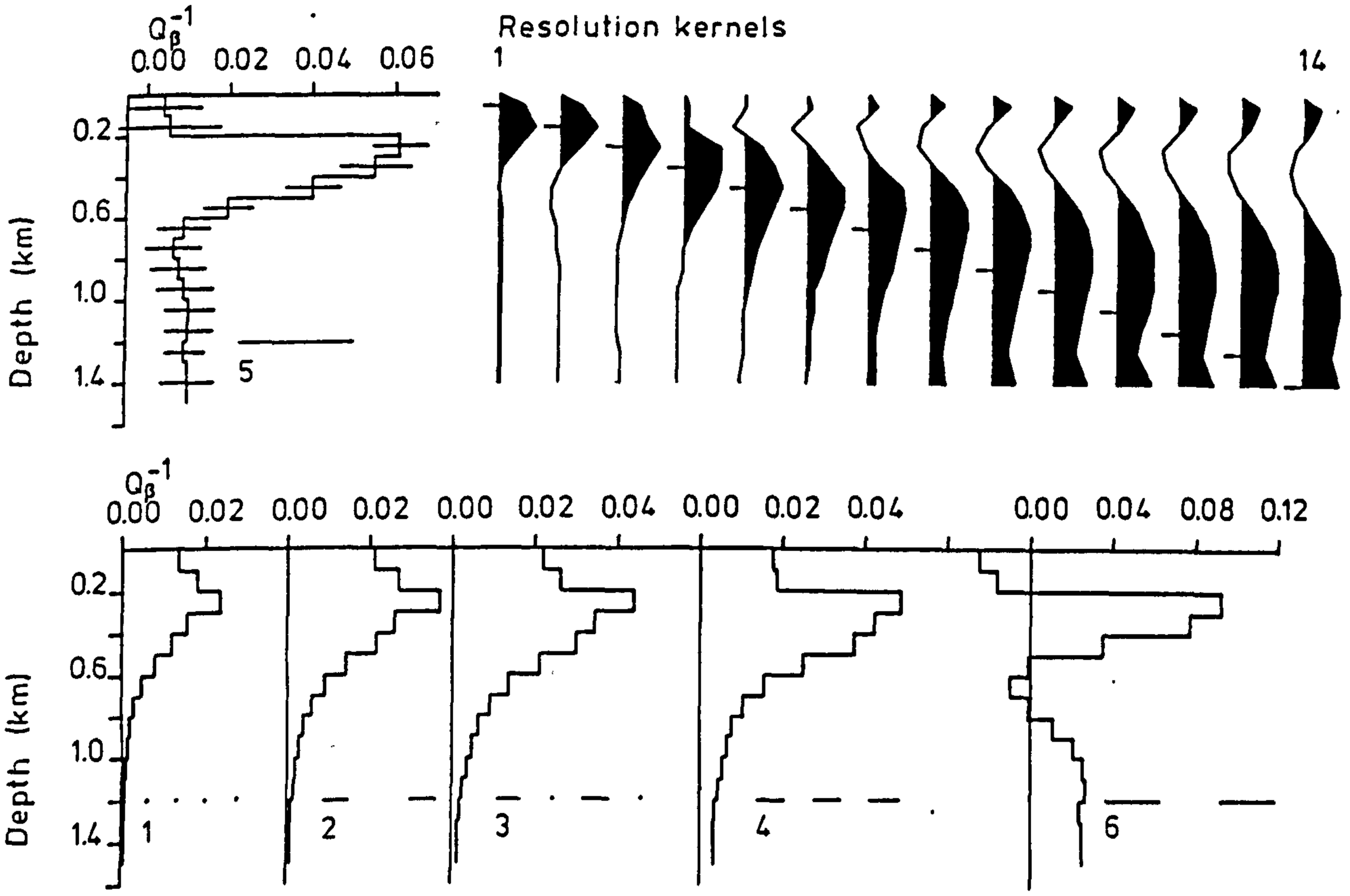
Q_β^{-1}
0.00 0.02 0.04 0.06
Resolution kernels
1
14
0.2
0.6
1.0
1.4
Depth (km)
5
Q_β^{-1}
0.00 0.02 0.00 0.02 0.00 0.02 0.04 0.00 0.02 0.04 0.00 0.04 0.08 0.12
0.2
0.6
1.0
1.4
Depth (km)
1
2
3
4
6

increases dramatically to a maximum Q_β^{-1} of 0.061 at 300 m and then decreases slowly to a depth of 500 m. At this depth a discontinuous decrease in Q_β^{-1} to values of approximately 0.01 was exhibited. Resolution kernels peaking at depths above the relevant layer show that the resolution of layers below 600 m is very poor.

A decrease in Q_β^{-1} with depth below 600 m is supported by the solution region from the simplex inversion technique (Fig 5.2). Below the upper layer, which is defined poorly, the intrinsic attenuation increases to 0.04 to 0.06 between 300-600 m. Whilst allowing for higher values of intrinsic attenuation the simplex model supports the trend of the distribution of Q_β^{-1} with depth given by the linear inversion technique.

Only three differently damped solution models were obtained from the linear inversion of the observed data QLST 1N (Fig 5.3). The three models show values of Q_β^{-1} very close to zero at depths below 1 km indicating that the problem is over damped. Model 3 was chosen as the preferred solution because the fit between the calculated and observed $Q_\gamma^{-1}(\nu)$ gave χ^2 less than one. The theoretical values of Q_γ^{-1} do not fit the maximum in the observations being underestimated between 2.7 - 3.5 Hz. This would imply that higher values of Q_β^{-1} were required near the surface and gives further evidence of the over damped nature of the solutions.

Small negative values of Q_β^{-1} were returned in model 3 at depths below 700 m. The resolution kernels for this model are broad and, except for the first 500 m, not located about the appropriate layer. Model 3 can be accepted as the preferred solution, therefore, provided that the values returned for the first five layers are understood to be underestimates of the intrinsic attenuation and that little information is given about deeper levels.

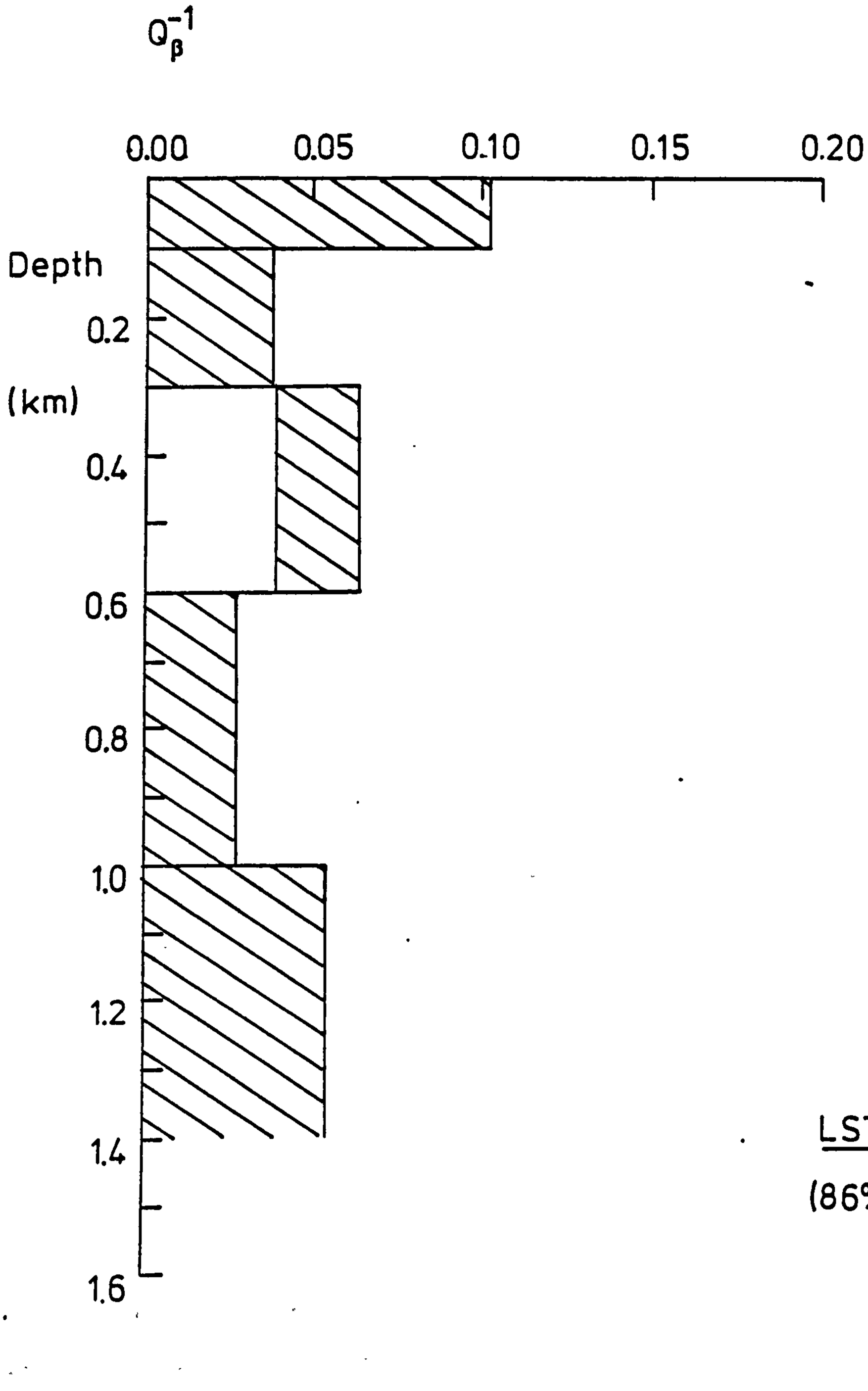

Figure 5.2 Linear programming inversion of the observed Rayleigh wave specific attenuation factor data for the intrinsic attenuation factor, $Q_\beta^{-1}(z)$, with depth for LST 1.

Figure 5.3 Linear inversion of the observed Rayleigh wave specific attenuation factor data for the intrinsic specific attenuation factor, $Q_\beta^{-1}(z)$, with depth for LST 1N. (Smoothing parameter of preferred solution, $\theta = 556.9$)

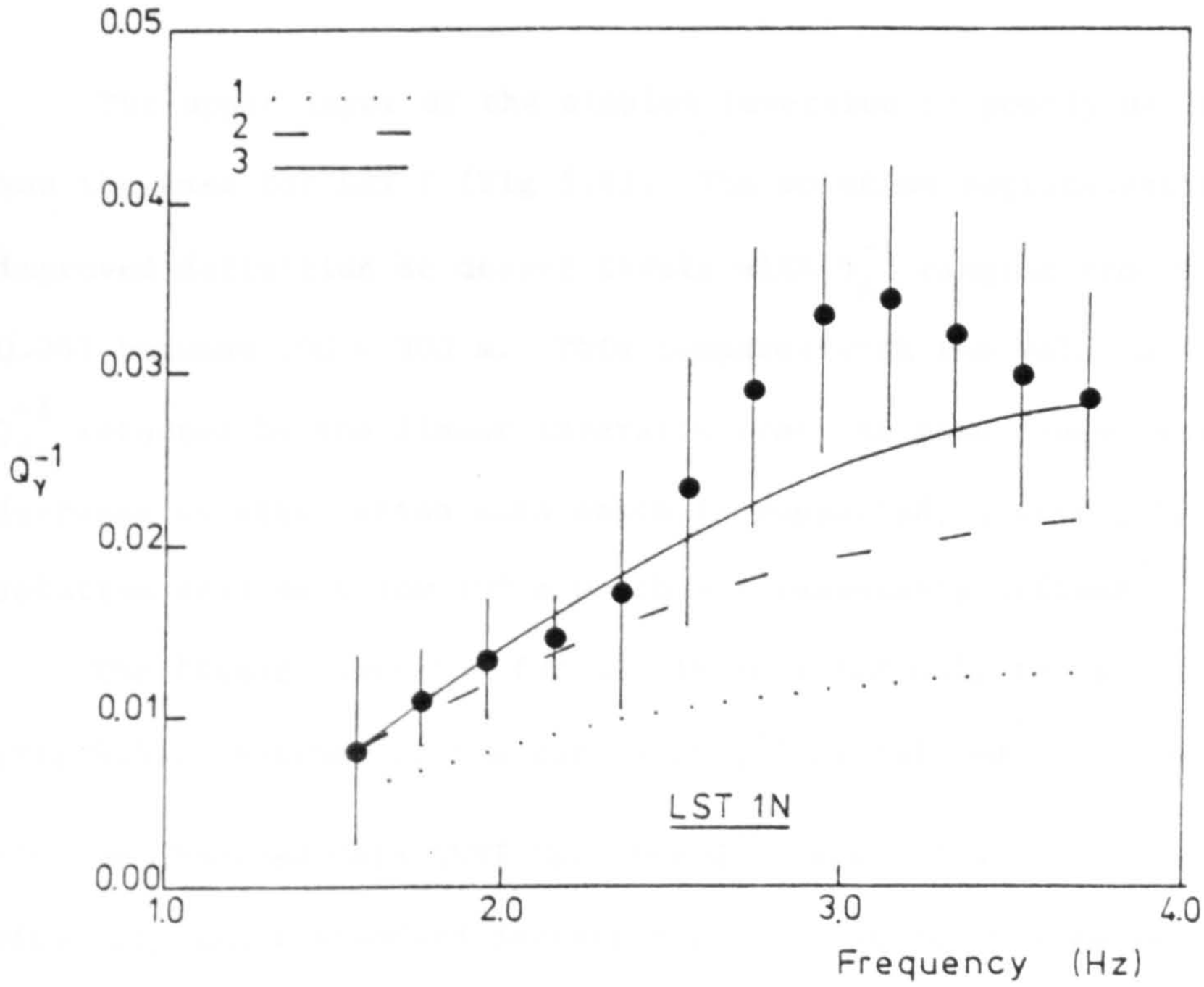
0.05
0.04
0.03
0.02
0.01
0.00
Q_γ^{-1}
1
2
3
LST 1N
1.0
2.0
3.0
4.0
Frequency (Hz)

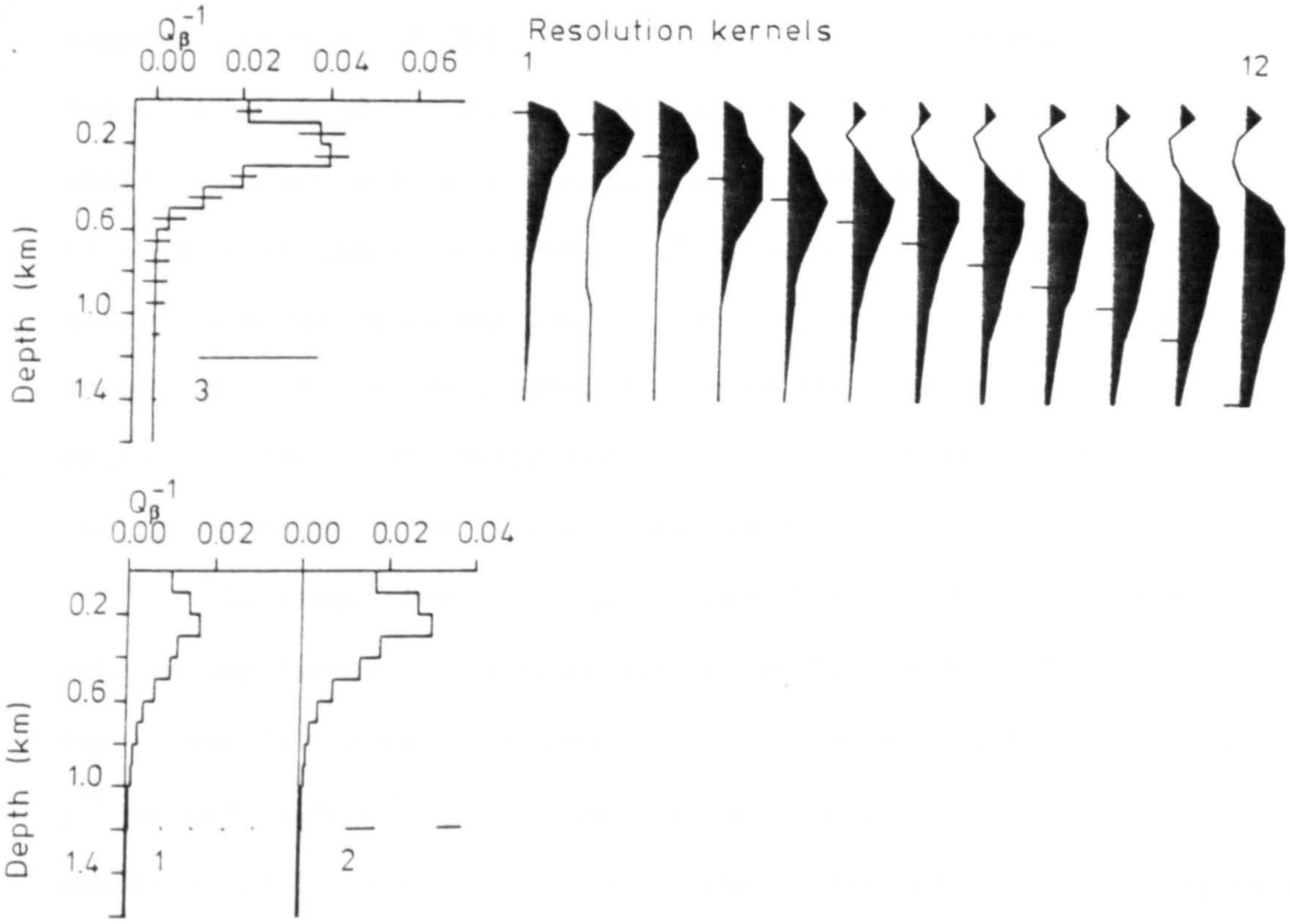
Q_β^{-1}
0.00 0.02 0.04 0.06
Resolution kernels
0.2
0.6
1.0
1.4
Depth (km)
3
Q_β^{-1}
0.00 0.02 0.00 0.02 0.04
1
2

The upper layer of the simplex inversion is poorly defined, as was the case for LST 1 (Fig 5.4). The solution regions exhibit improved definition at deeper levels with Q_β^{-1} ranging from 0.015 to 0.061 between 100 - 300 m. This compares with the value of 0.04 for Q_β^{-1} returned by the linear inversion over the same depth range. The decrease in attenuation with depth is supported, however, by the solution regions below 300 m which are reasonably defined.

The linear inversion for LST 1S provided only two solution models (Fig 5.5). Neither of the curves of Q_γ^{-1} calculated from the models fit the observed data QLST 1S. The Q_β^{-1} range from -0.0003 to 0.0809 with very small standard deviations. Resolution is also very poor with few kernels being located about the correct depth.

A feasible solution existed only at a very high tolerance for the simplex inversion of QLST 1S implying a poorly determined model (Fig 5.6). A value of Q_β^{-1} 0.00 - 0.02 is given for the first 500 m. A sharp increase in attenuation is shown to produce a high attenuation channel of thickness 300 m with Q_β^{-1} between 0.23 to 0.31. Below 800 m attenuation decreases but the solution regions are ill defined. The solutions from the two inversion schemes are contrasting; the simplex regions define considerably higher values of intrinsic attenuation at depth than those given by the linear inversion.

In the linear inversions presented above the intrinsic shear wave attenuation factor has been assumed to be independent of frequency. The assumption is based on laboratory observations which have shown Q^{-1} be independent of frequency and the contention of Jackson & Anderson (1970) that various mechanisms of dissipation, which may have a frequency dependence individually, combine to produce a negligible dependence on frequency. There is, however, a growing body of observational data which implies that the intrinsic attenuation within

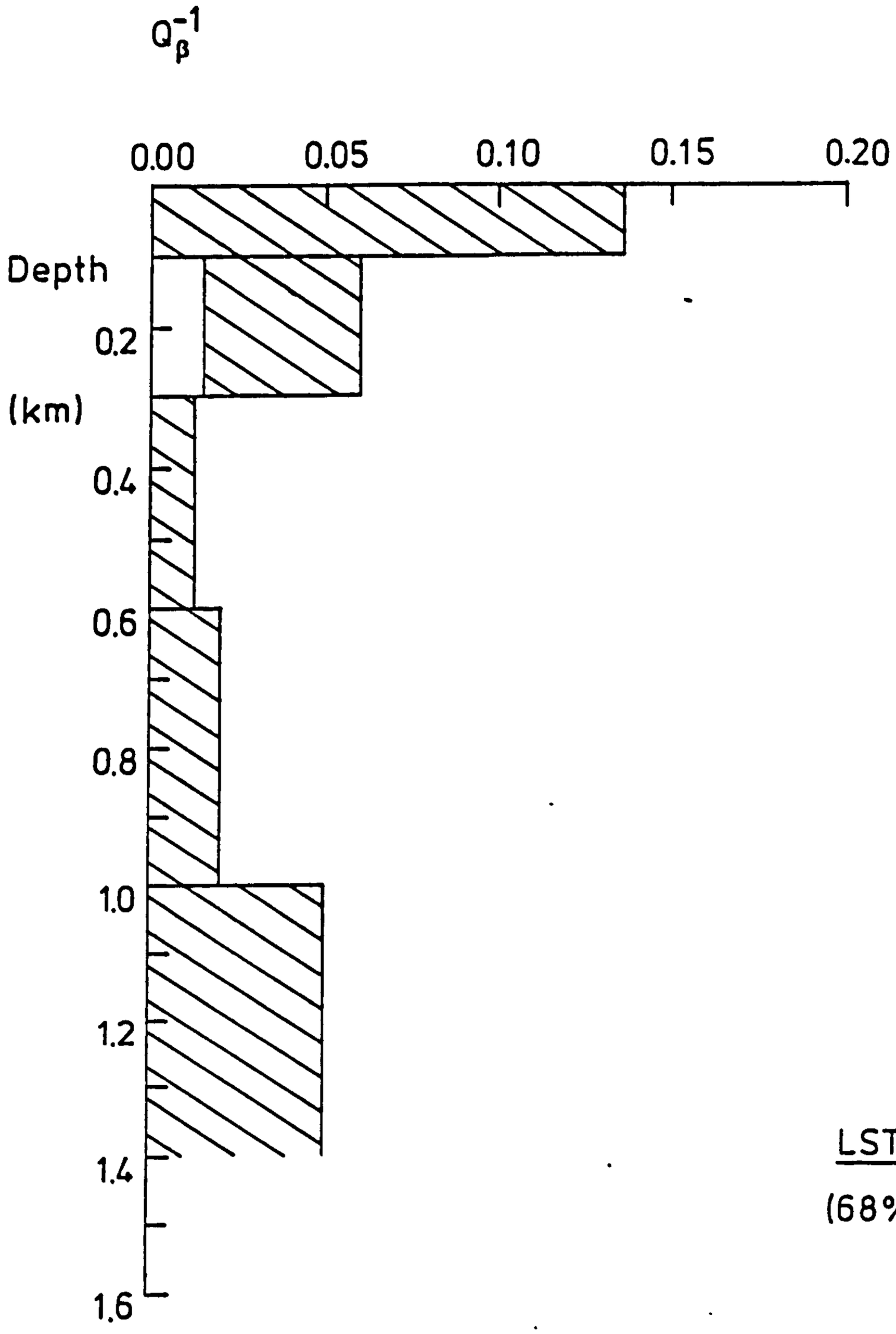

Figure 5.4 Linear programming inversion of the observed Rayleigh wave specific attenuation factor data for the intrinsic attenuation factor, $Q_\beta^{-1}(z)$, with depth for LST 1N.

Figure 5.5 Linear inversion of the observed Rayleigh wave specific attenuation factor data for the intrinsic specific attenuation factor, $Q_\beta^{-1}(z)$, with depth for LST 1S. (Smoothing parameter of preferred solution, $\theta = 1287.8$)

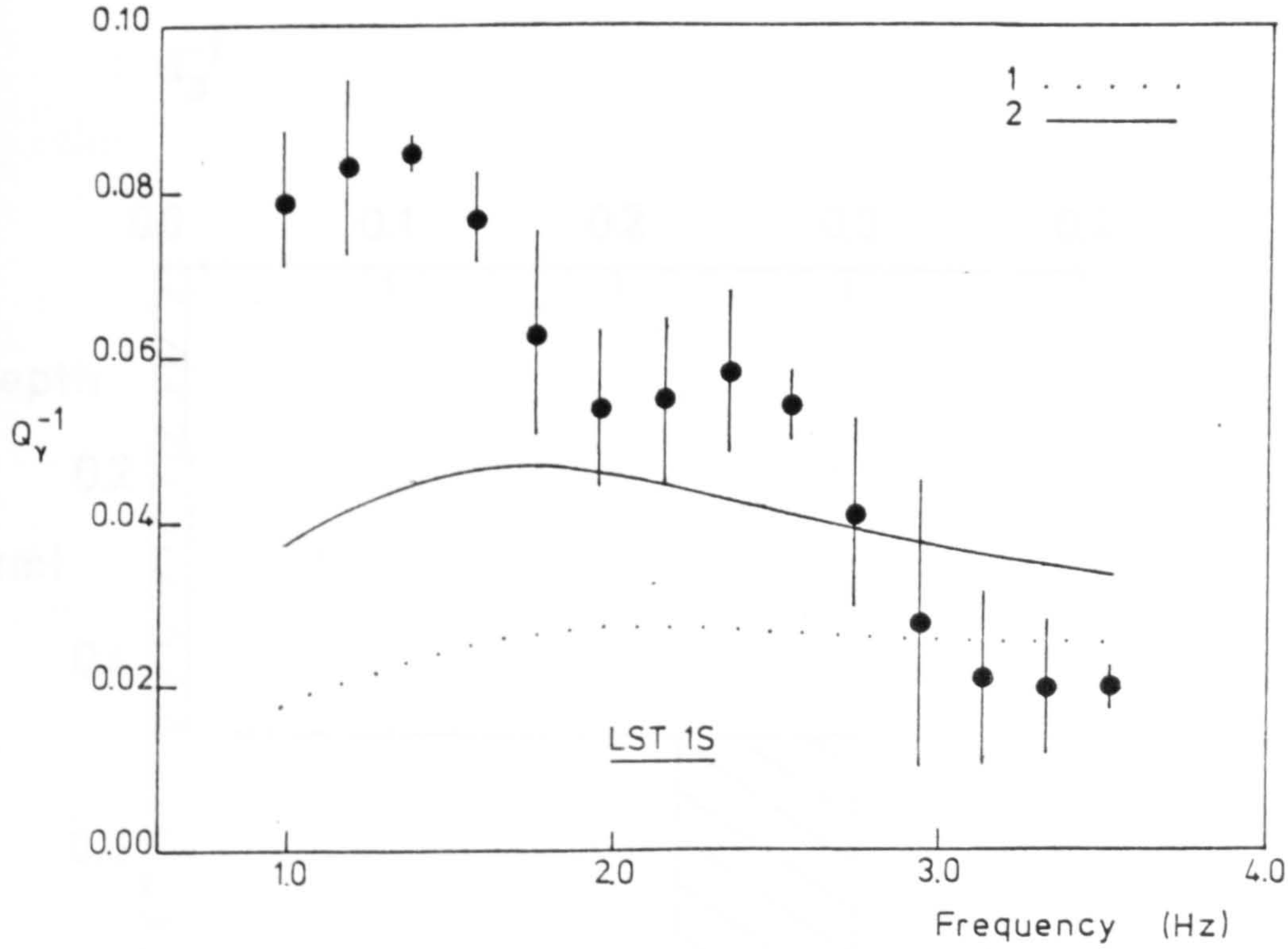
0.10
0.08
0.06
0.04
0.02
0.00
Q_Y^{-1}
1
2
LST 1S
1.0
2.0
3.0
4.0
Frequency (Hz)

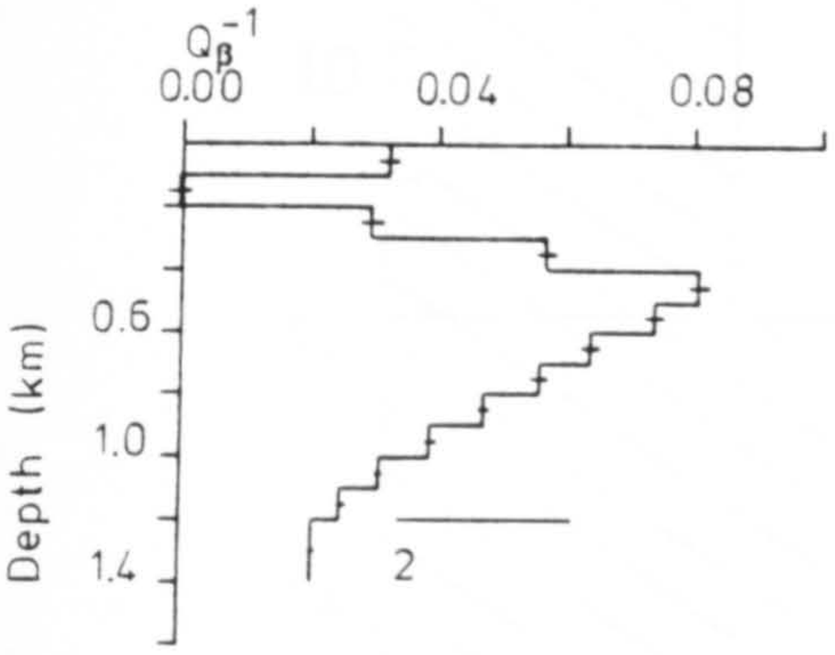
Q_β^{-1}
0.00
0.04
0.08
0.6
1.0
1.4
Depth (km)
2

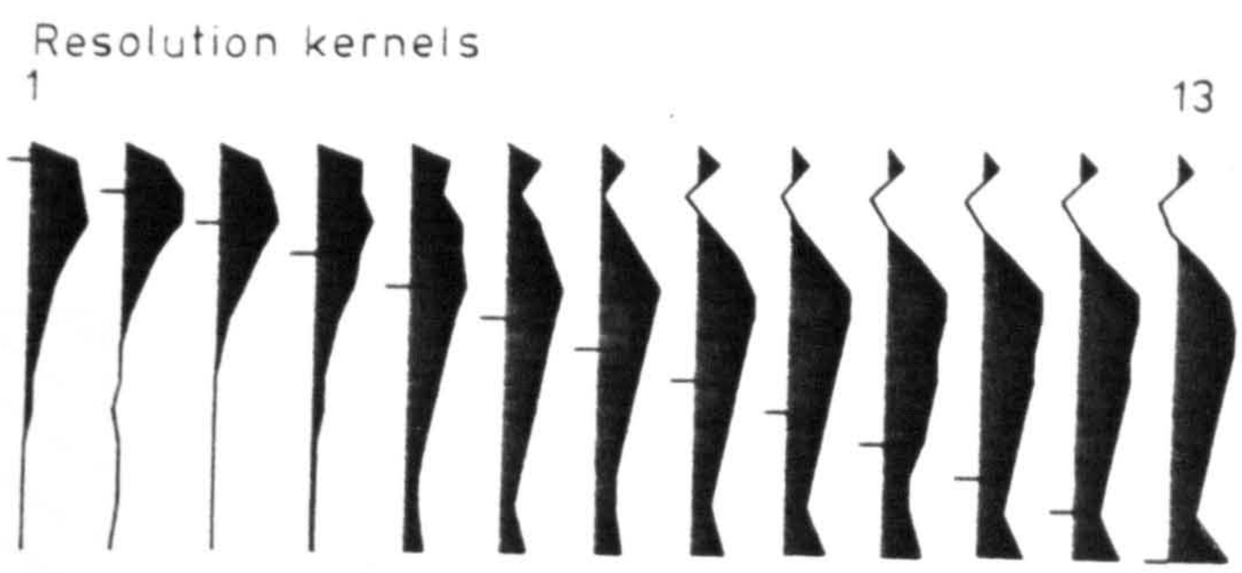
Resolution kernels
1
13

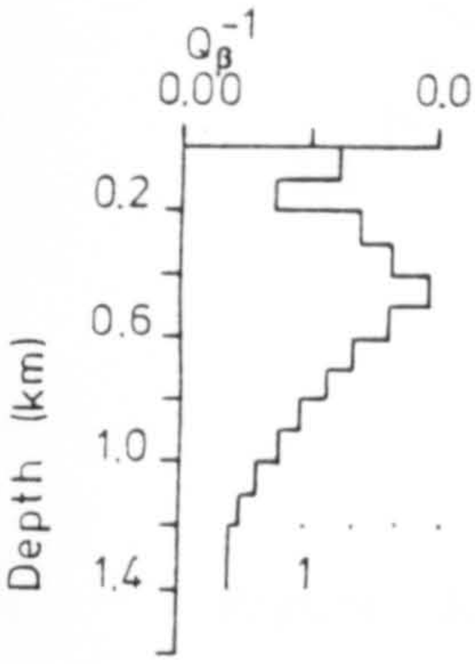
Q_β^{-1}
0.00
0.04
0.2
0.6
1.0
1.4
Depth (km)
1

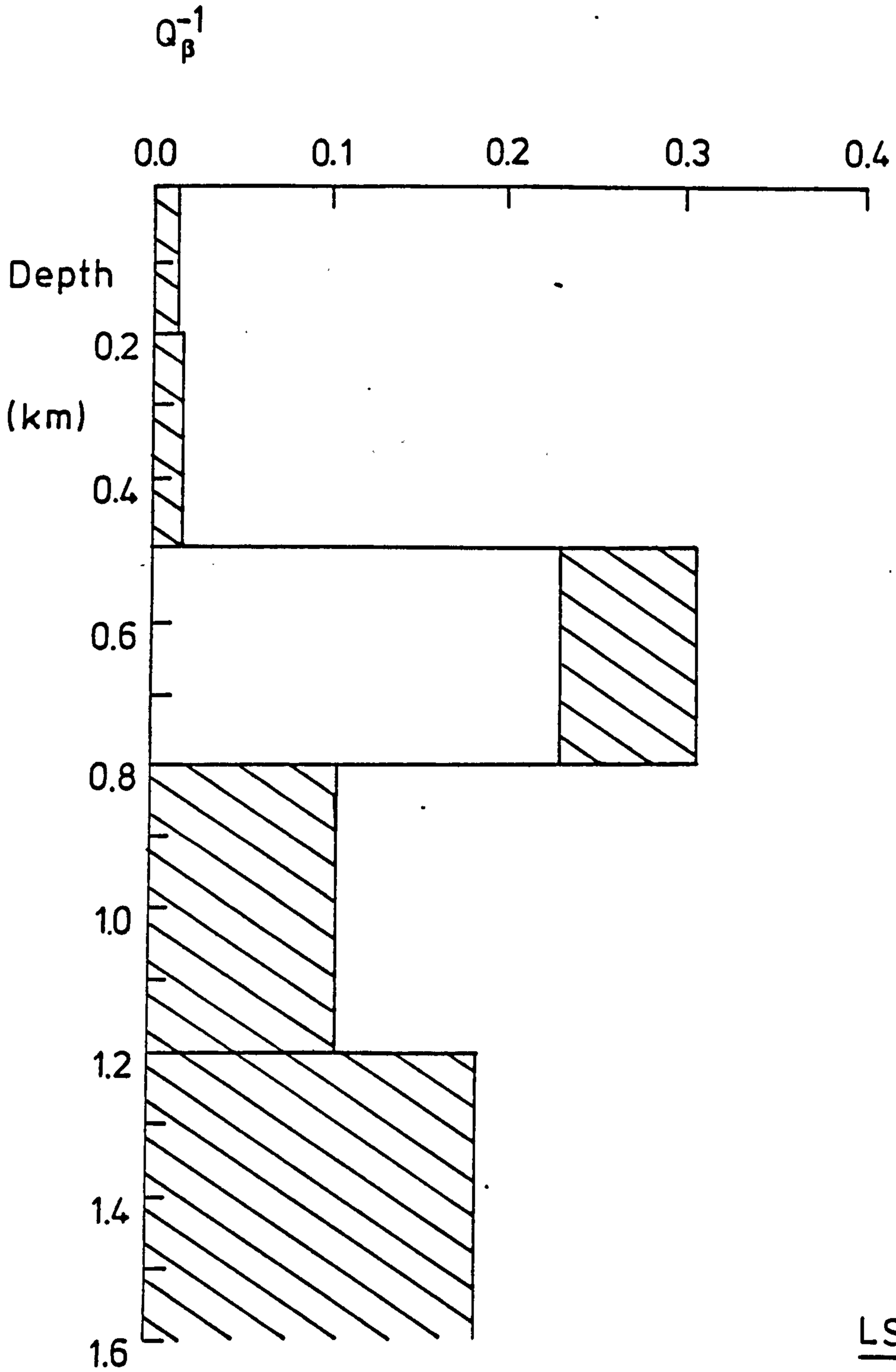

Figure 5.6 Linear programming inversion of the observed Rayleigh wave specific attenuation factor data for the intrinsic attenuation factor, $Q_\beta^{-1}(z)$, with depth for LST 1S.

the Earth is frequency dependent (Mitchell 1980, Souriau et al. 1980).

The linear inversion scheme can be modified to include a frequency dependence of the form given by equation (3.10). Provided that η, the exponent of the frequency dependence, is constant in each layer then the linearity of the problem is not impaired (Lee & Solomon 1975). Mitchell (1980) has suggested that $\eta = 0.5$ at 1 Hz for the upper crust but that a lower value may be more appropriate at higher frequencies.

The linear inversions were, therefore, conducted again assuming Q_β^{-1} to be frequency dependent with $\eta = 0.5$. The inversion solutions were not, however, improved by assuming this frequency dependence. In chapter 3 we obtained values of η more appropriate to the individual data sets of this study. Using the values presented in section 3.4 the solution models from the linear inversions of the observed data QLST 1N and QLST 1S were improved. The lack of improvement for LST 1, the district average was expected because the values of η obtained had little statistical significance.

For LST 1N (Fig 5.7) the inclusion of a frequency dependence permits five models to be determined before a solution of little physical meaning occurs. This contrasts to the frequency independent inversion in which only three models were obtained. Lower overall values of Q_β^{-1} are returned from the frequency dependent inversion. The preferred model 4 has a 200 m thick upper layer having Q_β^{-1} 0.001 - 0.002 underlain by a layer of higher attenuation with Q_β^{-1} 0.007 being 300 m in thickness. The attenuation then decreases monotonically with depth. The resolution kernels for the preferred model are only slightly improved in the upper layers when compared to those of the frequency independent inversions. Below 500 m the kernels are broad

Figure 5.7 Linear inversion of the observed Rayleigh wave specific attenuation factor data for the intrinsic specific attenuation factor, $Q_\beta^{-1}(z)$, with depth for LST 1N assuming a frequency dependent intrinsic attenuation. The frequency dependence has an exponent, $\eta = -1.681$. (Smoothing parameter of preferred solution, $\theta = 1468.1$)

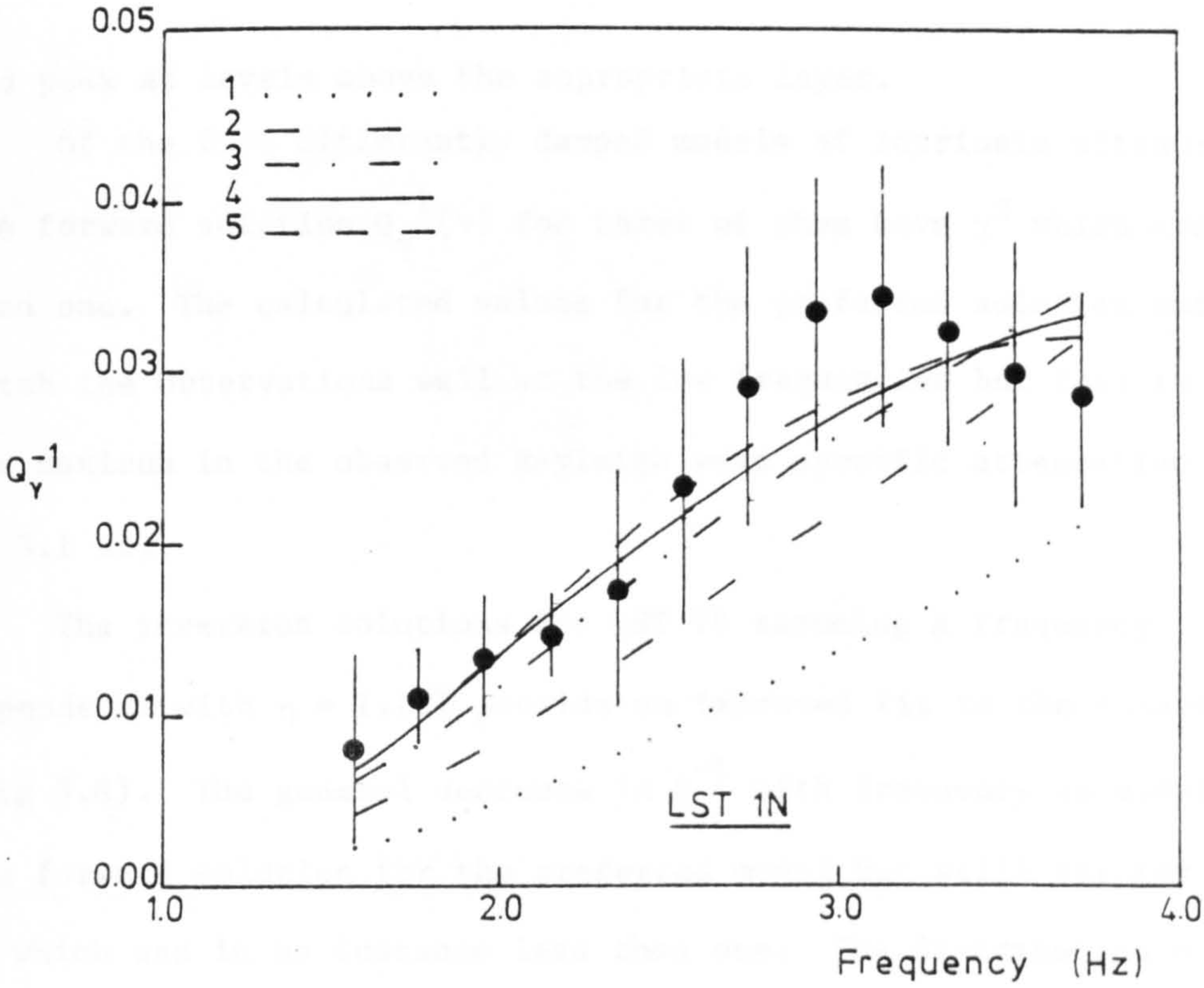
0.05
0.04
0.03
0.02
0.01
0.00
Q_Y^{-1}
1
2
3
4
5
LST 1N
1.0
2.0
3.0
4.0
Frequency (Hz)

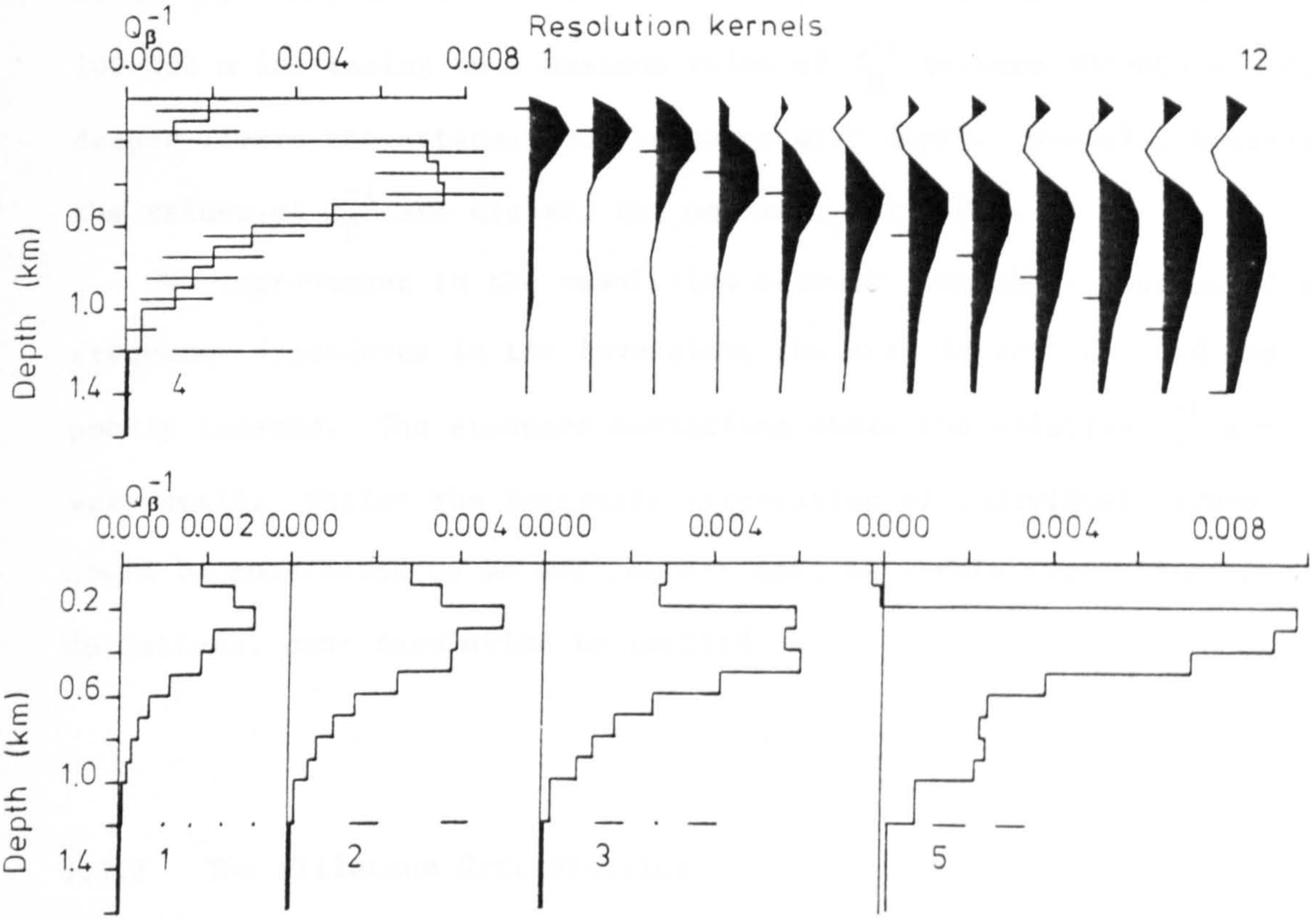
Q_β^{-1}
0.000
0.004
0.008
Resolution kernels
12
Depth (km)
0.6
1.0
1.4
4
Q_β^{-1}
0.000 0.002 0.000
0.004 0.000
0.004
0.000
0.004
0.008
0.2
0.6
1.0
1.4
1
2
3
5

and peak at levels above the appropriate layer.

Of the five differently damped models of intrinsic attenuation the forward solution $Q_\gamma^{-1}(\nu)$ for three of them have χ^2 which are less than one. The calculated values for the preferred solution model match the observations well at the low frequencies but fail to model the maximum in the observed Rayleigh wave specific attenuation factor at 3.1 Hz.

The inversion solutions for LST 1S assuming a frequency dependence with $\eta = 1.127$ provide an improved fit to the observed data (Fig 5.8). The general decrease in Q_γ^{-1} with frequency is modelled by the forward solution for the preferred model but still returns a high χ^2 which was in no instance less than one. The distribution of intrinsic attenuation with depth shows the same pattern as the frequency independent inversions with a low attenuation channel at 100-200 m increasing to a maximum value of Q_β^{-1} between 500-600 m. At deeper levels the attenuation decreases with depth. Overall, however, the values of Q_β^{-1} are higher, the maximum, being 0.2.

No improvement in the resolution accrues from the inclusion of a frequency dependence in the inversion; the kernels remain broad and poorly located. The standard deviations about the solution Q_β^{-1} are very small. Whilst the intrinsic attenuation of individual layers could be considered to be well determined, to within their standard deviations, poor resolution is implied.

5.3.2 The Millstone Grit District.

The linear inversion of the pure path data set QMG 1 provides six solution models at different degrees of damping of which the fifth is preferred (Fig 5.9). A channel of lower Q_β^{-1} 0.01 is exhibited between

Figure 5.8 Linear inversion of the observed Rayleigh wave specific attenuation factor data for the intrinsic specific attenuation factor, $Q_\beta^{-1}(z)$, with depth for LST 1S assuming a frequency dependent intrinsic attenuation. The frequency dependence has an exponent, $\eta = 1.127$. (Smoothing parameter of preferred solution, $\theta = 294.1$)

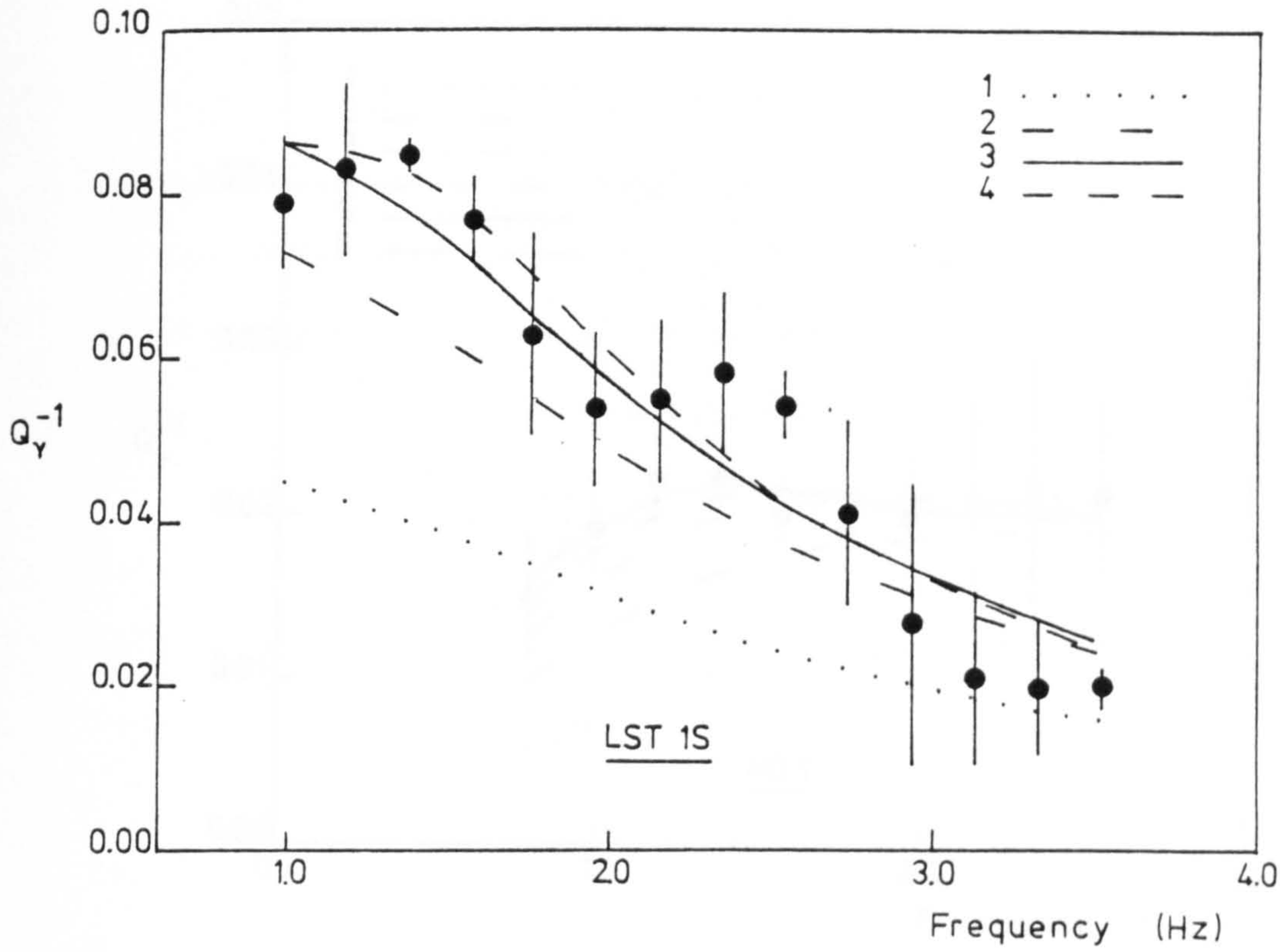
0.10
0.08
0.06
0.04
0.02
0.00
Q_γ^{-1}
1
2
3
4
LST 1S
1.0
2.0
3.0
4.0
Frequency (Hz)

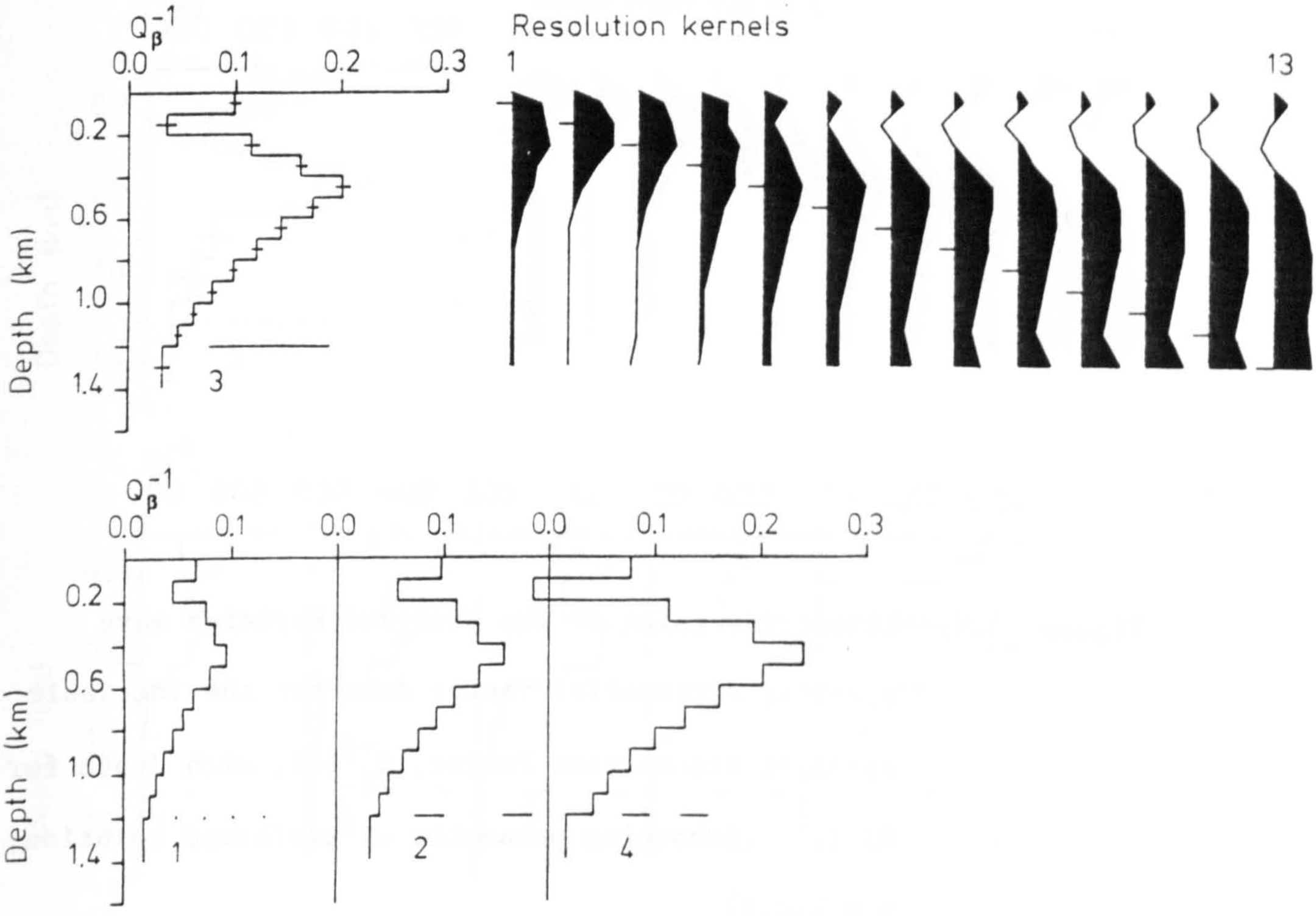
Q_β^{-1}
0.0
0.1
0.2
0.3
Resolution kernels
13
Depth (km)
0.2
0.6
1.0
1.4
3
Q_β^{-1}
0.0
0.1
0.0
0.1
0.0
0.1
0.2
0.3
Depth (km)
0.2
0.6
1.0
1.4
1
2
4

Figure 5.9 Linear inversion of the observed Rayleigh wave specific attenuation factor data for the intrinsic specific attenuation factor, $Q_\beta^{-1}(z)$, with depth for MG 1. (Smoothing parameter of preferred solution, $\theta = 210.5$)

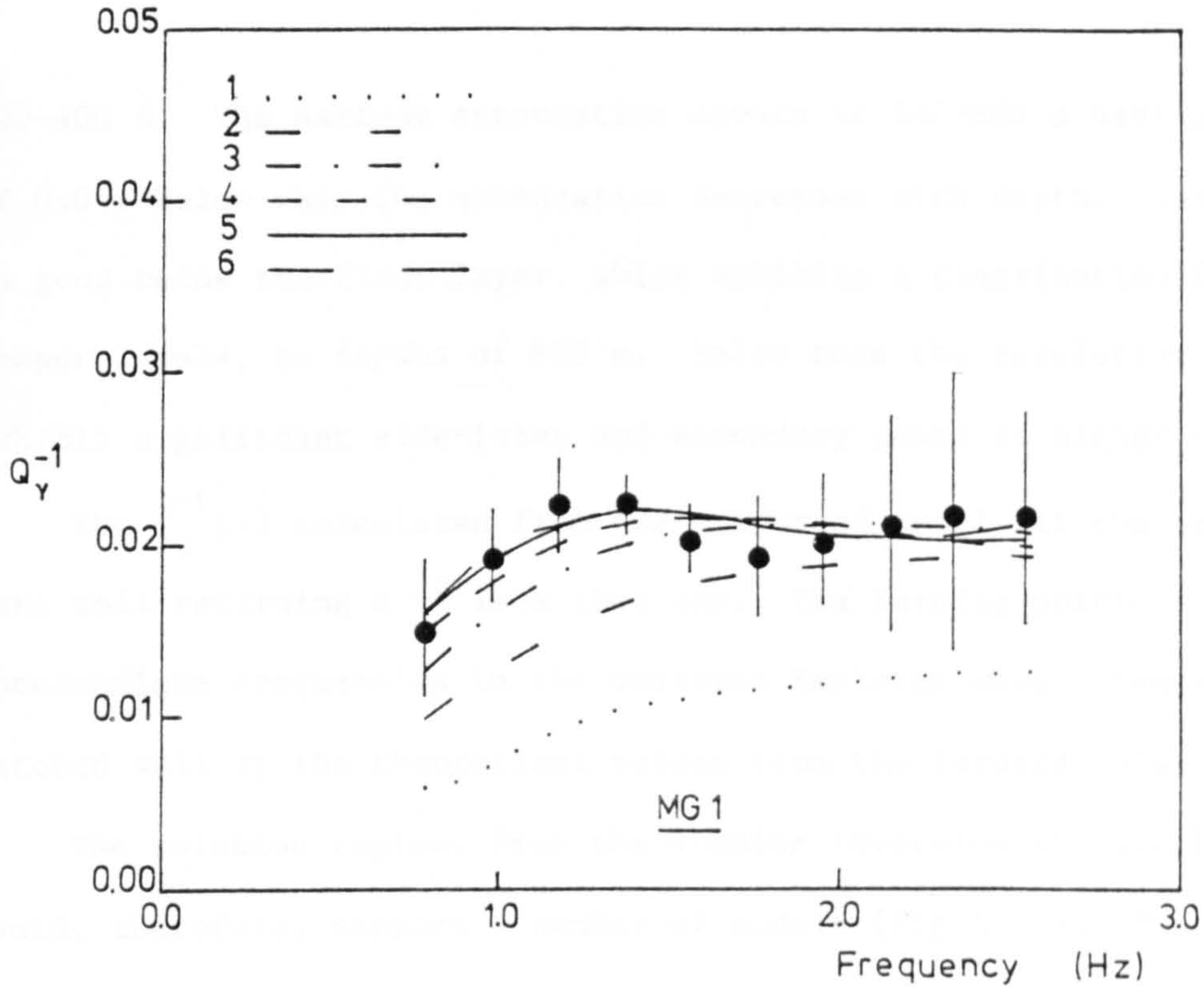
0.05
0.04
0.03
0.02
0.01
0.00
Q_γ^{-1}
1
2
3
4
5
6
MG 1
0.0
1.0
2.0
3.0
Frequency (Hz)

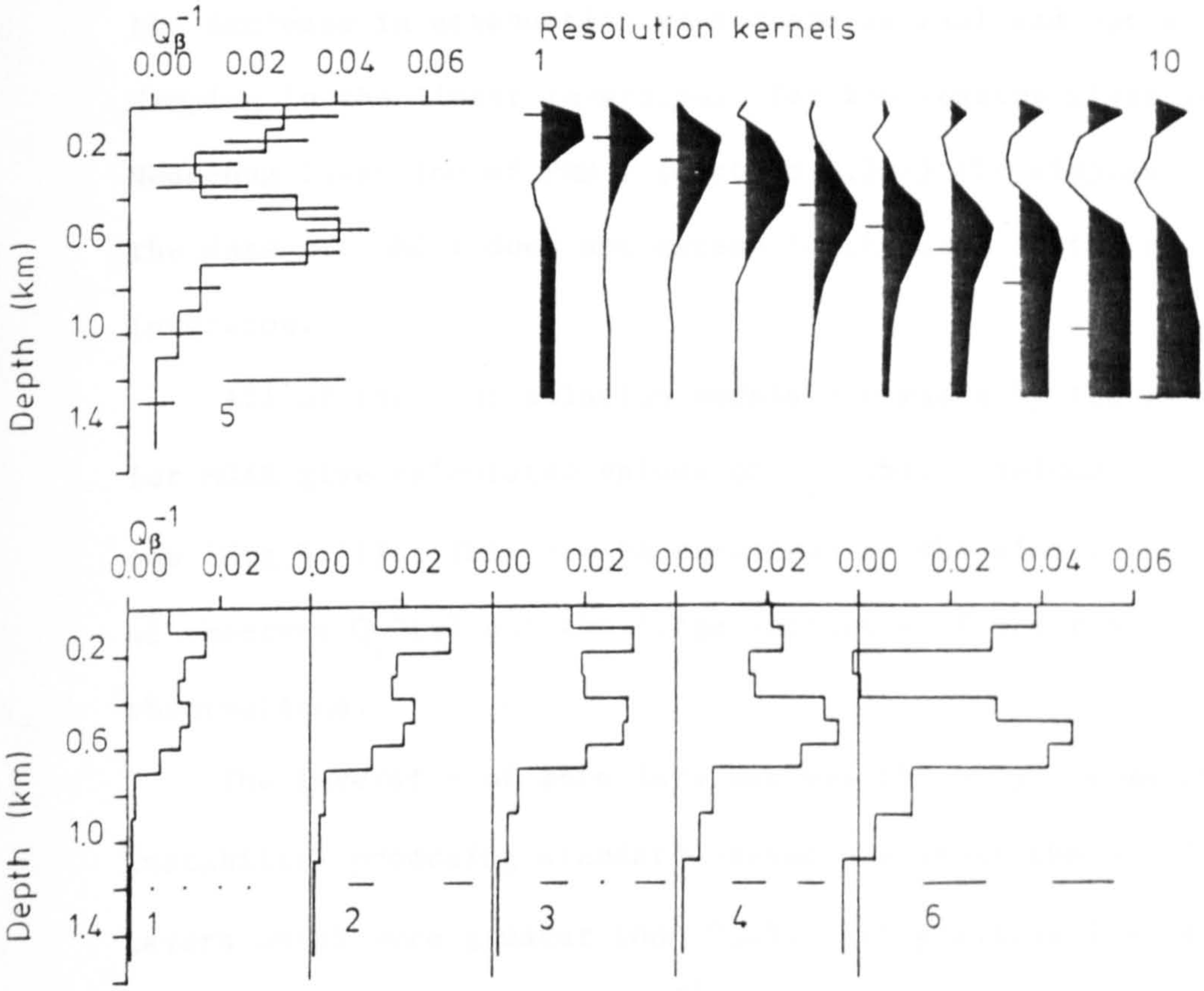
Q_β^{-1}
0.00 0.02 0.04 0.06
Resolution kernels
1
10
0.2
0.6
1.0
1.4
Depth (km)
5
Q_β^{-1}
0.00 0.02 0.00 0.02 0.00 0.02 0.00 0.02 0.00 0.02 0.04 0.06
1
2
3
4
6

200-400 m. The maximum attenuation occurs at 500-600 m having a Q_β^{-1} of 0.04. Below this the attenuation decreases with depth. Resolution is good below the first layer, which exhibits a contribution from deeper levels, to depths of 600 m. Below this the resolution kernels exhibit significant side-lobes and secondary peaks at higher levels.

The $Q_\gamma^{-1}(\nu)$ calculated from the preferred model fit the observed data well returning a χ^2 less than one. The turning points at intermediate frequencies in the observed Rayleigh wave attenuation are matched well by the theoretical values from the forward solution.

The solution regions from the simplex inversion all overlap and could, therefore, support a number of models (Fig 5.10). The definition on the solution region of the upper layer is poor. For deeper layers, however, the definition is improved and may indicate the decrease in attenuation with depth is real and not a facet of over damping in the linear inversion. For the reasons given for the Hedgehog inversion of PMG 1 (section 4.3.2) the simplex inversion of the data set QMG 1 does not extend to the same depths as the linear inversion.

All of the four solution models generated by the linear inversion for MGAR give calculated values of Q_γ^{-1} which yielded a χ^2 of less than one (Fig 5.11). This can be explained by the almost constant values of observed $Q_\gamma^{-1}(\nu)$ and the large estimates of error about these observations.

The inversion of this data set was the only one which ended by instability producing standard deviations about the Q_β^{-1} for certain layers which were greater than 0.05. All previous inversions were terminated because negative Q_β^{-1} occurred at some depths. A slight decrease in Q_β^{-1} is shown from 0.025 to 0.01 below 100 m by the solution values. The magnitudes of their standard deviations,

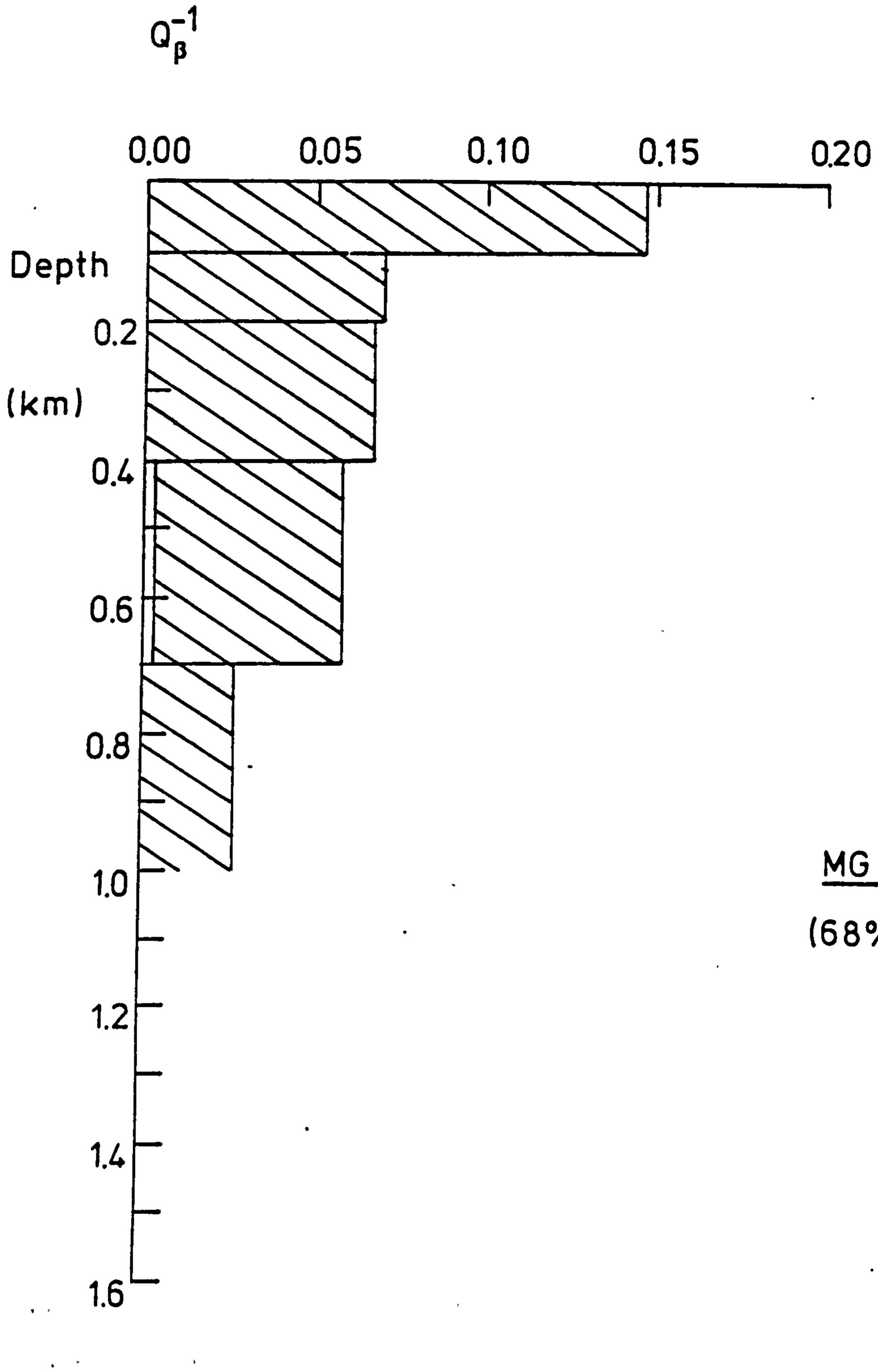

Figure 5.10 Linear programming inversion of the observed Rayleigh wave specific attenuation factor data for the intrinsic attenuation factor, $Q_\beta^{-1}(z)$, with depth for MG 1.

Figure 5.11 Linear inversion of the observed Rayleigh wave specific attenuation factor data for the intrinsic specific attenuation factor, $Q_\beta^{-1}(z)$, with depth for MGAR. (Smoothing parameter of preferred solution, $\theta = 90.1$)

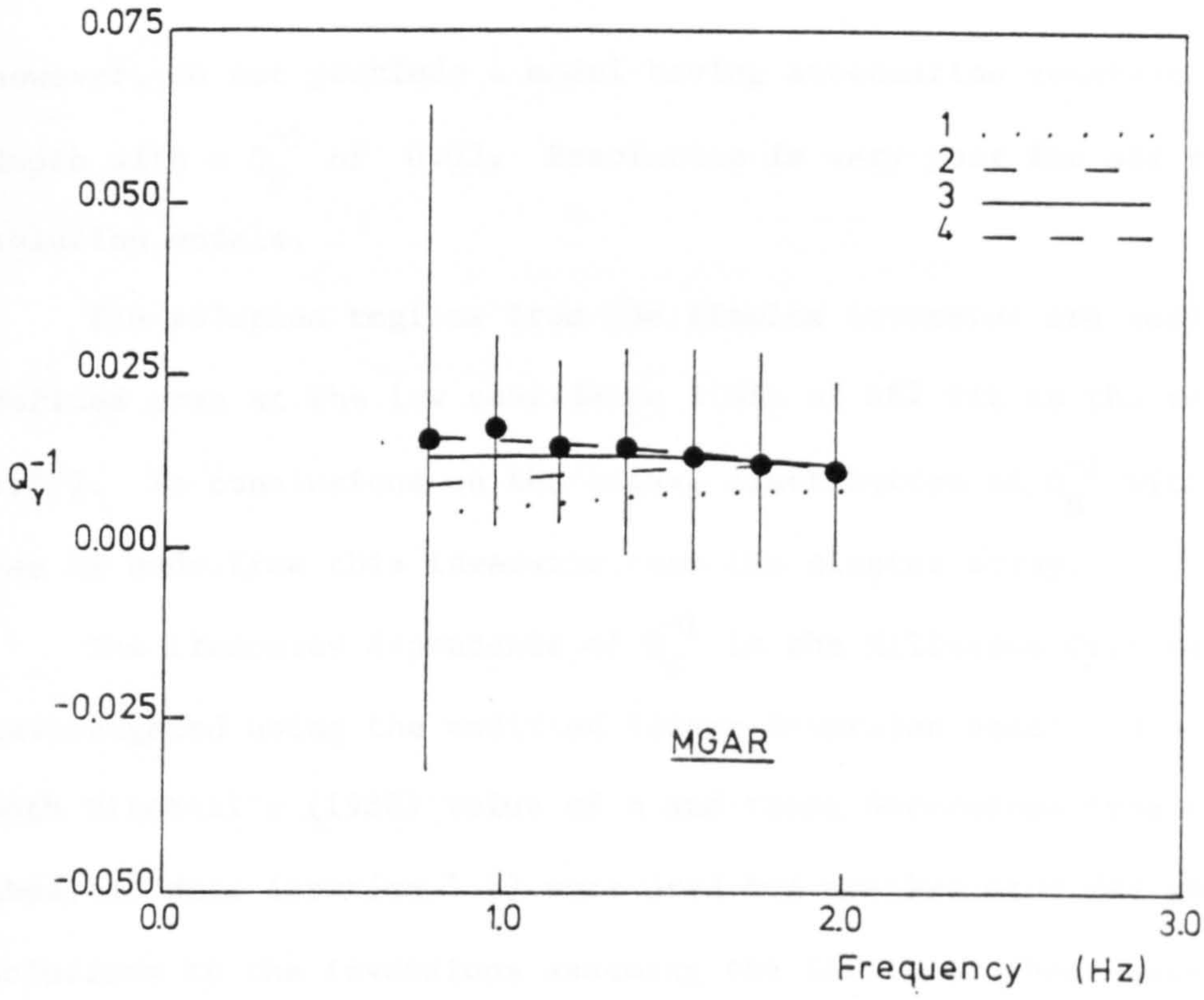
0.075
0.050
0.025
0.000
-0.025
-0.050
Q_Y^{-1}
1
2
3
4
MGAR
0.0
1.0
2.0
3.0
Frequency (Hz)

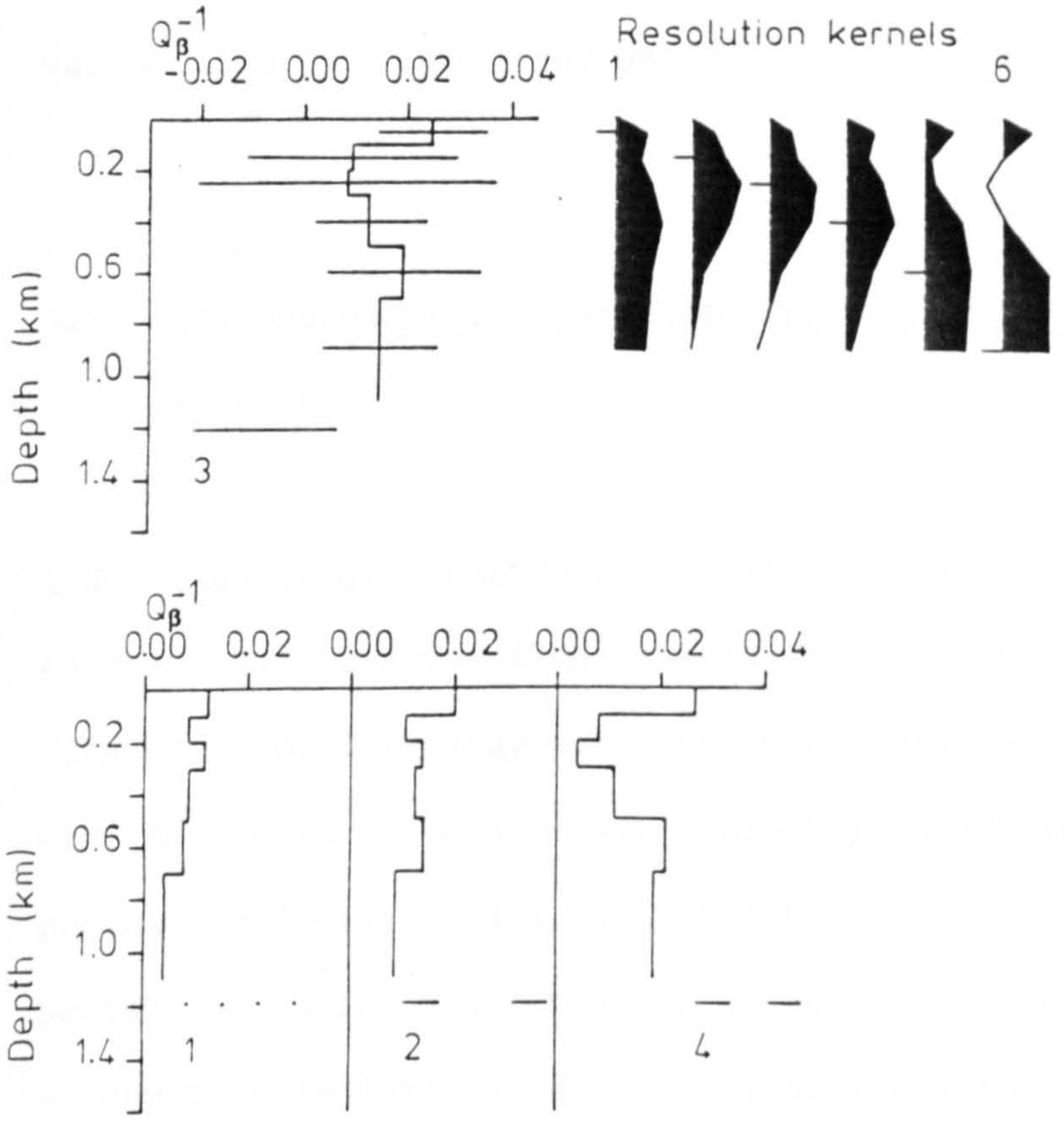
Q_β^{-1}
-0.02 0.00 0.02 0.04
Resolution kernels
1
6
0.2
0.6
1.0
1.4
Depth (km)
3
Q_β^{-1}
0.00 0.02 0.00 0.02 0.00 0.02 0.04
0.2
0.6
1.0
1.4
Depth (km)
1
2
4

however, do not preclude a model having attenuation constant with depth with a Q_β^{-1} of 0.02. Resolution is very poor for all the solution models.

The solution regions from the simplex inversion are very poorly defined even at the low confidence limit of 68% fit to the data (Fig 5.12). No conclusions on the actual distribution of Q_β^{-1} with depth can be made from this inversion over the cluster array.

The frequency dependence of Q_β^{-1} in the Millstone Grit was investigated using the modified linear inversion described previously. Both Mitchell's (1980) value of η and those determined from the observed data (section 3.4) were used but neither provided improved solutions to the inversions assuming the intrinsic shear wave attenuation factor to be independent of frequency. This result was expected due to the statistical insignificance of the calculated values of η from QMG 1 and QMGAR.

5.4 DISCUSSION of the INTRINSIC SHEAR WAVE ATTENUATION-DEPTH PROFILES.

A detailed interpretation of the shear wave velocity profiles (section 4.4) was possible because velocity has been shown to be diagnostic of lithology and there have been several laboratory experiments to measure seismic velocity in specific rock types. In general, velocity is less affected by changes in physical conditions pertaining in the shallow upper crust. In contrast, the intrinsic attenuation is influenced strongly by variations in physical conditions in addition to the rock type (section 1.3) making the assignation of lithology to obtained values of Q_β^{-1} difficult. The shear wave attenuation - depth profiles presented above, therefore,

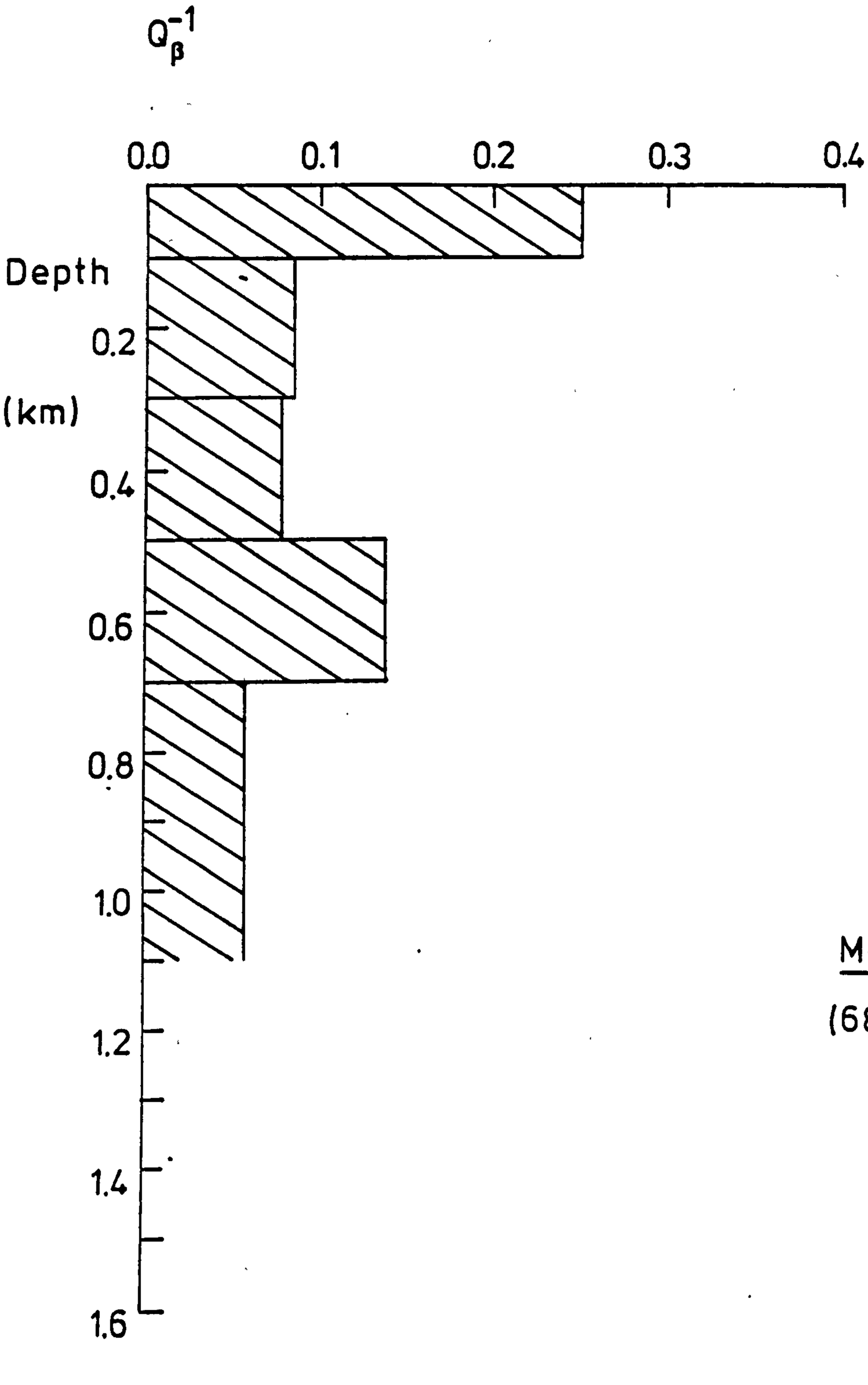

Figure 5.12 Linear programming inversion of the observed Rayleigh wave specific attenuation factor data for the intrinsic attenuation factor, $Q_\beta^{-1}(z)$, with depth for MGAR.

will be discussed in general terms.

Overall the results from the two inversion schemes show good similarity in the distribution of Q_β^{-1} with depth although the simplex method yields higher maximum values of attenuation. This may be because the estimates of Q_β^{-1} returned by the linear inversions have been, in some cases, depressed slightly by over damping.

The preferred solution models from the linear inversions are presented for comparison in Figure 5.13. In all cases the attenuation decreases with depth below a region of higher attenuation near the surface. Low apparent values of Q_β^{-1} at depth could be caused by forcing the inversions to depths at which there was little Rayleigh wave energy or by over damping the problem. This effect is similar to that described for the linearised inversion technique to obtain the shear wave velocity-depth profiles and can be resolved in the same manner by the use of an alternative inversion scheme. The Hedgehog inversion scheme can also be adapted to give shear wave attenuation-depth profiles using equation (5.7). This technique has been used previously by Burton & Kennet (1972), Burton (1977) and Evans (1981). It was found that with the data of the present study the Hedgehog inversion scheme failed to give meaningful results. Only when the mesh size was small and the acceptance criteria large did the Monte-Carlo search transfer from a random point to a knot. Having found this knot no further acceptable knots were found and the region was ended. This situation was clearly unrealistic as further random points satisfied the test conditions. For this reason the Hedgehog inversion technique was abandoned in favour of the linear programming, simplex method.

The two inversion schemes are, however, analogous and define the bounds of acceptable solutions in parameter space. Not all of the

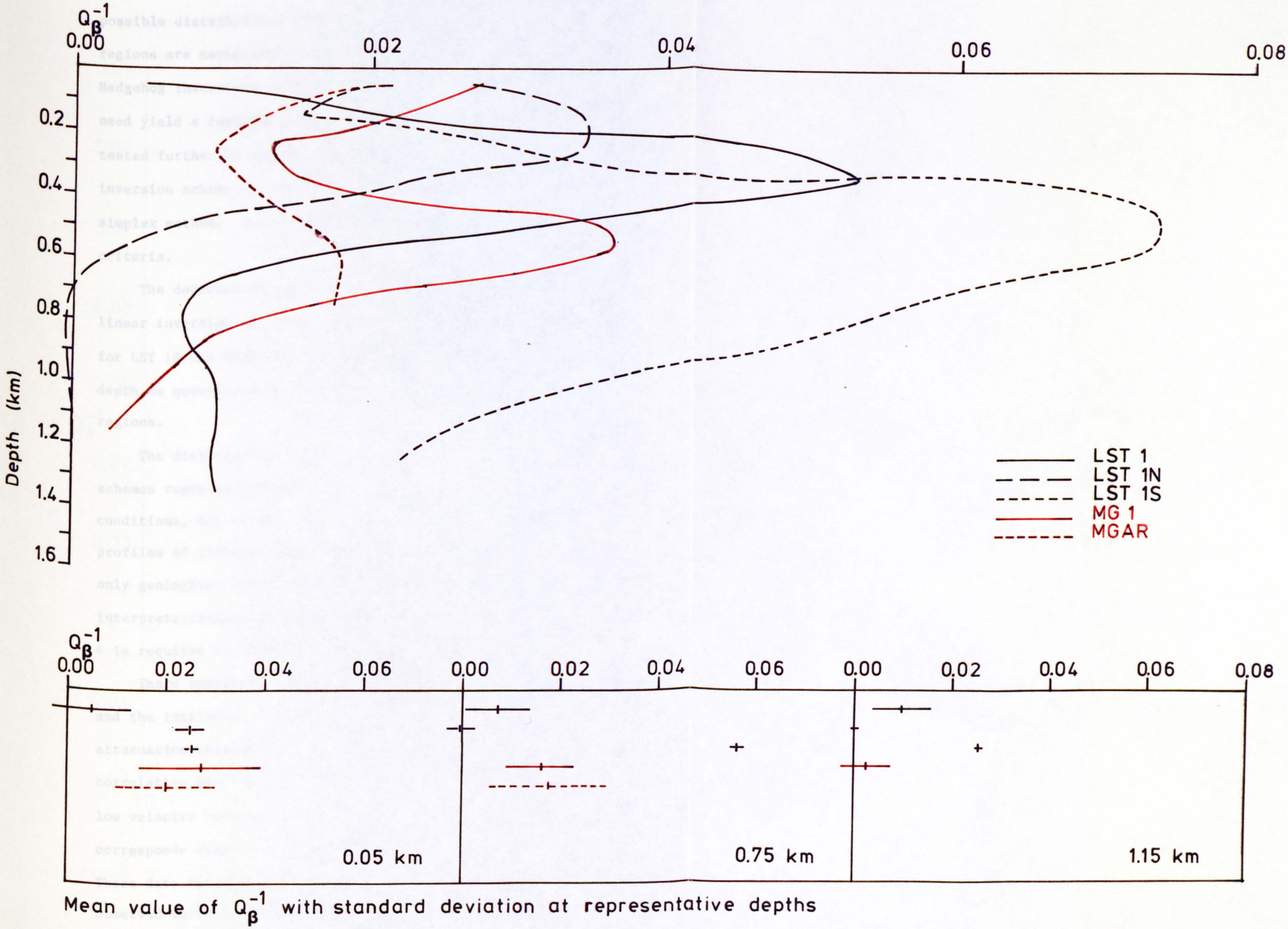

Figure 5.13 Comparison of the preferred solution intrinsic attenuation profiles from the linear inversion of the observed Rayleigh wave specific attenuation factor, $Q_\gamma^{-1}(\nu)$, data. A weighted 300 m running mean was used to smooth each profile. Standard deviations about mean velocities are shown for a selection of representative depths in each profile.

possible distributions of intrinsic attenuation within the solution regions are necessarily realistic models as is the case in the Hedgehog inversions where not every profile within the solution region need yield a feasible model. The equivalence of the two techniques was tested further by applying the acceptance criteria from the Hedgehog inversion scheme to the models used to define the boundaries in the simplex method. In all cases the models satisfied the Hedgehog test criteria.

The decrease in intrinsic attenuation at depth indicated by the linear inversion was supported by the simplex solution regions. Only for LST 1S and MGAR must the existence of this zone of low Q_β^{-1} at depth be questioned because of the poor definition of the solution regions.

The distribution of Q_β^{-1} with depth, obtained from the inversion schemes represent variations not only in rock type but in the physical conditions, for example saturation, existing in the upper crust. The profiles of intrinsic attenuation cannot, therefore, be used to infer only geological structure. For this reason a comparison with the interpretations of the shear wave velocity - depth profiles of chapter 4 is required to maintain geological compatibility.

There appears to be a correlation between the shear wave velocity and the intrinsic attenuation within individual provinces with low attenuation corresponding to high velocity and vice versa. This correlation was best demonstrated by the profile for MG 1 where the low velocity layer, β 1.3 - 1.5 km s^{-1}, between 400 - 700 m corresponds exactly to a layer of high attenuation, Q_β^{-1} 0.03 - 0.04. These data returned a correlation co-efficient of -0.9 with 81% of the observed variation being explained by a linear relation. The complete suite of data is presented in Figure 5.14.

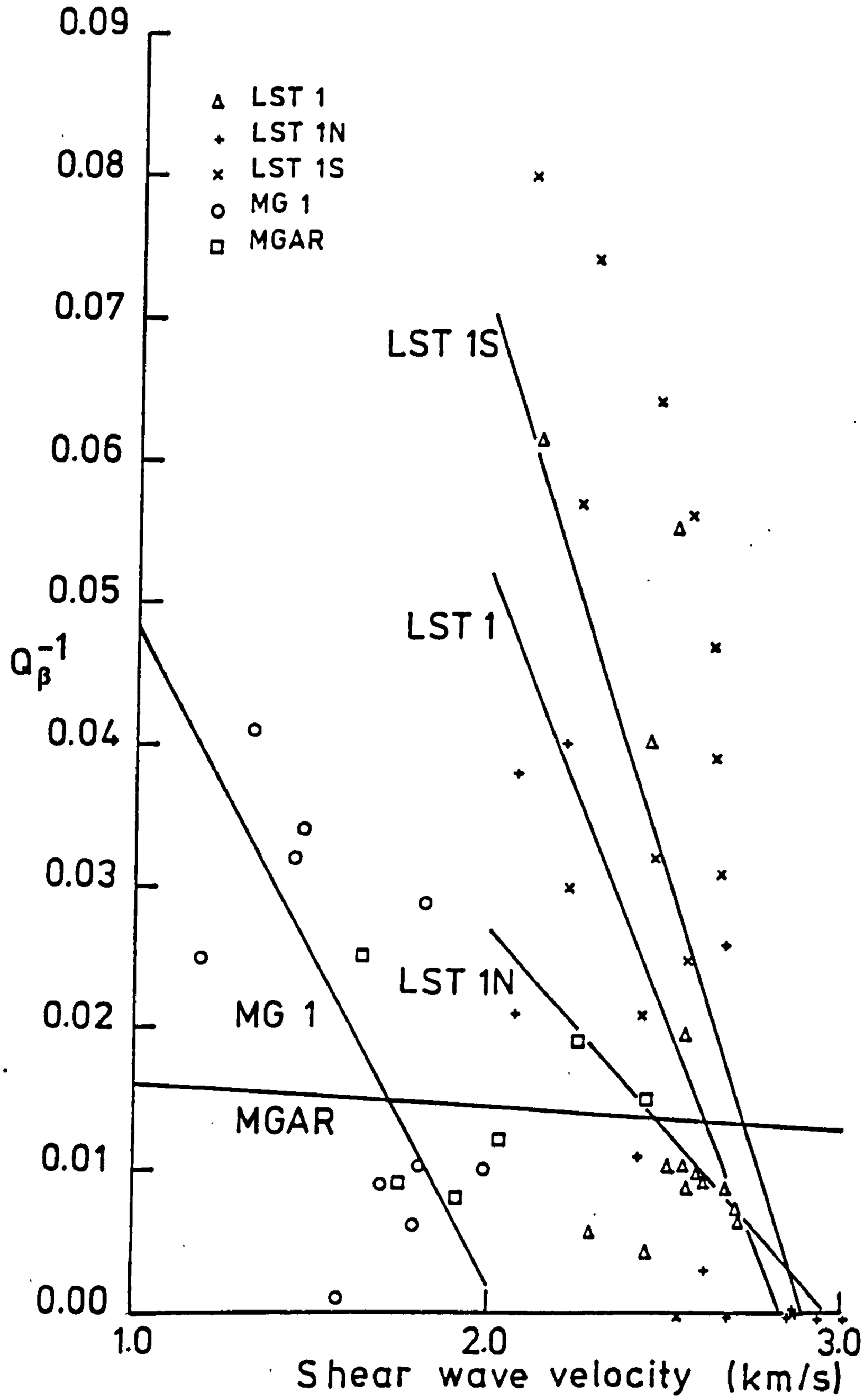

Figure 5.14 Correlation between intrinsic shear wave velocity and attenuation within individual provinces. (Least squares regression lines indicated.)

The correlation between intrinsic velocity and attenuation is less obvious when the Hedgehog (velocity) and simplex (attenuation) solution regions are compared. This is due to the coarser distribution of Q_β^{-1} and shear wave velocity implied by these inversion results.

Inferring from the shear wave velocity - depth profiles that the limestone is 200 - 300 m thick we obtained field estimates of Q_β^{-1} for limestone which range from 0.004 to 0.04. Laboratory determinations of attenuation for limestones at normal values of pressure, saturation and temperature give a range of Q_β^{-1} from 0.002 to 0.022, predominantly at the lower values (Table 1.1). These ranges of attenuation overlap but in general the field estimates are higher than the laboratory determinations. Saturation conditions have been shown to affect the intrinsic attenuation greatly. For example, measurements in the laboratory on a fully saturated sample of limestone gave a Q_β^{-1} of 0.083 (Toksöz et al. 1979). It is likely, therefore, that the high field estimates of attenuation are produced by some degree of saturation.

The corresponding range of Q_β^{-1} reported from the laboratory for sandstone is 0.006 - 0.042. In contrast to the limestone determinations, those for sandstone are more commonly at the higher limit of the range. The physical characteristics of the rocks (porosity, grain size, cementation et cetera) may influence the position in this range but few experiments have reported such characteristics for the specimens. In a study of attenuation in sandstones Clark et al. (1980) give a range of Q_β^{-1} from 0.006 to 0.022 for samples varying in porosity from 5% to 22%; the attenuation increasing, in general, with porosity.

Field estimates of intrinsic attenuation for the Millstone Grit

The correlation between intrinsic velocity and attenuation is less obvious when the Hedgehog (velocity) and simplex (attenuation) solution regions are compared. This is due to the coarser distribution of Q_β^{-1} and shear wave velocity implied by these inversion results.

Inferring from the shear wave velocity - depth profiles that the limestone is 200 - 300 m thick we obtained field estimates of Q_β^{-1} for limestone which range from 0.004 to 0.04. Laboratory determinations of attenuation for limestones at normal values of pressure, saturation and temperature give a range of Q_β^{-1} from 0.002 to 0.022, predominantly at the lower values (Table 1.1). These ranges of attenuation overlap but in general the field estimates are higher than the laboratory determinations. Saturation conditions have been shown to affect the intrinsic attenuation greatly. For example, measurements in the laboratory on a fully saturated sample of limestone gave a Q_β^{-1} of 0.083 (Toksöz et al. 1979). It is likely, therefore, that the high field estimates of attenuation are produced by some degree of saturation.

The corresponding range of Q_β^{-1} reported from the laboratory for sandstone is 0.006 - 0.042. In contrast to the limestone determinations, those for sandstone are more commonly at the higher limit of the range. The physical characteristics of the rocks (porosity, grain size, cementation et cetera) may influence the position in this range but few experiments have reported such characteristics for the specimens. In a study of attenuation in sandstones Clark et al. (1980) give a range of Q_β^{-1} from 0.006 to 0.022 for samples varying in porosity from 5% to 22%; the attenuation increasing, in general, with porosity.

Field estimates of intrinsic attenuation for the Millstone Grit

facies provide a range of Q_β^{-1} from 0.01 to 0.03 which falls within the range of the laboratory determinations. The comparison of the Millstone Grit is not unreasonable considering the composition of the facies.

These comparisons pose certain difficulties. Firstly, the values for limestone show higher attenuation than the laboratory determinations, made under normal conditions of pressure and saturation, whilst estimates for the Milstone Grit lie within the reported experimental range. Secondly, there is little difference between the values of Q_β^{-1} for both the limestone and Millstone Grit. This contrasts with the higher attenuation reported for sandstone compared with limestones in laboratory experiments.

The increase in attenuation with depth given by Evans (1981) for provinces within Scotland contrasts with the inversions above. To explain his observations Evans (1981) infers an increase in saturation with depth. The decrease in Q_β^{-1} with depth over the Derbyshire Dome and adjacent areas would be consistent with a frictional mechanism of dissipation (Born 1941; and others) in which cracks within the rocks close in response to the increase in pressure with depth. This mechanism has been challenged, however, for rocks at low pressures and strains (Winkler 1979).

Velocity is less sensitive to changes in physical conditions than attenuation (Toksöz et al. 1979) and may be used as a diagnostic of rock types. The correlation demonstrated between velocity and attenuation implies, therefore, that part of the attenuation is caused by the petrographic characteristics of the different lithologies. If the dissipation was caused predominantly by a mechanism pertaining to physical conditions, for example saturation, then the estimated attenuation-depth profiles would exhibit a reduced correlation with

the shear wave velocity distribution with depth.

The observed Rayleigh wave attenuation could be produced by scattering or mode conversions at velocity boundaries. Whilst this is believed to be a mechanism for high frequency compressional waves at near vertical incidence (O'Doherty & Anstey 1971) a similar effect for surface waves travelling horizontally is less likely. Further, scattering will only be of significance if the scatterer has dimensions of the order of a wavelength. The surface waves under consideration have wavelengths varying from 0.4 - 3.0 km which indicates that scattering would only occur at the higher frequencies where the wavelengths are similar to the size of the velocity discontinuities. Only in the Millstone Grit district and at the southern end of line LST 2 does the variation in topography approach dimensions similar to the shortest wavelength. Scattering, whether from velocity discontinuities or topography, is, therefore, unlikely to effect the observations of $Q_\gamma^{-1}(\nu)$ and subsequent inversions for $Q_\beta^{-1}(z)$ severely.

A frequency dependence determined previously by a least squares fit to the observed attenuation data (section 3.4) was also included in the linear inversion for $Q_\beta^{-1}(z)$. Consequently, an improved fit between the observed $Q_\gamma^{-1}(\nu)$ and those calculated from the obtained inversion models was achieved only for the provinces LST 1N and LST 1S. The resulting $Q_\beta^{-1}(z)$ models defined similar distributions of intrinsic attenuation with depth to the frequency independent results but with changes in the absolute values of Q_β^{-1} in each layer. Very high unrealistic estimates of Q_β^{-1} were returned for LST 1S when a frequency dependent intrinsic attenuation was assumed. In contrast, the inversion for LST 1N gave low values of Q_β^{-1} around 0.001 - 0.007 which whilst not being unrealistic would usually be expected for

estimates of Q_β^{-1} in the upper mantle (Mitchell 1976, Burton 1977, Nakanishi 1981).

Mavko & Nur (1979) have shown that fluid flow in parallel walled cracks theoretically would produce frequency dependent dissipation having an exponent which depended on the fluid flow regime and frequency. At low frequencies the attenuation is proportional to frequency; similar to the frequency dependence of Q^{-1} in liquids. For higher frequencies up to a critical value inertial flow dominates to give a dependence of $\nu^{3/2}$. Above this critical frequency whilst maintaining inertial flow the fluid becomes compressible resulting in a frequency dependence proportional to $\nu^{-3/2}$. The frequency dependence of Q_β^{-1} in LST 1N and LST 1S has been calculated as $\nu^{1.681}$ and $\nu^{-1.127}$ respectively and thus are not too dissimilar to those proposed by Mavko & Nur (1979).

It is unreasonable to infer from the frequency dependence a fluid flow mechanism of dissipation in LST 1S because the returned estimates of Q_β^{-1} at 0.2 are unrealistically high and the frequency dependence would imply that the fluid was compressible, a condition not encountered normally in geophysical situations. Similar strictures need not be placed on the results for LST 1N indicating that a fluid flow mechanism of dissipation may exist in this province. Such a mechanism would be consistent with the decrease in attenuation with depth determined by the inversions. An increase in pressure with depth would force the closure of cracks thereby inhibiting any fluid flow. Alternatively, fully saturated conditions would reduce the possible physical movement of fluid within or between cracks. If the latter is the case then a second mechanism, possibly thermal relaxation (Kjartansson & Denlinger 1977), may be dominant.

Whilst the intrinsic attenuation may be frequency dependent the

existence of such a dependence cannot be confirmed by these present data. Further, the implication from the invarient trends of the attenuation with depth is that only the absolute values of Q_β^{-1} are altered and that the true frequency dependence is indeterminate.

We have stated that partial saturation of the limestone could explain the high values of Q_β^{-1} in the limestone when compared to laboratory determinations. Also, evidence from the possible frequency dependence of the intrinsic attenuation of the limestone profiles would support partial saturation in the upper layers of the models. The water-table over the Derbyshire Dome is known to be at depths of about 200 m below the surface (Cox & Bridge 1977) showing the upper layers are partially saturated.

No evidence for frequency dependent intrinsic attenuation, and hence for a fluid flow mechanism of dissipation, has been found in the Millstone Grit. The sequence of sandstones and shales in the Millstone Grit produces a number of perched water-tables within the sandstones (Stevenson & Gaunt 1971). The district also has significant amounts of surface water. It is expected, therefore, that the Millstone Grit is fully saturated near the surface hence inhibiting dissipation by fluid flow implying that the intrinsic attenuation is related to the physical characteristics of the rocks.

These estimates of intrinsic attenuation for the limestone and the Millstone Grit show that the mechanism of dissipation in the shallow upper crust consists of two components which act together. The first component is produced by the physical characteristics of the different lithologies and the second caused by the degree of saturation and fluid flow. This conclusion about the mechanism of dissipation is equivalent to the 'jostling' and 'sloshing' mechanisms recognised in the laboratory by Wyllie *et al.* (1962).

To summarise, we have demonstrated a simple correlation between shear wave velocity and attenuation with high velocities corresponding to low values of Q_β^{-1} implying that physical characteristics of the rock types affect the attenuation. Laboratory determinations of Q_β^{-1} were comparable directly with the field estimates for the Millstone Grit facies. For the limestone, however, correspondence occurred only when laboratory results from specimens under high degrees of saturation were compared with the field estimates. It is difficult to use Q_β^{-1} as a diagnostic of lithology based on laboratory determinations. The attenuation, however, may be indicative of the physical state of the area of investigation for which the laboratory experiments provide a useful guide. Evidence for frequency dependent intrinsic attenuation over the limestone district supports a mechanism of dissipation based on fluid flow within cracks as does the overall decrease in attenuation with depth associated possibly with a corresponding decrease in the number of cracks and an increase in the degree of saturation. The intrinsic attenuation estimates for the limestone district imply partially saturated conditions in the upper layers. Over the Millstone Grit district fully saturated conditions are inferred from the estimates of attenuation. The overall intrinsic attenuation estimated within the shallow upper crust of the Derbyshire Dome and adjacent areas are believed to be produced by the combination of two mechanisms of dissipation; one of which involves the physical characteristics of the rock and the second which depends on the flow of fluids between cracks and hence on the degree of saturation.

CHAPTER SIX

CONCLUSIONS

6.1 THE PROJECT - a résumé.

This project has been an investigation into the anelastic properties of the shallow upper crust of the Derbyshire Dome and adjacent areas of central England. Its aim was to determine the distribution of shear wave velocity and intrinsic shear wave attenuation with depth thereby providing a more complete description of wave propagation within the region when considered together with the compressional wave velocity structures of previous seismic refraction studies. To achieve this aim reliable estimates of the group slowness dispersion and specific attenuation factor for fundamental mode Rayleigh waves had to be obtained. This necessitated the recording of high frequency, 0.5 - 5 Hz, Rayleigh waves generated by quarry blasts within the area. The study area was chosen to enable a comparison of the anelasticity within the Carboniferous Limestone outcrop forming the Derbyshire Dome with that in the Millstone Grit of the adjacent areas. It was also hoped to elucidate further the deep geology of the region.

The project divided conveniently into four separate phases: The design and implementation of field experiments to obtain suitable data, the preparation of the data with preliminary time domain observations, frequency domain analysis to obtain estimates of group slowness dispersion and $Q_\gamma^{-1}(\nu)$ and finally, the inversion of these data to determine the shear wave velocity and specific attenuation

factor structures with appropriate interpretation where possible.

The design of the field experiments was based around certain quarries within the limestone district which were known to blast regularly with large amounts of explosives. Quarry blasts form a convenient and repeatable source of seismic energy and have been utilised on a number of previous occasions. The effect of azimuthal variations in amplitude produced by the source was reduced by placing the seismometers in lines, of up to 30 km length, radiating from the principal quarry at Tunstead. Individual seismometer sites were chosen by considering the amount of equipment, the required station separation of about 2.5 km, the accessibility of the locations and the line-of-sight between the transmitting and recording stations. A few sites were also to be equipped with three component seismometer sets. Where possible the stations were to be restricted to discrete geologic provinces. A detailed study of the local topography and geology was required, therefore, to enable the selection of the sites.

To record the Rayleigh waves to their best advantage the characteristics of the instrumentation had to be considered. To obtain unclipped signals of optimum amplitude the gains of the amplifier-modulators increased with distance from the source according to a relation determined empirically from existing seismic refraction data. Hence, the experiments used 'gain-ranging' down the seismometer lines. To improve the recorded bandwidth and signal-to-noise ratio at low frequencies the period of the seismometers was extended from the usual setting of 1 s to 1.5 s. Careful calibration in the laboratory and later in the field was, therefore, necessitated.

Each site was prepared carefully to reduce the effect of noise

and poor coupling with the ground on the recorded amplitudes. The quality of the recorded data was monitored weekly during the experiments, which lasted six to eight weeks, to achieve the maximum return of data. During the field work, quarries were visited at the time of blasts to obtain accurate source locations and origin times.

To facilitate computer analysis the data were digitised at 50 Sps. The sampling rate was later halved to 25 Sps to reduce computational effort giving a Nyquist frequency of 12.5 Hz. During this phase of data preparation the magnitude of systematic errors in timing and amplitude was assessed and a correction applied when necessary. The parameters required to specify the instrument impulse response were also determined from the calibration pulses recorded whilst in the field.

Examination of complete suites of seismograms for individual events proved an invaluable aid to later frequency domain analysis and produced some results of geological and geophysical significance. Simple measurements of group velocity were made from the seismic sections produced for the individual lines. Estimates of phase velocity and azimuth of propagation were made using data from the small, two dimensional cluster array deployed in the Millstone Grit district to the north east of the Derbyshire Dome.

The data were analysed in the frequency domain using the techniques of Evans (1981) which were high frequency modifications of earlier methods. The signal was transformed into the frequency domain using the Fast Fourier Transform (Cooley & Tukey 1965) and the instrument transfer function removed by division of the relevant complex spectra. Group velocity as a function of frequency was determined through the application of the multiple filter technique

of Dziewonski et al. (1969). These operations were all achieved by a version of the Time Series Analysis Programme (Burton & Blamey 1972) modified by Evans (1981). The instaneous amplitudes of the envelope of each narrow bandpass filtered seismogram are used to form one column of an energy matrix the co-ordinates of which are frequency and velocity (time). By contouring this matrix the Rayleigh wave dispersion curve is displayed as a ridge of high energy which could be followed by a search algorithm (Evans 1981). Visual inspection of the energy matrix of instantaneous amplitude arrivals was required, for the data presented above, because of noise and the small separation in time between different phases characteristic of local recordings of small seismic events.

Having determined the group velocity at each station for all events the signals were revised by time windowing the seismogram more accurately about the Rayleigh wave using the dispersion curves as a guide. The spectral amplitudes of ground motion were then calculated for these revised signals by the FFT.

The repeatability of the source enables multiple recordings to be made over essentially the same propagation path between a given quarry and station. The best estimate of group slowness dispersion for the individual source-station pairs was obtained by a simple average over the number of events recorded at that station. To determine the observed Rayleigh wave group slowness dispersion and specific attenuation factor characteristic of each province identified by the time domain analysis an interstation procedure was used. The averaged group slownesses were converted to arrival times and plotted against distance for each frequency. The slopes of the least squares fit to these data giving the true slowness dispersion of each province. A similar technique was used to

determine Q_γ^{-1} by plotting amplitude against distance but this time for the individual events because of the different absolute amplitudes produced by each shot. The gradients, which are unaffected by the various dc levels, were later averaged to give statistically the best estimate of $Q_\gamma^{-1}(\nu)$ in each province.

The final phase was the inversion of the observed data to determine the shear wave velocity and intrinsic attenuation structure in the region. In both cases a solution to the forward problem was required to calculate theoretical values of group slowness dispersion and $Q_\gamma^{-1}(\nu)$ for a layered model.

Given a shear wave velocity-depth model the theoretical fundamental mode Rayleigh wave group slowness dispersion was calculated using Knopoff's (1964b) method through the application of a routine given by Schwab & Knopoff (1972). The compressional wave velocity was constrained by assuming a Poisson's ratio of 0.28 while the density was given by the empirical Nafe & Drake (1965) relation.

Theoretical $Q_\gamma^{-1}(\nu)$ were calculated using the theory given by Burton (1973), after Anderson & Archambeau (1964), for a $Q_\beta^{-1}(z)$ model. The compressional wave specific attenuation factor was constrained by assuming that no dissipation was associated with the bulk modulus (Burton & Kennet 1972).

Shear wave velocity-depth profiles were obtained by application of two inversion techniques. The linearised method calculates small corrections which must be applied to a starting model of shear wave velocity to improve the fit between the observed and theoretical dispersion calculated from the resulting model. By repeated correction of the model the best fit to the data can be found. This scheme is based on the determination of the inverse of non-square matrices using singular value decomposition (Lanczos 1961)

controlling the stability of the calculation by employing a smoothing parameter (Levenberg 1944, Marquardt 1963). Results from this iterative method may depend on the chosen starting model. Choice of starting models was guided by the initial time domain interpretation of seismograms and by the frequency domain observations of Rayleigh wave group slowness. The final solution was accepted on the basis of the fit to the observed data, the overall resolution and the standard deviations about the solution $\beta(z)$.

The second scheme employed, the Hedgehog inversion of Keilis-Borok & Yanovskaja (1967), is an improvement on trial-and-error forward modelling and defines the bounds within parameter space in which acceptable models are found. A Monte-Carlo random search in continuous parameter space is used to find a model which satisfies the acceptance criteria defined in the inversion scheme. The search then moves onto a discrete network of models which span the parameter space. In this manner a region of acceptable models is constructed without recourse to an initial starting model although it is confined to search within a finite region of parameter space.

A matrix method, similar to that given above, was utilised during the inversion of the observed Rayleigh wave specific attenuation factor data. The forward problem to obtain Q_γ^{-1} from the distribution of intrinsic Q_β^{-1} is immediately linear allowing the shear wave attenuation structure implied by the observed $Q_\gamma^{-1}(\nu)$ to be calculated in a single step and does not require a starting model of $Q_\beta^{-1}(z)$.

The bounds on acceptable models of $Q_\beta^{-1}(z)$ were determined by a linear programming technique (Garvin 1960) which is analogous to the

Hedgehog technique used for velocity.

The distributions of shear wave velocity and intrinsic attenuation with depth resulting from these inversions were then interpreted to provide models for the deep geology of the region, complementing previous seismic refraction work. Possible mechanisms of dissipation and physical conditions within the shallow upper crust were also discussed.

A summary of the results obtained at all phases of this project, along with some further tentative conclusions, is presented in the following section.

6.2 SUMMARY of RESULTS.

Careful planning and execution of the field experiments resulted in a high return of data. The deployment of extended period (1.5 s) seismometers was beneficial to this project with an improved signal-to-noise ratio being achieved for the lower frequency phases in the seismogram compared to the records from the usual short period (1 s) seismometers. Standardisation of the network by calibration and correct choice of amplifier-modulator gains to 'gain-range' down the seismometer lines assisted further in the data return.

Systematic errors could have been introduced during the data collection and preparation. The sources of such possible error were examined and shown to be negligible in most cases. To reduce timing errors caused by the mis-alignment of the record/replay magnetic heads, however, a correction had to be made to the start time of individual digital records. This implies that for any observational

project, and especially for higher frequency studies, the mis-alignment of the heads must be considered.

The existence of the fundamental mode Rayleigh wave in signals recorded from quarry blasts was confirmed by the use of particle motion plots. The individual records showed that the signal was repeatable provided that the shot was at approximately the same location within the quarry. The type of signal recorded depended on the position of the events in the quarry or the orientation of the quarry face to the line of instruments. Further, certain quarries were demonstrated to be more efficient at generating Rayleigh waves than others.

The reduced travel time sections showed that the limestone district had to be divided into smaller provinces with boundaries indicated by changes in the character and the velocity of the signal. The division between these provinces correlated directly with mapped geological features (Geological Survey 1:50 000 Sheet No. 111); the Bonsall Fault zone crossing the line LST 1 and the limestone/Millstone Grit boundary at the southern end of line LST 2. High frequency Rayleigh waves must be considered, therefore, to be sensitive indicators of changes in geological structure. No evidence of dramatic changes in structure produced by faulting was given for the Millstone Grit district to the north of the Derbyshire Dome. This is compatible with the geological mapping which shows little surface faulting over most of the line MG 1 (Geological Survey 1:50 000 Sheet No. 99).

Approximate group velocities were measured from the seismic sections. To the north of the Bonsall Fault zone a group velocity of 1.7 km s^{-1} obtains at 0.5 s period whilst to the south a higher velocity of 2.5 km s^{-1} for a period of 0.6 s is determined. For

the shorter line, LST 2, the corresponding velocities are 2.6 km s^{-1} in the limestone and 1.1 km s^{-1} having crossed the boundary into the Millstone Grit. Low values of group velocity are determined similarly for the Millstone Grit district with a value of 1.6 km s^{-1} at 1 s period along MG 1.

The assumption of circular wave fronts centred on the shot yielded a group velocity of 1.2 km s^{-1} over the cluster array. A higher phase velocity of 1.65 km s^{-1} was obtained when individual peaks were correlated. A better fit to the data was achieved when the restriction of centred, circular wave fronts was removed and an iterative technique used to solve for phase velocity and azimuth. This technique yielded a phase velocity of 1.5 km s^{-1} and implied an 11° refraction to the south of the direct source to station azimuth. The most likely cause of this refraction is the boundary between the limestone and Millstone Grit near Stoney Middleton (GR 42360 37510, Geological Survey 1:50 000 Sheet No. 99). These time domain observations are summarised in Figure 6.1.

Only seismograms showing clear Rayleigh wave packets were analysed using the frequency domain processing techniques. A total of 55 seismograms were analysed over the limestone district from Brier Low Quarry. More records were available over the Millstone Grit district with 98 seismograms from Tunstead Quarry being considered.

The amplitude spectra along the line LST 1 showed peak frequencies and bandwidths which decreased with distance as a direct consequence of dissipation. This dependence of amplitude with distance was not, however, exhibited along line LST 2 because of instrumental or local site effects.

The bandwidth of signals recorded in the Millstone Grit district (0.6-3.1 Hz) was narrower than for the limestone district

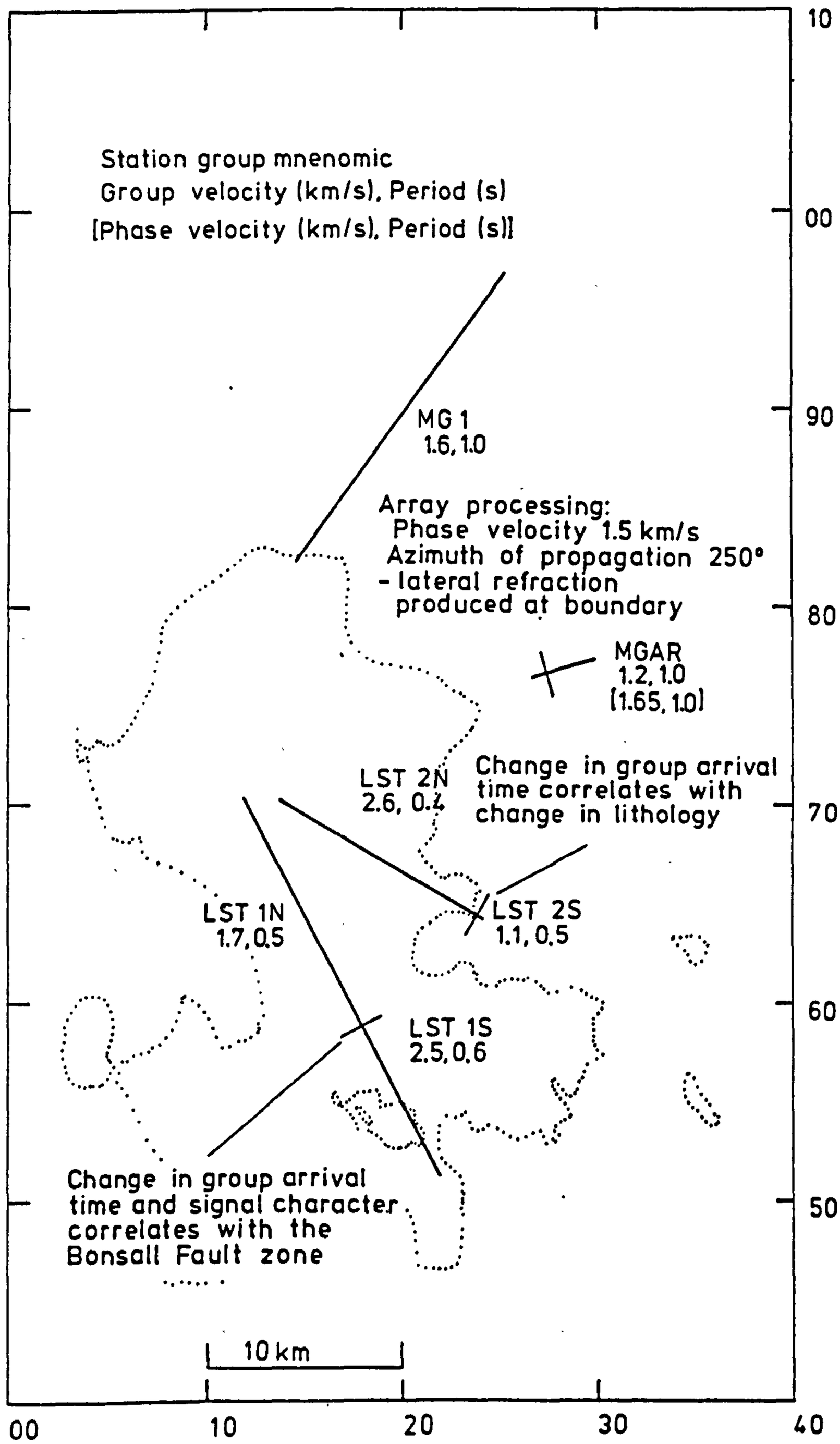

Figure 6.1 Summary of time domain observations.

(0.6-4.3 Hz). The frequency of the maximum amplitude did not change with distance although the amplitude of the spectral peak did decay with distance. These differences in the way the amplitude spectra vary with distance indicate that the two geological districts have different medium responses.

Values of group slowness and Q_γ^{-1} are given in Figure 6.2 as a summary of the results listed in Appendix B. Group slowness varies from 0.33 s km^{-1} to 0.56 s km^{-1} over the limestone and between 0.67 - 0.77 s km^{-1} within the Millstone Grit. In general, the slowness increases with frequency. Estimates of $Q_\gamma^{-1}(\nu)$ range from 0.01 to 0.08 in the limestone district and between 0.01 to 0.02 for the Millstone Grit.

Estimates of $Q_\gamma^{-1}(\nu)$ were made for five of the available slowness data sets, rather than the entire nine, because of inconsistent amplitude variations along the line LST 2. The frequency bandwidth of each of these data sets was smaller than that of the corresponding Rayleigh wave group slowness dispersion data set due to the effect of noise or lack of measurable amplitude decay with distance.

The values of group slowness were higher in the Millstone Grit than the limestone indicating that slowness is a characteristic of individual lithologies. In contrast, the specific attenuation factor for Rayleigh waves exhibits no such correlation with lithology. The dissipation must be produced by factors other than the physical characteristics of the rock types.

The iterative array processing technique can be modified to use frequency domain results of group slowness to give the variation in azimuth of propagation over the array. The low frequency phases showed a maximum deviation of 18° to the south of the direct

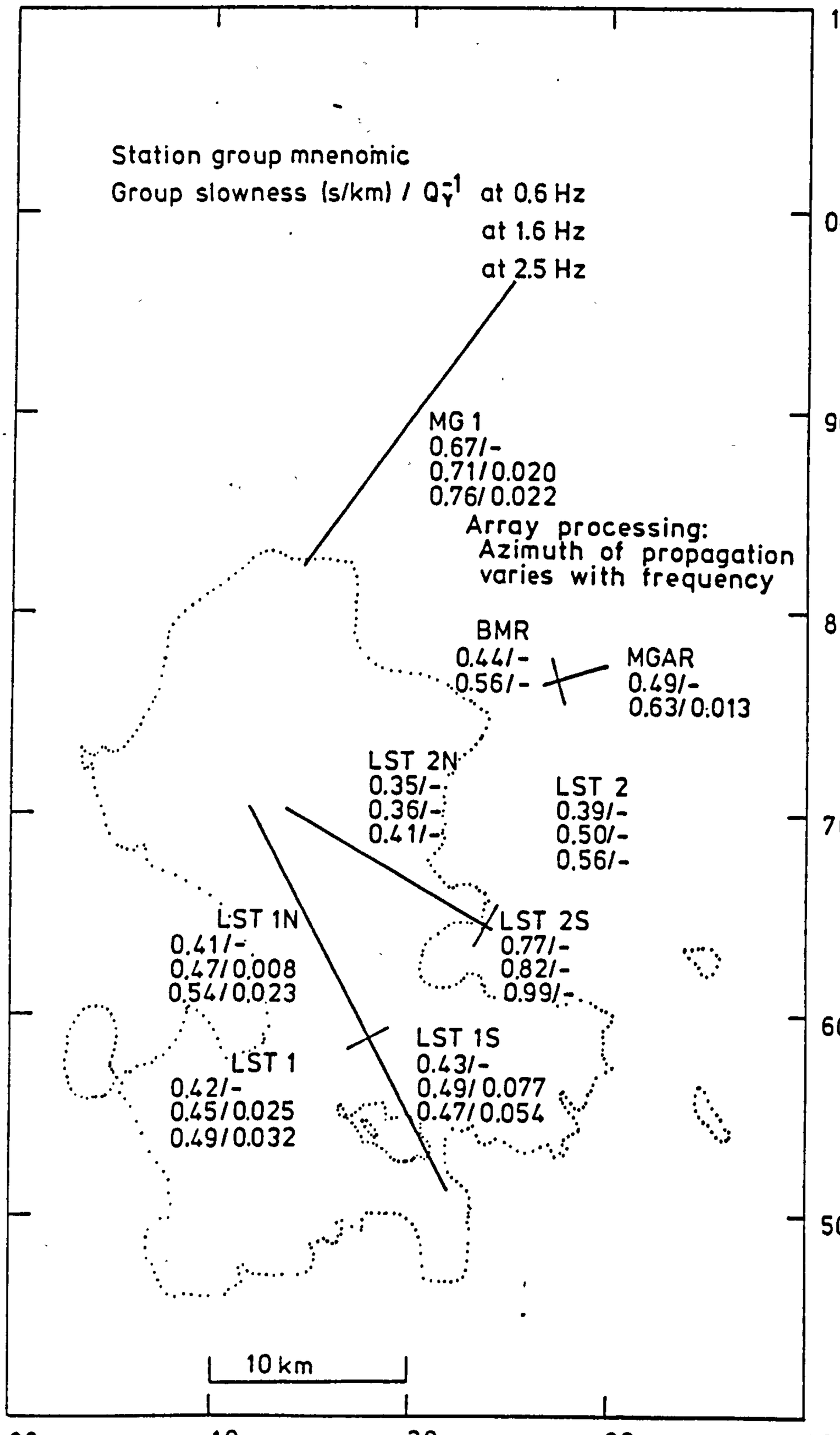

Figure 6.2 Summary of the results of the frequency domain analysis.

source-station azimuth. The higher frequencies showed little evidence of any lateral refraction. The structure which produces this frequency dependent refraction may be a wedge of Millstone Grit overlying a steeply dipping layer of Carboniferous Limestone which has a higher wave velocity.

The shear wave velocity and intrinsic attenuation distributions with depth obtained by inversion techniques given in chapters 4 and 5 are summarised in Figure 6.3. In general, the velocity decreases with depth below an initial increase to a maximum between the depths of 0.6 km and 1.2 km. The shear wave velocities tend to be lower than those calculated from the compressional wave velocities determined by seismic refraction studies (Bamford *et al.* 1978, Whitcombe & Maguire 1981, Rogers 1983). For compatibility these data may require that Poisson's ratio is higher than the 0.28 assumed, perhaps being 0.3.

The velocity-depth profiles were used to infer the deep geology of the region. The Bonsall Fault zone which separates the two provinces is believed to be the younger, surface manifestation of a basement fault. To the north the limestones are thought to be underlain by Ordovician mudstones and, at deeper levels, sediments of Cambrian age. To the south of the fault zone a different sequence is proposed with the limestones being underlain directly by Devonian sandstones. The Ordovician is again inferred at depth and implies that the basement fault down throws to the south contrary to the sense of motion at the surface. This interpretation differs from that of Rogers (1983) but is not inconsistent with the observations of Bamford *et al.* (1978) and Whitcombe & Maguire (1981). The interpretation of the profile to the north of the Dome is that of a deep sedimentary basin with a thickness of at least

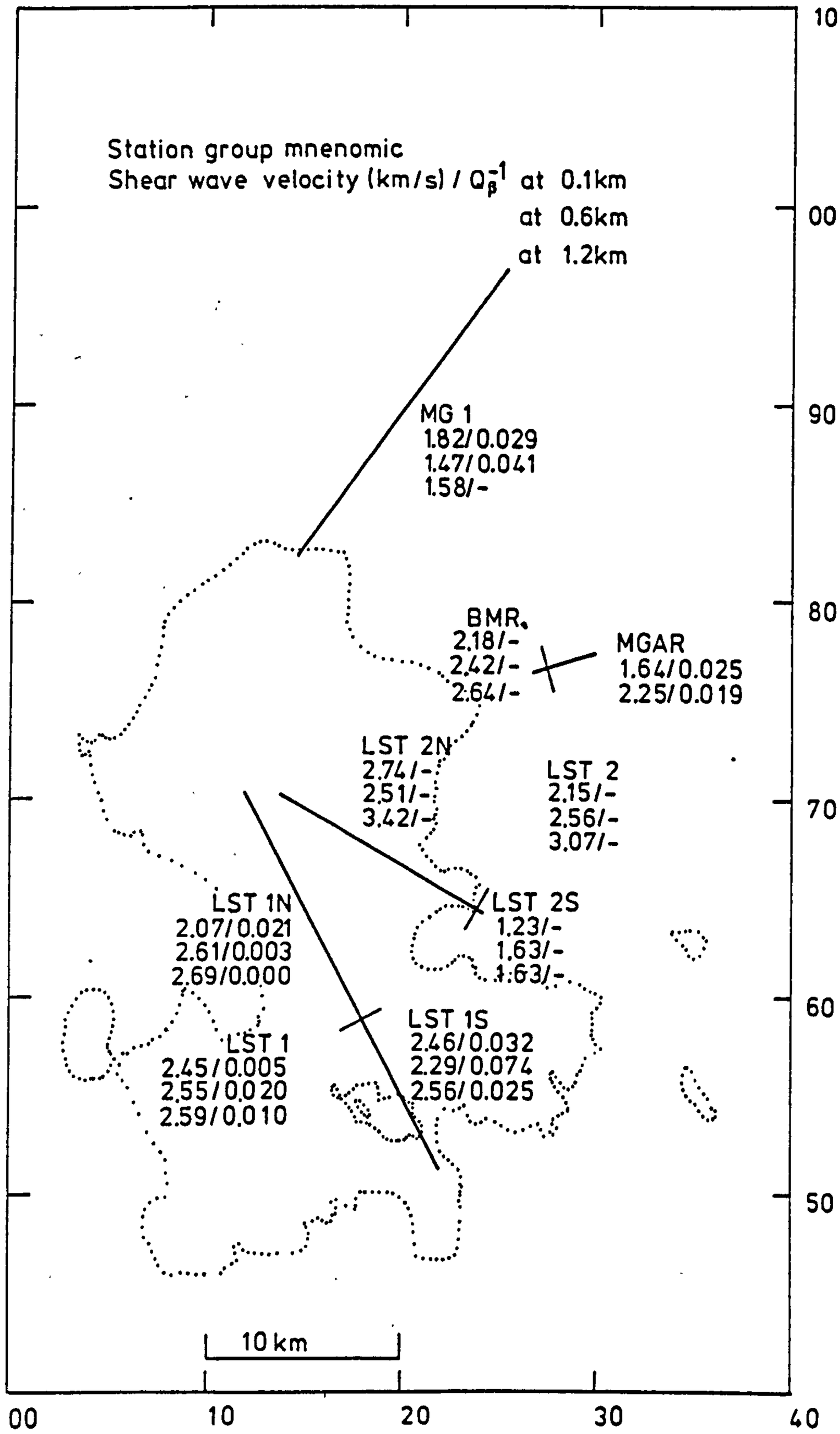

Figure 6.3 Summary of the results from the inversion techniques.

1.6 km. The Millstone Grit is assumed, but not shown, to be underlain by the Carboniferous Limestone.

Overall Q_β^{-1} found here tends to decrease with depth corresponding to the general increase in Q_γ^{-1} with frequency whereas Evans (1981) found that attenuation usually increased with depth in Scotland. As with the observed Q_γ^{-1}, the absolute values of intrinsic shear wave attenuation presented show no marked difference between each geologic province. Within each province separately, there exists, however, a clear association between the shear wave velocity and attenuation with high Q_β^{-1} corresponding to low velocities and vice versa.

Estimates of Q_β^{-1} for the Millstone Grit compare well with laboratory determinations of attenuation in sandstone under normal conditions of saturation. In contrast, the attenuation in the limestone only corresponded to the laboratory results for samples at higher degrees of saturation.

The intrinsic shear wave attenuation was assumed to be independent of frequency. Mitchell (1980), however, has indicated that Q_β^{-1} may have a frequency dependence of the form $\nu^{-0.5}$ above a frequency of 1 Hz in the upper crust. For a half-space this would produce a Q_γ^{-1} which varied as $\nu^{-0.5}$. A least squares procedure was used to fit curves of the form $\nu^{-\eta}$ to the observed Rayleigh wave data to yield values of η which ranges from -1.681 to 1.127 considerably different to Mitchell's (1980) values. Only the estimates of η for LST 1N and LST 1S were significant statistically and were the only provinces which resulted in an improved fit between the observed $Q_\gamma^{-1}(\nu)$ and those calculated from the $Q_\beta^{-1}(z)$ models obtained by assuming a frequency dependent inversion. The

resulting $Q_\beta^{-1}(z)$ profiles showed distinct changes in the absolute values compared to the frequency independent results with the estimates of $Q_\beta^{-1}(z)$ for LST 1S being unrealistically high. No change in the overall trend of the $Q_\beta^{-1}(z)$ models was shown. These data, however, cannot confirm that the intrinsic attenuation is frequency dependent.

The calculated frequency dependences for the two limestone provinces are similar to those proposed on theoretical grounds for dissipation produced by fluid flow in partially filled cracks by Mavko & Nur (1979). A fluid flow mechanism may, therefore, exist in LST 1N but a similar inference for LST 1S is unreasonable because the estimates of Q_β^{-1} are unrealistically high and the calculated frequency dependence would require the fluid to be compressible. Dissipation at least over part of the Derbyshire Dome is thought, therefore, to be caused not only by the nature of the rock but also the prevailing conditions of partial saturation. The decrease in intrinsic attenuation with depth is consistent with a fluid flow mechanism of dissipation. The increase in pressure with depth may force cracks to close, thus reducing the dissipation, or the rocks may become fully saturated which inhibits flow within the cracks. In the Millstone Grit district no significant frequency dependence could be determined, implying that the district may be fully saturated, with the mechanism of dissipation being more dependent on the petrographic characteristics of the rocks.

6.3 SUGGESTED FURTHER WORK and CONCLUDING COMMENTS.

The results summarised above form the major conclusions of this thesis. They should not be viewed as disparate observations. They are a necessary part of the seismologic description of the region and as such help to provide a complete geophysical and geological understanding of the Derbyshire Dome and adjacent areas. This understanding could be improved by further work on the existing data and by the development of refined techniques of data acquisition and processing.

Further analysis of the data presented above to obtain estimates of phase slowness might help to improve the shear wave velocity-depth profiles, and hence the inferred geologic structure, by removing a degree of non-uniqueness from the velocity inversions (Knopoff 1972). The cross multiplication technique (Bloch & Hales 1968) to obtain phase velocity or slowness has been used previously by Stuart (1978) for the North Sea and in the study of the upper crust of Scotland by Evans (1981). The direct relation between phase slowness dispersion and shear wave velocity structure would permit a more accurate initial model to be used in the linearised inversion technique for shear wave velocity.

From a close examination of the data it should also be able to obtain direct measurements of shear wave velocity. The three component recordings would be of most use here. It would then be possible with the estimates of compressional wave velocity to determine the actual Poisson's ratio pertaining in the shallow upper crust of the region.

The restriction of the inversions to horizontral, plane layers could produce non-realistic geological models in an area of

significant structural variations. This situation could be improved in two ways. For co-linear events, an interstation technique, perhaps using the cross-correlation method of Keen et al. (1979), between different pairs of stations could provide a suite of dispersion curves each characteristic of a short path length. Inversion of these data in the usual manner would define a series of velocity distributions which could be considered to be essentially one dimensional. A more realistic structure could then be defined by correlating between the velocity-depth profiles. This method would also incorporate a check on the consistency of the dispersion data and subsequent inversions by utilising all the possible pairings of stations along the line.

The second method of improving the structural analysis would be to use approximate numerical techniques to determine the theoretical dispersion. The finite element method has been used by Lysmer & Drake (1972) to model the propagation of Love and Rayleigh waves over a zone of irregular structure between two semi-infinite, horizontally layered zones. An alternative numerical method, that of finite differences, may be used to produce synthetic seismograms and to model the development of the wave field with time (Boore 1972). This technique may also include models of elastic constants which are not plane layered. For example, propagation across welded quarter spaces may be considered to be analogous to propagation across a fault (Bond 1979).

To obtain reasonable models of the structure these methods require some control on the structure either from existing bore holes or previous seismic work. Without such control any inversion scheme based on the finite element or difference techniques would have an increased degree of non-uniqueness. The use of such

numerical methods may be restricted, therefore, to the refinement of existing models rather than preliminary inversions.

Within the data base generated during this project are events from quarries which were broad side on to the station lines. Analysis of the signals from these events would permit the three dimensional nature of the region to be investigated. Of particular interest would be events in Cauldon Quarry along paths from the south west of the Dome recorded by stations north and south of the Bonsall Fault zone. The existence of a basement block tilting to the north east could be examined by inverting data recorded from Stoney Middleton or Hope Quarries by the stations comprising line LST 2.

The data base also includes recordings of local earthquakes. Hartzell et al. (1978) have found that for a shallow earthquake, strong motion records at a distance of 35 km from the epicentre are comprised mainly of high frequency Rayleigh waves. Such signals are likely to have a higher signal-to-noise ratio at the low frequency limit of the signal bandwidth. The inversion of these data would, therefore, improve the resolution and enable the model to extend to deeper levels. Inversions yielding models to a depth of 17 km have been presented by MacBeth (1983) using first and second order higher mode Rayleigh wave data from a local earthquake in Scotland. The analysis and interpretation of such signals would provide invaluable information on the nature of the basement within the region.

Further work on the source function for quarry blasts would remove the azimuthal restriction on the source-station disposition with estimates of attenuation being made through the application of the single station techniques of MacBeth (1983). The areal distribution of Q_{β}^{-1} could be determined from these techniques when

applied to the broad side quarry records. The determination of the areal distribution of intrinsic attenuation in the upper crust has important implications for the study of seismic hazard within active seismic regions. In future work it may be possible to utilise an experiment of the kind described above to relate the intrinsic attenuation determined from instrumentally recorded Rayleigh wave attenuation with the observed attenuation of macroseismic intensity.

The suggestions for further work given above can use the existing recordings of high frequency Rayleigh waves in the region. It is possible, however, that this data base can be improved. The variation in the source demonstrated between quarry blasts could be reduced if single hole shots were used as a source of seismic energy. The overall frequency bandwidth may not be significantly different from that of quarry blasts (Willis 1963) but the radiation pattern should have limited azimuthal amplitude variations removing the azimuthal restriction on the source-station disposition. It may also be possible to reduce the effect of the source medium by placing the shot away from anomalous structures such as quarry faces.

The estimates of observed Rayleigh wave attenuation could be improved by reducing the effect of noise and site variations on the record. This could be best achieved by deploying a small cluster of seismometers at each station with the spacing of the individual instruments designed to record the Rayleigh waves preferentially. Some measurements of very high frequency Rayleigh wave dispersion have been made by Al-Husseini et al. (1981) using data collected during standard noise tests conducted prior to seismic reflection profiling. The signal-to-noise ratio would be improved by the correct summation of the individual signals. The effect of

variations in the coupling of the seismometers with the ground would also be reduced because of its random nature. Although absolute amplitudes of ground motion would not be returned estimates of $Q_\gamma^{-1}(\nu)$ could still be achieved using the amplitude-distance analysis described above provided that the same processing was applied to each station cluster.

This technique would require radical changes in the instrumentation used. Firstly, a great many more seismometers would be required necessitating improved recording techniques. Secondly, the response of the instruments would have to be stable and within very strict limits. These requirements imply that the standard methods and equipment of data acquisition used in industrial seismic prospecting, except for the sensor, would be more appropriate in shallow, upper crustal studies. In general, the industrial geophone has a high frequency response (greater than 5 Hz) and so to obtain the desired frequency bandwidth alternative transducers would be required. It would be an advantage, however, if the robust characteristics of a geophone could be retained.

The geological interpretations of the velocity-depth profiles were speculative being based on variations of geophysical parameters with depth together with a knowledge of the regional geology. The definitive geologic structure can only be obtained through the use of deep bore holes but is limited to the depth and density of boring. The geophysical observations, however, identify a number of critical locations which could yield significant geological results. A total of four bore holes would be required each to a depth of 2 km. The cost of the proposed drilling programme would be very high. The important bore holes would be in the limestone provinces to the north and south of the Bonsall Fault zone and used

to examine the nature of the basement and the extent of the inferred Devonian sandstones in the southern province. The third bore hole would be placed on the eastern side of the Derbyshire Dome to sample the structure of that province and help elucidate the reasons for the unrealistic models returned by inversions over the line LST 2. The fourth, and least significant bore hole, would be sited in the Millstone Grit district to the north of the Dome with the purpose of determining the thickness of the proposed sedimentary basin.

This chapter has been a review of the project together with a summary of the results obtained. Some problems in data acquisition and processing have been identified and suggestions for further work to improve the results are given.

In conclusion, the declared aim of determining the anelastic structure of the shallow, upper crust of the field work area has been achieved. The large, high quality data base acquired during this project forms an excellent basis for further studies on the nature of anelasticity in the upper crust. The presented estimates of group slowness and $Q_\gamma^{-1}(\nu)$ are reliable measures of the high frequency Rayleigh wave dispersion and attenuation over the region. The subsequent inversions to give the shear wave velocity and intrinsic shear wave attenuation structures with depth complement earlier work and provide an improved geophysical and geological understanding of the Derbyshire Dome and adjacent areas.

APPENDIX A

INSTRUMENTAL CONSIDERATIONS

A.1 THE EFFECT of the INSTRUMENT on the RECORD.

The effect of the instrument is to magnify the amplitude of and introduce a phase shift in the true ground motion signal prior to recording. These instrumental effects are similar to those of a filter. Only in an instrument with a Dirac delta function for its impulse response would the recorded signal be a faithful reproduction of the ground motion. Unfortunately, such perfect instruments are not realisable physically.

In the time domain the recorded seismogram may be considered to be the convolution of the ground motion with the instrument impulse response. To extract the true ground motion signal the instrument response and the recorded seismogram must be deconvolved. In the frequency domain, however, the operation of instrument correction is greatly simplified. The spectrum of the recorded signal is formed by the product of the ground motion spectrum with the instrument transfer function. To obtain the ground motion spectrum, therefore, the spectrum of the recorded signal is divided by the instrument transfer function at each harmonic frequency of the spectrum. The instrument corrected seismogram may then be obtained by applying an inverse Fourier transformation to the corrected spectrum.

The reduction of the seismograms to true ground motion will standardise a network of disparate instruments provided that the responses of these instruments are known to sufficient accuracy.

Also, by performing this operation prior to the calculation of group velocity the dispersion curves resulting will have been corrected for the instrument group delay.

It is not always necessary to remove the instrument response from the records to obtain estimates of Rayleigh wave attenuation using the amplitude-distance analysis described above. All that is required in this case is that the response of each instrument within the network is the same. In this project, however, it was more convenient to standardise the network to true ground motion which necessitates the removal of the instrument transfer function from the spectra of the recorded seismograms.

A.2 INSTRUMENT RESPONSE.

The instruments used throughout this project consisted of Willmore Mk III seismometers, the output from which was recorded as frequency modulated, analogue signals.

All the instruments used to provide dispersion and attenuation estimates were Willmore Mk IIIa seismometers. Also deployed were three Willmore Mk IIIc force balance seismometers having a broad band response; these instruments will be discussed further in section A.4. Geophones of robust construction were used as shot timing transducers and are not considered further.

Within the frequency range of interest the response of the total system may be considered in two parts. First, the character of the Fourier spectrum is determined by the instrument and secondly, an overall gain factor is produced by the record/replay/digitiser system.

The Willmore Mk IIIa, an electro-mechanical instrument, uses feedback from the amplifier-modulator (amp-mod) to provide the necessary damping. The output voltage is proportional to the velocity of the mass with the governing equations given by Willmore (1960),

$$M\ddot{x} + D\dot{x} + Sx = M\ddot{X}, \qquad (a.1)$$

and

$$e = -K\dot{x}. \qquad (a.2)$$

Here M is the mass of the seismometer magnet (kg)

D is a damping constant (kg s^{-1})

S is the spring stiffness (kg s^{-1})

X is the ground displacement (m)

x is the displacement of magnet relative to frame (m)

K is the coupling factor (V m^{-1} s)

e is the output emf (V).

The Fourier transform of the solution of these equations for the displacement of a harmonic wave is

$$e(\omega) = \frac{j\omega^3 K}{(\omega_0^2 - \omega^2 + 2j\beta\omega\omega_0)} X, \qquad (a.3)$$

with $\omega_0^2 = S/M$

$\beta = D/2M$.

Both these quantities have a physical significance; ω_0 is the

natural period of the seismometer expressed as an angular frequency and β is the damping factor.

The digitised seismogram may be converted from digitiser units (d.u.) to output voltage from the seismometer using

$$A_d(\omega) = Ge(\omega), \qquad (a.4)$$

where $A_d(\omega)$ is the spectrum of the signal in d.u.

The system gain factor, G, is calculated from

$$G = \frac{5120}{V_{af}V_{df}}, \qquad (a.5)$$

where V_{af} is emf from amp-mod required to give full scale deflection (5 V) on replay

V_{df} is emf from replay system required to give full scale deflection (1024 d.u.) from the digitiser.

The parameters V_{af}, V_{df} depend on the gain switch setting of the amp-mod and digitiser respectively.

Combining (a.3) and (a.4) we obtain the displacement spectrum of ground motion

$$X(\omega) = \frac{A_d(\omega)}{GK}\left[\frac{j\omega^3}{(\omega_0^2 - \omega^2 + 2j\beta\omega\omega_0)}\right]^{-1}. \qquad (a.6)$$

The gain switch settings together with the instrument period and damping formed part of the information contained in the header block of each digital seismogram. The instrument response was calculated and corrected for by subroutines in TSAP with V_{af}, V_{df}

being found from look-up tables using the relevant gain switch setting.

There is a further part of the response of the record/replay system which takes effect at higher frequencies. The replay system introduces an amplitude decay which rolls off at a rate of 24 dB/octave above a cut off frequency which depends on the speed up factor between record and replay speeds. For the recording speed of 15/320 inches per second used throughout this project the cut off frequency is 16 Hz. This frequency is sufficiently above the maximum frequency contained in the signal that this additional response may be ignored.

A.3 CALIBRATION.

Calibration of the instruments serves a number of useful purposes. Initially, the instrument parameters may be set within given limits about nominal values in order to standardise the responses as much as possible. This procedure, conducted in the laboratory, will also highlight any faults in the instruments which may then be rectified. Secondly, the variation in response may be monitored by calibration, without alteration of the instrument parameters, at times throughout the experiment.

Calibration following transportation to the field area will indicate whether any instruments have drifted out of calibration. This change from the nominal parameter values may have been caused by incorrect handling and this calibration will permit the instruments to be repaired and reset prior to deployment in the field.

The Willmore Mk III seismometer relies on precision mechanical components for suspension and it is the setting of these elements which govern the period of the instrument. Such a system may undergo small physical changes which will, therefore, manifest themselves as an alteration of the natural period.

Creep within the springs can account for most of this variation but more discontinuous changes can be caused by a lack of sufficient care in handling the instruments. The diurnal temperature variation can also produce variations in response and should be compensated for either during construction or by controlling the range of the temperature variation.

The damping of the Willmore Mk III, in the mode used in this study, is provided by feedback from the amp-mod to an auxiliary coil, the resulting magnetic field from which opposes the motion of the magnetic mass. Because the damping is produced electronically it is thought that it will be more stable and less affected by external conditions than the period.

A second auxiliary coil in the Willmore Mk III provides a method by which the seismometer may be calibrated. Motion in the magnet may be induced by passing a current into this coil and monitoring the resultant output from the main coil in the usual manner.

The period may be set by introducing a sinusoidal current at the period required to be the natural period of the instrument. Adjustments to the suspension will bring the output from the main coil to 180° out of phase with the driving current. This occurs at resonance and the period is then set as required.

The damping may be set by adjustments to the output voltage of the feedback loop. An alternative method is to introduce a step in

current and then monitor the output curve. This method is employed by a micro-processor analyser (Houliston et al. 1982) and was used to set the damping of each instrument in the laboratory.

In the field calibration was achieved by introducing a step in current and recording the output on tape as usual to permit later analysis. For stations of the limestone district the field capabilities of the analyser were tested by using it to introduce the required step. For the later experiments a smaller device was used to inject the step in current.

For both surface wave experiments the recorded pulses were digitised at 100 Sps and analysed to given the period and damping. The inversion scheme used was a modified version of the programme given in Appendix 2 of Houliston et al. (1982). The correlation co-efficient

$$F = \frac{\Sigma(o_i - \bar{o})\ (c_i - \bar{c})}{(\Sigma(o_i - \bar{o})^2\ \Sigma(c_i - \bar{c})^2)^{\frac{1}{2}}}\ , \qquad (a.7)$$

is minimised where o_i is the i^{th} observation, and c_i the i^{th} value of the calculated calibration pulse and bars denote means. This obtains the best fitting shape between a model and the observations. This scheme eliminates the need to determine dc shift or gain terms. The standard minimisation procedure employed (Gill & Murray 1972) is contained in routine E04CGF of the NAG programme library (NAG 1980) and, provides the damping and natural frequency of the seismometer.

The resolution of the inversion programme has been investigated using a pulse calculated from the theoretical transfer function for

a number of period and damping values. The residual period, the difference between inverted and given periods, lies in the range -0.14 ms to 0.2 ms for all β, implying generally that it is underestimated. The residual damping for given values above 0.6, lies within the range -3.8×10^{-3} to 1.3×10^{-3} over a range of natural periods. Both of these ranges show the resolution to be good with each parameter estimated to within ±1% of the actual value (Fig A3.1).

Pulses recorded in the field can be affected by the ambient noise which may alter the shape or base level of the pulse. To examine this effect 'noisey' theoretical pulses were input to the inversion programme. For both parameters the resulting error was always less than 3% of the actual value when considering a base level shift or shape change due to noise. This value is smaller than the accuracy to which the parameters were set in the laboratory. The resolution of the inversion technique or the use of noisey data, therefore, do not form constraints on the determination of period and damping.

For the surface wave experiments 21 instruments each year were subjected to impulse calibration. In both experiments two transducers would not respond to the impulse in the field whilst still providing records of seismic signals; this was thought to be due to faulty wiring internal to the seismometers. There appears to be some degree of drift in both parameters with time but no consistent trend was indicated. The extent of the drift was small once the instruments had settled into their working environment.

Averaging the parameters for individual stations over the length of the experiment will provide estimates of the spread in parameters. The standard deviations of these means gives an

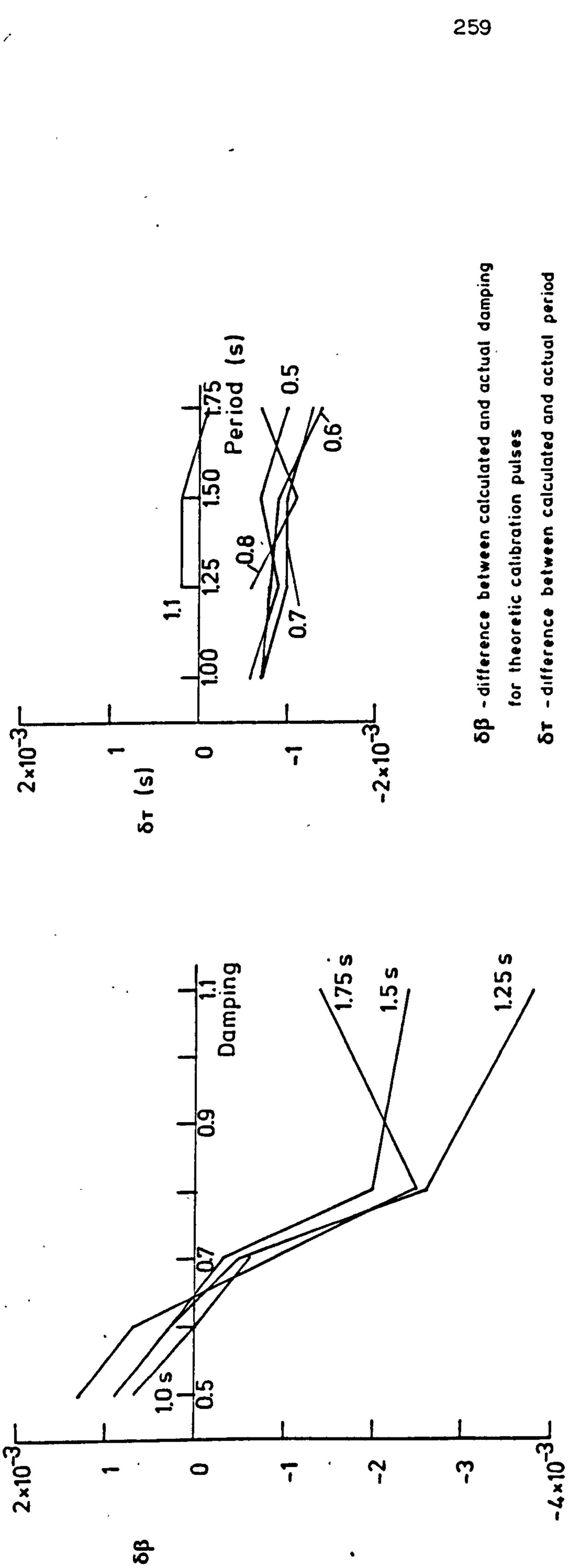
δβ - difference between calculated and actual damping
for theoretic calibration pulses
δτ - difference between calculated and actual period
for theoretic calibration pulses
Resolution of inversion process used to obtain the
instrument parameters of damping and period used to
define instrument transfer function. Obtained by
inverting various theoretical calibration pulses at
the different values of period and damping given.
δτ (s)
2×10⁻³
1
0
-1
-2×10⁻³
1.00
1.1
1.25
1.50
1.75
Period (s)
0.8
0.7
0.5
0.6
δβ
2×10⁻³
1
0
-1
-2
-3
-4×10⁻³
0.5
0.7
0.9
1.1
Damping
1.0 s
1.25 s
1.5 s
1.75 s

Figure A3.1

indication of the amount of drift in the instrument parameters.

It can be shown statistically that the four groups of data (period and damping for two experiments) are normally distributed with mean values which are all less than the nominal values set in the laboratory, Fig A3.2. If we assume that we are sampling a small portion of a population having means of the nominal values with the same variances then at the 95% significance level only the period data from the limestone experiment are from this parent distribution. From these observations we can see that whilst the distributions are normal their means are sufficiently different to the nominal values that errors may be incurred in the calculation of amplitudes by the use of the nominal values as a blanket response over the network. In any seismic experiment, therefore, it is appropriate that the transfer function of each instrument is calculated uniquely. It should also be realized that the determination of the instrument transfer function is of more importance than the individual instrument parameters (McGonigle & Burton 1980).

The amplitude and phase responses for displacement are given in Figure A3.3.

The low mean values of observed damping may have implications for previous determinations of damping. A discrepancy between the damping set by voltage measurements and that given by the micro-processor analyser has been observed. This would imply that the damping given in station details for networks other than those deployed in this study may be in error. Without further investigation the effect of this variation in damping on the instrument transfer function cannot be assessed.

The third parameter required to define the instrument response,

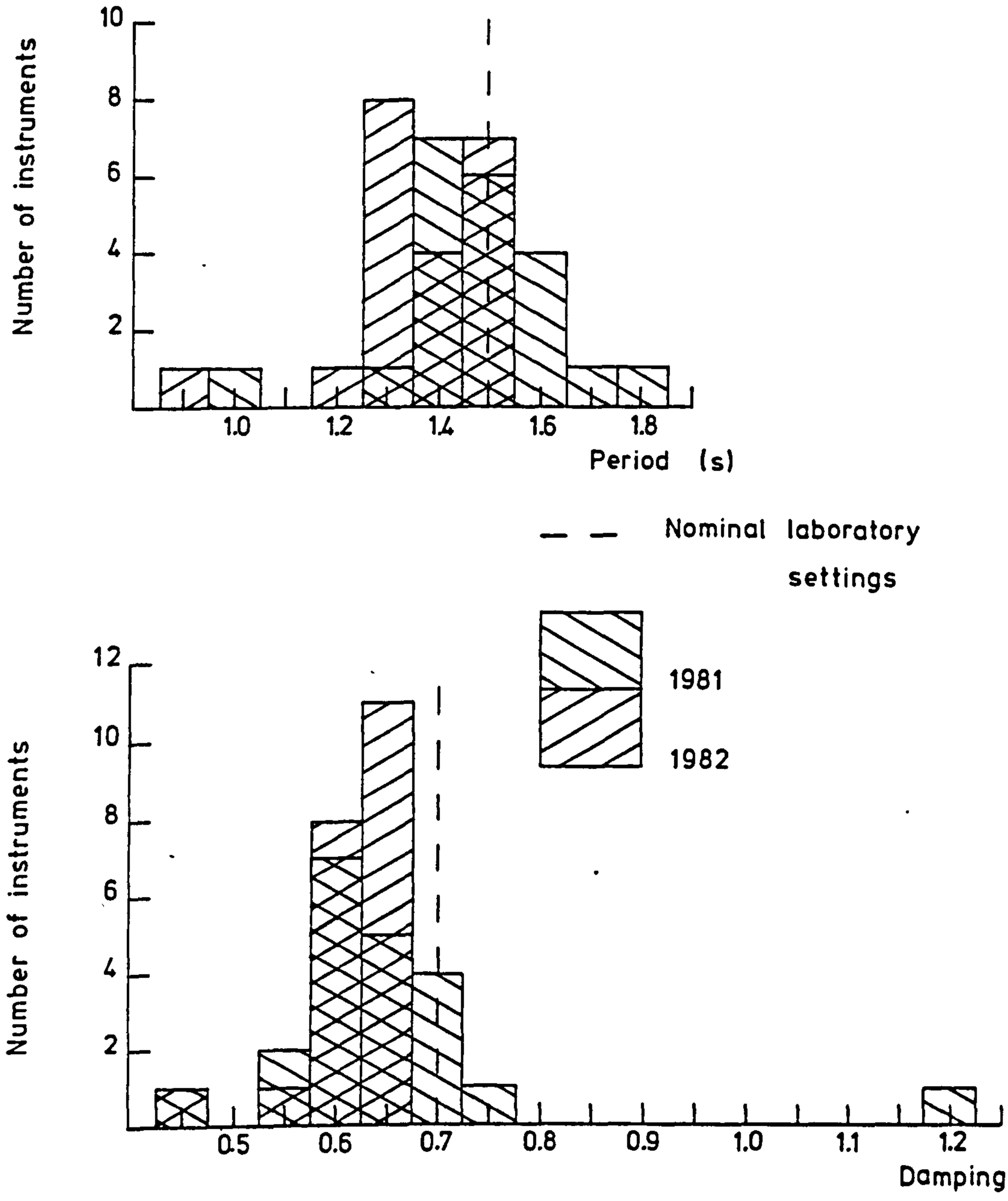

Figure A3.2 Distribution of instrument parameters from the averaged calibration results for each instrument deployed during the surface wave experiments in 1981 and 1982. (Total number of instruments in both cases was 21.)

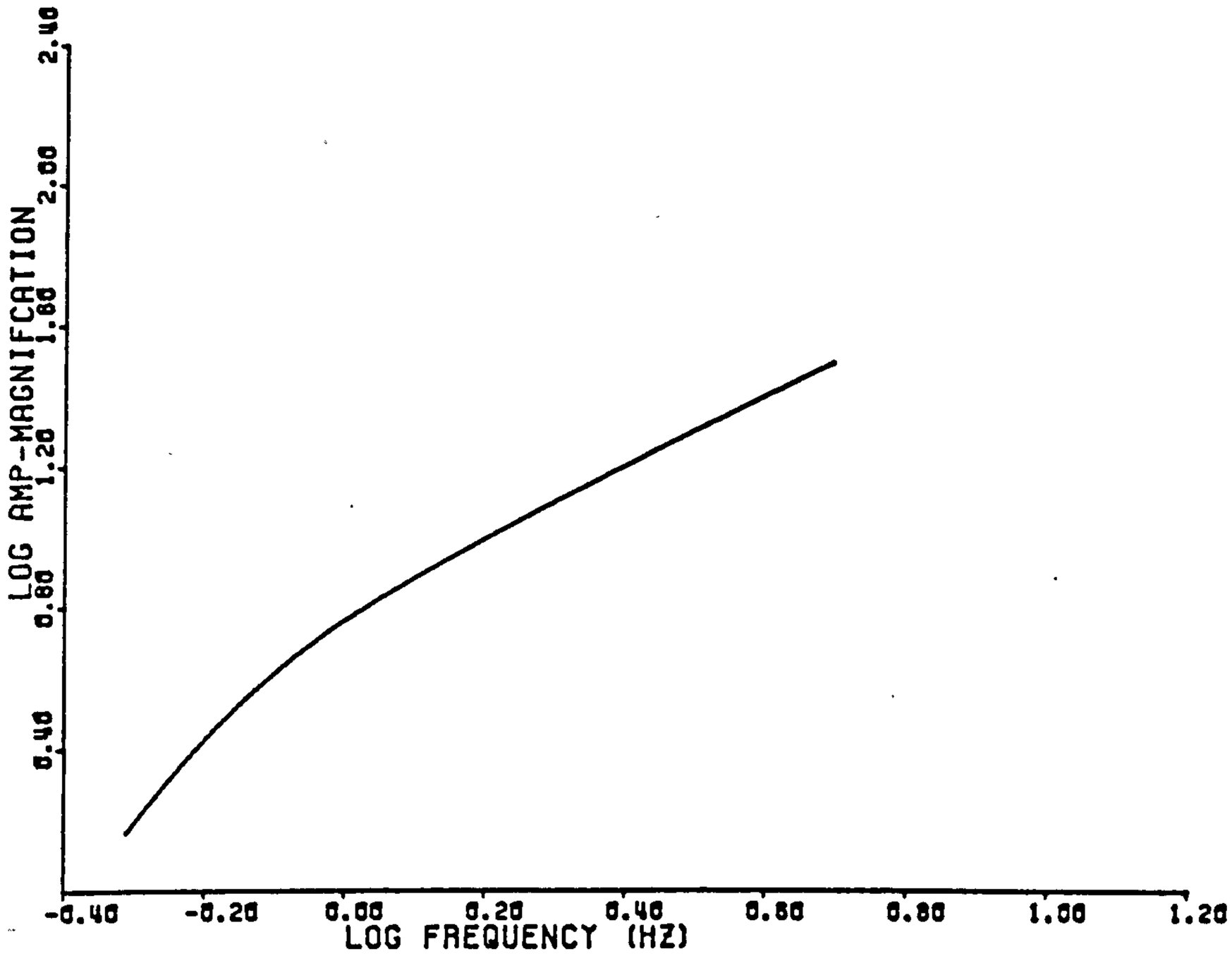

Amplitude response for nominal parameters: Period 1.5 s Damping 0.7

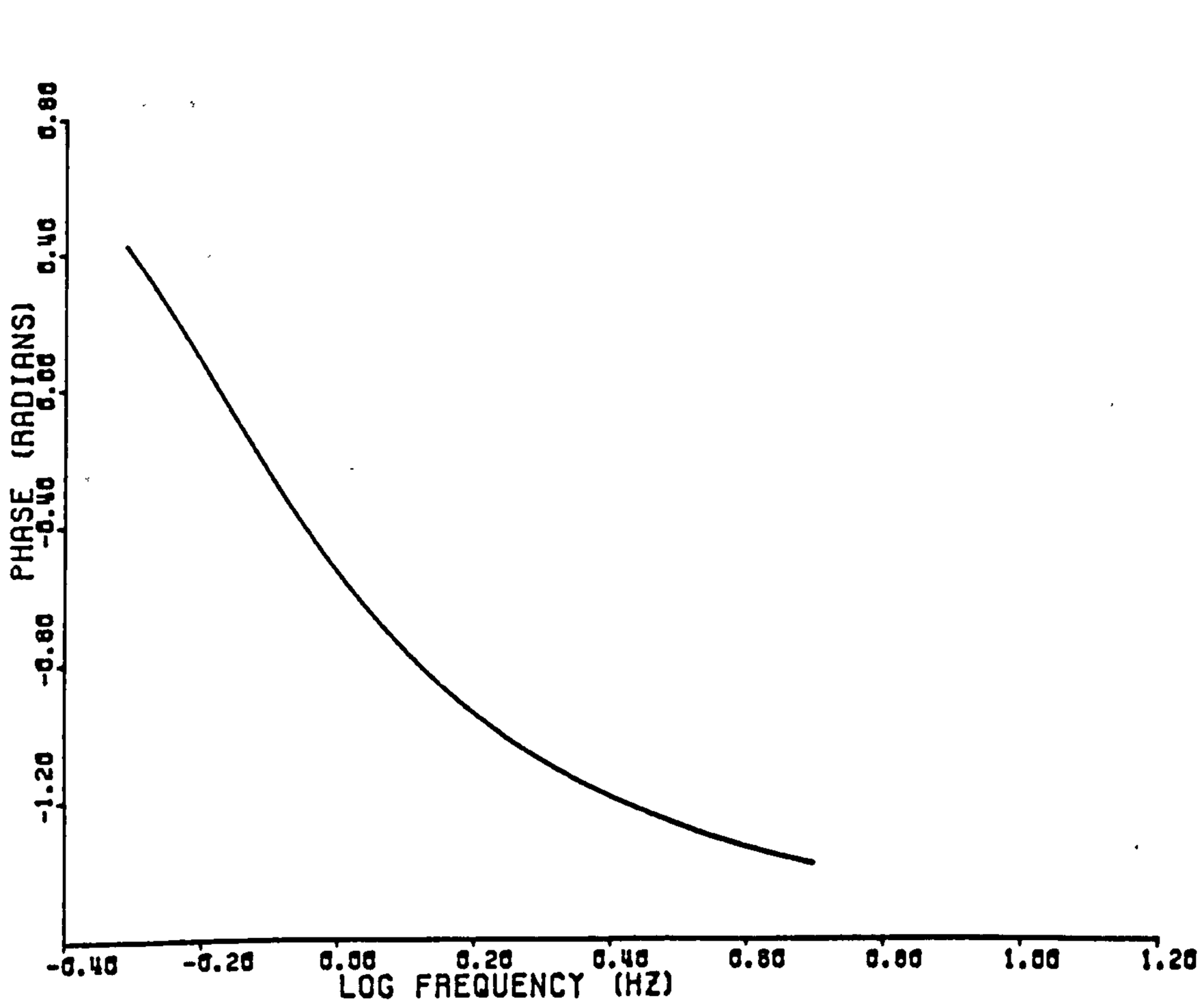

Phase response for nominal parameters: Period 1.5 s Damping 0.7

Figure A3.3 Amplitude and phase frequency responses for displacement of a Willmore Mk IIIa seismometer with a natural period of 1.5 s and damping of 0.7.

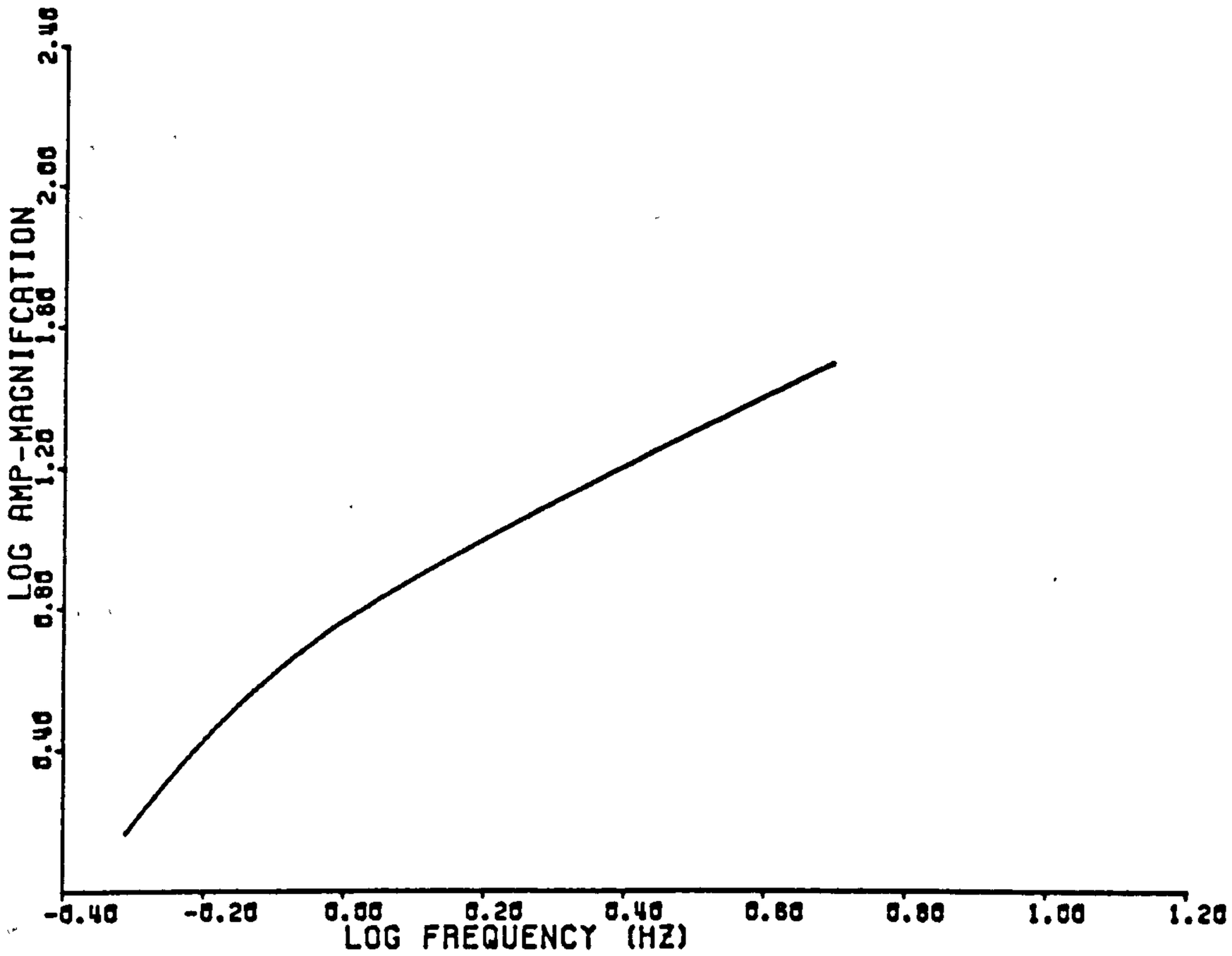

Amplitude response for nominal parameters: Period 1.5 s Damping 0.7

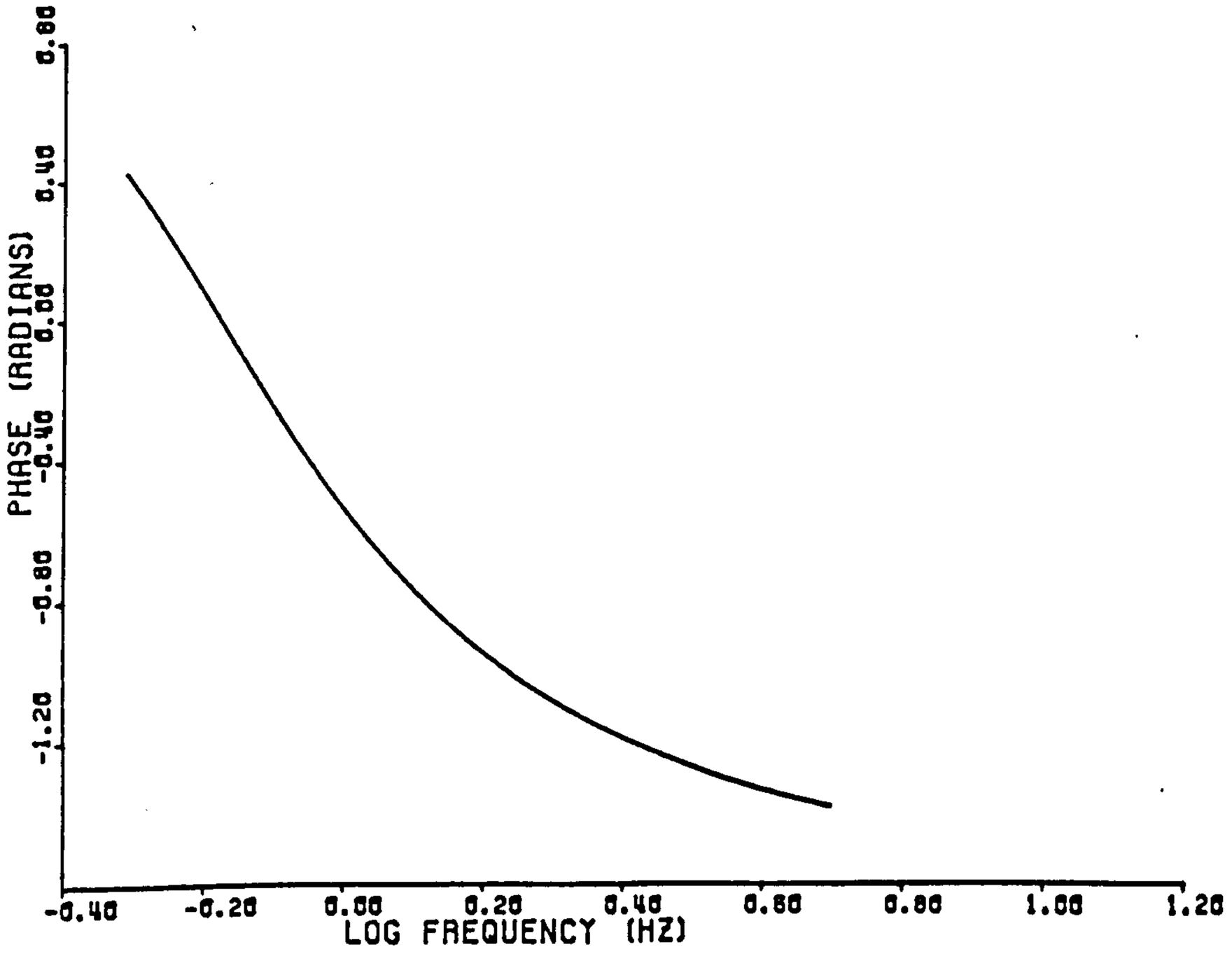

Phase response for nominal parameters: Period 1.5 s Damping 0.7

K the coupling factor, may be determined by monitoring the output voltage with frequency. Alternatively the system gain may be obtained by linear regression on the residuals of the computer inversion. Neither of these schemes were used in this study. Instead, an average value of K was found from the instrument test sheets. The error induced in the amplitudes by using this average will, therefore, become part of the errors associated with the observation.

Throughout the above discussion we have been concerned with the determination of two main instrument parameters to define the instrument response. The means by which this is achieved is not strictly analogous to the seismic situation. Any current input to the auxiliary coil will force the magnet-mass into motion which contrasts to the seismic case in which the instrument frame moves in response to ground motion. Further, the response is treated as being governed by a second order differential equation; whether this represents the true response is unknown. The only definitive way to determine the instrumental response would be to use a shaking table driven at a range of frequencies. This method, however, is impracticable for measurements in the field and we must, therefore, be content with impulse calibration and its inherent assumptions.

A.4 INSTRUMENT COMPARISONS.

Three types of seismometers have been deployed during various stages of the seismic investigation of the Derbyshire Dome. During the refraction study (Rogers 1983) the commonly used settings of 1.0 s and 0.7 for period and damping respectively were employed.

Following suggestions by Burton and later Evans (1981) the instrument period was altered for the surface wave experiments to 1.5 s with 0.7 damping being retained. For the purposes of this discussion the former instruments will be referred to as 'short period' (sp) whilst the latter group will be designated 'extended period' (ep). The third instrument type to be used consisted of force balance seismometers having a broad band response.

The principal reason for altering the instrument parameters is to facilitate the enhanced recording of lower frequency (less than 1 Hz) components of the signal. Observations at these lower frequencies provide better depth resolution in any subsequent inversions due to their penetration to deeper levels assuming normal dispersion.

The amplitude frequency response to ground velocity for the Willmore Mk IIIa indicates a change in slope at the natural frequency of the instrument. By increasing the period the 'knee point' is shifted to a lower frequency whilst the gradients of the lines remain the same. This should, theoretically, have the effect of increasing the frequency bandwidth over which the velocity response is flat; that is, decreasing the amount to which the recorded signal has undergone frequency variable amplification. For a ground motion signal having a flat amplitude spectrum over the frequency band of interest the recorded signals at 0.6 Hz and 1.0 Hz will exhibit a gain of 1.73 and 1.27 respectively for the extended period instruments over the short period seismometers. This increased bandwidth will reduce the shaping of the recorded wave packet caused by the instrument response.

A number of sites from the earlier refraction line along the axis of the Dome were reoccupied during experiment LST 1. This has

enabled a comparison of the instrument types for events from the same quarry. Details of the individual shots from the refraction experiment, recorded by the sp instruments, have not been documented implying that some of the observed differences may be due to differences between the sources. The amp-mod gain of the sp seismometers was also higher than those of the ep instruments and was also constant between stations.

Events from Tunstead are compared in Figures A4.1, A4.2. On the whole the records from the ep instruments appear to have a lower frequency content. This, however, is caused by the reduction in the difference in magnification between the lower and higher frequencies for the ep seismometers. This provides the first advantage of using extended periods in surface wave studies as the wave group is now more clearly displayed.

Once the instrument response has been removed there is little difference in the resulting spectral amplitudes of ground motion across the frequency bandwidth. What does become apparent is that the ep seismometers permit the removal of the instrument response to be conducted at slightly lower frequencies than with the sp transducers. This is because the lower magnification of the sp seismometers together with the low signal-to-noise ratio at these frequencies produces a more uncertain, possibly spurious, increase in the amplitude of the low frequency noise. The dispersion analysis on instrument corrected records from ep instruments was conducted down to 0.6 Hz but only to 0.8 Hz if short period records are used. This small increase in frequency bandwidth is especially important for shallow crustal studies using high frequency surface waves and implies an increase in penetration depth from 3 km to 4 km approximately.

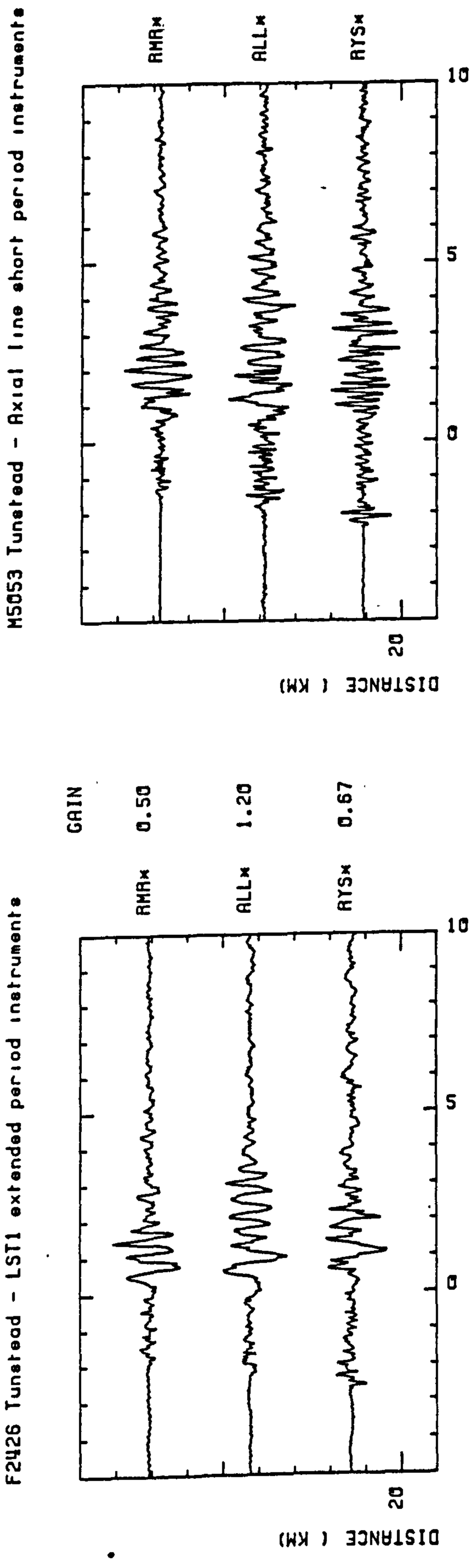

Figure A4.1 Comparison of signals recorded by extended (1.5 s) period and short (1.0 s) period seismometers for the stations given from similar type 1 events in Tunstead Quarry.

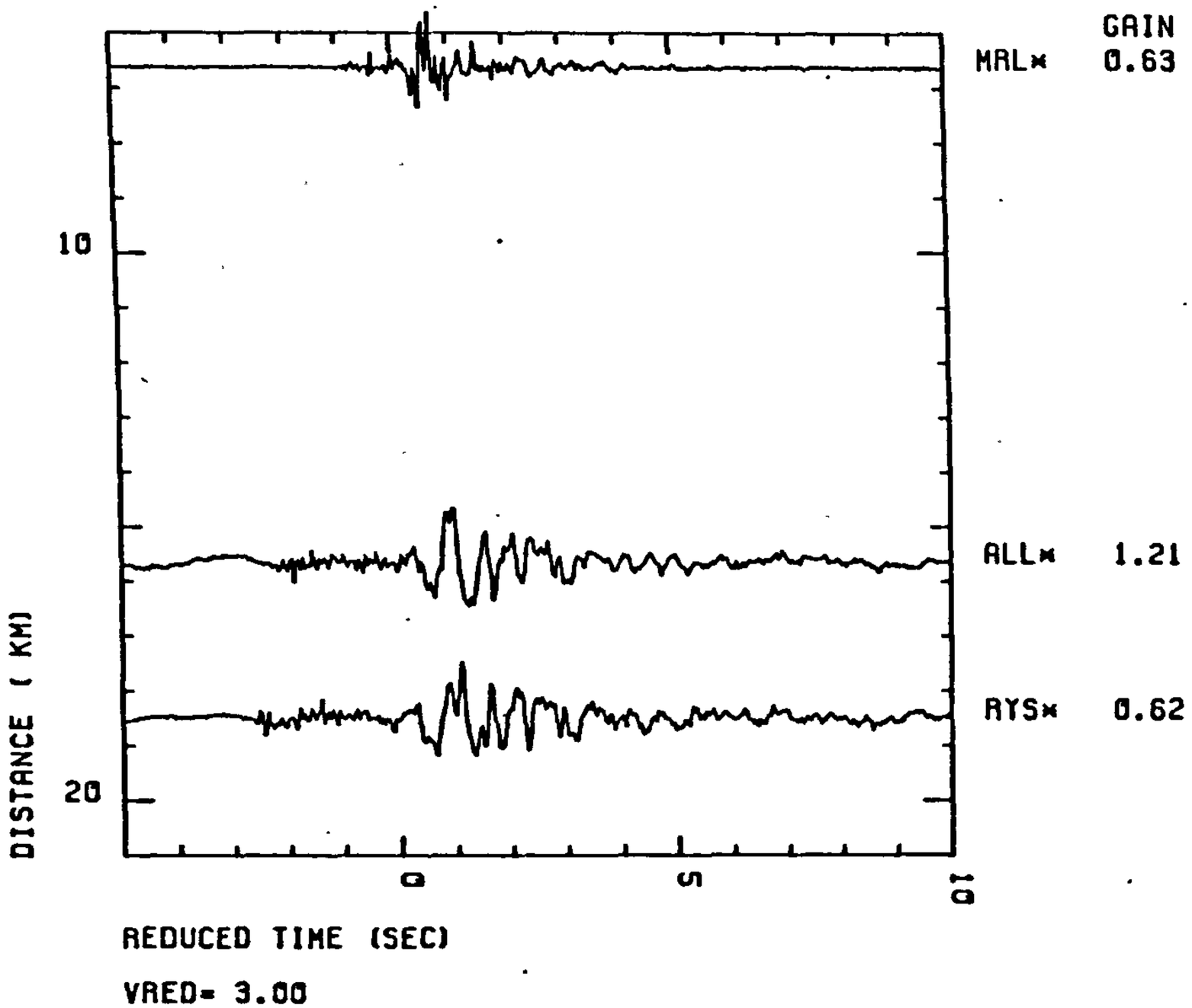

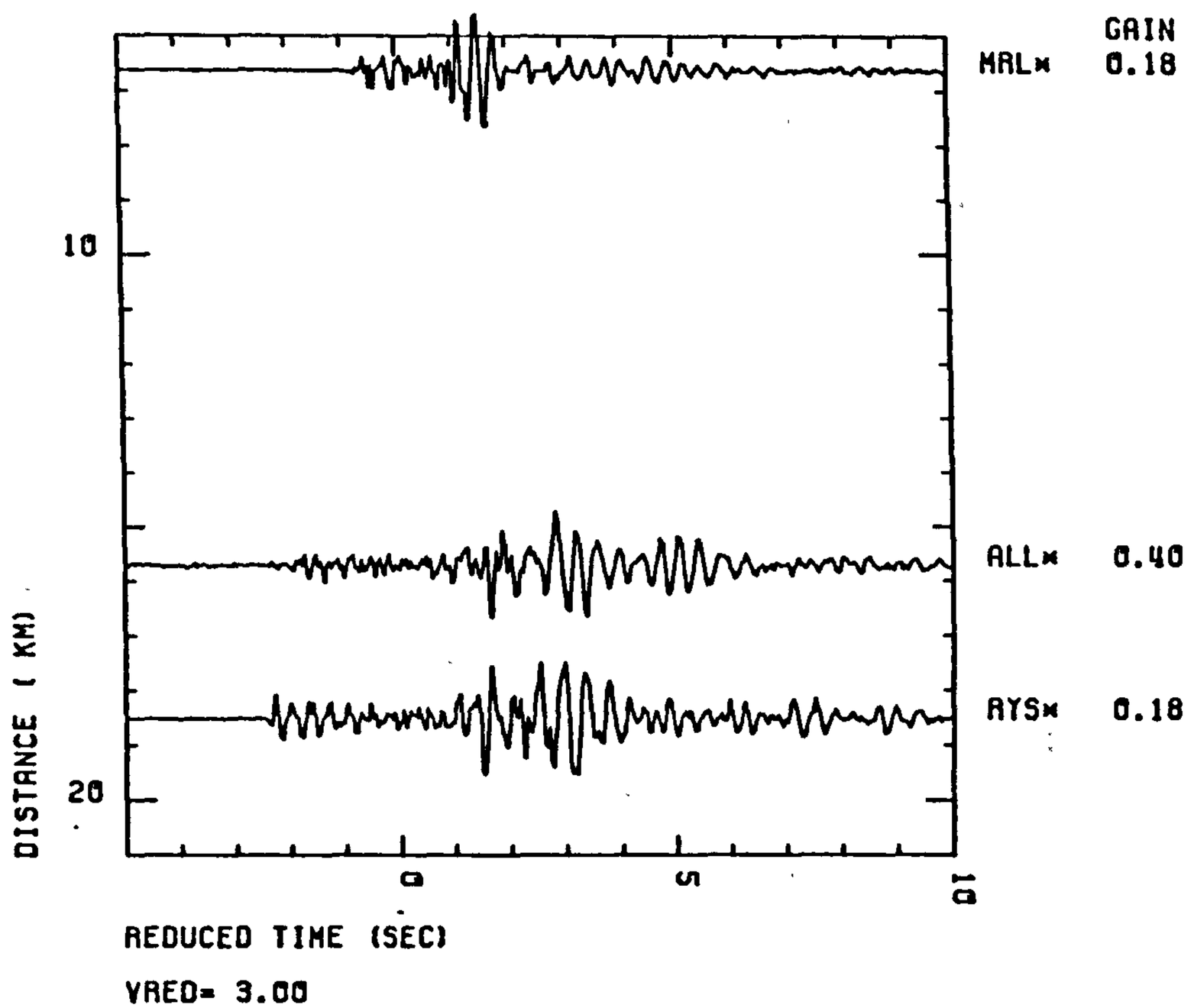

Figure A4.2 Comparison of signals recorded by extended (1.5 s) period and short (1.0 s) period seismometers for the stations given from similar type 2 events in Tunstead Quarry.

The broad band instruments were deployed specifically to look for and record any low frequencies which may be present in the signal and not recorded well by the other instrument types. These instruments were set to have a response which was flat to velocity from 0 - 5 Hz although their characteristics may be altered to suit the particular requirements of an experiment. Unfortunately, their operation in the field was restricted by their high power consumption resulting in a poor distribution of records.

Figures A4.3, A4.4 provide comparisons of broad band and extended period records for events in Tunstead and Brier Low Quarries. The effect of the long period micro-seismic energy can be seen clearly for records ALL and WNF. The long period component may be enhanced partially by the servo-assisted centring mechanism of these instruments as the energy is not well correlated between stations.

Visual inspection of the seismograms shows a similarity between the broad band and extended period records. In some cases (Fig A4.4, FWS record) there has been an equalisation of amplitudes in the wave packet. Individual cycles and periods in the signal are, however, directly comparable between the two data sets.

Except for the long period micro-seismic component superposed on the signal the amplitude spectra of the broad and extended period records are identical in shape. Spectral analysis of the ambient noise from both types of record shows it to increase in amplitude below 0.6 Hz achieving amplitudes greater than those seen in any of the signals. The 0.6 Hz limit to the analysis of extended period records must then represent the lowest frequency contained in the signal and not a constraint imposed by the instrument response. The use of the broad band seismometers, therefore, did not provide any

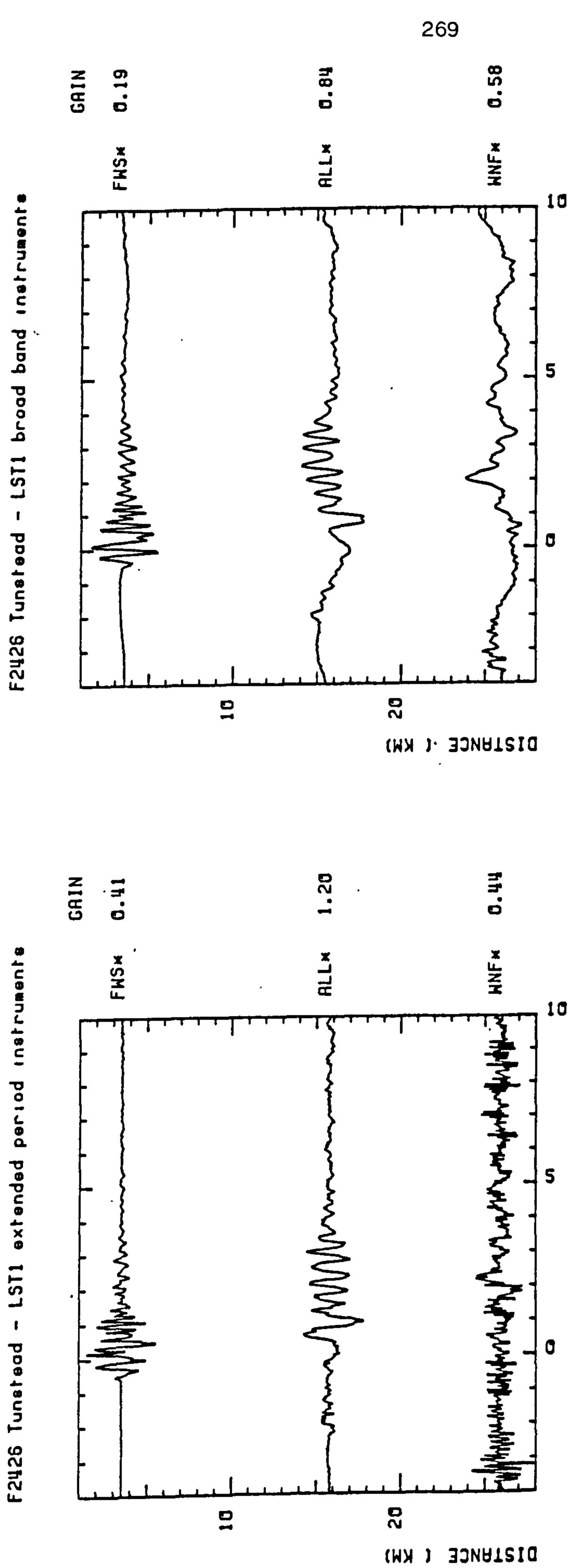

Figure A4.3 Comparison of signals recorded by extended (1.5 s) period and broad band seismometers deployed along the line LST 1 from event F2426 in Tunstead Quarry.

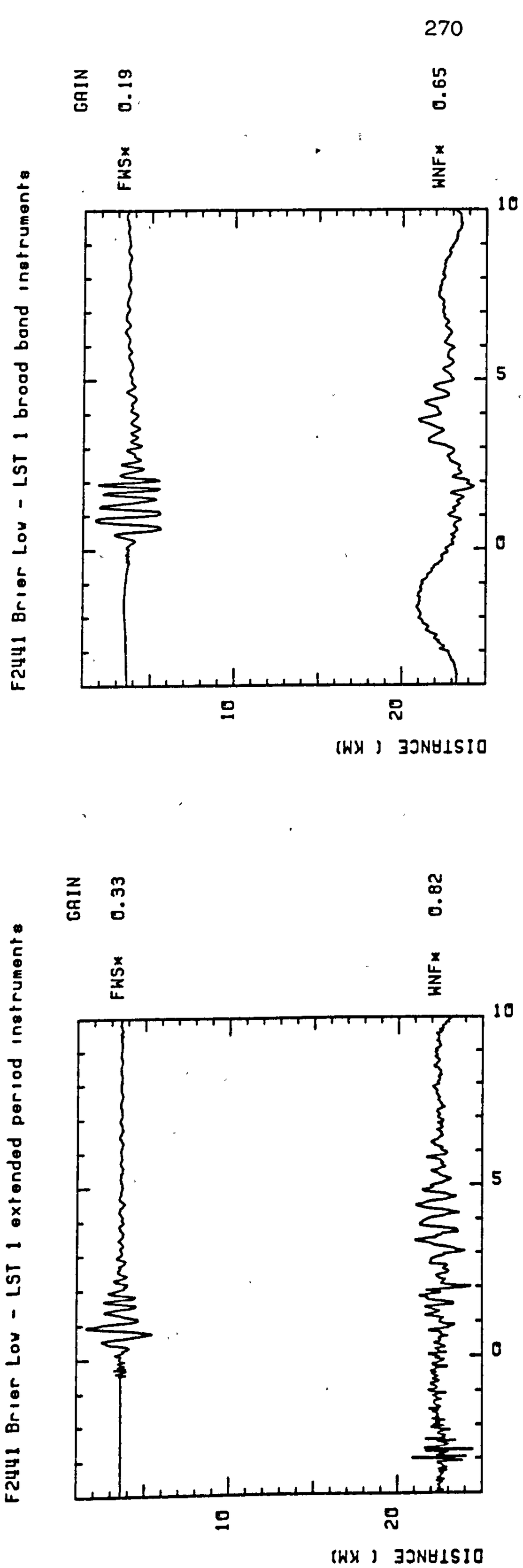

Figure A4.4 Comparison of signals recorded by extended (1.5 s) period and broad band seismometers deployed along the line LST 1 from event F2441 in Brier Low Quarry.

additional frequency data and demonstrated that the ep seismometers were able to record accurately all the lower frequency energy present in the seismic signals from the available sources.

Evans (1981) finds that for the Willmore Mk II seismometer deployed during the LISPB experiment in Scotland the minimum frequency to which the instrument correction operation could be extended was 0.4 Hz. This decrease in minimum frequency achieved with instruments set at 1.0 s and 0.7 damping, may be a result of the longer path lengths traversed during the LISPB experiment. Another explanation for the lower frequency is the nature of the source. The LISPB utilised a number of single shots on land and dispersed shots at optimum depth at sea (Bamford et al. 1976, Jacob 1975) and these may provide an improved frequency content compared to the dispersed quarry blasts used in this study.

A.5 CONCLUSIONS on INSTRUMENTATION.

The consideration of the instrumentation appropriate to this study formed an important part of the design of the experiments described herein. A number of important conclusions have been reached from this investigation on the instrumentation.

Firstly, careful calibration of the seismometers both in the laboratory and in the field will standardise a network of instruments as much as possible. Also, estimates of the instrument response and its variation may be obtained; a vital piece of information required to facilitate the removal of the effect of the instrument from the recorded signals. Furthermore, field calibration is essential as the instrument parameters may vary from

those set in the laboratory.

Secondly, extended period instruments provide enhanced recordings of high frequency surface waves. This in turn aids any subsequent analysis as the wave packet is more easily defined. Another advantage accruing from the extended period is the wider available bandwidth.

Thirdly, the usefulness of an exerise to assemble all the instrumentation and to record data overnight at the same location should not be disregarded. The results from each seismometer may be inspected and any instrumental fault detected. Further, the recorded information on the relative gains of the seismometer/amp-mod pairs is of importance to subsequent analysis.

The use of broad band instruments did not, in this instance, provide any further information to that given by the ep seismometers. A number of observations of local earthquakes and teleseisms made during the experiments, however, indicate the power of such instruments to provide the most complete record of such events.

Lastly, by comparing other suites of data it appears that the nature of the source, and perhaps local structure, plays an important part in the observed bandwidth. For studies of high frequency Rayleigh waves, therefore, a single, point source may be more appropriate to obtain a wider frequency bandwidth extending to lower frequencies.

APPENDIX B

OBSERVED RAYLEIGH WAVE DISPERSION and SPECIFIC ATTENUATION FACTOR DATA

The 14 tables given here contain the observed group slowness dispersion and specific attenuation factor data for Rayleigh recorded over the Derbyshire Dome and adjacent areas. These data complement the figures in chapter 3.

Each of the data sets is identified by a mnemonic which follows the convention of Table 3.1.

LST 1 Carboniferous Limestone district line 1

LST 1N Carboniferous Limestone district line 1 northern province

LST 1S Carboniferous Limestone district line 1 southern province

LST 2 Carboniferous Limestone district line 2

LST 2N Carboniferous Limestone district line 2 northern province

LST 2S Carboniferous Limestone district line 2 southern province

All observations made over the limestone district are from Brier Low Quarry

MG 1 Millstone Grit district main line

MGAR Millstone Grit district cluster array

BMR Single station observations from station BMR

All observations made over the Millstone Grit district are from Tunstead Quarry

Parameter prefixes: P observed group slowness data (s km^{-1}).

Q observed Rayleigh wave specific attenuation factor, $Q_\gamma^{-1}(\nu)$, data.

Hence PLST 1N is the group slowness data set from the northern province of line 1 over the Carboniferous Limestone.

All values of frequency are given in Hertz (Hz).

PLST 1 (Stations: MRL,HGF,RMR,ALL,RYS,BAL,WNF Quarry: Brier Low)

Frequency		Grp. slwns.	Std. dev.	Frequency		Grp. slwns.	Std. dev.
1	0.58594	0.42035	0.01436	2	0.78125	0.42008	0.01536
3	0.97656	0.42194	0.01456	4	1.17187	0.42807	0.01121
5	1.36719	0.43877	0.00911	6	1.56250	0.45279	0.00792
7	1.75781	0.46786	0.00801	8	1.95312	0.48104	0.00966
9	2.14844	0.48990	0.01102	10	2.34375	0.49400	0.01152
11	2.53906	0.49495	0.01144	12	2.73437	0.49468	0.01185
13	2.92969	0.49403	0.01313	14	3.12500	0.49283	0.01451
15	3.32031	0.49104	0.01535	16	3.51562	0.48875	0.01548
17	3.71094	0.48508	0.01625	18	3.90625	0.47949	0.02161
19	4.10156	0.47446	0.02222	20	4.29687	0.47201	0.03920

PLST 1N (Stations: MRL,HGF,RMR,ALL Quarry: Brier Low)

Frequency		Grp. slwns.	Std. dev.	Frequency		Grp. slwns.	Std. dev.
1	0.58594	0.40624	0.02124	2	0.78125	0.41465	0.02310
3	0.97656	0.42682	0.01919	4	1.17187	0.44067	0.00728
5	1.36719	0.45556	0.00321	6	1.56250	0.47327	0.00618
7	1.75781	0.49338	0.00584	8	1.95312	0.51241	0.00710
9	2.14844	0.52674	0.00947	10	2.34375	0.53594	0.01007
11	2.53906	0.54261	0.00834	12	2.73437	0.54922	0.00574
13	2.92969	0.55583	0.00566	14	3.12500	0.56066	0.00952
15	3.32031	0.56193	0.01361	16	3.51562	0.55766	0.01618
17	3.71094	0.54344	0.01795	18	3.90625	0.51377	0.02599
19	4.10156	0.47588	0.04524	20	4.29687	0.44512	0.06624

PLST 1S (Stations: RYS,BAL,WNF Quarry: Brier Low)

Frequency		Grp. slwns.	Std. dev.	Frequency		Grp. slwns.	Std. dev.
1	0.58594	0.42903	0.08368	2	0.78125	0.43803	0.09347
3	0.97656	0.45290	0.08288	4	1.17187	0.46931	0.04637
5	1.36719	0.48100	0.01530	6	1.56250	0.48668	0.01463
7	1.75781	0.48829	0.03195	8	1.95312	0.48787	0.04668
9	2.14844	0.48571	0.05333	10	2.34375	0.48075	0.05238
11	2.53906	0.47270	0.04266	12	2.73437	0.46350	0.02671
13	2.92969	0.45570	0.01294	14	3.12500	0.45033	0.00622
15	3.32031	0.44726	0.00168	16	3.51562	0.44585	0.00861

PLST 2 (Stations: OVW,MHO,BOL,GLW,BHL,SIP Quarry: Brier Low)

Frequency	Grp. slwns.	Std. dev.	Frequency	Grp. slwns.	Std. dev.
1 0.58594	0.39033	0.01882	2 0.78125	0.39202	0.01835
3 0.97656	0.40087	0.02101	4 1.17187	0.42224	0.02669
5 1.36719	0.45593	0.03201	6 1.56250	0.49542	0.03600
7 1.75781	0.52995	0.03859	8 1.95312	0.55131	0.03960
9 2.14844	0.55951	0.03972	10 2.34375	0.56046	0.03966
11 2.53906	0.55949	0.03960	12 2.73437	0.55854	0.03978
13 2.92969	0.55744	0.03996	14 3.12500	0.55589	0.03907
15 3.32031	0.55383	0.03676	16 3.51562	0.55071	0.03404
17 3.71094	0.54537	0.03126	18 3.90625	0.53823	0.02803
19 4.10156	0.53353	0.02591	20 4.29687	0.53479	0.02663

PLST 2N (Stations: OVW,MHO,BOL,GLW Quarry: Brier Low)

Frequency	Grp. slwns.	Std. dev.	Frequency	Grp. slwns.	Std. dev.
1 0.58594	0.35198	0.03662	2 0.78125	0.34176	0.02277
3 0.97656	0.33001	0.00526	4 1.17187	0.32532	0.01015
5 1.36719	0.33470	0.01382	6 1.56250	0.35615	0.01231
7 1.75781	0.38030	0.01609	8 1.95312	0.39719	0.01304
9 2.14844	0.40406	0.00536	10 2.34375	0.40516	0.00602
11 2.53906	0.40541	0.00777	12 2.73437	0.40683	0.00920
13 2.92969	0.41024	0.01278	14 3.12500	0.41695	0.01832
15 3.32031	0.42759	0.02347	16 3.51562	0.44038	0.02734
17 3.71094	0.45243	0.03243	18 3.90625	0.46241	0.04134
19 4.10156	0.47097	0.05361	20 4.29687	0.47799	0.15717

PLST 2S (Stations: BHL,SIP Quarry: Brier Low)

Frequency	Grp. slwns.	Std. dev.	Frequency	Grp. slwns.	Std. dev.
1 0.58594	0.76819	0.00000	2 0.78125	0.76883	0.00000
3 0.97656	0.77083	0.00000	4 1.17187	0.77431	0.00000
5 1.36719	0.78606	0.00000	6 1.56250	0.82104	0.00000
7 1.75781	0.87875	0.00000	8 1.95312	0.93208	0.00000
9 2.14844	0.95963	0.00000	10 2.34375	0.97181	0.00000
11 2.53906	0.99174	0.00000	12 2.73437	1.02639	0.00000
13 2.92969	1.06427	0.00000	14 3.12500	1.09047	0.00000
15 3.32031	1.10281	0.00000			

PMG 1 (Stations: FSF,CHF,FSD,TSD,MSC,HNF Quarry: Tunstead)

Frequency	Grp. slwns.	Std. dev.	Frequency	Grp. slwns.	Std. dev.
1 0.58594	0.67439	0.00864	2 0.78125	0.68910	0.00791
3 0.97656	0.70428	0.00497	4 1.17187	0.71184	0.01084
5 1.36719	0.71166	0.01579	6 1.56250	0.71181	0.01968
7 1.75781	0.71913	0.02710	8 1.95312	0.73192	0.04085
9 2.14844	0.74075	0.05553	10 2.34375	0.74885	0.06142
11 2.53906	0.76335	0.05922	12 2.73437	0.76728	0.04161
13 2.92969	0.75557	0.03126	14 3.12500	0.74852	0.07251

PMGAR (Stations: LDG,CTP,CTA,CTB,CTC Quarry: Tunstead)

Frequency	Grp. slwns.	Std. dev.	Frequency	Grp. slwns.	Std. dev.
1 0.58594	0.49102	0.01021	2 0.78125	0.50949	0.00918
3 0.97656	0.53984	0.01409	4 1.17187	0.57530	0.01558
5 1.36719	0.60524	0.01359	6 1.56250	0.62641	0.01284
7 1.75781	0.64045	0.01323	8 1.95312	0.65039	0.01322
9 2.14844	0.65750	0.01448	10 2.34375	0.66194	0.01808

PBMR (Station: BMR Quarry: Tunstead)

Frequency	Grp. slwns.	Std. dev.	Frequency	Grp. slwns.	Std. dev.
1 0.58594	0.44045	0.02681	2 0.78125	0.45101	0.01952
3 0.97656	0.47491	0.02485	4 1.17187	0.50717	0.01700
5 1.36719	0.53601	0.02101	6 1.56250	0.55681	0.03285
7 1.75781	0.56985	0.04273	8 1.95312	0.57612	0.04722
9 2.14844	0.57806	0.04614			

QLST 1 (Stations: MRL,HGF,RMR,ALL,RYS,BAL,WNF Quarry: Brier Low)

Frequency		Q_γ^{-1}	Std. dev.	Frequency		Q_γ^{-1}	Std. dev.
1	1.17187	0.01805	0.00797	2	1.36719	0.02215	0.00702
3	1.56250	0.02459	0.00560	4	1.75781	0.02359	0.00389
5	1.95312	0.02259	0.00331	6	2.14844	0.02481	0.00317
7	2.34375	0.02891	0.00388	8	2.53906	0.03249	0.00331
9	2.73437	0.03435	0.00289	10	2.92969	0.03406	0.00353
11	3.12500	0.03207	0.00285	12	3.32031	0.02894	0.00237
13	3.51562	0.02529	0.00453	14	3.71094	0.02218	0.00436

QLST 1N (Stations: MRL,HGF,RMR,ALL Quarry: Brier Low)

Frequency		Q_γ^{-1}	Std. dev.	Frequency		Q_γ^{-1}	Std. dev.
1	1.56250	0.00779	0.00543	2	1.75781	0.01099	0.00268
3	1.95312	0.01333	0.00352	4	2.14844	0.01445	0.00260
5	2.34375	0.01719	0.00706	6	2.53906	0.02284	0.00783
7	2.73437	0.02901	0.00822	8	2.92969	0.03324	0.00784
9	3.12500	0.03429	0.00759	10	3.32031	0.03240	0.00665
11	3.51562	0.02985	0.00787	12	3.71094	0.02834	0.00641

QLST 1S (Stations: RYS,BAL,WNF Quarry: Brier Low)

Frequency		Q_γ^{-1}	Std. dev.	Frequency		Q_γ^{-1}	Std. dev.
1	0.97656	0.07918	0.00840	2	1.17187	0.08294	0.01052
3	1.36719	0.08439	0.00190	4	1.56250	0.07687	0.00571
5	1.75781	0.06283	0.01180	6	1.95312	0.05379	0.00949
7	2.14844	0.05457	0.01029	8	2.34375	0.05805	0.00998
9	2.53906	0.05401	0.00378	10	2.73437	0.04096	0.01159
11	2.92969	0.02755	0.01805	12	3.12500	0.02091	0.01104
13	3.32031	0.01970	0.00843	14	3.51562	0.01980	0.00217

QMG 1 (Stations: FSF,CHF,FSD,TSD,MSC,HNF Quarry: Tunstead)

	Frequency	Q_γ^{-1}	Std. dev.		Frequency	Q_γ^{-1}	Std. dev.
1	0.78125	0.01531	0.00408	2	0.97656	0.01932	0.00290
3	1.17187	0.02237	0.00297	4	1.36719	0.02232	0.00169
5	1.56250	0.02028	0.00203	6	1.75781	0.01927	0.00339
7	1.95312	0.02031	0.00370	8	2.14844	0.02166	0.00607
9	2.34375	0.02189	0.00824	10	2.53906	0.02154	0.00625

QMGAR (Stations: LDG,CTP,CTA,CTB,CTC Quarry: Tunstead)

	Frequency	Q_γ^{-1}	Std. dev.		Frequency	Q_γ^{-1}	Std. dev.
1	0.78125	0.01598	0.04889	2	0.97656	0.01689	0.01338
3	1.17187	0.01560	0.01110	4	1.36719	0.01339	0.01496
5	1.56250	0.01303	0.01637	6	1.75781	0.01276	0.01524
7	1.95312	0.01078	0.01375				

REFERENCES

Abo-Zena, A.M., 1979. Dispersion function computations for unlimited frequencies in layered media. Geophys. J. R. astr. Soc. 58, 91-105

Aitkenhead, N., & Chisholm, J.I., 1982. A standard nomenclature for the Dinantian formations of the Peak District of Derbyshire and Staffordshire. Rep. Inst. Geol. Sci. no. 82/8

Al-Husseini, M.I., Glover, J.B., & Barley, B.J., 1981. Dispersion patterns of the ground roll in eastern Saudi Arabia. Geophysics 46, 121-137

Allen, J.R.L., 1960. The Mam Tor Sandstones - a "turbidite" facies of the Namurian deltas of Derbyshire. J. Sediment. Petrol. 30, 193-208

Anderson, D.L.,& Archambeau, C.B., 1964. The anelasticity of the Earth. J. geophys. Res. 69, 2071-2084

Anderson, D.L., Ben-Menaham, A., & Archambeau, C.B. 1965. Attenuation of seismic energy in the upper mantle. J. geophys. Res 70, 1441-1448

Anderton, R., Bridges, P.H., Leeder, M.R., & Sellwood, B.W., 1979. "A Dynamic Stratigraphy of the British Isles. A study in crustal evolution." Allen and Unwin (London)

Assumpção, M., & Bamford, D., 1978. LISPB-V Studies of crustal shear waves. Geophys. J. R. astr. Soc. 54, 61-73

Bache, T.C., Rodi, W.L., & Harkrider, D.G., 1978. Crustal structures inferred from Rayleigh wave signatures of NTS explosions. Bull. seism. Soc. Am. 68, 1399-1413

Backus, G., & Gilbert, F., 1967. Numerical applications of a formalism for geophysical inverse problems. Geophys. J. R. astr. Soc. 13, 247-276

Bamford, D., Faber, S., Jacob, B., Kaminski, W., Nunn, K., Prodehl, C., Fuchs, K., King, R., & Willmore, P., 1976. A lithospheric seismic profile in Britain - I Preliminary results. Geophys. J. R. astr. Soc 44, 145-160

Bamford, D., Nunn, K., Prodehl, C., & Jacob, B., 1978. LISPB - IV Crustal structure of northern Britain. Geophys. J. R. astr. Soc. 54, 43-60

Båth, M., 1968. "Mathematical Aspects of Seismology." Elsevier (Amsterdam)

Båth, M., 1974. "Spectral Analysis in Geophysics." Elsevier (Amsterdam)

Båth, M., 1975. Short period Rayleigh waves from near surface events. Phys. Earth Planet. Int. 10, 369-376

Bayerly, M., & Brooks, M., 1980. A seismic study of deep structure in South Wales using quarry blasts. Geophys. J. R. astr. Soc. 60, 1-19

Bemrose, H.H. Arnold, 1894. The microscopical structure of the Carboniferous dolerites and tuffs of Derbyshire. Quart. J. Geol. Soc. Lon. 50, 603-644

Bemrose, H.H. Arnold, 1907. The toadstones of Derbyshire; their field relations and petrography. Quart. J. Geol. Soc. Lon. 63, 241-281

Berry, M.J., & Fuchs, K., 1973. Crustal structure of the Superior and Greenville provinces of the north-eastern Canadian Shield, Bull. seism. Soc. Am. 63, 1393-1432

Birch, F., & Bancroft, D., 1938. Elasticity and internal friction in a long column of granite. Bull. seism. Soc. Am. 28, 243-254

Biot, M.A., 1956. Theory of propagation of elastic waves in a fluid saturated porous solid,

I Low frequency range. J. Acoust. Soc. Amer. 28, 168-178

II High frequency range. J. Acoust. Soc. Amer. 28, 179-191

Bloch, S., & Hales, A.L., 1968. New techniques for the determination of surface wave phase velocities. Bull. seism. Soc. Am. 58, 1021-1034

Bloch, S., Hales, A.L., & Landisman, M., 1969. Velocities in the crust and upper mantle of southern Africa from multi-mode surface wave dispersion. Bull. seism. Soc. Am. 59, 1599-1629

Bond, L.J., 1979. A computer model of the interaction of acoustic surface waves with discontinuities. Ultrasonics 17, 71-77

Boore, D.M., 1972. Finite difference methods for seismic wave propagation in heterogeneous materials. pp 1-37 in Bolt, B.A., (ed) "Methods in Computational Physics. Vol 11. Seismology: Surface Waves and Earth Oscillations." Academic Press (New York)

Born, W.T., 1941. The attenuation constant of Earth materials. Geophysics 6, 132-148

Braile, L.W., & Keller, G.R., 1975. Fine structure of the crust inferred from linear inversion of Rayleigh-wave dispersion. Bull. seism. Soc. Am. 65, 71-83

Brown, M.J., & Ogilvy, R.D., 1982. Geophysical and geochemical investigations over the Long Rake, Haddon Fields, Derbyshire. Mineral Reconnaissance Programme Rep. Inst. Geol. Sci. 56

Brune, J.N., 1962. Attenuation of dispersed wavetrains. Bull. seism. Soc. Am. 52, 109-112

Brune, J.N., Nafe, J.E., & Oliver, J.E., 1960. A simplified method for the analysis and synthesis of dispersed wavetrains. J. geophys. Res. 65, 287-304

Bullen, K.E., 1979. "An introduction to the theory of seismology." 3rd ed Cambridge University Press (Cambridge)

Bungum, H., & Capon, J., 1974. Coda pattern and multipath propagation of Rayleigh waves at NORSAR. Phys. Earth Planet. Int. 9, 111-127

Burton, P.W., 1973. Estimations of Q from seismic Rayleigh waves. Unpubl. PhD thesis University of Durham

Burton, P.W., 1974. Estimations of $Q_\gamma^{-1}(f)$ from seismic Rayleigh waves. Geophys. J. R. astr. Soc. 36, 167-189

Burton, P.W., 1977. Inversions of high frequency $Q_\gamma^{-1}(f)$. Geophys. J. R. astr. Soc. 48, 29-51

Burton, P.W., & Blamey, C., 1972. A computer program to determine the spectrum and dispersion characteristic of a transient signal. UKAEA AWRE Rep. no. O 48/72

Burton, P.W., & Kennet, B.L.N., 1972. Upper mantle zone of low Q. Nature Phys. Sci. 238, 87-90

Capon, J., 1969. High resolution frequency-wavenumber spectrum analysis. Proc. IEEE 57, 1408-1418

Capon, J., 1970. Analysis of Rayleigh-wave multipath propagation at LASA. Bull. seism. Soc. Am. 60, 1701-1731

Carpenter, E.W., & Davies, D., 1966. Frequency dependent seismic phase velocities; an attempted reconciliation between the Jeffreys/Bullen and the Gutenberg models of the upper mantle. Nature 212, 134-135

Chisholm, J.I., & Butcher, N.J.D., 1981. A borehole proving dolomite beneath the Dinantian limestones near Matlock, Derbyshire. Mercian Geol. 8, 225-228

Chow, R.A.C., Fairhead, J.D., Henderson, N.B., & Marshall, P.D., 1980. Magnitude and Q determinations in southern Africa using L_g. Geophys. J. R. astr. Soc. 63, 735-745

Clark, R.A., & Stuart, G.W., 1981. Upper mantle structure of the British Isles from Rayleigh wave dispersion. Geophys. J. R. astr. Soc. 67, 59-75

Clark, S.P., 1966. Handbook of physical constants. Geol. Soc. Am. Mem. 97

Clark, V.A., Tittmann, B.R., & Spencer, T.W., 1980. Effect of volatiles on attenuation (Q^{-1}) and velocity in sedimentary rocks. J. geophys. Res. 85, 5190-5198

Clee, T.E., Barr, K.G., & Berry, M.J., 1974. Fine structure of the crust near Yellowknife. Can. J. Earth. Sci. 11, 1524-1549

Collette, B.J., Lagaay, R.A., Ritsema, A.R., & Schouten, J.A., 1967. Seismic investigations in the North Sea,1 and 2. Geophys. J. R. astr. Soc. 12, 363-373

Collins, F., & Lee, C.C., 1956. Seismic wave attenuation characteristics from pulse experiments. Geophysics 21, 16-40

Cooley, J.W., & Tukey, J.W., 1965. An algorithm for the machine calculation of complex Fourier series. Mathematics of Computation 19, 297-301

Cope, F.W., 1973. Woo Dale bore hole near Buxton, Derbyshire. Nature 243, 29-30

Cope, F.W., 1979. The age of the volcanic rocks in the Woo Dale bore hole, Derbyshire. Geol. Mag. 116, 319-320

Correig, A.M., Susagna, M.T., & Lana, X., 1982. Lateral variations of attenuation coefficients, group and phase velocities of Rayleigh waves in Europe. Tectonophysics 82, 179-194

Cox, F.C., & Bridge, D.McC., 1977. The limestone and dolomite resources of the country around Monyash, Derbyshire: Description of 1:25 000 resource sheet SK 16. Miner. Assess. Rep. Inst. Geol. Sci. 26.

Cox, S.J., 1983. Upper crustal studies of a region west of Sheffield. Unpubl. MSc dissertation University of Leeds

Der, Z., Masse, R., & Landisman, M., 1970. Effects of observational errors on the resolution of surface waves at intermediate distances. J. geophys. Res. 75, 3399-3409

Dunham, K.C., 1952. "Fluorspar." 4th ed
Mem. Geol. Surv. Min. Res. 4

Dunham, K.C., 1973. A recent deep borehole near Eyam, Derbyshire. Nature Phys. Sci. 241, 84-85

Dziewonski, A.M., Bloch, S., & Landisman, M., 1969. A technique for the analysis of transient seismic signals. Bull. seis. Soc. Am. 59, 427-444

Dziewonski, A.M., Mills, J., & Bloch, S., 1972. Residual dispersion measurements - a new method of surface wave analysis. Bull. seism. Soc. Am. 62, 129-139

Dziewonski, A.M., & Hales, A.L., 1972. Numerical analysis of dispersed seismic waves. pp 39-85 in Bolt, B.A., (ed) "Methods in Computational Physics. Vol 11. Seismology: Surface Waves and Earth Oscillations." Academic Press (New York)

Eden, R.A., Stevenson, I.P., & Edwards, W., 1957. Geology of the country around Sheffield. Mem. Geol. Surv. GB. Sheet No 100

Edwards, W., & Trotter, F.M., 1954. British Regional Geology: The Pennines and Adjacent Areas. Institute of Geological Sciences (London)

Evans, A.C., 1981. Propagation and dissipation of VHF Rayleigh waves in Scotland.
Unpubl. PhD thesis University of Edinburgh

Evans, J.R., 1983. Effects of the free surface on shear wavetrains. Global Seismology Unit Rep. no. 190

Ford, T.D., 1968a. The Carboniferous Limestone. pp 59-82
in Sylvester-Bradley, P.C., & Ford, T.D., (eds) "The Geology of the East Midlands." Leicester University Press (Leicester)

Ford, T.D., 1968b. The Millstone Grit. pp 83-94
in Sylvester-Bradley, P.C., & Ford, T.D., (eds) "The Geology of the East Midlands." Leicester University Press (Leicester)

Ford, T.D., 1972. Supplement to the bibliography of the geology of the Peak District, Derbyshire. Mercian Geol. 4, 109-137

Ford, T.D., & Ineson, P.R., 1971. The fluorspar mining potential of the Derbyshire ore field. Trans. Inst. Min. Met. 80, B186-B210

Ford, T.D., & Mason, M.H., 1967. Bibliography of the Geology of the Peak District of Derbyshire. Mercian Geol. 2, 133-244

Francis, E.H., 1979. British Coalfields. Sci. Prog. 66, 1-23

Frisillo, A.L., & Stewart, T.J., 1980. Effect of partial gas/brine saturation on ultrasonic absorption in sandstone. J. geophys. Res. 85, 5209-5211

Futterman, W.I., 1962. Dispersive body waves. J. geophys. Res. 67, 5279-5291

Fyfe, C.J., 1982. PDP11/50 System software summary. Global Seismology Unit Rep. no. 153

Garvin, W.W., 1960. "Introduction to Linear Programming." McGraw Hill (New York)

Gill, P.E., & Murray, W., 1972. Quasi-Newton methods for unconstrained optimisation. Jour. Inst. Math. Appl. 9, 91-108

Gladwin, M.T., & Stacey, F.D., 1974. Ultrasonic pulse velocity as a rock stress sensor. Tectonophysics 21, 39-45

Godlewski, M.J.C., & West, G.F., 1978. Rayleigh wave dispersion over the Canadian shield. Bull. seism. Soc. Am. 67, 771-779

Gordon, R.B., & Davis, L.A., 1968. Velocity and attenuation of seismic waves in imperfectly elastic rock. J. geophys. Res. 73, 3917-3935

Grant, F.S., & West. G.F., 1965. "Interpretation Theory in Applied Geophysics." McGraw Hill (New York)

Griffiths, D.W., & Bollinger, G.A., 1979. The effect of Appalachian Mountain topography on seismic waves. Bull. seism. Soc. Am. 69, 1081-1105

Gupta, I.N., & Kisslinger, C., 1966. Radiation of body waves from near surface explosive sources. Geophysics 31, 1057-1065

Gupta, I.N., & Hartenberger, R.A., 1981. Seismic phases and scaling associated with small high explosive surface shots. Bull. seism. Soc. Am. 71, 1731-1741

Gutenberg, B., 1957. Effects of ground on earthquake motion. Bull. seism. Soc. Am. 47, 221-250

Habberjam, G.M., & Whetton, J.T., 1952. On the relationship between seismic amplitude and charge of explosive fired in routine blasting operations. Geophysics 17, 116-128

Hales, A.L., Muirhead, K.J., & Rynn, J.M.W., 1980. Crust and upper mantle shear velocities from controlled sources. Geophys. J. R. astr. Soc. 63, 659-670

Hall, J., 1978. LUST - a seismic refraction survey of the Lewisian basement complex in NW Scotland. J. geol. Soc. Lon. 135, 555-563

Hamilton, E.L., 1972. Compressional-wave attenuation in marine sediments. Geophsyics 37, 620-646

Hartzell, S.H., Brune, J.N., & Prince, J., 1978. The October 6, 1974 Acapulco earthquake: an example of the importance of short-period surface waves in strong ground motion. Bull. seism. Soc. Am. 68, 1663-1677

Haskell, N.A., 1953. Dispersion of surface waves on multi-layered media. Bull. seism. Soc. Am. 65, 71-83

Herrmann, R.B., 1969. The structure of the Cincinnati Arch as determined by short period Rayleigh waves. Bull. seism. Soc. Am. 59, 399-407

Herrmann, R.B., 1973. Some aspects of band-pass filtering of surface waves. Bull. seism. Soc. Am. 63, 663-671

Houliston, D.J., 1975. The seismic data-processing systems of the Institute of Geological Sciences in Edinburgh. Seismological Bulletin no. 2. Inst. Geol. Sci.

Houliston, D.J., Laughlin, J., & McGonigle, R.W., 1982. Impulse calibration of seismometers. Computers & Geosciences 8, 341-348

Ineson, P.R., & Ford, T.D., 1982. The South Pennine Orefield: Its genetic theories and eastward extension. Mercian Geol. 8, 285-303

Ineson, P.R., & Walters, S.G., 1983. Dinantian extrusive activity in the South Pennines. Mercian Geol. 9, 88-98

Institute of Geological Sciences., 1978. IGS Bore holes 1977. Rep. Inst. Geol. Sci. No. 78/21

Institute of Geological Sciences., 1981. Annual Report for 1980 and 1981. Institute of Geological Sciences (London)

Jackson, D.D., 1972. Interpretation of inaccurate, insufficient and inconsistant data. Geophys. J. R. astr. Soc. 28, 97-109

Jackson, D.D., & Anderson, D.L., 1970. Physical mechanisms of seismic wave attenuation. Rev. Geophys. Space Phys. 8, 1-64

Jacob, A.W.B., 1969a. Crustal structure in Ireland and the south of Scotland.
Unpubl. PhD thesis University of Dublin

Jacob, A.W.B., 1969b. Crustal phase velocities observed at the Eskdalemuir Seismic Array. Geophys. J. R. astr. Soc. 18, 189-197

Jacob, A.W.B., 1975. Dispersed shots at optimum depth - an efficient seismic source for lithospheric studies. J. Geophys. 41, 63-70

Johnston, D.H., Toksoz, M.N., & Timur, A., 1979. Attenuation of seismic waves in dry and saturated rocks. II Mechanisms. Geophysics 44, 691-711

Joyner, W.B., Warrick, R.E., & Fumal, T.E., 1981. The effect of Quarternary alluvium on strong ground motion in the Coyote Lake California, earthquake of 1979. Bull. seism. Soc. Am. 71, 1333-1349

Kanamori, H., & Anderson, D.L., 1977. Importance of physical dispersion in surface wave and free oscillation problems: review Rev. Geophys. Space Phys. 15, 105-112

Keen, C.E., Fricker, A., Keen, M.J., & Blinn, L., 1979. A study of the Reykjanes Ridge by surface waves using an earthquake-pair technique. Geol. Surv. Can. Paper 79-1A, 273-279

Keilis-Borok, V.I., & Yanovskaja, T.B., 1967. Inverse problems of seismology (structural review). Geophys. J. R. astr. Soc. 13, 223-234

Keller, G.R., Smith R.B., Braile, L.W., Heaney, R., & Shurbet, D.H., 1976. Upper crustal structure of the eastern Basin and Range, northern Colorado plateau and middle Rocky Mountains from Rayleigh dispersion. Bull. seism. Soc. Am. 66, 869-876

Kent, P.E., 1957. Triassic relics and the 1000 ft surface in the Southern Pennines. East Midland Geog. 1, 3-10

Kent, P.E., 1967. A contour map of the sub-Carboniferous surface in the north-east Midlands. Proc. Yorks. Geol. Soc. 36, 127-133

King, J.L., & Tucker, B.E., 1984. Observed variations of earthquake motions across a sediment filled valley. Bull seism. Soc. Am. 74, 137-151

Kjartansson, E., 1979. Attenuation of seismic waves in rocks and applications in energy exploration.
Unpubl. PhD thesis University of Stanford

Kjartansson, E., & Denlinger, R., 1977. Seismic wave attenuation due to thermal relaxation in porous media. (abstr) Geophysics 42, 1516

Knopoff, L., 1964a. Q. Reviews of Geophys. 2, 625-660

Knopoff, L., 1964b. A matrix method for elastic wave problems. Bull. seism. Soc. Am. 54, 431-438

Knopoff, L., 1969. Phase and group slowness in inhomogeneous media. J. geophys. Res. 74, 1701

Knopoff, L., 1972. Observation and inversion of surface wave dispersion. Tectonophysics 13, 497-519

Knopoff, L., & Porter, L.D., 1963. Attenuation of surface waves in a granular material. J. geophys. Res. 68, 2191-2197

Krishnamurthi, M., & Balakrishna, S., 1957. Attenuation of sound in rocks. Geophysics 22, 268-274

La Bas, M.J., 1972. Caledonian igneous rocks beneath central and eastern England. Proc. Yorks. Geol. Soc. 39, 71-86

Lanczos, C., 1961. "Linear Differential Operators." Van Nostrand (London)

Lee, W.B., & Solomon, S.C., 1975. Inversion schemes for surface wave attenuation and Q in the crust and mantle. Geophys. J. R. astr. Soc. 43, 47-71

Lee, W.B., & Solomon, S.C., 1978. Simultaneous inversion of surface wave phase velocity and attenuation: Love waves in western North America. J. geophys. Res. 83, 3389-3400

Leet, L.D., 1954. Quarry blasting with short period delay detonators. The Explosives Engineer (Sept-Oct), 142-154

Levenberg, K., 1944. A method for the solution of certain non-linear problems in least squares. Quant. Appl. Math. 2, 164-168

Levshin, A.L., Pisarenko, V.F., & Pogrebinsky, G.A., 1972. On a frequency-time analysis of oscillations. Ann. Geophys. 28, 211-218

Lewis, G.D., 1971. Earliest times to the Norman Conquest in "Peak District National Park." National Park Guide No 3 HMSO

Lysmer, J., & Drake, L.A., 1972. A finite element method for seismology. pp 181-216 in Bolt, B.A., (ed) "Methods in Computational Physics. Vol. 11. Seismology: Surface Waves and Earth Oscillations." Academic Press (New York)

MacBeth, C.D., 1983. Propagation and attenuation of seismic Rayleigh waves along single paths in Scotland. Unpubl. PhD thesis University of Edinburgh

MacBeth, C.D., & Burton, P.W., 1983. Single station Q: attenuation of 2 Hz Rayleigh waves along single isolated propagation paths in Scotland. Annls. Geophys. 1, 223-228

Mal, A.K., & Knopoff, L., 1965. Transmission of Rayleigh waves past a step change in elevation. Bull. seism. Soc. Am. 55, 319-334

Maroof, S.I., 1976. The structure of the concealed pre-Carboniferous basement of the Derbyshire Dome from Gravity data. Proc. Yorks. Geol. Soc. 41, 59-69

Marquardt, D.W., 1963. An algorithm for least-squares estimation of non-linear parameters. J. Soc. Ind. Appl. Math. 11, 431-441

Martel, L., Munasinghe, M., & Farnell, G.W., 1977. Transmission and reflection of Rayleigh wave through a step. Bull. seism. Soc. Am. 67, 1277-1290

Marshall, P.D., & Burton, P.W., 1971. The source-layering function of underground explosions and earthquakes - an application of a 'common path' method. Geophys. J. R. astr. Soc. 24, 533-537

Mavko, G.M., 1979. Frictional attenuation: An inherent amplitude dependence. J. geophys. Res. 84, 4769-4775

Mavko, G.M., Kjartansson, E., & Winkler, K., 1979. Seismic wave attenuation in rocks. Rev. Geophys. Space Phys. 17, 1155-1164

Mavko, G.M., & Nur, A., 1975. Melt squirt in the aesthenosphere. J. geophys. Res. 80, 1444-1448

Mavko, G.M., & Nur, A., 1979. Wave attenuation in partially saturated rocks. Geophysics 44, 161-178

McDonal, F.J., Angona, F.A., Mills, R.L., Sengbush, R.L., Van Nostrand, R.G., & White, J.E., 1958. Attenuation of shear and compressional waves in Pierre Shales. Geophysics 23, 421-439

McEvilly, T.V., & Stauder, W., 1965. The effect of sedimentary thickness on short period Rayleigh wave dispersion. Geophysics 30, 198-203

McGonigle, R.W., & Burton, P.W., 1980. Accuracy in LP electromagnetic seismograph calibration by least-squares inversion of the calibration pulse. Bull. seism. Soc. Am. 70, 2261-2273

Miller, J., & Grayson, R.F., 1982. The regional context of Waulsortian facies in N England. (in press?)

Mitchell, B.J., 1976. Anelasticity of the crust and upper mantle beneath the Pacific Ocean from the inversion of observed surface wave attenuation. Geophys. J. R. astr. Soc. 46, 521-533

Mitchell, B.J., 1980. Frequency dependence of shear wave internal friction in the continental crust of eastern North America. J. geophys. Res. 85, 5212-5218

Moseley, F., & Ahmed, S.M., 1967. Carboniferous joints in the North of England and their relation to earlier and later structures. Proc. Yorks. Geol. Soc. 36, 61-90

Nafe, J.E., & Drake, C.L., 1965. p200 in Grant, F.S., & West, G.F. "Interpretation theory in Applied Geophsyics." McGraw-Hill (New York)

NAG., 1980. "FORTRAN Library Manual." Numerical Algorithms Group (Oxford)

Nakanishi, I., 1981. Shear velocity and shear attenuation models inverted from the world-wide and pure-path average data of mantle Rayleigh waves ($_0S_{25}$ to $_0S_{80}$) and fundamental spheroidal modes ($_0S_2$ to $_0S_{24}$). Geophys. J. R. astr. Soc. 66, 83-130

Newman, P.J., & Worthington, M.H., 1980. In situ investigation of seismic body wave attenuation in heterogeneous media. 42nd meeting EAEG, Istanbul 1980

Nuttli, O.W., 1973. Sesimic wave attenuation and magnitude relations for eastern North America. J. geophys. Res. 78, 876-885

O'Brien, P.N.S., 1967. The use of amplitudes in seismic refraction survey. pp 85-117 in Musgrave, A.W., (ed) "Seismic Refraction Prospecting." SEG (Tulsa)

O'Connell, R.J., & Budiansky, B. 1977. Viscolelastic properties of fluid saturated cracked solids. J. geophys. Res. 82, 5719-5736

O'Doherty, R.F., & Anstey, N.A., 1971. Reflections on amplitudes. Geophys. Pros. 19, 430-458

Oliver, J., & Ewing, M., 1958. The effect of surficial sedimentary layers on continental surface waves. Bull. seism. Soc. Am. 48, 339-354

Panza, G.F., & Calcagnile, G., 1975. L_g, L_i, R_g from Rayleigh modes. Geophys. J. R. astr. Soc. 40, 475-487

Parker, R.L., 1977. Understanding inverse theory. Ann. Rev. Earth Planet. Sci. 5, 35-64

Patton, H., 1980. Crust and upper mantle structure of the Eurasian continent from phase velocity and Q of surface waves. Rev. Geophys. Space Phys. 18, 605-625

Pekeris, C.L., 1948. The theory of propagation of explosive sound in shallow water. Geol. Soc. Am. Mem. 27

Peselnick, L., & Zietz, I., 1959. Internal friction of fine grained limestones at ultrasonic frequencies. Geophysics 24, 285-296

Pilant, W.L., & Knopoff, L., 1970. Inversion of phase and group slowness dispersion. J. geophys. Res. 75, 2135-2136

Pinkerton, J.M.M., 1947. A pulse method for the measurement of ultrasonic absorption in liquids: Results for water. Nature 160, 128-129

Pollack, H.N. 1963. Effect of delay time and number of delays on the spectra of ripple-fired shots. Eq. Notes 34, 1-12

Prentice, J.E., 1951. The Carboniferous Limestone of the Manifold Valley region. Quart. J. geol. Soc. Lon. 106, 171-209

Ricker, N., 1953. The form and laws of propagation of seismic wavelets. Geophysics 18, 10-40

Rogers, D.E., 1980. Seismic studies on the Derbyshire Dome. (abstr) UKGA Supplement IV. Geophys. J. R. astr. Soc. 61, 199

Rogers, D.E., 1983. Seismic studies on the Derbyshire Dome. Unpubl. PhD thesis University of Leeds

Sabatier, P.C., 1977. On geophysical inverse problems and constraints. J. Geophys. 43, 115-137

Sanchez-Sesma, F.J., & Esquival, J.A., 1979. Ground motion on alluvial valleys under incident plane SH waves. Bull. seism. Soc. Am. 69, 1107-1120

Sato, Y., 1958. Attenuation, dispersion and wave guide of the G-wave. Bull. seism. Soc. Am. 48, 231-251

Savage, J.C., 1969. Comments on paper by R.B. Gordon and L.A. Davis 'Velocity and attenuation of seismic waves in imperfectly elastic rock'. J. geophys. Res. 74, 726-728

Schwab, F.A., & Knopoff, L., 1972. Fast surface wave and free mode computations. pp 87-180 in Bolt, B.A., (ed) "Methods in Computational Physics. Vol 11. Seismology: Surface Waves and Earth Oscillations." Academic Press (New York)

Shirley, J., 1959. The Carboniferous Limestone of the Monyash-Wirksworth area, Derbyshire. Quart. J. geol. Soc. Lon. 114, 411-429

Shirley, J., & Horsfield, E.L., 1945. The structure and ore deposits of the Carboniferous Limestone of the Eyam district, Derbyshire. Quart. J. geol. Soc. Lon. 100 (for 1944), 289-310

Souriau, A., Correig, A.M., & Souriau, M., 1980. Attenuation of Rayleigh waves across the volcanic area of the Massif Central, France. Phys. Earth Planet. Int. 23, 62-71

Stevenson, I.P., & Gaunt, G.D., 1971. Geology of the country around Chapel-en-le-Firth. Mem. Geol. Surv. GB Sheet No 99

Stuart, G.W., 1978. The upper mantle structure of the North Sea region from Rayleigh wave dispersion. Geophys. J. R. astr. Soc. 52, 367-382

Takeuchi, H., Dorman, J., & Saito, M., 1964. Partial derivatives of surface wave phase velocity with respect to physical parameter changes within the earth. J. geophys. Res. 69, 3429-3441

Telford, W.M., Geldart, L.P., Sheriff, R.E., & Keys, D.A., 1978. "Applied Geophysics." Cambridge University Press (Cambridge)

Thach, T.K., 1965. Sedimentology of Lower Carboniferous (Visean) Limestones in North Staffordshire and SW Derbyshire. Unpubl. PhD thesis University of Reading

Thoenen, J.R., & Windes, S.L., 1937. Earth vibrations caused by quarry blasting. Progress report 1. U.S. Bureau of Mines R.I. 3353

Thomson, W.T., 1950. Transmission of elastic waves through a stratified medium. J. Appl. Phys. 21, 89

Tittmann, B.R., Clark, V.A., Richardson, J.M., & Spencer, T.W., 1980. Possible mechanism for seismic attenuation in rocks containing small amounts of volatiles. J. geophys. Res. 85, 5199-5208

Toksöz, M.N., Johnston, D.H., & Timur, A., 1979. Attenuation of seismic waves in dry and saturated rocks: II Laboratory measurements. Geophysics 44, 681-690

Tryggvason, E., 1962. Crustal structure of the Iceland region from dispersion of surface waves. Bull. seism. Soc. Am. 52, 359-388

Tryggvason, E., 1965. Dissipation of Rayleigh energy. J. geophys. Res. 70, 1449-1455

Tsai, Y., & Aki, K., 1969. Simultaneous determination of the seismic moment and attenuation of seismic surface waves. Bull. seism. Soc. Am. 59, 275-287

Walsh, J.B., 1969. New analysis of attenuation in partially melted rock. J. geophys. Res. 74, 4333-4337

Walsh, P.T., Collins, P., Ijtaba, M., Newton, J.P., Scott, N.H., & Turner, P.R., 1980. Palaeocurrent directions and their bearing on the origin of the Brassington Formation (Miocene-Pliocene) of the Southern Pennines, Derbyshire, England. Mercian Geol. 8, 47-62

Walters, S.G., & Ineson, P.R., 1981. A review of the distribution and correlation of igneous rocks in Derbyshire, England. Mercian Geol. 8, 81-132

Waters, K.H., 1981. "Reflection Seismology." 2nd ed Wiley & Sons (New York)

Weaver, J.D., 1974. Systematic jointing in South Derbyshire. Mercian Geol. 5, 115-132

Whitcombe, D.N., & Maguire, P.K.H., 1980. An analysis of the velocity structure of the Precambrian rocks of Charnwood Forest. Geophys. J. R. astr. Soc. 63, 405-416

Whitcombe, D.N., & Maguire, P.K.H., 1981. Seismic refraction studies of the upper crust beneath Central England: Part 2 The investigation of a postulated basement ridge extending from the Derbyshire Dome to the west of Charnwood Forest. J. geol. Soc. Lon. 138, 653-660

Wiggins, R.A., 1972. The general linear inverse problem: implications of surface waves and free oscillations for earth structure. Rev. Geophys. Space Phys. 10, 251-285

Willis, D.E., 1963. A note of the effect of ripple firing on the spectra of quarry shots. Bull. seism. Soc. Am. 53, 79-85

Willmore, P.L., 1960. The detection of earth movements. pp 230-276 in Runcorn, S.K., (ed) "Methods and Techniques in Geophysics. Vol. 1" Interscience Publishers Ltd. (London)

Wills, L.J., 1978. A palaegeological map of the Lower Palaeozoic floor below the cover of Upper Devonian, Carboniferous and later formations with inferred and speculative reconstructions of the Lower Palaeozoic and Pre-Cambrian outcrops in adjacent areas. ed Leake, B.E., Geol. Soc. Lon. Mem. No. 8

Winkler, K.W., 1979. The effects of pore fluids and frictional sliding on seismic attenuation.
Unpubl. PhD thesis University of Stanford

Winkler, K.W., & Nur, A. 1979. Attenuation and velocity in dry and water saturated Massilon sandstone. (abstr) 48th Annual Int. SEG Meeting Geophsyics 44, 336

Wireless World. 1978. Time coded transmission - Details of the additional slow code. Wireless World (July), 68

Wyllie, M.R.J., Gardner, G.H.F., & Gregory, A.R., 1962. Studies of elastic wave attenuation in porous media: Geophysics 27, 569-589

Yu, G.K., & Mitchell, B.J., 1979. Regionalised shear velocity models of the Pacific upper mantle from observed Love and Rayleigh wave dispersion. Geophys. J. R. astr. Soc. 57, 311-341